UNIVERSITÀ DEGLI STUDI DI MILANO

Scuola di Dottorato in Fisica, Astrofisica e Fisica Applicata

Dipartimento di Fisica "Aldo Pontremoli"

Corso di Dottorato in Fisica, Astrofisica e Fisica Applicata
Ciclo XXXI

Continuous measurements and nonclassicality as resources for quantum technologies

Settore Scientifico Disciplinare FIS/03

Supervisore: Professor Matteo G. A. PARIS

Coordinatore: Professor Francesco RAGUSA

Tesi di Dottorato di:

Francesco ALBARELLI

Anno Accademico 2017-18

Commission of the final examination:

External Referees:

Dr. Alessio SERAFINI (University College London, UK)
Prof. Rajiah SIMON (Institute of Mathematical Sciences, Chennai, India)

External Members:

Prof. Fabio BENATTI (Università degli Studi di Trieste, Italy)
Prof. Lorenzo MACCONE (Università degli Studi di Pavia, Italy)

Internal Member:

Prof. Matteo G. A. PARIS (Università degli Studi di Milano, Italy)

Final examination:

Date: November 19th, 2018

Dipartimento di Fisica "Aldo Pontremoli"
Università degli Studi di Milano
via Celoria 16, 20133 Milano, Italy

MIUR subjects:

FIS/03

PACS:

03.67.-a
03.65.Yz

"There is no such thing as not worshipping. Everybody worships.
The only choice we get is what to worship. . . .
Worship your intellect, being seen as smart, you will end up feeling stupid,
a fraud, always on the verge of being found out."
— D. F. Wallace

To my family.

Contents

List of publications

As of November 18, 2018

Material discussed in this thesis

Publications in refereed journals

1. F. Albarelli, A. Ferraro, M. Paternostro, and M. G. A. Paris, "Nonlinearity as a resource for nonclassicality in anharmonic systems", Phys. Rev. A **93**, 032112 (2016).

2. F. Albarelli, T. Guaita, and M. G. A. Paris, "Quantum backflow effect and nonclassicality", Int. J. Quantum Inf. **14**, 1650032 (2016).

3. M. A. C. Rossi, F. Albarelli, and M. G. A. Paris, "Enhanced estimation of loss in the presence of Kerr nonlinearity", Phys. Rev. A **93**, 053805 (2016).

4. F. Albarelli, M. A. C. Rossi, M. G. A. Paris, and M. G. Genoni, "Ultimate limits for quantum magnetometry via time-continuous measurements", New J. Phys. **19**, 123011 (2017).

5. F. Albarelli, M. G. Genoni, M. G. A. Paris, and A. Ferraro, "Resource theory of quantum non-Gaussianity and Wigner negativity", Phys. Rev. A (in press), arXiv:1804.05763.

Publications in conference proceedings

1. F. Albarelli, M. A. C. Rossi, M. G. A. Paris, and M. G. Genoni, "Monitoring time and detectors efficiencies in time-continuous magnetometry" in P. F. Bortignon, G. Lodato, E. Meroni, M. Paris, L. Perini, A. Vicini (Eds.) *Toward a Science Campus in Milan*, Springer Proceedings in Physics (Springer, Heidelberg, 2018), in press.

Papers under review

1. F. Albarelli, M. A. C. Rossi, D. Tamascelli, and M. G. Genoni, "Restoring Heisenberg scaling in noisy quantum metrology by monitoring the environment", submitted to Quantum, arXiv:1803.05891.

Other material

Publications in refereed journals

6. F. Albarelli, M. G. Genoni, and M. G. A. Paris, "Generation of coherence via Gaussian measurements", Phys. Rev. A **96**, 012337 (2017).

Papers under review

2. F. Albarelli, U. Shackerley-Bennett, and A. Serafini, "Locally optimal control of continuous variable entanglement", submitted to Phys. Rev. A, arXiv:1711.11400.

Papers in preparation

- L. Seveso, F. Albarelli, M. G. Genoni, and M. G. A. Paris, "On the discontinuity of the quantum Fisher information and the validity of the Cramér-Rao bound".
- F. Albarelli, M. Menga and M. G. A. Paris, "Detecting two-qubit entanglement from classical correlations of noncommuting observables".
- H. Adnane, M. Bina, F. Albarelli and M. G. A. Paris "State engineering assisted by a non-deterministic linear amplifier".
- H. Adnane, F. Albarelli and M. G. A. Paris "Characterization of the gain of non-deterministic noiseless linear amplifiers at the quantum limit".

Acknowledgments

First and foremost I want to thank my supervisor Matteo Paris. I have a great number of reasons to be grateful to Matteo; just to name a few: his patience and kindness with me, all the things I've learnt from him and all the opportunities he provided for me. However, as a PhD student, I am most in debt to him for giving me the freedom to experiment with different things and to follow my own inclinations and ideas.

Second, I want to thank Marco Genoni, for introducing me to a new and exciting field (continuous measurements), for the countless discussions and e-mails and in general for his continuous support and encouragement.

The work presented in this thesis would not have been possible without my other collaborators, whom I have to thank: Matteo Rossi, Alessandro Ferraro, Mauro Paternostro, Dario Tamascelli, Tommaso Guaita. I am also very thankful to all the other people I had the pleasure to work with during these years: Alessio Serafini, Luigi Seveso, Matteo Bina, Hamza Adnane and Marina Menga. I need to thank my friend Alessandro Saltini, who first got me interested in physics and still helps me with anything related to physics, mathematics or programming, with unconditional dedication.

Finally, I also have some more technical acknowledgments. Thanks to Silvia Toson for producing Figure 3.1; thanks (again) to Matteo Rossi for producing Figures 4.3, 4.4 and 5.6, for contributing to Figure 4.1 and in general for the continuous help with numerical computations.

Introduction

Any word can be used both in a very precise and technical sense and in a broader colloquial sense; this is certainly true for the word *resource*. This word is becoming more and more popular in quantum information science and we want to explain why it appears in the title of this thesis.

Intuitively, if one can perform some particular task in a better way by having access to something, we can call this thing a resource. In scientific terms, improving the performance of a certain task is not only a qualitative concept, but it must be as quantitative as possible: any improvement must be a measurable increase in some suitable figure of merit. Therefore a resource for some task is something which can increase the relevant figure of merit. However, even by introducing this quantitative aspect, the definition of a resource is still vague and the word is still used with its colloquial meaning.

If one wants to be more precise, there exists a very general mathematical framework to talk about resources, the so-called resource theories. A resource theory can be built whenever there is some restriction on the operations than can be implemented on a system. This abstract construction becomes relevant in physics, where the system and the operations are *physical*. This framework is very general and it has found countless applications in quantum information science, mostly building on the pioneering work in entanglement theory.

In this thesis we are mostly concerned with the first "colloquial" meaning and for the most part we do not dwell on a precise mathematical definition of a resource. In particular, a substantial part of this thesis deals with the application of quantum mechanics to high precision measurements, the field of *quantum metrology*. In this context there are several figures of merit to quantify the precision of a given measurement scheme and we are interested in finding *metrological* resources, i.e. ways to achieve a better precision. On the other hand, we will also deal with the more rigorous connotation of the concept: in Chapter 8 we present a fully fledged resource theoretical framework for continuous variable quantum systems.

While the underlying and unifying aspect of the whole thesis is exactly this focus on resources, on a concrete level the presentation is divided into two parts. The first part deals with the topic of continuous (in time) quantum measurements, and it explores how and when they can be considered useful resources for quantum metrology.

On a very simple level, time-continuous measurements describe a situation where an experimenter does not get information out of a quantum system instantaneously, but continuously in time. In the standard "textbook" presentation of quantum mechanics, measurements are assumed to be instantaneous and to induce a strong perturbation on the system. On the contrary, continuous measurements can be seen as the continuous repetition of very weak measurements. Roughly speaking, at every instant only an infinitesimal amount of information is extracted from the system, which is thus only infinitesimally perturbed.

There is also a complementary way to frame the same concepts. Any quantum system interacts with an environment, usually modelled as a collection of external systems assumed to be out of experimental reach. This interaction causes a "noisy" evolution of the main system, which usually makes it lose its quantum properties. However, in many situations the environment is not truly out of reach. In this context, continuous measurements can be understood as a series of instantaneous "strong" measurements on the environment. This means that, by strongly and repeatedly measuring the environment, one implements weak (indirect) measurements on the main system.

Continuous measurements were historically introduced as an analogue to classical *filters*, which are methods to refine the estimate on the state of a classical system, by using a continuous stream of measurement data. Therefore it is not surprising that also in the quantum case there is a strong and deep connection with quantum metrology. As a matter of fact, we will show that this kind of evolution is a valuable metrological tool: it allows one to gain information about the system and also to prepare valuable *conditional* states. Moreover, in Chapter 4 we will show that it is possible to mitigate the negative effect of noisy dynamics on the metrological precision when the environment causing such dynamics can be measured. This fact can be intuitively understood by noting that the actual noisy evolution of the system (the so called *reduced* dynamics) corresponds to measuring the environment and discarding the results, keeping only the average state.

In order to rigorously study the metrological applications of continuous measurements we employ quantum estimation theory. The most celebrated result in quantum estimation theory is the quantum Cramér-Rao bound, which sets the limit on the achievable precision in estimating parameters encoded in quantum states. In Chapter (2) we will see that extending this bound to continuously monitored systems is not completely trivial and we will identify the correct figures of merit to use in this situation.

The second part of this thesis deals with nonclassical states of continuous variable systems and related topics. Continuous variable systems are infinite-dimensional and they are in general harder to study than discrete systems, where a mathematical description based only on linear algebra is sufficient. However, continuous variables systems are ubiquitous, the prime example is the quantum description of light, which fundamentally boils down to quantum harmonic oscillators.

The class of Hamiltonians given by quadratic polynomials of the canonical operators (i.e. position and momentum operators of a harmonic oscillator) plays a very important role. These Hamiltonians induce a genuinely quantum evolution, which however can be described in purely classical terms, using a phase-space description. Moreover, also ground and thermal states of quadratic Hamiltonians are very special. These are the

so-called Gaussian states; they are compactly described by a finite number of parameters and yet they display a great number of genuinely quantum features. For this reason they are the foundation of continuous variable quantum technologies.

The last important word in the title of this thesis is the word *nonclassicality*. Clearly, the challenge to precisely assess the demarcation line between a quantum and a classical description of a physical system is an extremely broad problem, which has engaged physicists for more than a century. In particular, in a quantum optical context, the concept of *nonclassicality* emerged to pinpoint all those effects not ascribable to a classical electromagnetic field. Since measurement results are described in statistical terms, we have a nonclassical effect whenever a classical statistical model is not enough to explain such results and we need the intrinsic statistical nature of quantum mechanics. The probabilities predicted by quantum mechanics have two ingredients: quantum states and quantum observables; nonetheless in the field of quantum optics, nonclassicality is usually understood as a property of the *states*.

The idea of nonclassical states is used here in a broader sense. Most notions of nonclassicality are connected to the impossibility of interpreting a quantum state as a classical probability distribution over some suitable phase-space. Quantum optical nonclassicality is based on the so called P-function, but we are also interested in a different phase-space description, the celebrated Wigner function. In this setting a state is nonclassical when the Wigner function takes negative values. Gaussian states are the most famous example of states with a positive Wigner function (it is a Gaussian distribution). From these definitions one many also introduce several non-equivalent ways to *quantify* nonclassicality of a quantum state.

Before diving completely into the study of nonclassical properties, Chapter 5 serves as connection between the two parts of this thesis. In this chapter we remain in the quantum metrology playground, but we abandon the topic of continuous measurements. Instead, we focus on a quartic Hamiltonian, the so-called self-Kerr interaction, which generates non-Gaussian/nonclassical states and we show that it can be useful for a particular task in metrology. Again, we can frame this finding by saying that such a nonlinear Hamiltonian[1] is a resource for the considered estimation problem.

Afterwards, we study anharmonic mechanical oscillators in Chapter 6 and some peculiar effects in the dynamics of a free massive particle in Chapter 7. Roughly speaking, the goal of these studies is to quantitatively compare different nonclassical properties and to assess what can be considered a resource for their generation. By studying anharmonic potentials we more or less confirm the idea that the degree of anharmonicity is a resource to generate nonclassical ground states.

Gaussian states can be highly nonclassical in the quantum optical sense; still, the generation of nonclassical Gaussian states in quantum optics is much easier than genuinely quantum non-Gaussian ones. The price to pay for such convenience (both analytical and experimental) is that many tasks in quantum technology cannot be implemented at all, or their performance suffers from this restriction. In Chapter 8 we start from these consider-

[1] We are going to use the term *nonlinear* to mean that the transformation induced on the canonical operators is nonlinear. Strictly speaking this implies that the Hamiltonian must be a polynomial of canonical operators of order greater than 2.

ations and we finally make use of the more rigorous meaning of the word resource, by building a proper mathematical resource theory for non-Gaussian states. This resource theory is truly quantum because we disregard "trivial" non-Gaussian states obtainable by classical means. We also find a connection to previously introduced measures of nonclassicality based on the negativity of the Wigner function. The work presented in this last chapter contains a complete framework and some examples, but yet not many general answers to fundamental questions. We hope that our work may set an appropriate stage for many more future investigations.

Organization of the thesis

The present PhD thesis consists of two parts plus a preliminary chapter, for a total of eight chapters. Part I is devoted to the topic of metrology with continuously monitored quantum systems and it is divided into three chapters. Part II deals with nonclassical and non-Gaussian continuous variable quantum states and it is composed by four chapters. Some slight variations have been made in the presentation of previously published results, to maintain consistency of style and to make the structure of the manuscript more coherent.

- In Chapter 1 we collect the basic notions needed to understand the rest of the work. We start by reviewing the mathematical description of quantum mechanics, with particular emphasis on how to model measurements. We review the description of Markovian open quantum systems and Markovian continuously monitored systems, with a brief derivation of stochastic master equations. We present the fundamentals of quantum estimation theory. We introduce continuous variable quantum systems, with a particular focus on the Gaussian formalism. Finally, we briefly present three different notions of nonclassicality, based on the P function, on the Wigner function and on the non-Gaussianity of the state.

- In Chapter 2 we set the stage for the original work of the following two chapters. We explain how to accommodate continuous measurements in the framework of quantum estimation theory and the correct figures of merit to use. We also present an efficient algorithm to compute said figures of merit, originally presented in [14].

- In Chapter 3 we apply quantum estimation theory to magnetometry with a large ensemble of atoms, continuously and collectively probed by an external light mode. These results are based on two published works [12, 13] and they show that, when such collective interaction can be implemented, this metrological scheme is very effective.

- In Chapter 4 we study the metrological problem of frequency estimation with qubits undergoing a noisy dynamics and we show the beneficial effect of measuring the environment. The results are mostly taken from [14], but we also present some new material.

- In Chapter 5 we study the problem of estimating the loss rate of a bosonic channel, modelled by a Markovian master equation. We show that the introduction of an

additional nonlinear Hamiltonian, describing the so-called self-Kerr effect, can be beneficial for the estimation. These results have been published in [243].

- In Chapter 6 we study the ground states of anharmonic potentials. We want to investigate how the nonlinearity of the Hamiltonian is quantitatively connected to the nonclassicality of the ground states, by considering different notions of nonclassicality. These results have been published in [9].

- In Chapter 7 we study a peculiar dynamical effect arising for a free particle prepared in a sufficiently nonclassical initial state, the so-called backflow effect. We compare this backflow effect with the negativity of the Wigner function and we find that, while negativity is a prerequisite, said effect is a more fragile phenomenon. These results have been published in [11].

- In Chapter 8 we introduce a resource theory for non-Gaussian states, which also applies to states with a negative Wigner function. The fundamental ingredient of this resource theory is the set of available operations, which is very broad and contains Gaussian unitaries, Gaussian measurements, classical randomness and conditioning on measurement outcomes. After defining these operations we prove that a logarithmic function of the volume of the negative part of the Wigner function is a good monotone and we proceed to analyse some classes of states and a simple protocol to concentrate negativity. This work has been presented in [10].

CHAPTER 1

Preliminaries

This chapter represents a brief overview of the fundamental concepts needed for the following parts of this thesis. The aim is to introduce all the relevant notions and set the notation, without giving an extensive presentation. We only show the derivations which we believe are useful to better understand the following results and we always proceed in a very intuitive manner, without dwelling on mathematical formalities.

We start with a review of the basic notions of quantum mechanics in Section 1.1. We then review the dynamics of Markovian open quantum systems in Section 1.2, introducing both Lindblad master equations and stochastic master equations, used to model continuously monitored quantum systems. In Section 1.3 we review quantum estimation theory, one of the main theoretical tools of quantum metrology. Finally, section 1.4 is devoted to the description of continuous variable quantum systems in the phase space representation of quantum mechanics, with particular attention to Gaussian systems. We also present some basic notions about nonclassicality of continuous variable systems.

1.1 Mathematical tools of quantum mechanics

In this section we review the fundamental mathematical tools of quantum mechanics from a modern point of view. In this treatment we do not deal in details we the *dynamical* aspects of quantum theory, meaning that we try to avoid time dependent descriptions and we focus on the abstract mathematical objects. The presentation roughly follows the structure of Ref. [127], but for obvious reasons it is much lighter; the reader is referred to that book for a more exhaustive and rigorous treatment, see also [282] for a similar approach. In particular, since part of this thesis is devoted to continuous variable systems, we try to point out the most relevant differences between quantum mechanics with finite dimensional and infinite dimensional systems; even though we are going to gloss over many mathematical details.

1.1.1 States and observables

The fundamental mathematical object to describe any quantum system is a Hilbert space $\mathcal{H}$. A vector space on the complex field endowed with a scalar product $\langle u|v\rangle$ is called a Hilbert space if it is also complete. Loosely speaking completeness means that every sequence of vectors which 'looks' convergent (a Cauchy sequence using the distance

induced by the scalar product) is indeed convergent. We recall that the scalar product is a sesquilinear form, i.e. $\langle \alpha u | \beta v \rangle = \alpha^* \beta \langle u | v \rangle \quad \forall |u\rangle, |v\rangle \in \mathcal{H}$, with $\alpha, \beta \in \mathbb{C}$. The requirement of completeness is always satisfied in any finite dimensional vector space, but it becomes a crucial requirement for infinite dimensional spaces. Moreover, for quantum mechanics in infinite dimension we also require separability of the Hilbert space, i.e. the existence of a numerable basis $\{|j\rangle, j \in \mathbb{N}\}$, so that every vector can be expressed as an infinite sum $|v\rangle = \sum_j^\infty v_j |j\rangle$.

For composite systems the global Hilbert space is obtained via tensor products of the Hilbert spaces $\mathcal{H}_i$ of the single components: $\mathcal{H} = \bigotimes_i \mathcal{H}_i$.

Operators on the Hilbert space

Quantum states and observables are represented by linear operators on $\mathcal{H}$. A particularly important class is the set of *bounded* operators $\hat{A} : \mathcal{H} \to \mathcal{H}$ which satisfy the condition $|\langle v | \hat{A} | v \rangle| \leq m \langle v | v \rangle$ for some positive real number $m \in \mathbb{R}^+$. For finite dimensional Hilbert spaces every linear operator is also bounded and continuous, while for infinite dimensional systems this is not the case. In infinite dimension we also say that an operator is "trace class" if $\mathrm{Tr}\left[\hat{A}\right] = \sum_j \langle e_i | \hat{A} | e_i \rangle < \infty$, where the sum is over the vectors of a complete orthonormal basis $\langle e_j | e_i \rangle = \delta_{ij}$.

Another fundamental class of operators is that of self-adjoint operators. The adjoint of an operator A is the unique operator $A^\dagger$ which satisfies $\langle v | \hat{A} u \rangle = \langle \hat{A}^\dagger v | u \rangle \quad \forall |v\rangle, |u\rangle \in \mathcal{H}$. An operator is said to be self-adjoint if $\hat{A} = \hat{A}^\dagger$; for finite dimensions this condition corresponds to having an Hermitian matrix satisfying $A_{ij} = A^*_{ji}$. On the contrary, in infinite dimensional spaces self-adjointness is a stronger the property than Hermiticity[1] and it requires that $\hat{A}$ and $\hat{A}^\dagger$ also have the same domain: it is not enough that $\langle v | \hat{A} u \rangle = \langle \hat{A} v | u \rangle \quad \forall |v\rangle, |u\rangle \in \mathcal{H}$. Even if this requirement is rather technical, it is crucial for the validity of the spectral theorem which states that a self-adjoint operator can be written as $\hat{A} = \sum_a a |a\rangle\langle a|$, with $a \in \mathbb{R}$; note that in general the sum corresponds to an integral with a given measure on a. In finite dimension the vectors $|a\rangle$ are orthonormal $\langle a | b \rangle = \delta_{ab}$, while in infinite dimension they can also correspond to improper vectors with infinite norm.

Finally, an operator is said to be positive if $\langle v | \hat{A} | v \rangle \geq 0 \quad \forall |v\rangle \in \mathcal{H}$. In finite dimension this corresponds to a positive semidefinite matrix with non-negative eigenvalues and thus implies Hermiticity.

Quantum states

Operationally, the state of a system is a way to express the knowledge about the *preparation* of the system. In classical physics this corresponds to a probability distribution on some suitable phase space; the distribution can collapse to a single point if the preparation is deterministic. In quantum mechanics on the other hand the most general way to define a quantum state is an operator on $\mathcal{H}$, satisfying certain properties to guarantee a sound statistical interpretation.

[1] Nonetheless in the following chapter we will often blur the terminology and refer to self-adjoint operators simply as Hermitian.

The convex set of quantum states is the set of normalized self-adjoint positive operators on $\mathcal{H}$[2]:

$$\mathcal{S}(\mathcal{H}) = \{\rho \in \mathcal{B}(\mathcal{H}) | \rho \geq 0, \, \mathrm{Tr}[\rho] = 1\}, \tag{1.1}$$

in the following we equivalently call $\rho \in \mathcal{S}(\mathcal{H})$ a state, a density operator or a density matrix. Any quantum state admits a spectral decomposition $\rho = \sum_j \lambda_j |e_j\rangle\langle e_j|$, where the vectors $|e_j\rangle$ form an orthonormal basis; the coefficients are positive $\lambda_j \geq 0$ thanks to the positivity of ρ and form a normalized probability distribution $\sum_j \lambda_j = 1$, thanks to the condition $\mathrm{Tr}\rho = 1$. As usual, in the infinite dimensional case the sums might need to be replaced by integrals.

Pure state corresponds to projectors on a normalized vector $|\psi\rangle\langle\psi|$, or equivalently to rank-1 density operators with only one non-zero eigenvalue $\lambda_0 = 1$. Pure states are the extremal points of the convex set $\mathcal{S}(\mathcal{H})$, since every non-pure state can be expressed as a convex combination (also called a mixture) of pure states $\rho = \sum_j p_j |v_j\rangle\langle v_j|$. We can see that any ensemble of pure states $\{|v_j\rangle\langle v_j|\}$, each appearing with probability p_j, gives rise to some density operator ρ. However, infinitely-many ensembles of pure states correspond to the same density operator, the ensemble given by the spectral decomposition is only a particular choice.

From this discussion it should be clear that pure states are *deterministic* preparations of a quantum system, whilst when we deal with uncertain preparations we need to consider mixed (non-projective) states[3] The main point is that, differently from classical mechanics, a deterministic preparation is not a point on phase-space manifold, but it is, in its most simple form, a vector[4] and this makes it possible that the outcome of an experiment are uncertain even if the preparation is deterministic.

Given a bipartite system, a quantum state on the global Hilbert space $\rho_{AB} \in \mathcal{S}(\mathcal{H}_A \otimes \mathcal{H}_B)$ is mapped to local states on the two Hilbert spaces via the partial trace operation

$$\rho_A = \mathrm{Tr}_B[\rho_{AB}] = \sum_i {}_B\langle i| \, \rho_{AB} \, |i\rangle_B \ , \tag{1.2}$$

where the sum is taken over an orthonormal basis $\{|i\rangle_B\}$ of $\mathcal{H}_B$.

Observables

Having introduced quantum states as a way to describe the preparation of a system, we now need the mathematical description of observables. The process of measuring a quantum system is one of the most discussed fundamental aspects of the whole quantum theory and it can be described at different levels of detail. The intrinsic randomness of measurement outcomes is a key feature of the theory, which is a tool to predict the probability of such outcomes, but not single occurrences. Here, with the word "observable"

[2]Even if operators are usually denoted by a hat sign, we omit the symbol on quantum states.

[3]However keep in mind that a mixed state can also be prepared without uncertainty, starting from a pure global state and disregarding (tracing away) some subsystem. In this situation the randomness involved in the mixture is not due to some uncertain preparation.

[4] Actually, pure states correspond to an equivalence classes of vectors w.r.t. the multiplication with a phase $e^{i\theta}$ (these equivalence classes are called "rays"). However, for the sake of simplicity we usually refer to pure states as vectors.

we mean a mathematical object that captures the statistical description of the measurement process, but it does not describe how the state changes because of the measurement. This distinction is not present in classical physics and only quantum systems are perturbed by measuring them. [5]

The most general observable on a quantum system is a positive valued operator measure (POVM). Informally a POVM is a collection of positive operators $\{\hat{\pi}_\mu\}$ (also called effects), which satisfy the fundamental property

$$\sum_{\mu\in\mathcal{M}} \hat{\pi}_\mu = \mathbb{1}\,, \tag{1.3}$$

where $\mathcal{M}$ represents the outcome space and the label μ corresponds to a single measurement outcome. The outcomes μ can be either discrete quantities or real valued vectors, in such a case the sum is replaced by the appropriate integral. The recipe to obtain the probability of an outcome is the celebrated Born rule

$$p(\mu) = \mathrm{Tr}\left[\rho\hat{\pi}_\mu\right]\,, \tag{1.4}$$

when μ assumes discrete values the real numbers $0 \leq p(\mu) \leq 1$ represent probabilities. On the other hand, when μ is a continuous variable $p(\mu) \geq 0$ is a normalized probability density: $\int_{\mathcal{M}} \mathrm{d}\mu p(\mu) = 1$, thanks to (1.3). Later, we will see that this difference has non-trivial consequences for continuous variable quantum systems. We also note that sometimes we explicitly write $p(\mu|\rho)$, since this probability obtained from the Born rule can be thought as a *conditional* probability given the initial state ρ, which represents our knowledge on the preparation of the system.

In the traditional formulation of quantum mechanics, observables correspond to self-adjoint operators $\hat{O} = \hat{O}^\dagger$ and the statistical moments of the observable are obtained as $\langle\hat{O}\rangle = \mathrm{Tr}\left[\hat{O}^n\rho\right]$, in particular for $n = 1$ we have the expected (average) value of the observable. Since $\hat{O}$ is Hermitian, thanks to the spectral decomposition $\hat{O} = \sum_i o_i|e_i\rangle\langle e_i|$ it corresponds to a set of projections on its eigenstates $\hat{O}|e_i\rangle = o_i|e_i\rangle$. These observables are called *sharp* and correspond to projective POVMs since we have $\sum_i |e_i\rangle\langle e_i| = \mathbb{1}$.

Finally, we want to stress again that observables described as POVMs, as introduced in this Section, are only a way to *assign probabilities* and there is no information about the state of the system *after* the measurement has taken place. In many cases this description is sufficient, because either there is no way to access the state of the quantum system after the measurement or the measurement process itself destroys the quantum system. Following the point of view of Ref. [127] we believe that it is conceptually clearer to keep different levels of description separate. As a matter of fact, to describe the state of a system *after* the measurement we need more information than the set of positive operators $\{\pi_\mu\}$. In the next Section, after introducing transformations between quantum states, we will describe the most general way to perform this post-measurement update of a quantum state and obtain the so-called conditional states.

[5] In statistical mechanics the state of a system is a probability distribution in phase space and such a distribution is updated after a measurement according to Bayes' theorem. However, this is only a change in our ignorance about the system, while in quantum mechanics the state is perturbed even if there is no uncertainty (a pure state).

1.1.2 CP maps and quantum instruments

In the previous section we discussed the statistical interpretation of quantum states and observables, but we did not address the question of how a quantum state can be transformed into other states. Now we study this question in full generality, but abstractly, without a proper dynamical description. In Sec. 1.2 we show more in detail how to relate the abstract description with a more physical description which explicitly involves time and Hamiltonians.

Let us now introduce the mathematical definition of quantum channels. A map $\mathcal{E}$ between density operators must satisfy the following requirements

1. Linearity: $\mathcal{E}[\alpha\rho + \beta\sigma] = \alpha\mathcal{E}[\rho] + \beta\mathcal{E}[\sigma] \quad \forall\alpha,\beta \in \mathbb{C} \quad \forall\rho,\sigma \in \mathcal{S}(\mathcal{H})$
2. Complete positivity: $\mathcal{E} \otimes \mathcal{I}_{\text{anc}}(|\psi\rangle\langle\psi|) \geq 0 \quad \forall|\psi\rangle \in \mathcal{H} \otimes \mathcal{H}_{\text{anc}}$[6]
3. Trace preservation: $\text{Tr}[\mathcal{E}[\rho]] = \text{Tr}[\rho] = 1$.

Maps satisfying requirements 1-3 are called quantum channels or CPT (completely positive trace-preserving) maps. The first and the third requirements are needed to preserve the statistical interpretation of density operators, while the requirement of complete positivity is more subtle and requires further explanation. As a matter of fact positivity of the map $\mathcal{E}$, i.e. $\mathcal{E}[\rho] \geq 0 \quad \forall\rho \in \mathcal{S}(\mathcal{H})$, would be enough to preserve the statistical interpretation of the density operator. Complete positivity is a stronger mathematical condition, it obviously implies positivity of $\mathcal{E}$, but it is strongly connected to entanglement. Complete positivity ensures that if the system under scrutiny is entangled with some other ancillary system living in the Hilbert space $\mathcal{H}_{\text{anc}}$, applying the channel $\mathcal{E}$ on the system still produces a physical evolution of the global system. Moreover, this must hold for all possible dimensions of the ancillary space. On slightly more practical grounds, when the channels satisfies a semigroup property $\mathcal{E}_{t+s} = \mathcal{E}_t \circ \mathcal{E}_s$, the complete positivity of $\mathcal{E}_t$ is a necessary and sufficient condition for the positivity of the map $\mathcal{E}_t \otimes \mathcal{E}_t$ [29].

Another crucial point is that complete positivity allows for a nice mathematical characterization of quantum channels, whereas the set of positive maps is harder to characterize. A particularly useful result is that every CP map can be written in the so-called Kraus form

$$\tilde{\mathcal{E}}[\bullet] = \sum_{\mu} \hat{K}_\mu \bullet \hat{K}_\mu^\dagger; \tag{1.5}$$

the operators K_μ are usually called the Kraus operators (again, the sum might need to be replaced by an integral in general); the Kraus representation of CP maps is not unique. If $\tilde{\mathcal{E}}$ is also trace preserving the Kraus operators must satisfy the identity $\sum_\mu \hat{K}_\mu^\dagger \hat{K}_\mu = \mathbb{1}$.

We are going to show that trace non-increasing maps play a fundamental role in quantum theory, in this case the condition on the Kraus operators is $\sum_\mu \hat{K}_\mu^\dagger \hat{K}_\mu \leq \mathbb{1}$ and they are usually denoted by a tilde, i.e. $\text{Tr}\big[\tilde{\mathcal{E}}[\rho]\big] \leq \text{Tr}[\rho]$. Completely positive trace non-increasing maps are sometimes called quantum operations to distinguish them from trace-preserving quantum channels; we mostly call them only CP maps. Such CP maps

[6] $\mathcal{I}_{\text{anc}}$ represents the identity map on the ancillary Hilbert space: $\mathcal{I}_{\text{anc}}[\rho_{\text{anc}}] = \rho_{\text{anc}} \quad \forall\rho_{\text{anc}} \in \mathcal{S}(\mathcal{H}_{\text{anc}})$

still describe valid operations on quantum states, albeit non deterministic ones, i.e. the renormalized output state ρ' is obtained with probability p:

$$\rho' = \frac{\tilde{\mathcal{E}}[\rho]}{p} \qquad p = \mathrm{Tr}\left[\tilde{\mathcal{E}}[\rho]\right] , \tag{1.6}$$

Even if the state ρ' is obtained by a *nonlinear* map acting on ρ, it is usually simpler to work with the unnormalized state $\tilde{\rho}' = \tilde{\mathcal{E}}[\rho]$ and apply the normalization at the end.

A special class of quantum channels is given by unitary transformations acting on the density operator, i.e. $\rho \mapsto \hat{U}\rho\hat{U}^\dagger$, with $\hat{U}\hat{U}^\dagger = \hat{U}^\dagger\hat{U} = \mathbb{1}$. Unitary channels correspond to CPT maps with a single Kraus operator and they send pure states into pure states, their action is most easily seen at the level of vectors and it is given by the mapping $|\psi\rangle \mapsto \hat{U}|\psi\rangle$.

To end this section, we note that the description we have given so far is in the Schrödinger picture, where quantum channels act on states and observables remain unchanged. We can equivalently work in the Heisenberg picture, where channels are applied to the observables instead. Mathematically, a linear mapping on the space of states $\mathcal{S}(\mathcal{H})$ defines a dual mapping on the dual space [7] of observables (effects) as follows

$$\mathrm{Tr}[\mathcal{E}[\rho]\pi] = \mathrm{Tr}[\rho\mathcal{E}^*[\pi]] \; ; \tag{1.7}$$

this map is well defined since $\mathrm{Tr}\left[\hat{A}^\dagger\hat{B}\right]$ defines a scalar product on the space of linear operators on $\mathcal{H}$, the Hilbert-Schmidt product. From an operational point of view this means that the probability distributions given by the Born rule do not change, so the two pictures are equivalent. In this thesis we almost always work in the Schrödinger picture.

Quantum instruments

Now that we have introduced CP maps, we can finally go back to the question of how the state of a system is perturbed after a measurement. For simplicity we restrict our statements to the case of countable outcome sets $\mathcal{M}$, for more general statements see [127].

A quantum instrument is a collection of CP trace-nonincreasing maps $\{\tilde{\mathcal{E}}_\mu\}_{\mu\in\mathcal{M}}$, such that the sum of all the maps is trace preserving $\mathrm{Tr}\left[\sum_{\mu\in\mathcal{M}}\tilde{\mathcal{E}}_\mu[\rho]\right] = \mathrm{Tr}[\rho]$ for every positive operator ρ. The probability of measuring the outcome μ is then $p(\mu|\rho) = \mathrm{Tr}\left[\tilde{\mathcal{E}}_\mu[\rho]\right]$. As we already saw in (1.6) the normalized conditional states are given by

$$\rho_\mu = \frac{\tilde{\mathcal{E}}_\mu[\rho]}{p_\mu} \; . \tag{1.8}$$

A quantum instrument describes a *conditional* evolution, since the evolution is conditioned on the observation of the outcome μ.

Each quantum instrument is also associated to a trace preserving channel $\mathcal{E}_{\mathrm{unc}} = \sum_{\mu\in\mathcal{M}}\tilde{\mathcal{E}}_\mu$, which gives the so-called *unconditional* evolution, i.e. the state obtained on average by measuring the system and discarding the results; it is easy to see that

[7] We refer the reader to [127] for the precise statement about the duality between states and effects.

$\mathcal{E}_{\text{unc}}[\rho] = \sum_{\mu\in\mathcal{M}} p(\mu)\rho_\mu$. Furthermore, every CP map in the collection has Kraus decomposition $\mathcal{E}_\mu[\bullet] = \sum_j \hat{K}_{\mu,j} \bullet \hat{K}^\dagger_{\mu,j}$, thus the unconditional channel has a Kraus decomposition $\mathcal{E}_{\text{unc}}[\bullet] = \sum_\mu \sum_j \hat{K}_{\mu,j} \bullet \hat{K}^\dagger_{\mu,j}$. Since the unconditional channel is deterministic (trace-preserving) the sum of all the Kraus operators satisfies $\sum_{\mu,j} \hat{K}^\dagger_{\mu,j}\hat{K}_{\mu,j} = \mathbb{1}$.

This description is obviously consistent with the statistical description given in term of POVMs. Given a POVM $\left\{\hat{\pi}_\mu\right\}_{\mu\in\mathcal{M}}$ there are infinitely many quantum instrument which reproduce its statistics. A particularly useful instrument is the Lüders instrument (also called a bare instrument): $\tilde{\mathcal{E}}_{\text{Lüd},\mu}[\bullet] = \sqrt{\hat{\pi}_\mu} \bullet \sqrt{\hat{\pi}_\mu}$. There is larger class often considered in the literature: quantum instruments in which all the CP maps have only one Kraus operator. This means that every element of the POVM is written as

$$\hat{\pi}_\mu = \hat{M}^\dagger_\mu \hat{M}_\mu \tag{1.9}$$

and the (unnormalized) conditional states are obtained as $\tilde{\rho}_\mu = \hat{M}_\mu \rho \hat{M}^\dagger_\mu$. It is easy to see that these instruments are given by the Lüders instrument followed by a unitary transformation (in general a different one for every measurement outcome), this is nothing more than the polar decomposition of the operators: $\hat{M}_\mu = \hat{U}_\mu \sqrt{\pi_\mu}$. More generally, it can be proven that the whole class of instruments leading to a POVM is given by the Lüders instrument of the POVM, followed by a CPT map dependent on the measurement outcome, i.e. conditional map is $\tilde{\mathcal{E}}_\mu[\bullet] = \mathcal{E}_\mu\left[\sqrt{\hat{\pi}_\mu} \bullet \sqrt{\hat{\pi}_\mu}\right]$.

1.1.3 The church of the larger Hilbert space

Even though we formulated quantum mechanics in terms of density operators and channels there is no contradiction with the older traditional formulation. Crucially, the fundamental postulates remain the same [222]:

1. *States:* States of a quantum system corresponds to vectors (up to multiplication for a global phase factor) in a suitable Hilbert space.

2. *Measurements:* Observables correspond to Hermitian operators on the Hilbert space and the state of the system after the measurement is an eigenstate of the observable corresponding to the observed eigenvalue.

3. *Dynamics:* The evolution of states is given by unitary operators.

The conciliation between the traditional and the modern approach has been called "going to the church of the larger Hilbert space". The idea is that by enlarging the Hilbert space of the system under investigation it is always possible to go back to a description in terms of vectors, unitaries and projective measurements; this procedure is often called a "purification". This point of view is backed up by a very important mathematical result, Stinespring's dilation theorem.

When applied to observables Stinespring's dilation theorem is known as Naimark's theorem. Naimark's theorem states that each observable can be built from the unitary interaction of the system with a pure state of an ancillary system and a subsequent projective measurement of the ancillary system. Formally, for any POVM $\{\hat{\pi}_\mu\}_{\mu\in\mathcal{M}}$ there is an

ancillary Hilbert space $\mathcal{H}_{\rm anc}$, an ancillary fixed pure state $|\omega\rangle \in \mathcal{H}_{\rm anc}$, a fixed unitary interaction $\hat{U} : \mathcal{H}_{\rm syst} \otimes \mathcal{H}_{\rm anc} \to \mathcal{H}_{\rm syst} \otimes \mathcal{H}_{\rm anc}$ and a projective measurement $\{\hat{P}_\mu = |\mu\rangle\langle\mu|\}_\mu$ with $\hat{P}_\mu \hat{P}_\nu = \delta_{\mu\nu}$ such that $\mathrm{Tr}_{\rm syst}[\rho\hat{\pi}_\mu] = \mathrm{Tr}_{\rm syst}\mathrm{Tr}_{\rm anc}\{\hat{U}(\rho \otimes |\omega\rangle\langle\omega|)\hat{U}^\dagger(\mathbb{1} \otimes \hat{P}_\mu)\} \quad \forall \mu \in \mathcal{M}, \forall \rho \in \mathcal{S}(\mathcal{H}_{\rm syst})$. As expected the extension of a given POVM is not unique.

The other important consequence of Stinespring's theorem is that each quantum channel can be obtained as the unitary interaction with an ancillary system in a pure state, which is then discarded. Formally, the action of a CPT map $\mathcal{E}$ on any state ρ can be expressed as

$$\mathcal{E}[\rho] = \mathrm{Tr}_{\rm anc}\left[\hat{U}(\rho \otimes |\omega\rangle\langle\omega|)\hat{U}^\dagger\right], \tag{1.10}$$

for a certain ancillary Hilbert space $\mathcal{H}_{\rm anc}$, pure state $|\omega\rangle \in \mathcal{H}_{\rm anc}$ and unitary interaction $\hat{U} : \mathcal{H}_{\rm syst} \otimes \mathcal{H}_{\rm anc} \to \mathcal{H}_{\rm syst} \otimes \mathcal{H}_{\rm anc}$; again, this construction is not unique. This result is due to Kraus and it is equivalent to specifying the Kraus form of the channel (1.5); if we write the CPT map in Kraus form as $\mathcal{E}[\bullet] = \sum_\mu \hat{M}_\mu \bullet \hat{M}_\mu^\dagger$, the Kraus operators are written as

$$\hat{M}_\mu = \langle\mu|\,\hat{U}|\omega\rangle\ ; \tag{1.11}$$

this is a partial scalar product of $\hat{U}$ with vectors in $\mathcal{S}(\mathcal{H}_{\rm anc})$, so that the result is an operator on $\mathcal{H}_{\rm syst}$. This channel also corresponds to the unconditional channel given by the instrument with CP maps $\tilde{\mathcal{E}}[\bullet] = \hat{M}_\mu \bullet \hat{M}_\mu^\dagger$, which in turn generates the POVM (1.9).

1.2 Markovian conditional and unconditional quantum dynamics

In this section we introduce the relevant dynamical equations which are employed in the rest of this thesis. These equations are to the celebrated Gorini-Kossakowski-Sudarshan-Lindblad master equation (which we mostly call only Lindblad equation, for semantical convenience) and Markovian stochastical master equations, both diffusive and jump-like. We do not give rigorous proofs, but we try to sketch the main ideas behind the derivations of the equations, following the presentation in [100, 102, 256, 295]. Some other standard references on these subjects are [144, 146, 298], we also refer to the introductory section of [118] for a brief but self-contained presentation, which clearly highlights all the relevant assumptions in this approach. We stress that we only deal with Markovian dynamics.

Hamiltonian dynamics

Let us briefly recall how the unitary dynamics we described in the previous section is physically generated by the Hamiltonian of the system, which is a self-adjoint operator with a spectrum bounded from below [8]. The differential equation which dictates the dynamic of a pure state is the Schrödinger equation

$$\frac{\mathrm{d}\,|\psi(t)\rangle}{\mathrm{d}t} = -i\hbar\hat{H}(t)\,|\psi(t)\rangle\ ; \tag{1.12}$$

this is equivalent to an equation for an observable O in the Heisenberg picture:

$$\frac{\mathrm{d}\hat{O}(t)}{\mathrm{d}t} = i\hbar\left[\hat{H}(t), \hat{O}(t)\right]\ . \tag{1.13}$$

[8] We remark that in some cases we will work with *effective* Hamiltonians that are not bounded from below.

Eq. (1.12) in the Schrödinger picture can equivalently be rewritten as a Liouville-Von Neumann equation for the density operator

$$\frac{\mathrm{d}\rho(t)}{\mathrm{d}t} = -i\hbar\big[\hat{H}(t), \rho(t)\big] \,, \tag{1.14}$$

this equation has the same form as (1.13), but with the opposite sign. The unitary operator expressing the solution to equations (1.14) and (1.12) can formally be written as

$$\hat{U}(t, t_0) = \mathcal{T} \exp\left[\frac{-i}{\hbar} \int_{t_0}^{t} dt' \hat{H}(t')\right] \,, \tag{1.15}$$

the time-ordering operator $\mathcal{T}$ has the effect of putting non-commuting operators in the correct chronological order. Formally we have

$$\mathcal{T}\big(\hat{H}(t_1)\hat{H}(t_2)\big) = \begin{cases} \hat{H}(t_1)\hat{H}(t_2) & \text{if} \quad t_1 < t_2 \\ \hat{H}(t_2)\hat{H}(t_1) & \text{if} \quad t_1 > t_2 \end{cases} \tag{1.16}$$

and analogously for more than two operators; this definition is applied to exponential (1.15) by Taylor expansion. When the Hamiltonian is time independent, we do not need time ordering and the evolution is homogeneous in time (it is only described by the elapsed time t):

$$\hat{U}(t) = \exp\big[-it\hat{H}\big] \,; \tag{1.17}$$

note that from now on we always rescale units appropriately such that $\hbar = 1$. Unitary evolutions are due only to the Hamiltonian of the system, therefore they describe *closed* quantum systems. As we already pointed out, more general evolutions arise when the system interacts with an external ancillary system. In many cases instead of an "ancillary system" the interaction is with an external environment; the environment itself is treated as a quantum mechanical system. Usually the dimension of the Hilbert space of the environment is much larger than the dimension of the principal system. When the dynamics of a quantum system is also caused by the interaction with an environment we usually talk of *open* quantum systems.

The topic of this section is precisely open quantum systems dynamics, both when we do not have any access to the degrees of freedom of the environment (unconditional evolution) and when we can actually access and measure them (conditional evolution).

1.2.1 Lindblad master equation

This derivation is obtained using input-output theory, in a way that is going to make the transition to stochastic master equations (SME) transparent. The intuition behind this Markovian input-output theory is that the environment can be thought as an infinite collection of uncorrelated quantum systems, all in the same state and that the principal system interacts at each time with a different system from this collection. More formally: the global Hilbert space of the environment is partitioned in an (uncountable) infinity of

subspaces labelled by the time variable t and the global state is a factorized state with the same reduced state on every subspace.[9]

The input modes are a collection of bosonic modes[10] $\{\hat{b}_{\text{in}}(t)\}_t$, labelled by the time variable t, that satisfy the following commutation relations

$$\left[\hat{b}_{\text{in}}(t), \hat{b}_{\text{in}}(t')^\dagger\right] = \delta(t-t') \,, \tag{1.18}$$

these operators are also called "white noise" operators, as their commutation relations implies that they are delta-correlated in time, exactly like classical white noise. In a quantum optical setting the input operators $\hat{b}_{\text{in}}(t)$ represent travelling light fields, while the system (usually an optical cavity) is fixed and localized and interacts with the travelling light impinging on it. For this reason we often refer to the excitations of this bosonic field as photons.

In this section and in the next we always assume that the state of each mode is the vacuum $|0\rangle_t$, satisfying $\hat{b}_{\text{in}}(t)\,|0\rangle_t = 0$ and $\hat{b}_{\text{in}}(t)^\dagger\,|0\rangle_t = |1\rangle_t$ (a single photon state) at each t. This choice implies that the expectation value of the anti-commutator is again a Dirac delta

$$\left\langle \left\{\hat{b}_{\text{in}}(t), \hat{b}_{\text{in}}(t')^\dagger\right\} \right\rangle = \delta(t-t') \,. \tag{1.19}$$

This last condition and the one in (1.18) encode our Markovianity assumptions. The physical meaning is that the environment subsystems interacting at different times are completely uncorrelated and the interaction itself is instantaneous. This is clearly an idealisation which relies on a separation of timescales between the dynamics of the system and the environment. Roughly speaking we are assuming that the correlation time of the environment is much shorter than the timescales governing the evolution of the system[11].

The interaction Hamiltonian between the input modes and the system is the following

$$\hat{H}_{\text{int}}(t) = i\sqrt{\gamma}\Big(\hat{c}\otimes\hat{b}_{\text{in}}(t)^\dagger - \hat{c}^\dagger\otimes\hat{b}_{\text{in}}(t)\Big), \tag{1.20}$$

where $\hat{c}$ represent a generic (Hermitian or non-Hermitian) operator on the Hilbert space of the system and γ quantifies the strength of the coupling. Notice that in the context of quantum optical cavities the rotating wave approximation usually brings to a non-Hermitian operator $\hat{c}$, but there are methods to obtain the coupling with an Hermitian operator, see [71]. Nonetheless, in other physical setups Hermitian collapse operators appear more naturally.

We can see that the commutator (1.18) at equal times is not a well defined quantity, so we heuristically go around this problem by integrating the input operators as [256]

$$\delta\hat{b}_{\text{in}}(t) = \int_t^{t+\delta t} \hat{b}_{\text{in}}(t')dt' \tag{1.21}$$

[9] For the sake of the derivations we work with a continuous time variable t and infinitesimal time increments dt, a more rigorous approach is to discretize time first and then take the limit for $\Delta t \to 0$ at the end, see e.g. [55, 118].

[10] Bosonic continuous variable systems are introduced in more detail in Section 1.4, here we assume a basic knowledge on the subject.

[11] Alternatively, we could say that in this approximation dt is mathematically an infinitesimal quantity, but physically corresponds to the smallest timescale of the system and anything happening on shorter timescales can be disregarded.

which implies

$$\left[\delta\hat{b}_{\text{in}}(t), \delta\hat{b}^{\dagger}_{\text{in}}(t)\right] = \mathbb{1}\delta t \,. \tag{1.22}$$

For an infinitesimal δt we have that $\delta\hat{b}_{\text{in}}(t) = \hat{b}_{\text{in}}(t)dt$; this leads to the following identity

$$\left[\hat{b}_{\text{in}}(t), \hat{b}^{\dagger}_{\text{in}}(t)\right] dt^2 = \mathbb{1}dt \,. \tag{1.23}$$

We now define a new set of bosonic operators $\hat{b}'_{\text{in}}(t)$ satisfying the relation $\hat{b}_{\text{in}}(t)dt = \hat{b}'_{\text{in}}(t)\sqrt{dt}$ [12], these operators are proper creation and annihilation operator at each time, i.e.

$$\left[\hat{b'}_{\text{in}}(t), \hat{b'}^{\dagger}_{\text{in}}(t)\right] = \mathbb{1} \,. \tag{1.24}$$

We can thus write the unitary evolution corresponding to the Hamiltonian (1.20), which evolves the system from a time t to a time $t + dt$, as a function of the operators $\hat{b'}_{\text{in}}(t)$ as follows

$$\begin{aligned} \hat{U}(t, t+dt) = e^{-i\hat{H}_{\text{int}}(t)} &= \exp\left[\sqrt{\gamma}dt\left(\hat{c}\otimes\hat{b}^{\dagger}_{\text{in}}(t) - \hat{c}^{\dagger}\otimes\hat{b}_{\text{in}}(t)\right)\right] \\ &= \exp\left[\sqrt{\gamma\, dt}\left(\hat{c}\otimes\hat{b'}^{\dagger}_{\text{in}}(t) - \hat{c}^{\dagger}\otimes\hat{b'}_{\text{in}}(t)\right)\right] ; \end{aligned} \tag{1.25}$$

The key feature of the form (1.25) is that it is an exponential of the dimensionless variable $\sqrt{\gamma dt}$. Thus, to obtain terms up to first order in dt, we need to expand the exponential up to second order as follows

$$\begin{aligned} \hat{U}(t, t+dt) \approx &\mathbb{1}\otimes\mathbb{1} + \left(\hat{c}\otimes\hat{b'}^{\dagger}_{\text{in}}(t) - \hat{c}^{\dagger}\otimes\hat{b}'_{\text{in}}(t)\right)\sqrt{\gamma dt} + \\ &+ \frac{1}{2}\left(\hat{c}^{\dagger 2}\otimes\hat{b'}^{2}_{\text{in}}(t) + \hat{c}^{2}\otimes\hat{b'}^{\dagger 2}_{\text{in}}(t) - \hat{c}\hat{c}^{\dagger}\otimes\hat{b'}^{\dagger}_{\text{in}}\hat{b}'_{\text{in}}(t) - \hat{c}^{\dagger}\hat{c}\otimes\hat{b}'_{\text{in}}\hat{b'}^{\dagger}_{\text{in}}(t)\right)\gamma dt \,; \end{aligned} \tag{1.26}$$

we note here that sometimes we are going to include the parameter γ in the definition of the operator $\hat{c}$ by rescaling it as $\hat{c} \to \sqrt{\gamma}\hat{c}$.

Now we bring into the calculation the assumption that at each time the state is factorized as $\rho(t)\otimes|0\rangle_t\langle 0|$ and we compute the evolution of the density matrix of the system as

$$\rho(t+dt) = \text{Tr}_t\left[\hat{U}(t, t+dt)(\rho(t)\otimes|0\rangle_t\langle 0|)\hat{U}(t, t+dt)^{\dagger}\right] , \tag{1.27}$$

where with Tr_t we mean that we are tracing over the Hilbert space labelled by t, the one where the operator $\hat{b}_{\text{in}}(t)$ acts. By inserting the expansion (1.26) and explicitly computing the trace we get to

$$\rho(t+dt) = \rho(t) + \gamma\hat{c}\rho\hat{c}^{\dagger} - \frac{\gamma}{2}\left\{\hat{c}^{\dagger}\hat{c}, \rho\right\} , \tag{1.28}$$

which we can rewrite as a proper differential equation:

$$\frac{d\rho(t)}{dt} = \gamma\mathcal{D}[\hat{c}]\rho(t) \,, \tag{1.29}$$

[12] In more mathematical literature the operator $d\hat{b}_{\text{in}} \equiv \hat{b}'_{\text{in}}(t)\sqrt{dt}$ is called a quantum Wiener increment.

where we introduced the dissipation superoperator $\mathcal{D}$, defined as

$$\mathcal{D}[\hat{A}]\bullet = \hat{A}\bullet\hat{A}^\dagger - \frac{1}{2}\left\{\hat{A}^\dagger\hat{A},\bullet\right\}. \tag{1.30}$$

More in general, we can also insert an Hamiltonian acting on the system into the master equation (1.29), albeit we should make sure that the evolution due to the system Hamiltonian is slow enough not to break the derivation. The Markovianity assumption of considering the system "frozen" while interacting with each environmental mode could break down.

Furthermore, the case with a single $\hat{c}$ can be generalized to a collection $\{\hat{c}_j\}$, often called collapse operators. The general form of a Markovian Lindblad master equation is then

$$\frac{d\rho(t)}{dt} = \mathcal{L}\rho(t) = -i\left[\hat{H},\rho(t)\right] + \sum_i \gamma_i \mathcal{D}[\hat{c}_i]\rho(t)\,, \tag{1.31}$$

with $\gamma_i \geq 0 \quad \forall i$. To obtain this general form, we have to consider n independent input modes $\hat{b}_{\text{in}}^{(j)}(t)$, one for each noise operator c_j, that satisfy Bosonic commutation relations

$$\left[\hat{b}_{\text{in}}^{(j)}(t), \hat{b}_{\text{in}}^{(k)\dagger}(t')\right] = \delta_{jk}\delta(t-t')\,. \tag{1.32}$$

In Eq. (1.31) we also introduced the time independent Lindbladian superoperator $\mathcal{L}$. This is a *linear* operator on $\mathcal{S}(\mathcal{H})$ and from this point of view it is easy to see that the CPT map generated by Eq. (1.31) are obtained by exponentiation of $\mathcal{L}$ as

$$\mathcal{E}_t = e^{t\mathcal{L}}\,. \tag{1.33}$$

These solutions satisfy a semi-group property

$$\mathcal{E}_t \circ \mathcal{E}_s = \mathcal{E}_{s+t} \quad \forall t,s \in \mathbb{R}\,; \tag{1.34}$$

the fact that this is a semi-group and there is no inverse, at variance with the purely unitary case, makes clear that this kind of evolution is irreversible. More in general, if a collection of CPT maps $\mathcal{E}_t$ satisfies the semi-group property (1.34), the generator $\mathcal{L}$ must have the form given by the master equation (1.31); this is the original result of Lindblad [166] and Gorini et al. [114].

1.2.2 Stochastic master equation

Here we will show that a stochastic dynamical equation arises when we are able to measure the environmental degrees of freedom at each time t instead of tracing them out. In particular we consider only two kinds of measurements: the so called homodyne measurements, which corresponds to a Hermitian observable $\hat{x}_\theta = (e^{i\theta}\hat{b}'_{\text{in}} + e^{-i\theta}\hat{b}'^\dagger_{\text{in}})/\sqrt{2} = \cos\theta\hat{x}_{\text{in}} - \sin\theta\hat{p}_{\text{in}} = \int |x_\theta\rangle\langle x_\theta|\, dx_\theta$ and on-off photo-detection which corresponds to the binary POVM, with elements $\hat{\pi}_0 = |0\rangle\langle 0|$ and $\hat{\pi}_1 = \mathbb{1} - |0\rangle\langle 0|$. Note that, by dealing with states with at most one photon, the projection on the subspace orthogonal to $|0\rangle$ is restricted to a projection on single photon subspace $\hat{\pi}_1 = |1\rangle\langle 1|$.

We derive stochastic differential equations, but do not explain in details the theory of stochastic processes and we only introduce the bits of information needed in this context. We refer to [143] for a comprehensive, yet straight-forward, treatment.

Photo detection

We start again from the expansion of the interaction unitary up to order dt in (1.26) and we compute the Kraus operator as prescribed by (1.11)

$$\hat{K}_0(t) = {}_t\langle 0|\,\hat{U}(t,t+dt)\,|0\rangle_t = \mathbb{1} - \frac{\gamma dt}{2}\hat{c}^\dagger\hat{c} \tag{1.35}$$

$$\hat{K}_1(t) = {}_t\langle 1|\,\hat{U}(t,t+dt)\,|0\rangle_t = \sqrt{\gamma dt}\hat{c}\,; \tag{1.36}$$

we have the POVM elements (keeping terms up to order dt)

$$\hat{\pi}_0(t) = \hat{K}_0(t)^\dagger\hat{K}_0(t) = \mathbb{1} - \gamma dt\hat{c}^\dagger\hat{c} \tag{1.37}$$

$$\hat{\pi}_1(t) = \hat{K}_1(t)^\dagger\hat{K}_1(t) = \gamma dt\hat{c}^\dagger\hat{c}\,; \tag{1.38}$$

this is a well defined POVM, since $\hat{\pi}(t)_0 + \hat{\pi}(t)_1 = \mathbb{1}$.

The state at $t + dt$ can assume two different values:

$$\rho_0^{(c)}(t+dt) = \frac{\hat{K}_0(t)\rho^{(c)}(t)\hat{K}_0(t)^\dagger}{\mathrm{Tr}\left[\hat{K}_0(t)\rho^{(c)}(t)\hat{K}_0(t)^\dagger\right]} = \frac{\rho^{(c)}(t) - \frac{\gamma}{2}dt(\hat{c}^\dagger\hat{c}\rho^{(c)}(t) + \rho^{(c)}(t)\hat{c}^\dagger\hat{c})}{1 - \gamma dt\mathrm{Tr}\left[\hat{c}^\dagger\hat{c}\rho^{(c)}(t)\right]} \tag{1.39}$$

$$\rho_1^{(c)}(t+dt) = \frac{\hat{K}_1(t)\rho^{(c)}(t)\hat{K}_1(t)^\dagger}{\mathrm{Tr}\left[\hat{K}_1(t)\rho^{(c)}(t)\hat{K}_1(t)^\dagger\right]} = \frac{\hat{c}\rho^{(c)}(t)\hat{c}^\dagger}{\mathrm{Tr}\left[\hat{c}^\dagger\hat{c}\rho^{(c)}(t)\right]}, \tag{1.40}$$

where the superscript (c) signals a conditional state. This evolution is discontinuous in time and the evolution due to the Kraus operator $\hat{K}_1$ in (1.36), which corresponds to the detection of a photon, is often called a "quantum jump".

If we expand the denominator of (1.39) up to order dt we get to

$$\rho_0^{(c)}(t+dt) = \rho^{(c)}(t) - \frac{\gamma}{2}dt(\hat{c}^\dagger\hat{c}\rho^{(c)}(t) + \rho^{(c)}(t)\hat{c}^\dagger\hat{c}) + \gamma dt\mathrm{Tr}\left[\hat{c}^\dagger\hat{c}\rho^{(c)}(t)\right]\rho^{(c)}(t) + O(dt). \tag{1.41}$$

We now introduce a Poisson increment[13] dN_t with mean

$$\mathbb{E}(dN_t) = 0\cdot\mathrm{Tr}\left[\hat{\pi}_0(t)\rho^{(c)}(t)\right] + 1\cdot\mathrm{Tr}\left[\hat{\pi}_1(t)\rho^{(c)}(t)\right] = \gamma\mathrm{Tr}\left[\rho^{(c)}(t)\hat{c}^\dagger\hat{c}\right]dt; \tag{1.42}$$

being a two-outcome distribution, it is completely described by its mean value. Therefore one can combine the two possible outcomes into a single equation

$$\begin{aligned} d\rho^{(c)}(t) &= \rho^{(c)}(t+dt) - \rho^{(c)}(t) = \\ &= dN_t\left(\rho_1^{(c)}(t+dt) - \rho^{(c)}(t)\right) + (1-dN_t)\left(\rho_0^{(c)}(t+dt) - \rho^{(c)}(t)\right). \end{aligned} \tag{1.43}$$

This equation can be simplified by noting that the term $dtdN_t$ can be discarded, since it gives contributions of order greater than dt. This can be understood intuitively from (1.42) and it can be proven rigorously in the theory of stochastic processes [143].

[13] A Poisson increment dN_t with rate $\gamma(t)$ is a stochastic process with two outcomes: 0 and 1. The probability that dN_t assumes the value 1 in the time interval dt is $\lambda(t)dt$, and the probability that it takes the value 0 is $1-\lambda(t)dt$. Informally, the probability that dN_t is 1 in any infinitesimal time interval is vanishingly small and thus dN is zero most of the time. However, sometimes dN_t takes the value 1, and the value of $N(T) = \int_0^T dN_t$ "jumps" by 1; $N(t)$ is called a Poisson *process*. A fundamental property of Poisson increments is that $(dN_t)^2 = dN_t$.

If we also add an Hamiltonian term we get to the more general equation

$$\rho^{(c)} = -i\Big[\hat{H},\rho^{(c)}\Big] - \frac{\gamma}{2}\Big(\hat{c}^\dagger\hat{c}\rho^{(c)} + \rho^{(c)}\hat{c}^\dagger\hat{c}\Big)dt + \gamma \mathrm{Tr}\Big[\hat{c}^\dagger\hat{c}\rho^{(c)}\Big]\rho^{(c)}dt + \left(\frac{\hat{c}\rho^{(c)}\hat{c}^\dagger}{\mathrm{Tr}\big[\hat{c}\rho^{(c)}\hat{c}^\dagger\big]} - \rho^{(c)}\right)dN_t$$
$$= -i\Big[\hat{H},\rho^{(c)}\Big] - \frac{\gamma}{2}\mathcal{H}[\hat{c}^\dagger\hat{c}]\rho^{(c)}dt + \left(\frac{\hat{c}\rho^{(c)}\hat{c}^\dagger}{\mathrm{Tr}\big[\hat{c}\rho^{(c)}\hat{c}^\dagger\big]} - \rho^{(c)}\right)dN_t\,, \tag{1.44}$$

where in the last line we introduced the superoperator $\mathcal{H}$ defined as

$$\mathcal{H}[\hat{A}]\bullet = \hat{A}\,\bullet + \bullet\,\hat{A}^\dagger - \mathrm{Tr}\Big[\bullet(\hat{A}+\hat{A}^\dagger)\Big]\,\bullet\ . \tag{1.45}$$

The unconditional state is obtained by taking averaging over the Poisson process: $\rho(t) = \mathbb{E}\Big[\rho^{(c)}(t)\Big]$. In order to see it explicitly it is useful to introduce the following stochastic calculus rule [298]

$$\mathbb{E}\Big[dN_t f(\rho^{(c)})\Big] = \gamma dt \mathbb{E}\Big[\mathrm{Tr}\Big[c^\dagger c\rho^{(c)}\Big]f(\rho^{(c)})\Big]\,, \tag{1.46}$$

for any function of the density matrix; this is consistent with (1.42) when $f = 1$. By making use of (1.46) one can average over the Poisson increment and get from the stochastic master equation (1.44) for the conditional state to the Lindblad master equation (1.29) for the unconditional state.

If instead of considering a generic initial state ρ_0, the system starts in a pure state $|\psi_0\rangle$, the stochastic evolution maintains the state pure at all times and can be rewritten as an equation for a conditional state vector $|\psi_c(t)\rangle$:

$$d\,|\psi^{(c)}(t)\rangle = \left[-iHdt + \frac{\gamma}{2}\Big(\big\langle\hat{c}^\dagger\hat{c}\big\rangle - \hat{c}^\dagger\hat{c}\Big)dt + \left(\frac{\hat{c}}{\sqrt{\langle\hat{c}^\dagger\hat{c}\rangle}} - 1\right)dN_t\right]|\psi^{(c)}(t)\rangle\ , \tag{1.47}$$

this equation is called a stochastic Schrödinger equation (SSE); for compactness we introduced the expectation value on the conditional state: $\langle\psi^{(c)}(t)|\,\bullet\,|\psi^{(c)}(t)\rangle = \langle\bullet\rangle$. Historically, solutions to stochastic Schrödinger equations are called *quantum trajectories*; however we also use the term more freely also for solutions of stochastic master equations.

By writing the infinitesimal increment for the projector representing the pure state

$$d\rho^{(c)} = (d\,|\psi^{(c)}\rangle)\,\langle\psi^{(c)}| + |\psi^{(c)}\rangle\,(d\,\langle\psi^{(c)}|) + (d\,|\psi^{(c)}\rangle)(d\,\langle\psi^{(c)}|)\,, \tag{1.48}$$

one can check the consistence between (1.47) and (1.44), taking into account the property of Poisson increments $(dN_t)^2 = dN_t$. Note that it is necessary to retain also the second order term in Eq. (1.48).

The stochastic variable $N_T = \int_0^T dN_t$ represents how many jumps have occurred up to time T, i.e. how many photons have been detected. However, the 'measurement record' corresponding to an experiment contains more information than just N_T, the complete information is a list of times $0 \le t_1, \le \cdots \le t_{N_T} \le T$ corresponding to each photo-detection.

Every master equation in Lindblad form can be rewritten in terms of stochastic Schrödinger equations and the solution of the master equation is obtained by averaging

over the stochastic process. This procedure is called "unravelling" the master equation and Eq. (1.47) is a specific unravelling based on a discontinuous jump-like evolution. As we have seen, a stochastic Schrödinger equation has a physical meaning, however it is also useful as a tool to numerically solve Lindblad master equations [63]. The advantage is that only state vectors are needed instead of density matrices, the price to pay is that one has to accumulate enough statistics to reduce fluctuations by generating many trajectories.

Homodyne detection

For homodyne detection we use a slightly different approach to derive a stochastic master equation. Starting from the expansion of the interaction unitary up to order dt (1.26), instead of computing the Kraus operators, we can directly compute the unnormalized conditional state

$$\begin{aligned}\tilde{\rho}^{(c)}(t+dt) &= \mathrm{Tr}_t\Big[\hat{U}(t,t+dt)(\rho(t)\otimes|0\rangle_t\langle 0|)\hat{U}(t,t+dt)^\dagger(\mathbb{1}\otimes|x_\theta\rangle\langle x_\theta|)\Big] = \\ &= {}_t\langle x_\theta|\,\hat{U}(t,t+dt)(\rho(t)\otimes|0\rangle_t\langle 0|)\hat{U}(t,t+dt)^\dagger\,|x_\theta\rangle_t\end{aligned} \tag{1.49}$$

and the corresponding probability

$$p_{t+dt}(x_\theta) = \mathrm{Tr}[\tilde{\rho}(t+dt)]\ ; \tag{1.50}$$

the normalized state is then

$$\rho^{(c)}(t+dt) = \frac{\tilde{\rho}^{(c)}(t+dt)}{p_{t+dt}(x_\theta)}\ . \tag{1.51}$$

Differently from the previous case, we only need an expansion of the numerator and the denominator in (1.51) up to order $\sqrt{\gamma dt}$, since all the relevant terms of order γdt come out as a result. Due to vacuum fluctuations the probability distribution for x_θ at time t, before the interaction, is a Gaussian with variance $\frac{1}{2}$ and mean value 0, i.e. $p_t(x_\theta) = |{}_t\langle x_\theta|0\rangle_t|^2 = \frac{1}{\sqrt{\pi}}e^{-x_\theta^2}$.

The expansion of the conditional state yields

$$\begin{aligned}\tilde{\rho}^{(c)}(t+dt) =& |{}_t\langle x_\theta|0\rangle_t|^2\rho^{(c)}(t)+ \\ &+\Big(\hat{c}\rho^{(c)}(t)_t\langle x_\theta|1\rangle_t\langle 0|x_\theta\rangle_t + \rho^{(c)}(t)\hat{c}^\dagger{}_t\langle x_\theta|0\rangle_t\langle 1|x_\theta\rangle_t\Big)\sqrt{\gamma dt} + O(\sqrt{\gamma dt}) = \\ =& p_t(x_\theta)\Big[\rho^{(c)}(t) + \Big(\hat{c}\rho^{(c)}(t)e^{i\theta} + \rho^{(c)}(t)\hat{c}^\dagger e^{-i\theta}\Big)x_\theta\sqrt{2\gamma dt}\Big] + O(\sqrt{\gamma dt})\end{aligned} \tag{1.52}$$

where to get the second expression we used the identity ${}_t\langle x_\theta|1\rangle_t = \sqrt{2}x_\theta e^{i\theta}{}_t\langle x_\theta|0\rangle_t$. The expansion of the probability distribution yields

$$\begin{aligned}p_{t+dt}(x_\theta) = \mathrm{Tr}\Big[\tilde{\rho}^{(c)}(t+dt)\Big] &= p_t(x_\theta)\Big(1+\sqrt{2\gamma dt}x_\theta\langle\hat{c}e^{i\theta}+\hat{c}^\dagger e^{-i\theta}\rangle_t\Big) + O(\sqrt{\gamma dt}) \\ &\approx \frac{1}{\sqrt{\pi}}\exp\left[-\left(x_\theta - \sqrt{\frac{\gamma dt}{2}}\left\langle\hat{c}e^{i\theta}+\hat{c}^\dagger e^{-i\theta}\right\rangle_t\right)^2\right],\end{aligned} \tag{1.53}$$

up to order $\sqrt{dt}$ it is equivalent to a Gaussian distribution with variance $\frac{1}{2}$ and mean value $\sqrt{\frac{\gamma dt}{2}}\langle \hat{c}e^{i\theta} + \hat{c}^\dagger e^{-i\theta}\rangle_t$. We can introduce a new stochastic increment dy_t and a stochastic process I_t such that

$$dy_t = I_t dt = \sqrt{2dt}x_\theta = \sqrt{\gamma}\langle \hat{c}e^{i\theta} + \hat{c}^\dagger e^{-i\theta}\rangle_t dt + dw_t \,, \tag{1.54}$$

where here dw_t a Gaussian random variable with variance dt and zero mean $\mathbb{E}[dw_t] = 0$. The stochastic variable $y_T = \int_0^T dy_t$ represents the so-called integrated photo-current. The continuous stream of outcomes is usually understood in terms of the so-called photocurrent $I_t = \frac{dy_t}{dt}$. The photocurrent I_t is equal to the expectation value of the operator $\hat{c}e^{i\theta} + \hat{c}^\dagger e^{-i\theta}$ at time t, plus a white noise term:

$$I(t) = \sqrt{\gamma}\langle \hat{c}e^{i\theta} + \hat{c}^\dagger e^{-i\theta}\rangle_t + \xi_t \tag{1.55}$$

where $\xi_t = \frac{dw_t}{dt}$ represents white noise.

In the theory of stochastic processes dw_t is called a Wiener increment. The defining and remarkable property of a Wiener increment is that its square (in principle a random variable) is actually *not* random, but satisfies $dw_t^2 = dt$. This identity is formally known as Itô's lemma and it is the basis of Itô stochastic calculus. The assumption leading to a Itô stochastic differential equation is that integral (1.21), needed to define the "physical" operators $\hat{b}'_{\text{in}}(t)$, does not involve modes at times preceding t.

By inserting expressions (1.52) and (1.53) into (1.51) and expanding the denominator we can finally get to

$$d\rho^{(c)}(t) = -i\Big[\hat{H}, \rho^{(c)}(t)\Big]dt + \gamma\mathcal{D}[\hat{c}]\rho^{(c)}(t)dt + \sqrt{\gamma}\mathcal{H}[\hat{c}]\rho^{(c)}(t)dw_t = \tag{1.56}$$

$$= -i\Big[\hat{H}, \rho^{(c)}(t)\Big]dt + \gamma\mathcal{D}[\hat{c}]\rho^{(c)}(t)dt + \sqrt{\gamma}\mathcal{H}[\hat{c}]\rho^{(c)}(t)\Big(dy_t - \sqrt{\gamma}\langle \hat{c} + \hat{c}^\dagger\rangle_t dt\Big) \tag{1.57}$$

where we also added the usual Hamiltonian term and in the second line we wrote the equation in term of the observed photocurrent. In the following we suppress the explicit dependence on θ which comes from measuring a different quadrature, since it is simply equivalent to the substitution $\hat{c} \mapsto \hat{c}e^{i\theta}$; also note that the dissipative part does not depend on θ: $\mathcal{D}[\hat{c}] = \mathcal{D}\big[\hat{c}e^{i\theta}\big]$. This stochastic master equation is called a diffusive unravelling, since the stochastic part is represented by a diffusive stochastic process[14].

Similarly to the discontinuous jump-like case we can alternatively write a stochastic Schrödinger equation if the initial state is pure:

$$\begin{aligned} d\,|\psi^{(c)}(t)\rangle = \Bigg\{ \Bigg[-i\hat{H} + \frac{\gamma}{2}\left(\hat{c}^\dagger\hat{c} - \Big\langle \hat{c} + \hat{c}^\dagger \Big\rangle \hat{c} + \frac{\big\langle \hat{c} + \hat{c}^\dagger \big\rangle^2}{4} \right) \Bigg] dt \\ + \sqrt{\gamma}\left(\hat{c} - \frac{\langle \hat{c} + \hat{c}^\dagger \rangle}{2} \right) dw_t \Bigg\} |\psi^{(c)}(t)\rangle \;; \end{aligned} \tag{1.58}$$

[14] *Diffusive* means that something initially localized spreads out in time. This can be seen by considering the Wiener process $W(t) \equiv \int dw_t$, which is a Gaussian random variable with variance t (linearly increasing in time).

to check the equivalence with the previous equation for the density matrix we need to use again Eq. (1.48) and to apply Itô's rule. Due to the fact that dw_t has zero mean $\mathbb{E}[dw_t] = 0$, it is straight forward to check that the average of (1.56) gives back the Lindblad equation (1.29), which corresponds to the particular case $\hat{H} = 0$.

Inefficient detection

The previous equations were derived assuming that the measurement on the output modes was a perfect projective measurement (actually a sharp observable, since we are only interested in the statistics). However this assumption is not fulfilled in many practical and interesting scenarios. The simplest way to model inefficient detection is to assume that the measurement happens with probability $\eta \in [0,1]$ and fails with probability $1-\eta$. This is equivalent to placing a beam-splitter with trasmissivity η before the measurement device, which accounts for the lost photons. Another equivalent way to model this inefficiency is to rewrite the master equation for the unconditional dynamics as

$$\frac{d\rho(t)}{dt} = \eta\gamma\mathcal{D}[\hat{c}]\rho(t) + (1-\eta)\mathcal{D}[\hat{c}]\rho(t) \tag{1.59}$$

and then unravel only the term proportional to η [298].

The steps presented in the previous sections can be reproduced and we get to a stochastic master equation for photo-detection

$$d\rho^{(c)} = -i\Big[\hat{H},\rho^{(c)}\Big]dt - \eta\frac{\gamma}{2}\mathcal{H}[\hat{c}^\dagger\hat{c}]\rho^{(c)}dt + \left(\frac{\hat{c}\rho^{(c)}\hat{c}^\dagger}{\mathrm{Tr}\big[\hat{c}\rho^{(c)}\hat{c}^\dagger\big]} - \rho^{(c)}\right)dN_t + (1-\eta)\gamma\mathcal{D}[\hat{c}]\rho^{(c)}dt\,, \tag{1.60}$$

where now the Poisson increment has expectation value $\mathbb{E}[dN_t] = \eta\gamma\mathrm{Tr}\Big[\rho^{(c)}\Big]dt$. Analogously, we have a diffusive stochastic master equation for homodyne detection with finite efficiency

$$d\rho^{(c)}(t) = -i\Big[\hat{H},\rho^{(c)}(t)\Big]dt + \gamma\mathcal{D}[\hat{c}]\rho^{(c)}(t)dt + \sqrt{\gamma\eta}\,\mathcal{H}[\hat{c}e^{i\theta}]\rho^{(c)}(t)dw_t\,. \tag{1.61}$$

As expected, both equations give back the unconditional Lindblad master equation for $\eta \to 0$.

In Sec. 2.3 we will generalize these stochastic master equations to the case of more than one collapse operator. This is done by considering not only one input field, i.e. one "environment", but a collection of input field, one for each collapse operator: the stochastic master equation has as many independent stochastic increments as collapse operators. In this way it is possible to unravel a generic master equation in Lindblad form.[15]

[15] Master equations with more than one collapse operator can also arise by considering mixed states (usually thermal states) of the environment instead of the vacuum. In such cases the corresponding SME contains *less* independent stochastic increments than collapse operators.

1.3 Quantum estimation theory

In Section 1.1.1 we described the measurement process in quantum mechanics. We have shown that even when every aspect of an experiment is under control and the resulting state is prepared deterministically the outcomes of a measurement on the quantum system are in general random variables. From this intuitive understanding, we immediately sense that statistical analysis of measurement data is fundamental in quantum physics. Some quantum mechanical observables corresponding to self-adjoint operators, such as energy and angular momentum, have a very clear physical interpretation. However, many other quantities of interest in physics do not naturally correspond to Hermitian operators, two notable examples being optical phases and temperatures. To assign a value to such quantities, one has to measure proper quantum mechanical observables and then *infer* their value.

Even classically, the general problem of characterizing a probability distribution from empirical data is exceedingly hard. However, very often one is able to restrict the problem to a class of probability distributions parametrized by a certain finite number of real parameters. Estimation theory is the branch of statistics that deals with estimating the true values of such parameters from empirical data. The parametrized probability distribution is also called a statistical model. In Subsection 1.3.1 we introduce the most relevant concepts in estimation theory and review some important results.

In the quantum case, the parameters to be estimated appear in a quantum state rather than in a classical probability distribution. This is the starting point of quantum estimation theory, which is presented in 1.3.2. There is a deep connection between classical and quantum estimation theory, as one would expected from the Born rule.

Within the the scope of this thesis, we are interested in single parameter estimation only, i.e. statistical models, classical or quantum, parametrized by a single real variable. Actually, many results in estimation theory can be generalized to the multidimensional case without too many conceptual difficulties. The same is not true for the quantum case, where multi-parameter estimation introduces a new set of challenges.

1.3.1 Classical parameter estimation

A standard reference on classical estimation theory is [165], where proofs for most of these statements can be found; we only present a brief overview. We approach parameter estimation in the framework of frequentist statistics, rather than Bayesian, therefore it is always assumed that the parameter to be estimated has a *true* value and correspondingly the statistics of the observed data obeys the true probability distribution.

The statistical model is denoted as $p(x|\lambda)$ and it simply represents a collection of probability distributions for the random variable x[16] , labelled by a real parameter λ. The true value of the parameter is λ_0 and the corresponding probability is $p(x|\lambda_0)$. The starting point of the statistical analysis is a set of M independent empirical observations $\Omega = \{x_1, \ldots, x_M\}$; in practical terms the M data points are usually obtained from M rep-

[16]Here we leave x generic, it can correspond either to a discrete variable or to a vector of continuous variables. With a modern measure theoretical approach to probability both cases can be treated equivalently.

etitions of an experiment with identical initial preparations. We now define an *estimator*[17], which is, roughly speaking, a function from the set of measurement outcomes to the space of parameters

$$\hat{\lambda}(\Omega) = \lambda(x_1, \ldots, x_M) \; ; \tag{1.62}$$

being a function of random variables, the estimator itself is a random variable.

We can then introduce several figures of merit to quantify the error in the estimation, the most common choice is the mean square error, defined as:

$$\mathrm{MSE}(\hat{\lambda}) = \mathbb{E}\Big[\big(\hat{\lambda} - \lambda_0\big)^2\Big] = \int \big(\hat{\lambda}(\Omega) - \lambda_0\big)^2 p(\Omega) d\Omega \; , \tag{1.63}$$

where the probability distribution of the outcomes is $p(\Omega)d\Omega = \prod_{n=1}^{M} p(x_i|\lambda_0)dx_i$, since the variables are independent and identically distributed (i.i.d.). The variance of the estimator is defined as

$$\mathrm{Var}(\hat{\lambda}) = \mathbb{E}\Big[\big(\hat{\lambda} - \mathbb{E}\big[\hat{\lambda}\big]\big)^2\Big] \; ; \tag{1.64}$$

it does not quantify the error in the estimation, but only the spread around the expected value. An estimator is *unbiased* if the expected value is equal to the true value: $\mathbb{E}\big[\hat{\lambda}\big] = \lambda_0$. For unbiased estimators the variance and the mean square error clearly coincide. A lower variance corresponds to less uncertainty in the estimation of the true value λ_0 from the observed data.

One of the fundamental results in estimation theory is that it is possible to give a lower bound to the variance of *any* unbiased estimator for the parameter λ_0 in terms of local properties of the statistical model $p(x|\lambda)$ around λ_0. This result is the celebrated Cramér-Rao bound

$$\mathrm{Var}\big[\hat{\lambda}\big] \geq \frac{1}{M\mathcal{F}[p(x|\lambda_0)]} \; , \tag{1.65}$$

given in terms of the Fisher information (FI)

$$\mathcal{F}[p(x|\lambda)] = \int dx p(x|\lambda)[\partial_\lambda \log p(x|\lambda)]^2 = \int dx \frac{[\partial_\lambda p(x|\lambda)]^2}{p(x|\lambda)} \; ; \tag{1.66}$$

the FI can be interpreted as a measure of statistical distinguishability between neighbouring probability distributions. Under a reparametrization of the statistical model $\theta(\lambda)$, the FI changes as

$$\mathcal{F}[p(x|\theta)] = \left(\frac{d\theta(\lambda)}{d\lambda}\right)^2 \mathcal{F}[p(x|\lambda(\theta))] \; . \tag{1.67}$$

Only *relative* increments of $p(x|\lambda)$ are relevant for the FI and thus proper normalisation is not important: any function $\kappa(x) \cdot p(x|\lambda)$, with $\partial_\lambda \kappa(x) = 0$ can be used to compute the Fisher information.

The Cramér-Rao bound (1.65) can be proven under some regularity conditions on the function $p(x|\lambda)$, see [165]. In particular, the sample space of the probability distribution $p(x|\lambda)$ must not depend on λ.

[17] Confusingly enough, in statistical literature estimators are usually denoted with a hat, which clashes with the notation we used for operators on Hilbert space. We hope that the difference between the two should be clear from the context.

When the variance of an estimator is equal to the r.h.s of the Cramér-Rao inequality (1.65), the estimator is said to be efficient. The existence of an efficient estimator is guaranteed only for some statistical models and for particular choices of parametrization. However, much more is known for the asymptotic limit of a very large number of observations $M \to \infty$. An estimator is said to be asymptotically unbiased if it becomes unbiased in the asymptotic limit. Two asymptotically unbiased and asymptotically efficient estimators for every (well behaved) statistical model are the maximum likelihood estimator and the Bayesian estimator, that is presented at the end of this section and employed in Chapter 3.

Finally, we want to point out the deep connection between statistics and geometry, which goes under the name of information geometry. The basic idea is that the statistical model $p(x|\lambda)$ has the structure of a manifold with coordinates λ, to each point on the manifold corresponds a probability distribution. In this geometrical picture the Fisher information plays an important role: it defines a Riemannian metric on the manifold. The reparametrization of the statistical model thus corresponds to a change of coordinates on the manifold and the behaviour of the FI (1.67) obeys the transformation rules for the components of a tensor. We only considered the singe-parameter case, where the metric tensor is simply a scalar.

Bayesian estimator

Here we introduce an estimator commonly used in practical scenarios, the Bayesian estimator. In the Bayesian approach, one starts with some prior information about the value of the parameter, which is treated like a random variable with some initial probability distribution. This initial probability is then conditioned by the observed data and the updated probability is used to get an estimate of the true value.

Bayes's rule is a recipe to compute the conditioned probability distribution of some random variable x, given some observed value of some other random variable y:

$$p(x|y) = \frac{p(y|x)p(x)}{p(y)} \,. \tag{1.68}$$

This is due to the relationship between the joint probability and the conditional probabilities $p(x,y) = p(x|y)p(y) = p(y|x)p(x)$ (the joint probability is symmetrical in its arguments).

In the case of parameter estimation the ruled is applied as follows. We consider a dataset $\Omega = \{x_i\}_i^M$ with M empirical observations of a certain random variable X. The probability of obtaining the outcomes in Ω given that the value of the parameter is λ is $p(\Omega|\lambda)$.[18] From Bayes rule we get that

$$p(\lambda|\Omega) = \frac{p(\Omega|\lambda)p(\lambda)}{\int_\Lambda p(\Omega|\lambda)p(\lambda)d\lambda} \tag{1.69}$$

where the integral is carried out over the whole parameter space Λ. The probability distribution $p(\lambda)$ is called the *prior* distribution and it has to be chosen to reflect previous

[18] This object is also called the likelihood function of the statistical model given the observed data.

information about the true value of the parameter λ_0. $p(\lambda|\Omega)$ is the posterior distribution and it represents the information we have *a posteriori*, after observing the data Ω.

The most common Bayesian estimator is the expected value of the posterior distribution:

$$\hat{\lambda}_B(\Omega) = \int_\Lambda \lambda p(\lambda|\Omega) d\lambda \,, \tag{1.70}$$

this is also called the minimum mean square error estimator and it can be shown that it minimizes the average mean square error

$$\mathrm{MSE}\left[\hat{\lambda}\right] = \iint \left(\hat{\lambda} - \lambda\right)^2 p(x,\lambda) d\Omega d\lambda \,, \tag{1.71}$$

where the expected value is taken w.r.t. to the joint distribution of the data and the parameter. Since $p(x,\lambda) = p(\Omega|\lambda)p(\lambda)$, this is equivalent to averaging the mean square error (1.63) over the prior distribution on the parameter.

For the estimator given by (1.70) the average mean square error is equal to the variance of the posterior distribution, i.e.

$$\mathrm{Var}\left[\hat{\lambda}_B\right] = \int_\Lambda \lambda^2 p(\lambda|\Omega) d\lambda - \left[\hat{\lambda}_B(\Omega)\right]^2 \,; \tag{1.72}$$

this quantity is taken as the figure of merit to asses the precision of the estimator $\hat{\lambda}_B$. It can be shown that, under some regularity assumptions, in the limit $M \to \infty$ the prior becomes unimportant and the estimator becomes asymptotically unbiased and efficient (Bernstein–von Mises theorem). In this limit the variance (1.64) and the Bayesian variance (1.72) both tend to $(M\mathcal{F}[p(x|\lambda_0)])$. Moreover, in the asymptotic limit only *local* properties of the statistical model $p(x|\lambda)$ in a neighbourhood of the true value λ_0 are important.

Please note that in this analysis the prior distribution is used only for the estimation, but it does not enter in the Cramér-Rao bound. If one wants to seriously consider the prior as part of the statistical model a more general bound is needed, known as Bayesian Cramér-Rao bound or Van Trees inequality [112, 283]. The two approaches become equivalent only in the asymptotic limit [147, 165].

1.3.2 Quantum Cramér-Rao bound

Quantum estimation theory (QET) was pioneered by Helstrom [128] and Holevo [130], but the field became more relevant for metrological applications when Braunstein and Caves explicitly showed the connection with classical estimation theory [37]. This presentation is mainly based on a more recent review [221], but see also [68].

A quantum statistical model is represented by a manifold of density operators $\rho_\lambda \in \mathcal{S}(\mathcal{H})$. The goal of QET is to find the best POVM to precisely estimate the true value λ_0 of a parameter. We can distinguish two approaches to QET; *global* QET aims at minimising a suitable cost functional, averaged over all possible values of the parameter to be estimated. The result is thus a POVM independent of the true value of the parameter to be estimated. On the contrary, in local QET one looks for the POVM maximizing the resulting classical Fisher information, thus minimizing the variance of the estimator, at a fixed value of the parameter.

Intuitively, we expect that local QET should provide better performances, since the optimization is tailored to a specific value of the parameter. We are going to see that this approach yields an optimal POVM that depends on the true value λ_0. This conundrum is resolved in the asymptotic limit by implementing adaptive measurement strategies [26, 90] which asymptotically yield the same precision of the true optimal POVM.

Given a quantum state $\rho_\lambda \in \mathcal{S}(\mathcal{H})$ and a POVM $\{\hat{\pi}_x\}_{x\in\mathcal{X}}$, from the Born rule we have the (conditional) probability $p(x|\lambda) = \mathrm{Tr}[\hat{\pi}_x\rho_\lambda]$. The classical FI (1.66) is thus

$$\mathcal{F}[p(x|\lambda)] = \int dx \frac{(\partial_\lambda \mathrm{Tr}[\hat{\pi}_x\rho_\lambda])^2}{\mathrm{Tr}[\hat{\pi}_x\rho_\lambda]} \,. \tag{1.73}$$

Let us introduce the symmetric logarithmic derivative (SLD), an operator implicitly defined as

$$\partial_\lambda \rho_\lambda = \frac{L_\lambda\rho_\lambda + \rho_\lambda L_\lambda}{2} \tag{1.74}$$

more precisely, this equation defines the operator L_λ only on the support of the operator ρ_λ (the subspace spanned by its non-zero eigenvectors). The part of the operator L_λ acting on the null space of ρ is left undetermined; there is a unique solution if and only if the state ρ is full-rank. Using the SLD we can express the derivative in (1.73) as

$$\partial_\lambda \mathrm{Tr}[\hat{\pi}_x\rho_\lambda] = \mathrm{Tr}[\hat{\pi}_x\partial_\lambda\rho_\lambda] = \mathrm{Re}(\mathrm{Tr}[L_\lambda\rho_\lambda\hat{\pi}_x]) \tag{1.75}$$

and rewrite the FI as

$$\mathcal{F}[p(x|\lambda)] = \int dx \frac{\{\mathrm{Re}(\partial_\lambda \mathrm{Tr}[L_\lambda\rho_\lambda\hat{\pi}_x])\}^2}{\mathrm{Tr}[\hat{\pi}_x\rho_\lambda]} \,. \tag{1.76}$$

This FI quantifies the precision that can be obtained by implementing a suitable estimator on the outcomes of the POVM $\{\hat{\pi}_x\}$.

This last expression for the FI can be analytically maximized [37] over all possible POVMs [19] and the result is the celebrated *quantum* Fisher information (QFI), which thus provides an upper bound the classical FI for every POVM:

$$\mathcal{Q}[\rho_\lambda] \equiv \max_{\{\hat{\pi}_x\}}\{\mathcal{F}[p(x|\lambda)]\} = \mathrm{Tr}\left[\rho_\lambda L_\lambda^2\right] \geq \mathcal{F}[p(x|\lambda)] \,. \tag{1.77}$$

This inequality implies that there is a bound imposed by quantum mechanics to the precision in the estimation of a parameter λ with true value λ_0, this is the quantum Cramér-Rao bound:

$$\mathrm{Var}[\hat{\lambda}] \geq \frac{1}{M\mathcal{Q}[\rho_{\lambda_0}]} . \tag{1.78}$$

The single-parameter quantum Cramér-Rao bound is tight: one can show that a projection on the eigenstates of L_λ saturates the inequality (1.77) [221]. This bound depends solely on the quantum statistical model ρ_λ, analogously to the classical Cramér-Rao bound that depends only on the classical statistical model.

[19] We remark that there are some pathological cases where this optimization fails due to the fact that the POVMs depend non-trivially on the parameter to be estimated. In some instances this fact can actually be exploited to achieve better precision [259, 260].

To obtain an explicit expression for the QFI we note that Eq (1.74) is a Lyapunov equation for the operator L, which can be formally solved as[20]

$$L_\lambda = 2\int_0^\infty e^{-t\rho_\lambda}(\partial_\lambda\rho_\lambda)e^{-t\rho_\lambda}dt\ . \tag{1.79}$$

A more explicit solution can be obtained in terms of the spectral decomposition of the density matrix $\rho_\lambda = \sum_n p_n|\psi_n\rangle\langle\psi_n|$:

$$L_\lambda = \sum_{n,m}\frac{\langle\psi_m|\,\partial_\lambda\rho_\lambda\,|\psi_n\rangle}{p_m+p_n}|\psi_m\rangle\langle\psi_n|\ , \tag{1.80}$$

this sum is over all terms for which $p_n + p_m \neq 0$. By applying the definition (1.77) we get to an explicit expression for the QFI

$$\mathcal{Q}[\rho_\lambda] = \sum_{n,m}\frac{|\langle\psi_m|\,\partial_\lambda\rho_\lambda\,|\psi_n\rangle|^2}{p_m+p_n}\ . \tag{1.81}$$

We point out a subtlety here: even though the SLD is defined only on the support of ρ_λ, it is very important to consider also orthonormal vectors belonging to the null-space of ρ_λ. As a matter of fact in Eqs. (1.80) and (2.3.2) the condition is not $p_n \neq 0$ and $p_m \neq 0$, but $p_n + p_m \neq 0$, therefore terms for which $p_m = 0$ but $p_n \neq 0$ have to be included in the sum. It is possible to derive expressions for the QFI where summations run only on non-zero eigenvalues [167], thereby explicitly showing that only the support of ρ_λ is relevant.

We now state some general properties of the QFI. The first is monotonicity under CPT maps:

$$\mathcal{Q}[\rho_\lambda] \geq \mathcal{Q}[\mathcal{E}[\rho_\lambda]]\ , \tag{1.82}$$

for every CPT map $\mathcal{E}$ which does not depend on λ [231], this holds also for CPT maps between operators on Hilbert spaces of different dimensions. The second is invariance under (parameter-independent) unitary transformations $\mathcal{Q}[\rho_\lambda] = \mathcal{Q}\big[U\rho_\lambda U^\dagger\big]$. The third property is the so-called extended convexity [15, 206]. For every mixture of quantum states $\rho_\lambda = \sum_x p(x|\lambda)\rho_{x|\lambda}$ the QFI is upper bounded as follows

$$\mathcal{Q}[\rho_\lambda] \leq \mathcal{F}[p(x|\lambda)] + \sum_x p(x|\lambda)\mathcal{Q}\Big[\rho_{x|\lambda}\Big]\ , \tag{1.83}$$

the quantity on the r.h.s. is the Fisher information of the classical probability distribution plus the average QFI of the states in the mixture; this quantity is going to be important in the following chapters. When the mixing probability is independent from the parameter, i.e. $\partial_\lambda p(x|\lambda) = 0$ and $\mathcal{F}[p(x|\lambda)] = 0$, this property reduces to the ordinary convexity of the functional $\mathcal{Q}$.

For pure states one can easily derive a simple expression for the QFI [221]

$$\mathcal{Q}[|\psi_\lambda\rangle] = 4\Big[\langle\partial_\lambda\psi_\lambda|\partial_\lambda\psi_\lambda\rangle + (\langle\partial_\lambda\psi_\lambda|\psi_\lambda\rangle)^2\Big] \tag{1.84}$$

$$= 4\Big[\langle\partial_\lambda\psi_\lambda|\partial_\lambda\psi_\lambda\rangle - (\mathrm{Im}\langle\partial_\lambda\psi_\lambda|\psi_\lambda\rangle)^2\Big]\ , \tag{1.85}$$

[20] When the state is not full-rank this expression must be handled with care, see [240] for an explicit account.

where the last equality is due to the fact that the overlap between a normalized complex vector and its derivative has to be a purely imaginary number: $\mathrm{Re}\langle\partial_\lambda\psi_\lambda|\psi_\lambda\rangle = \langle\partial_\lambda\psi_\lambda|\psi_\lambda\rangle + \langle\psi_\lambda|\partial_\lambda\psi_\lambda\rangle = \partial_\lambda\langle\psi_\lambda|\psi_\lambda\rangle = 0$.

The geometrical interpretation remains valid in the quantum domain. A quantum statistical model corresponds to a differentiable manifold with coordinates λ and the QFI is connected to a Riemaniann metric on the manifold. In particular, the QFI corresponds to the metric tensor (here a scalar, for a single parameter) obtained from the Bures distance, which is defined as

$$D_B[\rho_1,\rho_2] = \sqrt{2(1-F[\rho_1,\rho_2])}\,, \tag{1.86}$$

where we also introduced the fidelity:

$$F[\rho_1,\rho_2] = \mathrm{Tr}\left[\sqrt{\sqrt{\rho_1}\rho_2\sqrt{\rho_1}}\right], \tag{1.87}$$

which quantifies *similarity* between states. The metric coming from the Bures distance is obtained by an infinitesimal expansion and it can be shown that it is proportional to the QFI:

$$ds_B^2 = D_B^2[\rho_\lambda,\rho_{\lambda+d\lambda}] = 4\mathcal{Q}[\rho_\lambda]d\lambda^2\,. \tag{1.88}$$

More explicitly, we can write the QFI in terms of the infinitesimal change in the fidelity

$$\mathcal{Q}[\rho_\lambda] = \lim_{\epsilon\to 0}\frac{8(1-F[\rho_\lambda,\rho_{\lambda+\epsilon}])}{\epsilon^2}\,. \tag{1.89}$$

For pure states the fidelity reduces to the overlap, i.e. $F[|\psi_1\rangle,|\psi_2\rangle] = |\langle\psi_1|\psi_2\rangle|$, so we can write a compact expression for the QFI of pure states [121] in terms of the overlap:

$$\mathcal{Q}\left[|\psi_{\lambda_0}\rangle\right] = 4\,\partial_{\lambda'}\partial_\lambda\left(\log|\langle\psi_\lambda|\psi_{\lambda'}\rangle|\right)|_{\lambda=\lambda'=\lambda_0}\,. \tag{1.90}$$

To end this section, we want to quickly mention some recent developments about non-asymptotic QET, even though we always will employ the standard asymptotic analysis based on the QFI. The restriction to unbiased estimators is a strong constraint, especially for a small number of observations, in fact it has been shown that biased estimators can actually reduce the mean square error [168]. Furthermore, in the non-asymptotic case a fully Bayesian analysis is believed to be more appropriate, for a discussion and a comparison with the asymptotic "orthodox" approach see [246] and references therein.

1.4 Continuous variable quantum systems

Historically, quantum mechanics was employed to study the motional degrees of freedom of non-relativistic particles. The standard approach is to define n pairs of position and momentum self-adjoint operators, satisfying the so-called canonical commutation relations

$$\left[\hat{x}_i,\hat{p}_j\right] = i\hbar\delta_{ij}\mathbb{1}\,, \tag{1.91}$$

from now on we work in natural units so that $\hbar = 1$. In analogy with classical Hamiltonian mechanics $\hat{x}$ and $\hat{p}$ are called *canonical* operators. It is customary to introduce the non-Hermitian creation and destruction operators

$$\hat{a}_i = \frac{\hat{x}_i + i\hat{p}_i}{\sqrt{2}} \qquad \hat{a}_i^\dagger = \frac{\hat{x}_i - i\hat{p}_i}{\sqrt{2}} \,, \tag{1.92}$$

for which the commutation relations become

$$\left[\hat{a}_i, \hat{a}_j^\dagger\right] = \delta_{ij}\mathbb{1} \,. \tag{1.93}$$

These operators have the effect to annihilate or create a quantum of energy in the quantum description of harmonic oscillators. In the framework of quantum field theory they represent the creation and destruction of particles. As a matter of fact, in second quantization each pair of canonical operators represents field operators of a bosonic field, instead of position and momentum; therefore, systems described by canonical operators are also called "bosonic" systems. The best known example of a bosonic field is the electromagnetic field, where the canonical operators represents the quantum description of the magnetic and electric fields (in one polarization direction). Each canonical degree of freedom is also referred to as a single 'mode', a terminology stemming from quantum optics. We are interested in systems with a finite number of degrees of freedom[21].

These commutation relations define an algebra of operators, which however do not allow any finite dimensional representation, i.e. they cannot be represented as finite-dimensional matrices. However, it is possible to find infinite-dimensional representations, considering the space of square integrable functions $L^2(\mathbb{R}^N)$, so that

$$\hat{x}_j \left|f\right\rangle = x_j f(\boldsymbol{x}) \tag{1.94}$$

$$\hat{p}_j \left|f\right\rangle = -i\frac{\partial f(\boldsymbol{x})}{\partial x_j} \quad \forall \left|f\right\rangle \equiv f(\boldsymbol{x}) \in L^2(\mathbb{R}^n) \tag{1.95}$$

We can also define a vector of canonical operators $\hat{\boldsymbol{r}} = (\hat{x}_1, \hat{p}_1, \ldots, \hat{x}_n, \hat{p}_n)$. For later convenience, we also introduce the corresponding vector of classical phase space variables $\boldsymbol{r} = (x_1, p_1, \ldots, x_n, p_n) \in \mathbb{R}^{2n}$. The canonical bosonic commutation relations can be rewritten as [256]

$$\left[\hat{\boldsymbol{r}}, \hat{\boldsymbol{r}}^\mathsf{T}\right] = i\Omega \,, \tag{1.96}$$

where the canonical symplectic form Ω is a matrix in block-diagonal form:

$$\Omega = \bigoplus_{i=1}^{N} \Omega_1, \qquad \Omega_1 = \begin{pmatrix} 0 & 1 \\ -1 & 0 \end{pmatrix}. \tag{1.97}$$

The external product notation of Eq. (1.96) is defined by components as $\left[\hat{r}_i, \hat{r}_j\right] = i\Omega_{ij}$.

Even if the eigenstate of the canonical operators are not functions in $L^2(\mathbb{R}^n)$ they are expressed in Dirac notation as $|x_j\rangle$ and $|p_j\rangle$. Formally, this notation denotes linear forms

[21] Actually in our treatment of input operators in Section 1.2, we already used a series of modes labeled by a continuous value t (time), i.e. a bosonic system with an infinite number of degrees of freedom. For that particular purpose a full treatment in terms of quantum field theory is not necessary.

acting on $L^2(\mathbb{R}^n)$, so that $\langle \boldsymbol{x}|f\rangle = f(\boldsymbol{x}) \quad \forall\, |f\rangle \equiv f(\boldsymbol{x}) \in L^2(\mathbb{R}^n)$, where $|\boldsymbol{x}\rangle = \bigotimes_{k=1}^n |x_j\rangle$. The operators $\hat{x}_j$ and $\hat{p}_j$ admit a spectral decomposition in terms of projectors on these improper eigenvectors, e.g. $\hat{x} = \int_{-\infty}^{\infty} dx\, x|x\rangle\langle x|$. Since their eigenvalues cover the whole real line, it is customary to refer to systems described by pairs of canonical operators as "quantum continuous variables". Moreover, for a trace-class operator O, the trace can be expressed as

$$\mathrm{Tr}\left[\hat{O}\right] = \int_{-\infty}^{\infty} \langle x|\, \hat{O}\, |x\rangle\, dx\,. \tag{1.98}$$

From these properties we can see that the continuous set $|x\rangle$ can be used as a "continuous" basis of the Hilbert space.

1.4.1 Phase space representation

The Weyl operators (or displacement operators) are the bridge to connect quantum states on the Hilbert space to a description in terms of phase space; they are defined as follows

$$\hat{D}_{\boldsymbol{r}} = e^{i\boldsymbol{r}^{\mathsf{T}}\Omega\hat{\boldsymbol{r}}}\,. \tag{1.99}$$

They can equivalently be defined in terms of complex space variables, i.e. the n-dimensional complex vector $\boldsymbol{\alpha}$ with components $\alpha_j = \frac{x_j + ip_j}{\sqrt{2}}$, as follows

$$\hat{D}_{\boldsymbol{\alpha}} = \bigotimes_j^n e^{\alpha_j \hat{a}_j^\dagger - \alpha^* \hat{a}_j} = \hat{D}_{-\boldsymbol{r}}\,. \tag{1.100}$$

We remark that the Weyl operators are in tensor product form, therefore they act locally on each subsystem. By applying them on a vacuum state, i.e. the state satisfying $\hat{a}_j\,|0\rangle = 0\ \forall j$, we have the so called coherent states

$$|\boldsymbol{\alpha}\rangle = \bigotimes_j^N |\alpha_j\rangle = \hat{D}_{\boldsymbol{\alpha}}\,|0\rangle \tag{1.101}$$

For bounded operators $\hat{O}$ the following important relation holds [45, 256]

$$\hat{O} = \int_{\mathbb{R}^{2n}} \mathrm{Tr}\left[\hat{D}_{-\boldsymbol{r}}\hat{O}\right]\hat{D}_{\boldsymbol{r}} \tag{1.102}$$

Roughly speaking displacement operators can be thought as a basis on the space of bounded operators, where the scalar product is the Hilbert-Schmidt product; they also satisfy an orthogonality condition:

$$\mathrm{Tr}\left[\hat{D}_{\boldsymbol{r}}\hat{D}_{-\boldsymbol{s}}\right] = (2\pi)^n \delta^{2n}(\boldsymbol{r}-\boldsymbol{s})\,. \tag{1.103}$$

Let us define the characteristic function of an operator $\hat{O}$ as

$$\chi_{\hat{O}}(\boldsymbol{r}) = \mathrm{Tr}\left[\hat{O}\hat{D}_{-\boldsymbol{r}}\right]\,, \tag{1.104}$$

from the previous discussion we can see that this is an equivalent representation of a bounded operator.

There is another important mapping between Hilbert space operators and functions on the phase space, known as Wigner transform [46, 62]. The Wigner transform of a generic bounded operator on the infinite dimensional Hilbert space is simply the Fourier transform of the characteristic function:

$$\mathcal{W}[\hat{O}](\boldsymbol{r}) = \frac{1}{(2\pi)^{2N}} \int_{\mathbb{R}^{2N}} \mathrm{d}\boldsymbol{v}\, e^{i\boldsymbol{v}^\intercal \Omega \boldsymbol{r}} \mathrm{Tr}\left[\hat{O} e^{-i\boldsymbol{v}^\intercal \Omega \hat{\boldsymbol{r}}}\right], \tag{1.105}$$

which is of course a basis-independent definition[22]. The Wigner transform is also called the Wigner function of the operator (a term that we mostly use to refer to Wigner functions of quantum states) and contains all the information about the operator, just like the characteristic function. Crucially, the Wigner function of a self-adjoin operators correspond to a *real* valued function on the phase space. If we evaluate the trace in position basis $\hat{\boldsymbol{x}}|\boldsymbol{s}\rangle_x = \boldsymbol{s}|\boldsymbol{s}\rangle_x$[23] we get the equivalent expression

$$\mathcal{W}[\hat{O}](\boldsymbol{x}, \boldsymbol{p}) = \frac{1}{\pi^N} \int_{\mathbb{R}^N} \mathrm{d}\boldsymbol{y}\, {}_x\langle \boldsymbol{x} + \boldsymbol{y}|\hat{O}|\boldsymbol{x} - \boldsymbol{y}\rangle_x\, e^{-2i\boldsymbol{p}\cdot\boldsymbol{y}}\,, \tag{1.106}$$

which is most often encountered in the literature.

A fundamental property of the Wigner transform is that the trace of two operators can be expressed as an integral in phase space

$$\mathrm{Tr}[\hat{O}_1 \hat{O}_2] = (2\pi)^N \int_{\mathbb{R}^{2N}} \mathrm{d}\boldsymbol{r} \mathcal{W}[\hat{O}_1](\boldsymbol{r}) \mathcal{W}[\hat{O}_2](\boldsymbol{r}), \tag{1.107}$$

in particular this can be used to express the Born rule

$$p(\boldsymbol{a}|\rho) = (2\pi)^N \int_{\mathbb{R}^{2N}} \mathrm{d}\boldsymbol{r} \mathcal{W}[\rho](\boldsymbol{r}) \mathcal{W}[\Pi_{\boldsymbol{a}}](\boldsymbol{r}), \tag{1.108}$$

where $\int_\Omega \mathrm{d}\mu(\boldsymbol{a}) \Pi_{\boldsymbol{a}} = \mathbb{1}$ is a generic POVM. The integral measure $\mu(\boldsymbol{a})$ on the outcome space Ω is generic, e.g. the the Lebesgue measure for general-dyne measurements or the counting measure for photon-counting measurements (for which $\int d\mu(a) \to \sum_a$) The Wigner functions of the effects of the POVM satisfy

$$\int_\Omega \mathrm{d}\mu(\boldsymbol{a}) \mathcal{W}[\Pi_{\boldsymbol{a}}](\boldsymbol{r}) = \frac{1}{(2\pi)^N}, \tag{1.109}$$

where we used the linearity of the Wigner transform and the fact that $\mathcal{W}[\mathbb{1}](\boldsymbol{r}) = 1/(2\pi)^N$ (we implicitly assume that all the conditions to exchange the integration order hold true). When the Wigner transform of the POVM effects $\mathcal{W}[\Pi_{\boldsymbol{a}}](\boldsymbol{r})$ is a Gaussian function we refer to these as Gaussian measurements. It is also important to consider the limiting case of projection on position or momentum eigenstates (or rotations thereof); in this case the corresponding Wigner transform is proportional to a Dirac delta function and the Born

[22] This mapping is one to one only for bounded operators, however we use it also for some unbounded operators, in particular projectors over position/momentum eigenstates. In these particular cases everything remains consistent with the definitions given here.

[23] In some situations, to avoid confusion, we explicitly denote the eigenvectors of a quadrature operator by a subscript, so that arbitrary letters can be used to label the eigenvalues.

rule is equivalent to an integration over all the other phase-space variables, e.g. for a single mode

$$p(x) = \int_{\mathbb{R}} \mathrm{d}p\, \mathcal{W}[\rho](x,p)\ . \tag{1.110}$$

In this formalism the trace rule (1.107) can be generalized also to the partial trace, which is just the marginal Wigner function [214]:

$$\mathcal{W}[\mathrm{Tr}_B[\rho_{AB}]](\boldsymbol{r}_A) = \int \mathrm{d}\boldsymbol{r}_B \mathcal{W}[\rho_{AB}](\boldsymbol{r}_A,\boldsymbol{r}_B)\ . \tag{1.111}$$

Consequently, the rule for the unnormalized conditional states after a measurement on one subsystem can be written as

$$\mathcal{W}[\mathrm{Tr}_B[\rho_{AB}\mathbb{1}\otimes\Pi_{\boldsymbol{a}}]](\boldsymbol{r}_A) = (2\pi)^{N_B}\int \mathrm{d}\boldsymbol{r}_B \mathcal{W}[\rho_{AB}](\boldsymbol{r}_A,\boldsymbol{r}_B)\mathcal{W}[\Pi_{\boldsymbol{a}}](\boldsymbol{r}_B). \tag{1.112}$$

To get a normalized Wigner function the previous expression should be divided by the probability density $p(\boldsymbol{a})$ given by the Born rule (1.108). Moreover, the tensor product operation is simply given by multiplication of Wigner functions

$$\mathcal{W}\big[\hat{O}_1\otimes\hat{O}_2\big](\boldsymbol{r}_1,\boldsymbol{r}_2) = \mathcal{W}\big[\hat{O}_1\big](\boldsymbol{r}_1)\mathcal{W}\big[\hat{O}_2\big](\boldsymbol{r}_2). \tag{1.113}$$

The Wigner transform is not the only mapping between operators and phase space. However, it is the only one with the following properties [30, 81]: it is real for any quantum state, it is a linear functional over density operators, its marginals are the probability distributions of canonical observables and the trace rule (1.107) holds.

Another particularly relevant class of phase-space mappings is obtained by considering the s-ordered characteristic functions; we only give a very brief introduction, for more details see [27]. For a single mode the s-ordered displacement operator is defined as

$$\chi_s(\alpha) = \mathrm{Tr}\big[\hat{D}_\alpha\rho\big]e^{\frac{s}{2}|\alpha|^2}\ , \tag{1.114}$$

clearly for $s=0$ we get the previously introduced characteristic function. By taking the Fourier transform of χ_s it is possible to define the s-ordered quasiprobability distributions[24]. In particular, for $s=1$, we have the so called Glauber P-function, which allows to write a density operator as an integral over coherent state projectors:

$$\rho = \int_{\mathbb{C}} d\alpha P(\alpha)|\alpha\rangle\langle\alpha|\ . \tag{1.115}$$

Note that in general this is not a mixture of coherent states, since the function P does not need to be positive and actually it might be a very singular object, not even a tempered distribution. Nonetheless it is always possible to formally write the integral (1.115) for *any* continuous variable quantum state [158].

[24] In Section 7.3 we explain more in detail how the quasiprobability distributions for different s are connected by Gaussian convolutions.

1.4.2 Gaussian systems

Gaussian states of bosonic systems have played a fundamental role for continuous-variable (CV) quantum technologies and quantum information. The theoretical analysis of Gaussian states is made simpler by the fact that they can be compactly described by first and second statistical moments, yet they can manifest many genuinely quantum properties. A number of books and reviews deals with this subject extensively [2, 39, 80, 129, 256, 291]. Experimentally, the generation and manipulation of Gaussian states has been made possible by the availability of second order non-linearities (Gaussian-preserving operations) in various physical platforms, including optical, atomic, and opto-mechanical systems.

Let us consider a Hamiltonian that is a quadratic polynomial in the canonical operators (the constant factors are irrelevant)

$$\hat{H}_G = \frac{1}{2}\hat{\boldsymbol{r}}^{\mathsf{T}} H \hat{\boldsymbol{r}} + \hat{\boldsymbol{r}}^{\mathsf{T}} \boldsymbol{h}, \tag{1.116}$$

where H is a symmetric $2N \times 2N$ matrix and $\boldsymbol{h}$ is a $2N$ real vector. Such Hamiltonian corresponds to a linear transformation in the Heisenberg picture (the so-called Gaussian unitaries)

$$\hat{U}_G^\dagger \hat{\boldsymbol{r}} \hat{U}_G = S\hat{\boldsymbol{r}} + \boldsymbol{d}, \tag{1.117}$$

where $\hat{U}_G = \exp[-it\hat{H}_G]$ and S is a symplectic matrix satisfying $S^{\mathsf{T}}\Omega S = \Omega$, which implies $\det S = 1$ (on a classical level this means that the phase space volume element is conserved). The symplectic matrix S and the vector $\boldsymbol{d}$ are obtained in terms of the Hamiltonian as follows:

$$S = e^{\Omega H} \qquad \boldsymbol{d} = -H^{-1}\boldsymbol{h}\,. \tag{1.118}$$

More formally, the matrix S belongs to the symplectic group $\mathrm{Sp}(2n, \mathbb{R})$, while the whole transformation belongs to the affine symplectic group $\mathrm{ISp}(2n, \mathbb{R})$. A crucial property is that every Wigner function is covariant with respect to Gaussian unitary evolutions:

$$\mathcal{W}[\hat{U}_G \rho \hat{U}_G^\dagger](\boldsymbol{r}) = \mathcal{W}[\rho](S^{-1}\boldsymbol{r} - S^{-1}\boldsymbol{d})\,. \tag{1.119}$$

This identity shows that a quadratic Hamiltonian induces an evolution in the quasiprobability distribution which is exactly the *classical* Liouville evolution of a classical probability distribution in phase-space. We are going to comment more about this point in Chapter 7.

Gaussian states are defined as thermal states of Hamiltonians of the form (1.116):

$$\rho_G = \frac{e^{-\beta \hat{H}_G}}{\mathrm{Tr}\left[e^{-\beta \hat{H}_G}\right]}, \tag{1.120}$$

where pure states correspond to ground states and are obtained in the limit $\beta \to \infty$. A Gaussian state has a complete parametrization in term of first and second statistical moments (the covariance matrix σ)

$$\bar{\boldsymbol{r}} = \mathrm{Tr}[\rho_G \hat{\boldsymbol{r}}] \qquad \sigma = \mathrm{Tr}\left[\rho_G \left\{(\hat{\boldsymbol{r}} - \bar{\boldsymbol{r}}), (\hat{\boldsymbol{r}} - \bar{\boldsymbol{r}})^{\mathsf{T}}\right\}\right] \tag{1.121}$$

and its Wigner function is a Gaussian function of the form

$$\mathcal{W}[\rho_G](\boldsymbol{r}) = \frac{1}{\pi^N \sqrt{\det \boldsymbol{\sigma}}} e^{-(\boldsymbol{r}-\bar{\boldsymbol{r}})^{\mathsf{T}} \boldsymbol{\sigma}^{-1} (\boldsymbol{r}-\bar{\boldsymbol{r}})}. \tag{1.122}$$

For clarity, we remark that according to definition (1.121) the variance of a canonical observable $\hat{r}_j$ is equal to *half* the respective diagonal element of the covariance matrix: $\mathrm{Tr}\left[\rho \hat{r}_j^2\right] - \mathrm{Tr}\left[\rho \hat{r}_j\right]^2 = \sigma_{jj}/2$ (e.g. the covariance matrix of the vacuum state is the identity). For Gaussian states the evolution due to quadratic Hamiltonians in Eq. (1.119) entails a simple expression in terms of covariance matrix and first moments:

$$\boldsymbol{\sigma}' = S \boldsymbol{\sigma} S^{\mathsf{T}} \qquad \bar{\boldsymbol{r}}' = S \bar{\boldsymbol{r}} + \boldsymbol{d} \,. \tag{1.123}$$

As previously mentioned, we can also define Gaussian measurements; in the ideal case they correspond to projections on pure Gaussian states with the same covariance matrix but labeled by different values of the first moments. These measurement can be obtained by Gaussian unitaries followed by projective measurements of the canonical operators $\hat{\boldsymbol{r}}$, which in optics correspond to *homodyne* measurements. An ideal Gaussian measurement is not a projective measurement in general, e.g. for a projection on coherent states we have the usual heterodyne detection of quantum optics. More in general, some noise can be present in the detector. As long as the noise obeys a Gaussian description (such as loss, or thermal noise) a convenient parametrization for Gaussian POVMs is the following [100, 256]

$$\int_{\mathbb{R}^N} d\boldsymbol{r}_{\mathrm{m}} \; \hat{\pi}_{\boldsymbol{r}_{\mathrm{m}}} = \int_{\mathbb{R}^N} d\boldsymbol{r}_{\mathrm{m}} \; \frac{\hat{D}_{-\boldsymbol{r}_{\mathrm{m}}} \rho_{\mathrm{m}} \hat{D}_{\boldsymbol{r}_{\mathrm{m}}}}{(2\pi)^N} = \mathbb{1} \,, \tag{1.124}$$

where ρ_{m} is a generic Gaussian state with zero first moments, thus completely characterized by its covariance matrix $\boldsymbol{\sigma}_{\mathrm{m}}$.

Acting with such POVMs on a Gaussian state, the Born rule (1.108) gives a Gaussian distribution

$$p(\boldsymbol{r}_{\mathrm{m}}) = \frac{e^{-\frac{1}{2}(\boldsymbol{r}_m - \bar{\boldsymbol{r}})^{\mathsf{T}} (\boldsymbol{\sigma} + \boldsymbol{\sigma}_{\mathrm{m}})^{-1} (\boldsymbol{r}_{\mathrm{m}} - \bar{\boldsymbol{r}})}}{(2\pi)^n \sqrt{\det(\boldsymbol{\sigma} + \boldsymbol{\sigma}_{\mathrm{m}})}} \,. \tag{1.125}$$

Let us consider a bipartite Gaussian state with global covariance matrix and first moments

$$\boldsymbol{\sigma} = \begin{pmatrix} \boldsymbol{\sigma}_A & \boldsymbol{\sigma}_{AB} \\ \boldsymbol{\sigma}_{AB}^{\mathsf{T}} & \boldsymbol{\sigma}_B \end{pmatrix} \qquad \bar{\boldsymbol{r}}_{AB} = \begin{pmatrix} \bar{\boldsymbol{r}}_A & \bar{\boldsymbol{r}}_B \end{pmatrix} . \tag{1.126}$$

If we measure the subsystem B with a Gaussian POVM, Eq. (1.112) gives the following mapping for the conditional state on subsystem A[25]:

$$\sigma_A \mapsto \sigma_A - \boldsymbol{\sigma}_{AB} (\boldsymbol{\sigma}_B + \boldsymbol{\sigma}_{\mathrm{m}})^{-1} \boldsymbol{\sigma}_{AB}^{\mathsf{T}} \tag{1.127}$$

$$\bar{\boldsymbol{r}}_A \mapsto \bar{\boldsymbol{r}}_A + \boldsymbol{\sigma}_{AB} (\boldsymbol{\sigma}_B + \boldsymbol{\sigma}_{\mathrm{m}})^{-1} (\boldsymbol{r}_{\mathrm{m}} - \bar{\boldsymbol{r}}_B) \,. \tag{1.128}$$

[25] If in the rule for the covariance matrix we put $\boldsymbol{\sigma}_{\mathrm{m}} = 0$ we get the Schur complement of the matrix $\boldsymbol{\sigma}$ w.r.t. the submatrix $\boldsymbol{\sigma}_B$, which would give the classical Gaussian conditional probability after observing $\boldsymbol{r}_B$. Notice how in the quantum case there is an additional uncertainty $\boldsymbol{\sigma}_{\mathrm{m}}$ due to the POVM.

Entropy of a Gaussian state

Any covariance matrix can be diagonalized by symplectic matrices so each eigenvalue has multiplicity two. The N different values ν_j are usually called symplectic eigenvalues. The von Neumann entropy of a Gaussian state is a function of the symplectic eigenvalues only [104, 131, 256] and one does not need the eigenvalues of the infinite dimensional density operator to compute it. For a generic N-mode Gaussian state we have

$$S(\rho_G) = \sum_j^N h(\nu_j), \tag{1.129}$$

where $\{\nu_j, j \in [1, \dots, N]\}$ are the symplectic eigenvalues and we defined the following function

$$h(x) = \left(\frac{x+1}{2}\right)\log\left(\frac{x+1}{2}\right) - \left(\frac{x-1}{2}\right)\log\left(\frac{x-1}{2}\right). \tag{1.130}$$

In particular, for single mode systems the only symplectic eigenvalue is the square root of the determinant of the covariance matrix and we have

$$S(\rho_G) = h(\sqrt{\det\sigma}). \tag{1.131}$$

Examples of Gaussian unitary operations

As an example, let us consider a couple of Gaussian unitary operations that are going to be useful in the following chapters. First we consider single mode squeezing:

$$\hat{S}(\xi) = \exp\left[\frac{\xi}{2}\left(\hat{a}^\dagger\right)^2 - \frac{\xi^*}{2}\hat{a}^2\right] = \exp\left[\frac{i}{2}r\sin\psi\left(\hat{q}^2 - \hat{p}^2\right) - \frac{i}{2}r\cos\psi(\hat{q}\hat{p} + \hat{p}\hat{q})\right] \tag{1.132}$$

where $\xi = re^{i\psi}$, the corresponding symplectic matrix is thus

$$S(r,\psi) = \begin{pmatrix} \cosh r + \cos\psi\sinh r & \sin\psi\sinh r \\ \sin\psi\sinh r & \cosh r - \cos\psi\sinh r \end{pmatrix}. \tag{1.133}$$

For $\psi = 0$ we get a squeezing of the momentum fluctuations; since $S(r,0)^\dagger(\hat{p},\hat{x})S(r,0) = (e^r\hat{x}, e^{-r}\hat{p})$ the variance in momentum $\Delta\hat{p} = \langle\hat{p}^2\rangle - \langle\hat{p}\rangle^2$ is transformed as $\Delta\hat{p} \to e^{-2r}\Delta\hat{p}$, while the variance of the position operator increases as $\Delta\hat{x} \to e^{2r}\Delta\hat{x}$. Another important Gaussian unitary is the one for the beam splitter

$$\hat{U}_{\mathsf{bs}}(\phi,\theta) = e^{\phi e^{i\theta}\hat{a}_1^\dagger\hat{a}_2 - \phi e^{-i\theta}\hat{a}_1\hat{a}_2^\dagger} = \exp[i\phi\cos\theta(\hat{p}_1\hat{x}_2 - \hat{x}_1\hat{p}_2) + i\phi\sin\theta(\hat{x}_1\hat{x}_2 + \hat{p}_1\hat{p}_2)]. \tag{1.134}$$

We can parametrize the beam splitter with the trasmissivity $T = \cos^2\phi$ and choose a particular $\theta = \pi$; the corresponding symplectic matrix is then

$$S_{\mathsf{bs}}(T) = \begin{pmatrix} \sqrt{T} & 0 & \sqrt{1-T} & 0 \\ 0 & \sqrt{T} & 0 & \sqrt{1-T} \\ -\sqrt{1-T} & 0 & \sqrt{T} & 0 \\ 0 & -\sqrt{1-T} & 0 & \sqrt{T} \end{pmatrix}. \tag{1.135}$$

1.4.3 Conditional and unconditional Gaussian dynamics

Let us apply our treatment of Markovian dynamics in Sec. (1.2) to the class of continuous variable systems we have just introduced. In doing so, we mostly follow Refs. [96, 100, 256]; as usual we favour physical intuition over mathematical rigour. Alternative parametrizations for the same dynamics are found in [297, 298]. We also mention that there is also a more formal way of dealing with this very topic, which is closer in spirit to how classical linear systems are handled; see for example [209].

Let us introduce a vector of input modes, described in terms of the canonical operators:

$$\left[\hat{\boldsymbol{r}}_{\rm in}(t), \hat{\boldsymbol{r}}_{\rm in}(t')^{\mathsf{T}}\right] = i\Omega\delta(t-t') \tag{1.136}$$

$$\left\langle \left\{\hat{\boldsymbol{r}}_{\rm in}(t), \hat{\boldsymbol{r}}_{\rm in}(t')^{\mathsf{T}}\right\}\right\rangle = \boldsymbol{\sigma}_{\rm in}\,\delta(t-t')\,, \tag{1.137}$$

in terms of the previously used input operators (1.32) this corresponds to $\hat{\boldsymbol{r}}_{\rm in}(t)^{\mathsf{T}} = (\hat{x}^{(1)}_{\rm in}, \hat{p}^{(1)}_{\rm in}, \ldots \hat{x}^{(n)}_{\rm in}, \hat{p}^{(n)}_{\rm in})$ with $\hat{x}^{(j)}_{\rm in} = (b^{(j)}_{\rm in} + b^{(j)\dagger}_{\rm in})/\sqrt{2}$ and analogously for the other canonical operators. At variance with Sec. (1.2), where we only considered input modes in the vacuum state, now we allow them to be in a generic Gaussian state with covariance matrix $\boldsymbol{\sigma}_{\rm in}$.

We can also collect the canonical operators of the system and those of the input at a certain time t in a single vector $\hat{\boldsymbol{r}}^{\mathsf{T}}_{\rm s,in} = \left(\hat{\boldsymbol{r}}^{\mathsf{T}}, \hat{\boldsymbol{r}}_{\rm in}(t)^{\mathsf{T}}\right)$. The instantaneous interaction between the system and the input modes is then assumed to be a generic quadratic one, so that the interaction Hamiltonian reads

$$\hat{H}_{\rm tot} = \hat{\boldsymbol{r}}^{\mathsf{T}} C\, \hat{\boldsymbol{r}}_{\rm in}(t) = \frac{1}{2}\hat{\boldsymbol{r}}^{\mathsf{T}}_{\rm s,in} H_c \hat{\boldsymbol{r}}_{\rm s,in} = \frac{1}{2}\hat{\boldsymbol{r}}^{\mathsf{T}}_{\rm s,in}\begin{pmatrix} 0 & C \\ C^{\mathsf{T}} & 0 \end{pmatrix}\hat{\boldsymbol{r}}_{\rm s,in}\,, \tag{1.138}$$

where H_C is symmetric, but C is an arbitrary real matrix.

Then we define the so-called quantum Wiener increment, as previously done

$$d\hat{\boldsymbol{r}}_{\rm in}(t) = \hat{\boldsymbol{r}}_{\rm in}(t)dt = \hat{\boldsymbol{r}}'_{\rm in}(t)\sqrt{dt}, \tag{1.139}$$

so that the operators $\hat{r}'_{\rm in}$ at time t obey canonical commutation relations:

$$\left[\hat{\boldsymbol{r}}'_{\rm in}(t), \hat{\boldsymbol{r}}'_{\rm in}(t)\right] = i\Omega\,. \tag{1.140}$$

The symplectic matrix corresponding to the unitary interaction must be written in terms of the operators $\hat{r}'_{\rm in}$ using (1.118) and it has to be expanded up order dt, as previously done in (1.25):

$$e^{\Omega H_C\sqrt{dt}} \approx \mathbb{1} + \Omega H_C\sqrt{dt} + \frac{(\Omega H_C)^2}{2}dt\,. \tag{1.141}$$

This symplectic transformation can then be used to obtain the covariance matrix at $t + dt$

$$e^{\Omega H_C\sqrt{dt}}(\boldsymbol{\sigma}\oplus\boldsymbol{\sigma}_b)e^{(\Omega H_C)^{\mathsf{T}}\sqrt{dt}} \approx (\boldsymbol{\sigma}\oplus\boldsymbol{\sigma}_b) + \left(A\boldsymbol{\sigma} + \boldsymbol{\sigma}A^{\mathsf{T}} + D\right)\otimes\tilde{\boldsymbol{\sigma}}_{\rm in} + \boldsymbol{\sigma}_{\rm s,in}\sqrt{dt}\,, \tag{1.142}$$

where

$$A = \Omega H_{\rm s} + \frac{\Omega C\Omega C^{\mathsf{T}}}{2} \qquad D = \Omega C\boldsymbol{\sigma}_{\rm in}C^{\mathsf{T}}\Omega^{\mathsf{T}} \tag{1.143}$$

are the so called drift[26] and diffusion matrices and the other matrices appearing in the expression are defined as follows

$$\boldsymbol{\sigma}_{\mathrm{s,in}} = \begin{pmatrix} 0 & \Omega C \boldsymbol{\sigma}_{\mathrm{in}} + \boldsymbol{\sigma} C \Omega^{\mathsf{T}} \\ \boldsymbol{\sigma}_{\mathrm{in}} C^{\mathsf{T}} \Omega^{\mathsf{T}} + \Omega C^{\mathsf{T}} \boldsymbol{\sigma} & 0 \end{pmatrix} \tag{1.144}$$

$$\tilde{\boldsymbol{\sigma}}_{\mathrm{in}} = \frac{\Omega C^{\mathsf{T}} \Omega C \boldsymbol{\sigma}_{\mathrm{in}} + \boldsymbol{\sigma}_{\mathrm{in}} C^{\mathsf{T}} \Omega C \Omega}{2} + \Omega^{\mathsf{T}} C^{\mathsf{T}} \boldsymbol{\sigma} C \Omega \, . \tag{1.145}$$

In a similar fashion we can obtain the first moments at $t + dt$:

$$e^{\Omega H_C \sqrt{dt}} \begin{pmatrix} \boldsymbol{r} \\ \boldsymbol{r}_{\mathrm{in}} \end{pmatrix} \approx \left(\mathbb{1} + \Omega H_c \sqrt{dt} + \frac{(\Omega H_C)^2}{2} dt \right) \begin{pmatrix} \boldsymbol{r} \\ \boldsymbol{r}_{\mathrm{in}} \end{pmatrix} \approx \begin{pmatrix} \boldsymbol{r} + A \boldsymbol{r} dt \\ \Omega C^{\mathsf{T}} \boldsymbol{r} \sqrt{dt} \end{pmatrix} , \tag{1.146}$$

where we assume $\boldsymbol{r}_{\mathrm{in}} = \mathbf{0}$, i.e. the input modes have no displacement.

Tracing away the input mode, we can straight-forwardly obtain the unconditional dynamics for the first moments and the covariance matrix

$$\frac{d\boldsymbol{r}_t}{dt} = A \boldsymbol{r}_t + \boldsymbol{u} \tag{1.147}$$

$$\frac{d\boldsymbol{\sigma}_t}{dt} = A \boldsymbol{\sigma}_t + \boldsymbol{\sigma}_t A^{\mathsf{T}} + D \, . \tag{1.148}$$

We also added a linear drive term $\boldsymbol{u}$, so that the dynamics given by this equations with A and D in (1.143) can now accommodate a generic system Hamiltonian with quadratic and linear terms $\hat{H}_s = \frac{1}{2} \hat{\boldsymbol{r}}^{\mathsf{T}} H_S \hat{\boldsymbol{r}} + \boldsymbol{u}^{\mathsf{T}} \Omega \hat{\boldsymbol{r}}$. At the Hilbert space level this dynamics is expressed as a Lindblad equation with collapse operators linear in $\hat{\boldsymbol{r}}$, so that the action in the master equation is at most quadratic.

If instead of tracing away the modes $\hat{r}'_{\mathrm{in}}$ we perform a generic Gaussian (general-dyne) measurement, we get the Gaussian probability density (1.125) for the outcome $\boldsymbol{r}_m$, which is centred around a value proportional to the first moments of the state $\bar{\boldsymbol{r}}_m = \Omega C^{\mathsf{T}} \boldsymbol{r} \sqrt{dt}$ and has a covariance matrix which is independent from the state of the system: $\boldsymbol{\Sigma} = (\boldsymbol{\sigma}_m + \boldsymbol{\sigma}_{\mathrm{in}})/2$.

Since $\boldsymbol{r}_m$ is a Gaussianly distributed random variable it is possible to introduce another random variable

$$d\boldsymbol{w} = \boldsymbol{\Sigma}^{-1/2} (\boldsymbol{r}_m - \bar{\boldsymbol{r}}_m) \sqrt{dt} \, , \tag{1.149}$$

which corresponds to a vector of Wiener increments with the following properties $\mathbb{E}[d\boldsymbol{w}] = 0$ and $\left\{ d\boldsymbol{w}, d\boldsymbol{w}^{\mathsf{T}} \right\}/2 = \mathbb{1} dt$ (for the components this means $dw_i dw_j = \delta_{ij} dt$). The measurement output is usually expressed in term of the vector of currents (corresponding to (1.54) in the case of a single input operator):

$$\begin{aligned} d\boldsymbol{y}_t &= \sqrt{2} \Sigma^{-1/2} \boldsymbol{r}_m \sqrt{dt} = \sqrt{2} \Sigma^{-1/2} \bar{\boldsymbol{r}}_m \sqrt{dt} + d\boldsymbol{w} = \\ &= \sqrt{2} (\boldsymbol{\sigma}_{\mathrm{in}} + \boldsymbol{\sigma}_m)^{-1/2} \Omega C^{\mathsf{T}} \boldsymbol{r}_t \sqrt{dt} + d\boldsymbol{w} \, . \end{aligned} \tag{1.150}$$

[26] To keep the derivation cleaner, we did not include any Hamiltonian operator for the system alone. However, the drift matrix presented also contains the contribution of a quadratic term in the system Hamiltonian $\hat{H}_s = \frac{1}{2} \hat{\boldsymbol{r}}^{\mathsf{T}} H_S \hat{\boldsymbol{r}}$

By applying the formula for conditional Gaussian states, the following equations for the first and second statistical moments can be derived [100, 256]:

$$d\boldsymbol{r}_t = A\boldsymbol{r}_t dt + \boldsymbol{u}dt + \left(\frac{\sigma_t B + N}{\sqrt{2}}\right) d\boldsymbol{w} \tag{1.151}$$

$$\frac{d\sigma_t}{dt} = A\sigma_t + \sigma_t A^{\mathsf{T}} + D - (\sigma_t + N)(\sigma_t B + N)^{\mathsf{T}} \tag{1.152}$$

where we introduced two matrices $B = C\Omega^{\mathsf{T}}\boldsymbol{\Sigma}^{-1/2}$ and $N = \Omega C\sigma_{\text{in}}\boldsymbol{\Sigma}^{-1/2}$.

A very remarkable feature of the conditional Gaussian dynamics is that the equation for the covariance matrix is deterministic and it has the form of a continuous-time Riccati differential equation. The stochasticty coming from the random output of measurements is reflected only on the first moments of the conditional state.

1.4.4 Nonclassicality of continuous variable states

In the most general terms, a quantum state is said to be nonclassical if the methods of classical statistics fail to describe its properties and phenomenology. This definition is usually made precise by using quasiprobability distributions in phase space, but several different flavours of the concept of nonclassicality exist; for our purposes it is sufficient to present two of the most common ones.

In the context of quantum optics, the concept of *nonclassicality* is tied to genuine quantum traits of optical systems [182] and it is usually based on the Glauber P-function of a quantum state; we dub this concept P-nonclassicality. On the other hand, we refer to nonclassicality based on the negativity Wigner function as W-nonclassicality. In the following we present some suitable *quantifiers* of nonclassicality, but we do not discuss *witnesses* of nonclassicality. In any case we only cover a small part of the possible approaches to the subject, see the introduction of Ref. [195] for a concise overview.

Finally, we also present a way to quantify the non-Gaussianity of a quantum state. This notion is connected to the other notions of nonclassicality, but gives a very distinct characterization when mixed states are considered.

P-nonclassicality

According to Glauber, Titulauer and Mandel [113, 181, 278], a quantum state of light is nonclassical when its P function fails to be interpreted as a probability distribution in the phase space. This definition is very meaningful for states of the electromagnetic field, since the P function is the only quasiprobability distribution which can give a description that can be completely modelled using classical electrodynamics, see for example [152] for a recent account of this point of view. Intuitively, this definition means that the state can be properly represented as a mixture of coherent states, therefore it has no coherences on the (overcomplete) basis of coherent states. This argument has recently been made rigorous in the context of quantum resource theories, see [274, 300].

The best known way to quantify P-nonclassicality is the nonclassical depth [164]. Operationally, it quantifies the amount of thermal noise that is needed to render the P function of a given state a well-behaved probability distribution and the corresponding

state classical. Nonetheless we do not present this measure in detail, because it gives a very coarse quantification for pure states, as a matter of fact *any* pure non-Gaussian state saturates this measure to its maximal value [174]. For this reason we introduce a different quantifier, which is particularly easy to compute for pure states of a single bosonic mode.

It has long been known that coherent states are the only pure states that produce uncorrelated outputs when mixed by a passive linear-optics device [4]. Specifically, P-nonclassicality has been identified as a necessary condition for having entangled states at the output of a beam splitter [156, 299]. The idea is thus to quantify nonclassicality of a single mode state as the two mode entanglement at the output of a linear optic device, as introduced by Asbóth et al. [22]. In particular, it was shown that the optimal entangler is simply a beam splitter with vacuum as an auxiliary state. By restricting to this setup, nonclassicality of the input state becomes a necessary and sufficient condition for output entanglement. As a consequence, entanglement at the output of a linear mixer may be used as a faithful quantitative measure of P-nonclassicality. This measure is usually referred to as entanglement potential and it is defined as

$$\mathcal{E}[\rho] = E\Big[\hat{B}(\rho \otimes |0\rangle\langle 0|)\hat{B}^\dagger\Big], \tag{1.153}$$

where ρ is the density matrix of the state under scrutiny, $|0\rangle$ is the vacuum state at the ancillary port of the beam splitter, $\hat{B} \equiv \hat{U}_{\mathsf{bs}}\big(\pi, \frac{\pi}{4}\big)$ is the balanced beam splitter operator (1.134), and $E[\rho]$ is a suitable measure of entanglement. If we restrict to pure input states, $E[\rho]$ can be chosen, with no ambiguity, as the the entanglement entropy, i.e. the von-Neuman entropy of the reduced state.

W-nonclassicality

While the P function can be a singular object, the Wigner function is always well behaved, even if it can attain negative values. W-nonclassicality is only a sufficient condition for P-nonclassicality and there are W-classical states which are P-nonclassical, for example squeezed states.

The notion of W-nonclassicality has gained an operational meaning as follows: the evolution of a system which is in a W-nonclassical state cannot be efficiently simulated with classical resources [185, 287]; we are going to comment more about this point in Chapter 8. The most common way to quantify W-nonclassicality is the volume of the negative part of the Wigner function [151], defined as

$$\Delta[\rho] = \frac{1}{2}\left(\int_{\mathbb{R}^{2n}} \mathrm{d}\boldsymbol{r}\ |\mathcal{W}[\rho](\boldsymbol{r})| - \int_{\mathbb{R}^{2n}} \mathrm{d}\boldsymbol{r}\ \mathcal{W}[\rho](\boldsymbol{r})\right) = \frac{1}{2}\left(\int_{\mathbb{R}^{2n}} \mathrm{d}\boldsymbol{r}\ |\mathcal{W}[\rho](\boldsymbol{r})| - 1\right); \tag{1.154}$$

however many slight variations on this definition can be employed. First, we can introduce a normalized version of this measure

$$\nu[\rho] = \frac{2\Delta[\rho]}{1 + 2\Delta[\rho]}, \tag{1.155}$$

which gives $\nu \in [0, 1]$ and that we use in Chapter 6. On the other hand in Chapter 8 we employ both the Wigner negativity $\mathcal{N}[\rho] = 2\Delta[\rho]$ and the so-called CV mana $\mathsf{M}[\rho] = \log(\mathcal{N}[\rho] + 1)$.

Let us stress that the W and P-nonclassicality single out different quantum features. In particular, the Hudson theorem [136, 263] guarantees that the sole pure states with a positive Wigner function are Gaussian ones, i.e. squeezed coherent states for a single mode. Hence, there exist pure states that have zero W-nonclassicality (e.g. squeezed states) but non-zero P-nonclassicality. In this sense the entanglement potential can reveal more detailed features of quantumness. Note that alternative measures of W-nonclassicality based on the geometric distance between quantum states have also been introduced [186].

Non-Gaussianity

Gaussian states are not P-classical, as they include squeezed states. They have a positive Wigner function and yet they do not represents the whole class of W-classical states. Nonetheless, quadratic Hamiltonians can be truly considered classical, since they generate a classical evolution in phase space. Being thermal states of such Hamiltonians, Gaussian state thus embody yet another notion of classical quantum states; these observations are expanded in Chapter 8. It is thus interesting to study a quantitative characterization of the non-Gaussian character of a continuous variable state. Several different ways to quantify non-Gaussianity [104, 105, 141, 187] have been introduced and also exploited to assess the properties of experimentally generated non-Gaussian states of optical systems [18, 19, 25]. In this Thesis we focus on the entropic approach proposed in [106, 187].

To quantify the non-Gaussianity of a generic state ρ, we introduce a reference Gaussian state τ having the same covariance matrix and displacement vector as ρ, computed via (1.121). A quantitative measure of non-Gaussianity can then be given by some suitable distance functional between ρ and τ. A particularly useful choice is the quantum relative entropy

$$S(\rho\|\tau) = \mathrm{Tr}[\rho(\ln\rho - \ln\tau)] \,. \tag{1.156}$$

Even if $S(\rho\|\tau) = 0$ iff $\rho = \tau$, the relative entropy is not symmetric in its arguments, therefore it is not a proper distance. Nonetheless it has a clear operational meaning and quantifies the distinguishability of two states in the asymptotic regime of many copies.

This leads to the definition of the entropic measure of non-Gaussianity

$$\delta[\rho] = S(\rho\|\tau) = \mathrm{Tr}[\rho\ln\rho] - \mathrm{Tr}[\rho\ln\tau] = S(\tau) - S(\rho), \tag{1.157}$$

where S denotes the von Neumann entropy and, because of how τ is defined, we have that $-\mathrm{Tr}[\rho\ln\tau] = -\mathrm{Tr}[\tau\ln\tau] = S(\tau)$. This term is the entropy of a Gaussian state and can be easily computed by finding the symplectic eigenvalues via (1.129).

This measure satisfies a series of quite useful properties [104]: it is additive under the tensor product operation, and invariant under symplectic transformations. We alternatively call this measure *relative entropy of non-Gaussianity*, because it can equivalently be defined as the relative entropy between the state under scrutiny and the whole *set* of Gaussian states [187], which means

$$\delta[\rho] = \min_{\rho_G}[S(\rho||\rho_G)] \,, \tag{1.158}$$

where ρ_G is a generic Gaussian state. We are going to comment more about this point of view in Chapter 8, after introducing resource theories.

Summary

- Quantum states are described by density operators acting on a Hilbert space. Observables are described by positive operator valued measures, a collection of positive operators summing to the identity. Deterministic evolutions are described by completely-positive trace preserving maps, while probabilistic (conditional) evolutions by completely positive trace non-increasing maps; a collection of such CP maps summing to a CPT map represents a quantum instrument, which gives both a POVM and the rule to update the quantum state after observing a certain outcome. Everything is consistent with the standard postulates of quantum mechanics by enlarging the Hilbert space and considering purifications.
- Under a Markovian approximation, the evolution of a quantum system in contact with an environment obeys a Lindblad master equation. This can be achieved by modelling the environment as a set of independent modes instantaneously interacting with the system and being discarded immediately afterwards. When the modes are measured instead of discarded the evolution of the principal system is described by a stochastic master equation. For photo-detection the evolution is governed by a jump-like Poisson process, for homodyne-detection by a diffusive Wiener process.
- When dealing with a probability distribution with a smooth dependence on a parameter, the classical Cramér-Rao bound gives the best precision of any unbiased estimator for the true value of the parameter. The figure of merit quantifying such precision is the Fisher information. By optimizing the FI of the probability coming from the Born rule over all possible POVMs we have the quantum Cramér-Rao bound, defined in terms of the quantum Fisher information, which depends only on the quantum state. In the asymptotic limit of a large number of experiments, both the classical and the quantum bounds can usually be saturated. An estimator which saturates them is the Bayesian estimator, i.e. the mean of the posterior distribution, given the observed data.
- Continuous variable quantum systems obey the canonical Heisenberg commutation relations and live in a infinite dimensional Hilbert space. They can be equivalently described as functions on the phase space, rather than operators. The class of Gaussian states and Gaussian operations is special because everything can be described in terms of finite-dimensional first-moments vectors and covariance matrices. Markovian conditional and unconditional dynamics can be recast in a simple form for Gaussian systems. Quantum continuous variable states can be nonclassical in different ways, the most important criteria are: not being mixtures of coherent states (P-nonclassicality) and having a negative Wigner function (W-nonclassicality); both notions can be numerically quantified. It also possible to quantify the non-Gaussianity of quantum states.

Part I

Quantum metrology with continuous measurements

CHAPTER 2

Quantum estimation with continously monitored systems

This chapter illustrates the conceptual framework needed to rigorously analyse the precision of quantum estimation with continuous measurements. We introduce and explain all the theoretical and numerical tools needed for Chapters 3 and 4, which are devoted to particular applications.

The content of the chapter is a mixture of existent results taken from the literature and new results, originally presented together with their applications in [12, 14]. The idea is to lay down a coherent and unified framework, clarifying the relationship between older and newer concepts.

2.1 Cramér-Rao bound for conditional quantum evolution

We believe it is more instructive to first introduce the relevant QET concepts more abstractly in terms of quantum channels and instruments. We leave the dynamical details about a proper continuous measurement scenario, described by stochastic master equations, at the end of the presentation.

Classical Fisher information in terms of conditional probabilities

We start by considering a classical estimation problem of a parameter λ described by a conditional probability over two random variables $p(z, y|\lambda)$. The corresponding Fisher information can be evaluated as

$$\begin{aligned}\mathcal{F}[p(z,y|\lambda)] &= \int dy\, dz\, p(z,y|\lambda)(\partial_\lambda \log p(z,y|\lambda))^2 \\ &= \int dy\, dz\, p(z|y,\lambda)p(y|\lambda)\Big[(\partial_\lambda \log p(z|y,\lambda))^2 + \\ &\qquad + 2(\partial_\lambda \log p(z|y,\lambda))\,(\partial_\lambda \log p(y|\lambda)) + (\partial_\lambda \log p(y|\lambda))^2\Big]\end{aligned} \tag{2.1}$$

where the second expression has been obtained by the identity $p(z, y|\lambda) = p(z|y, \lambda)p(y|\lambda)$. In the following, we omit the dependence on the parameter λ and we denote by $\mathbb{E}_{p(x)}[\cdot]$ the average over a probability distribution $p(x)$. By considering each term inside the

integral separately one obtains

$$\mathbb{E}_{p(z,y)}\Big[(\partial_\lambda \log p(z|y))^2\Big] = \mathbb{E}_{p(y)}[\mathcal{F}[p(z|y)]] \tag{2.2}$$

$$\mathbb{E}_{p(z,y)}[\partial_\lambda \log p(z|y)\, \partial_\lambda \log p(y)] = \int dy\, (\partial_\lambda p(y)) \int dz\, (\partial_\lambda p(z|y)) = 0 \tag{2.3}$$

$$\mathbb{E}_{p(z,y)}\Big[(\partial_\lambda \log p(y))^2\Big] = \mathcal{F}[p(y)] \tag{2.4}$$

where we have used the property $\int dz\, \partial_\lambda p(z|y) = \partial_\lambda \int dz\, p(z|y) = \partial_\lambda (1) = 0$. As a consequence, for any unbiased estimator $\hat{\lambda}$ built on M observations $\{(y_i, z_i)\}_{i=1}^M$, we can write the Cramér-Rao bound as follows:

$$\mathrm{Var}[\hat{\lambda}] \geq \frac{1}{M\Big(\mathcal{F}[p(y|\lambda)] + \mathbb{E}_{p(y)}[\mathcal{F}[p(z|y,\lambda)]]\Big)}\ ; \tag{2.5}$$

the first term at the denominator $\mathcal{F}[p(y|\lambda)]$ is the Fisher information corresponding to a measurement with outcomes y, while the second term is the average of the Fisher information $\mathcal{F}[p(z|y,\lambda)]$ for measurement of x conditioned upon the observation of y.

The bound in Eq. (2.5) is rather general and formally identical to the Bayesian Cramér-Rao bound [283] (Van Trees inequality). The Bayesian inequality is obtained via the substitutions $p(y|\lambda) \to p(\lambda)$ and $p(z|y,\lambda) \to p(z|\lambda)$, i.e. there is only one observed variable x, but the parameter to be estimated λ is also a random variable. This situation is conceptually very different, because in our case we are able to observe the variable y, while in the Bayesian approach the distribution $p(\lambda)$ cannot be sampled directly (for this reason its fundamental meaning is very debated).

For the following discussion it is useful to think about the conditioning of probabilities in temporal terms. We consider a scenario where the random variable y is the result of some initial measurement, while the variable z represents a final measurement, which is thus conditioned by the previously observed outcome y.

2.1.1 Effective quantum Fisher information

We can now connect the classical result of the previous section to a quantum measurement model. In what follows we consider a *selective* quantum evolution, which is formally expressed by a quantum instrument, introduced in Section 1.1.2.

Let us consider a quantum state ρ_0 which undergoes a selective evolution, represented by a quantum instrument, i.e. a collection of CP trace non-increasing maps $\left\{\mathcal{E}_y^{(\lambda)}\right\}$ labeled by the variable y, with the associated unconditional trace-preserving map $\mathcal{E}_{\mathrm{unc}}^{(\lambda)} = \sum_y \mathcal{E}_y^{(\lambda)}$. The superscript indicates that the maps depend on the parameter λ.

We can think about this evolution as a non-destructive measurement, such that we have access both to the measurement outcomes y and to the post-measurement states, which we define as in Section 1.1.2:

$$\rho_{y|\lambda} \cdot p(y|\lambda) = \tilde{\rho}_{y|\lambda} = \mathcal{E}_y^{(\lambda)}[\rho_0] \quad \text{with} \quad p(y|\lambda) = \mathrm{Tr}\Big[\tilde{\rho}_{y|\lambda}\Big], \tag{2.6}$$

We call the states $\rho_{\mu|\lambda}$ the *conditional* states, while we denote the *unconditonal* state obtained by discarding the measurement outcomes, i.e. the average state, as

$$\rho_{\mathrm{unc},\lambda} = \mathcal{E}^{(\lambda)}_{\mathrm{unc}}[\rho_0] = \sum_y \mathcal{E}^{(\lambda)}_y[\rho_0] = \sum_y \tilde{\rho}_{\mu|\lambda} = \sum_y p(y|\lambda)\rho_{\mu|\lambda} \,. \tag{2.7}$$

We want to perform another measurement on the conditional states $\rho_{y|\lambda}$, but for this last measurement we only need a description in terms of POVMs, since we are not interested the evolution of the system *after* measuring it. In many cases this final measurement can correspond to a *destructive* measurement which actually destroys the system under investigation.

In general one may choose a different POVM $\left\{\hat{\pi}_{z|y}\right\}_{z\in\mathcal{Z}}$ for each outcome y of the first instrument. However, we assume that the set of outcomes $\mathcal{Z}$ is the same for each of these POVMs. As customary, we also assume that the POVM operators $\hat{\pi}_{z|y}$ do not depend on the parameter λ.

After performing the final measurement the joint distribution of (y,z) and the conditional distribution can be easily obtained as

$$\begin{aligned} p(z|y,\lambda) &= \mathrm{Tr}[\rho_{y|\lambda}\hat{\pi}_{z|y}] \,, \\ p(z,y|\lambda) &= p(z|y,\lambda)\, p(y|\lambda) = \mathrm{Tr}[\tilde{\mathcal{E}}^{(\lambda)}_y[\rho_0]\hat{\pi}_{z|y}] \,. \end{aligned} \tag{2.8}$$

It should be clear that we are exactly in the situation considered in the previous section and thus the Cramér-Rao bound can written as in (2.5).

Now we consider the maps $\tilde{\mathcal{E}}^{(\lambda)}_y$ as fixed, but we suppose to be able to optimize over *each one* of the final measurements $\{\hat{\pi}_{z|y}\}$. We can then apply the quantum Cramér-Rao bound (1.65) to the conditional states $\rho_{y|\lambda}$, stating that $\mathcal{F}[p(z|y,\lambda)] \leq \mathcal{Q}[\rho_{y|\lambda}]$. The result is a more fundamental quantum Cramér-Rao bound for estimation strategies where the parameter is encoded by this kind of evolutions:

$$\mathrm{Var}(\hat{\lambda}) \geq \frac{1}{M\Big(\mathcal{F}[p(y|\lambda)] + \mathbb{E}_{p(y|\lambda)}\Big[\mathcal{Q}[\rho_{y|\lambda}]\Big]\Big)} \,. \tag{2.9}$$

Two important remarks are in order. First, by optimizing the FI of each conditional state independently, we are assuming that such states can only be accessed one at a time. We call this a *sequential* evolution and we have in mind a temporal description where the conditional states are generated sequentially one after the other. In some other situations it could be possible to retain the global state $\bigotimes_y \rho_{y|\lambda}$ (or part of it) and perform a joint measurement on it.

Second, while in the classical case the expression is at least formally identical to the Van-Trees inequality, in the quantum case the situation is quite different. As a matter of fact, the optimal measurement on each conditional state in general depends on the observed outcome y, this amounts to knowing what is the conditional state before measuring it. From a Bayesian perspective it is not possible to know in advance the state that is going to be measured and therefore the optimization problem is much harder, see [188] for a recent discussion.

In the following we refer to the precision achievable by the bound in Eq. (2.9) with a figure of merit that we dub *effective* QFI [12], denoted by a tilde

$$\tilde{\mathcal{Q}}[\rho_0] = \sum_y p(y|\lambda)\mathcal{Q}\left[\rho_{y|\lambda}\right] + \mathcal{F}[p(y|\lambda)]\,; \tag{2.10}$$

we repeat again that this figure of merit is optimized on all the possible final POVMs, but is obtained for a fixed initial state ρ_0 as well as a fixed quantum instrument encoding the parameter. This quantity has been considered a number of times, in different contexts [48, 60, 261].

In particular, the effective QFI (2.10) is equal to the ordinary QFI of the following state [261]:

$$\rho = \sum_y p(y|\lambda)\rho_{y|\lambda} \otimes |y\rangle\langle y|, \tag{2.11}$$

where we introduced an ancillary Hilbert space with a set of orthonormal vectors labelled by the outcomes y, so that each conditional state lives in an orthogonal subspace.

The unconditional state given by (2.7) is a mixture of all the conditional states with weights $p(y|\lambda)$. Hence, the extended convexity [16, 206] of the QFI (1.83) implies that the QFI of the unconditional state is never greater than the effective QFI given by these sequential strategy: $\mathcal{Q}[\rho_{\text{unc},\lambda}] \leq \tilde{\mathcal{Q}}[\rho_0]$. This result is both important and intuitive: having access to the measurement outcomes is never worse than discarding them and considering only the average conditional state.

This last inequality can be understood also from the monotonicity of the QFI [231]; the argument goes as follows. The unconditional state (2.7) is obtained from the state (2.11) by partial tracing over the ancillary Hilbert space. Since the partial trace is a CPT map (from operators acting in a Hilbert space to operators acting on a reduced Hilbert space), the monotonicity of the QFI under CPT maps guarantees the result.

2.1.2 Application to continuous measurements

The estimation strategy we described so far is of particular interest when we deal with continuously monitored quantum systems.

It is possible to apply what we presented in the previous section, by considering that the evolution is not conditioned on the value of some random variable y, but on the realization of some stochastic process. Roughly speaking, the photocurrent $I(t)$ for homodyne detection represents the outcome of a measurement, even if this outcome is not instantaneous but continuous in time. The same is true for photo-detection, where the outcome is represented by the list of times at which all the photo-detections occurred, i.e. the times of the jumps in the stochastic process $N(t)$. In Sec. 2.2.1 we are going to see that to each nonlinear stochastic master equation corresponds a linear SME for the unnormalized conditional state, which plays the role of the CP trace non-increasing maps in the definition of quantum instrument.

We can more easily see the comparison if we subdivide the time interval $[0, T]$ of the conditional evolution into discrete time intervals Δt. The output photocurrent $I(t)dt$ becomes a finite vector of random variables y_j, where the index $j = 0, \ldots, N$ corresponds

to the time $t_j = j\Delta t$, so that $T = t_N = N\Delta t$. In the case of homodyne measurements y_j are real random variables, while for photo-detection they are binary random variables. We can collect the whole sequence of random variables in a vector $\boldsymbol{y}_T$, which corresponds to the realization of the stochastic process in the limit $\Delta t \to 0$.

The evolution is *sequential* and we can associate each measurement outcome y_k to a CP trace non-increasing map $\tilde{\mathcal{E}}_{y_k}$. The total evolution is given by the sequential application of those CP maps: $\tilde{\mathcal{E}}_{\boldsymbol{y}_T} = \tilde{\mathcal{E}}_{y_N} \circ \tilde{\mathcal{E}}_{y_{N-1}} \circ \cdots \circ \tilde{\mathcal{E}}_{y_2} \circ \tilde{\mathcal{E}}_{y_1}$ For the system initially prepared in a state ρ_0, after obtaining the stream of outcomes $\boldsymbol{y}_T$ the conditional state reads

$$\rho^{(c)}_{\boldsymbol{y}_T} = \frac{\tilde{\mathcal{E}}_{\boldsymbol{y}_T}[\rho_0]}{\mathrm{Tr}\big[\tilde{\mathcal{E}}_{\boldsymbol{y}_T}[\rho_0]\big]}\,. \tag{2.12}$$

where the probability of obtaining the outcomes $\boldsymbol{y}_T$ is $p(\boldsymbol{y}_T|\lambda) = \mathrm{Tr}\big[\tilde{\mathcal{E}}_{\boldsymbol{y}_T}[\rho_0]\big]$. The *strong* (destructive) measurement at the end of the evolution is described by POVM operators $\{\hat{\pi}_z\}$ on the conditional state, and the whole measurement strategy is described by the conditional probabilities

$$\begin{aligned} p(z|\boldsymbol{y}_T,\lambda) &= \mathrm{Tr}[\rho_{\boldsymbol{y}_T}\hat{\pi}_z]\,, \\ p(z,\boldsymbol{y}_T|\lambda) &= p(z|\boldsymbol{y}_T,\lambda)\,p(\boldsymbol{y}_T|\lambda) = \mathrm{Tr}\big[\tilde{\mathcal{E}}_{\boldsymbol{y}_T}[\rho_0]\hat{\pi}_z\big] \end{aligned} \tag{2.13}$$

Obviously, this is identical to the previous case and the Cramér-Rao bound (2.9) holds. In this case it can be written as

$$\mathrm{Var}_{\hat{\lambda}}(\lambda) \geq \frac{1}{M\Big(\mathcal{F}[p(\boldsymbol{y}_T)] + \mathbb{E}_{p(\boldsymbol{y}_T)}\big[\mathcal{Q}[\rho_{\boldsymbol{y}_T}]\big]\Big)}\,. \tag{2.14}$$

Clearly, this bound can be readily applied to the time-continuous case in the limit $\Delta t \to 0$, when $\boldsymbol{y}_T$ becomes a continuous stochastic process. Intuitively, we can write the effective QFI for continuous measurements as

$$\widetilde{\mathcal{Q}}_{\mathrm{unr}} = \mathcal{F}[p_{\mathsf{traj}}] + \sum_{\mathsf{traj}} p_{\mathsf{traj}}\,\mathcal{Q}[\rho^{(c)}]\,, \tag{2.15}$$

where we also stress out this quantity depends on the choice of the unravelling, i.e. how the environmental modes are measured. In what follows we only consider photo-detection and homodyne detection, but more general strategies can be employed.

In Section 2.2 we explain a clever method to compute the classical Fisher information of the probability distribution of the trajectories. Building up on those ideas, in Section 2.3 we are going to present a stable numerical method to efficiently compute not only the classical FI, but the whole effective QFI for continuously monitored systems.

2.2 Fisher information for continuous measurements

In Section 2.2.1 we show that to any nonlinear stochastic master equation for the density operator we can associate a class of *linear* stochastic equations for the unnormalized state. The trace of the unnormalized state is proportional to the probability of obtaining the trajectory. Solutions of the linear SME are often called linear quantum trajectories.

The idea to use this method of linear trajectories for statistical inference on the parameters governing the dynamics has been very fruitful and dates back at least to [177]. More recently, Gammelmark and Mølmer [92] have shown how to derive an additional stochastic equation to handily compute the the Fisher information $\mathcal{F}[p_{\text{traj}}]$. This result is going to be fundamental for the following chapters and it is presented in Section 2.2.2.

2.2.1 Linear quantum trajectories

We have seen that the evolution of a quantum system conditioned on a certain measurement outcome is given by a trace non-increasing linear CP map. On the other hand, the map which gives the *normalized* conditional state is non-linear, because of the renormalization. Analogously, it is possible to derive *linear* stochastic master equations describing the evolution of the unnormalized conditional state [296].

In the stochastic master equations (1.44) for photo-detection the nonlinear terms are due to the scalar coefficient $\text{Tr}\left[\hat{c}^\dagger \hat{c} \rho^{(c)}\right]$, which is related to the Poisson process representing the measurement outcomes as $\mathbb{E}[dN_t] = \gamma \text{Tr}\left[\hat{c}^\dagger \hat{c} \rho^{(c)}\right] dt$. If we perform the substitution $\text{Tr}\left[\hat{c}^\dagger \hat{c} \rho^{(c)}\right] \to \beta$ for any $\beta > 0$ we get the following linear equation

$$d\tilde{\rho}^{(c)} = \left(-i\left[\hat{H}, \tilde{\rho}^{(c)}\right] - \frac{\gamma}{2}\left\{\hat{c}^\dagger \hat{c}, \tilde{\rho}^{(c)}\right\} + \beta\gamma\tilde{\rho}^{(c)}\right)dt + \left(\frac{\hat{c}\tilde{\rho}^{(c)}\hat{c}^\dagger}{\beta} - \tilde{\rho}^{(c)}\right)dN_t \,, \tag{2.16}$$

where now the Poisson process dN_t satisfies $\mathbb{E}_{p_{\text{ost}}}[dN_t] = \beta\gamma dt$ (the meaning of the probability p_{ost} will be explained in a few lines). It is straight-forward to see that (2.16) generates the correct unconditional Lindblad master equation for any value of β.

In order to have both a linear equation and to reproduce the correct Lindblad dynamics when averaged, the probability of the Poisson increments must be independent from the norm of the state. Therefore the resulting Poisson process $dN(t)$ does not represents the true observed record of photo-detections, but it is distributed according to a reference probability distribution p_{ost}.[1] The *true* probability of a photo-detection, obtained by solving the normalized SME, is proportional to the trace of the unnormalized state and the proportionality constant is exactly the reference probability p_{ost} [92]:

$$p_{\text{true}}(dN_t) = p_{\text{ost}}(dN_t)\text{Tr}\left[\tilde{\rho}^{(c)}(t)\right] \,. \tag{2.17}$$

Everything is consistent: when we choose $\beta = \text{Tr}\left[\hat{c}^\dagger \hat{c} \rho^{(c)}\right]$ the trace has value 1 and $p_{\text{ost}} = p_{\text{true}}$. Usually it is convenient to simply set $\beta = 1$ to solve the equation.

The situation is analogous for homodyne detection, where we can apply the substitution $\text{Tr}\left[(\hat{c} + \hat{c}^\dagger)\rho^{(c)}\right] \to \mu$ and get the linear equation

$$d\tilde{\rho}^{(c)} = \left(-i\left[\hat{H}, \tilde{\rho}^{(c)}\right] + \mathcal{D}[c]\tilde{\rho}^{(c)}\right)dt + \left(\hat{c}\tilde{\rho}^{(c)} + \tilde{\rho}^{(c)}\hat{c}^\dagger - \mu\tilde{\rho}^{(c)}\right)(dy_t - \mu dt) \,, \tag{2.18}$$

[1] The superscript "ost" stands for ostensible probability, the name introduced by Wiseman [296, 298], we find more clear to call it a reference probability, in accordance to [92].

where dy_t now must be considered as a stochastic increment with mean value μ and variance dt, i.e. $dy_t = \mu dt + dw_t$. Again, it is straight-forward to see that the averaged equation reproduces the Lindblad master equation for any $\mu \in \mathbb{R}$. Similarly to the previous case, the probability density of the true observed increment is proportional to the trace of $\tilde{\rho}^{(c)}$:

$$p_{\text{true}}(dy_t) = p_{\text{ost}}(dy_t)\text{Tr}\left[\tilde{\rho}^{(c)}(t)\right] , \tag{2.19}$$

where now p_{ost} is the Gaussian distribution of a stochastic increment with variance dt and mean μdt. By setting $\mu = \text{Tr}\left[(\hat{c} + \hat{c}^\dagger)\rho^{(c)}\right]$ we get back the nonlinear equation and the stochastic process has the correct statistics, i.e. again we have $p_{\text{ost}} = p_{\text{true}}$. Usually, it is convenient to choose $\mu = 0$, so that dy_t corresponds to a standard Wiener increment when solving the linear equation.

From this discussion we can conclude that the probability of observing a trajectory is *not equal* to the trace of the corresponding unnormalized operator $\tilde{\rho}^{(c)}(t)$ obtained by solving the linear SME, but only proportional to it. The important thing to remember is that all the dependence on parameters characterizing the dynamics is contained in $\text{Tr}\left[\tilde{\rho}^{(c)}(t)\right]$. It follows that for all statistical inference applications, such as estimation or hypothesis testing, the quantity $\text{Tr}\left[\tilde{\rho}^{(c)}(t)\right]$ still represents a valid likelihood function. If one is interested only in relative changes when a parameter λ is varied, then the proportionality factor, which is dependent on the outcomes but not on the parameter, is not important.

For the FI this invariance property is clear because any multiplicative constant not depending on the parameter λ is killed by the partial derivative ∂_λ in the definition. Since we are only interested in the unnormalized state to obtain the FI, from now on we forget about the reference probability and by abusing the notation we simply consider $p_{\text{traj}} = \text{Tr}\left[\tilde{\rho}^{(c)}_\lambda(t)\right]$.

2.2.2 Stochastic equation for the Fisher information

In order to obtain the FI pertaining to a continuous measurement one has to compute the following quantity

$$\mathcal{F}[p_{\text{traj}}] = \mathbb{E}_{\text{traj}}\left[\frac{(\partial_\lambda p_{\text{traj}})^2}{p_{\text{traj}}^2}\right] = \sum_{\text{traj}} \frac{(\partial_\lambda p_{\text{traj}})^2}{p_{\text{traj}}} , \tag{2.20}$$

where again p_{traj} informally represents the probability distribution of the trajectories.

In some situations it is possible to obtain analytical expressions both for p_{traj} and the conditional states [145], but in general it is a hard task. However, by simulating numerically the nonlinear SME one can generate trajectories distributed according to p_{traj}. A straight-forward approach to compute this kind of expectation values is a crude Monte-Carlo: the quantity of interest is evaluated for a randomly generated trajectory and this step is repeated a sufficiently high number of times, then all the values are summed up and the is total divided by the number of generated trajectories. We will show that it is possible to obtain the FI by employing this Monte-Carlo approach.

The starting point to make the computation more manageable it to define an operator τ as follows [92]

$$\tau = \frac{\partial_\lambda \tilde{\rho}^{(c)}}{\mathrm{Tr}[\tilde{\rho}^{(c)}]}\,, \tag{2.21}$$

then the FI can be written as the expectation value over the trajectories of this operator

$$\mathcal{F}[p_{\mathrm{traj}}] = \mathbb{E}\Big[\mathrm{Tr}[\tau]^2\Big]\,, \tag{2.22}$$

since we explained that $p_{\mathrm{traj}} = \mathrm{Tr}\Big[\tilde{\rho}^{(c)}\Big]$.

Interestingly, it is possible to write down a stochastic equation for the operator τ which involves only the operator τ itself and the normalized operator $\rho^{(c)}$. From a numerical point of view this is very convenient, because those matrices are well-behaved and do not become vanishingly small as it happens with $\tilde{\rho}^{(c)}$.

Concretely, let us write the equation for τ in the case of photo-detection:

$$\begin{aligned} d\tau = &\left(-i\big[\hat{H},\tau\big] - \frac{1}{2}\Big\{\hat{c}^\dagger\hat{c},\tau\Big\} + \mathrm{Tr}\Big[\hat{c}^\dagger\hat{c}\rho^{(c)}\Big]\tau - i\Big[(\partial_\lambda\hat{H}),\rho^{(c)}\Big] - \frac{1}{2}\Big\{\partial_\lambda(\hat{c}^\dagger\hat{c}),\rho^{(c)}\Big\}\right)dt + \\ &+ \Big(\hat{c}\tau\hat{c}^\dagger + (\partial_\lambda\hat{c})\rho^{(c)} + \rho^{(c)}(\partial_\lambda\hat{c}^\dagger) - \tau\Big)dN_t\,; \end{aligned} \tag{2.23}$$

this expression can be obtained directly from Eq. (2.16). This equation needs to be solved together with the nonlinear SMEs (1.44) for $\rho^{(c)}$ and the sampled valued of dN_t must coincide in both equations to obtain meaningful results.

The same thing can be done for the diffusive SME, starting from Eq. (2.18); eventually we get to the following dynamical equation for τ:

$$\begin{aligned} d\tau = &\Big\{-i\big[\hat{H},\tau\big] + \mathcal{D}[\hat{c}]\tau + i\Big[(\partial_\lambda\hat{H}),\rho^{(c)}\Big] + (\partial_\lambda\mathcal{D})[\hat{c}]\rho^{(c)}\Big\}dt + \\ &+ \Big\{\mathcal{M}[\hat{c}]\tau + (\partial_\lambda\mathcal{M})[\hat{c}]\rho^{(c)} - \mathrm{Tr}\Big[\mathcal{M}[\hat{c}]\rho^{(c)}\Big]\tau\Big\}dy_t\,, \end{aligned} \tag{2.24}$$

where some additional superoperators have been introduced, defined as follows

$$(\partial_\lambda\mathcal{D})[\hat{c}]\bullet = \partial_\lambda\hat{c}\,\bullet\,c^\dagger + \hat{c}\,\bullet\,(\partial_\lambda\hat{c}^\dagger) - \frac{1}{2}\Big\{\partial_\lambda(\hat{c}\hat{c}^\dagger),\bullet\Big\} \tag{2.25}$$

$$\mathcal{M}[\hat{c}]\bullet = \hat{c}\,\bullet + \bullet\,\hat{c}^\dagger \qquad (\partial_\lambda\mathcal{M})[\hat{c}]\bullet = (\partial_\lambda\hat{c})\,\bullet + \bullet\,(\partial_\lambda\hat{c}^\dagger)\,. \tag{2.26}$$

Also in this case, one needs to solve (2.24) together with the respective SME (1.56), being careful to use the same generated increments dy_t for both.

In Section 2.3 we present an alternative and more convenient way to compute the evolution of τ numerically. Before discussing the numerical algorithm we show how to adapt this scheme to the realm of Gaussian states and linear dynamics, where it is easier to obtain analytical results.

2.2.3 Gaussian case

The classical Fisher information obtained by a Gaussian measurement continuous in time can be computed in a more efficient way; this result has been presented in [96]. The stochastic dynamics for Gaussian systems is described in Subsection 1.4.3 and it is particularly simple, since the evolution of the covariance matrix is always deterministic.

Let us consider the Gaussian distribution (1.125) describing the outcomes $\boldsymbol{r}_m$ of a general-dyne measurement on the environment at time $t + dt$. This distribution is a Gaussian with covariance matrix $\Sigma = \sigma_m + \sigma_{\text{in}}$ and first moments $\bar{\boldsymbol{r}}_m = \Omega C^{\mathsf{T}} \boldsymbol{r}_t \sqrt{dt}$, where $\boldsymbol{r}_t$ is the vector of first moments of the system. The FI of a parameter encoded in the first moments of Gaussian distribution has the following expression

$$\mathcal{F}[p(\boldsymbol{r}_m|\lambda)] = (\partial_\lambda \bar{\boldsymbol{r}}_m)^{\mathsf{T}} \Sigma^{-1} (\partial_\lambda \bar{\boldsymbol{r}}_m) \,, \tag{2.27}$$

which is easy to check by directly applying the definition of FI.

By applying this formula for the FI to the distribution of the outcomes (1.125) we get the infinitesimal FI for a single trajectory

$$d\mathcal{F}_t^{\text{traj}} = 2(\partial_\lambda \boldsymbol{r}_t)^{\mathsf{T}} C\Omega^{\mathsf{T}} (\sigma_m + \sigma_{\text{in}})^{-1} \Omega C^{\mathsf{T}} (\partial_\lambda \boldsymbol{r}_t) dt \,. \tag{2.28}$$

The dependence of this quantity on the particular trajectory is contained in the vector $\partial_\lambda \boldsymbol{r}_t$ which has a stochastic evolution. The evolution of the vector $\partial_\lambda \boldsymbol{r}_t$ can be computed by partial derivation of Eqs. (1.151) and (1.152), the final result is given by

$$\begin{aligned} d(\partial_\lambda \boldsymbol{r}_t) =& (\partial_\lambda A)\boldsymbol{r}_t \, dt + A(\partial_\lambda \boldsymbol{r}_t) \, dt + (\partial_\lambda \boldsymbol{u}) \, dt + (\sigma_t + N) B^{\mathsf{T}} (\partial_\lambda \boldsymbol{r}_t) dt \\ &+ \frac{(\partial_\lambda \sigma_t) B}{\sqrt{2}} d\boldsymbol{w} \end{aligned} \tag{2.29}$$

$$\begin{aligned} \frac{d(\partial_\lambda \sigma_t)}{dt} =& (\partial_\lambda A)\sigma_t + \sigma_t (\partial_\lambda A)^{\mathsf{T}} + A(\partial_\lambda \sigma_t) + (\partial_\lambda \sigma_t) A^{\mathsf{T}} \\ &- (\partial_\lambda \sigma_t) B (\sigma_t B + N)^{\mathsf{T}} - [(\partial_\lambda \sigma_t) B]^{\mathsf{T}} \end{aligned} \tag{2.30}$$

In computing the above equations it is important to keep in mind that, even though the vector of Wiener increments $d\boldsymbol{w}$ represents the stochastic part of the evolution, the actual measurement outcome is $\boldsymbol{r}_m$ and therefore $\partial_\lambda \boldsymbol{r}_m = 0$ because the outcomes must be considered as fixed quantities given by the experiment. On the other hand the derivative of the Wiener increment is not zero [97]; from the definition (1.149) we get $\partial_\lambda d\boldsymbol{w} = \sqrt{2} B^{\mathsf{T}} (\partial_\lambda \boldsymbol{r}_t) dt$.

The FI at time $t + dt$ can then be found by averaging over all possible outcomes

$$d\mathcal{F}_t = \mathbb{E}_{p(\boldsymbol{r}_m|\lambda)} \left[d\mathcal{F}_t^{\text{traj}} \right] . \tag{2.31}$$

Since all the observations at every infinitesimal time step are independent, we can exploit the additive property of the FI and the total FI for the whole measurement current is obtained by integration

$$\mathcal{F}\left[p_{\text{traj}}\right] = \int_{t'=0}^{t} d\mathcal{F}_{t'} \,. \tag{2.32}$$

2.3 Efficient numerical implementation

In this section we present the ideas behind the numerical implementation of an algorithm to compute the effective QFI. This method was introduced in [14] where it is also applied to a particular problem, presented in Chapter 4. In this presentation we consider a single a parameter appearing only in the Hamiltonian and not in the collapse operators.

At variance to what we have done in Section 1.2, we now consider SME with N collapse operators; conceptually it is not very different from the simple case $N = 1$. One has to consider N independent input modes $\hat{b}_{\text{in}}^{(j)}(t)$, one for each noise operator $\hat{c}_j$, that satisfy the commutation relations (1.32), i.e. $[\hat{b}_{\text{in}}^{(j)}(t), \hat{b}_{\text{in}}^{(k)\dagger}(t')] = \delta_{jk}\delta(t-t')$.

The stochastic master equation corresponds to the physical situation in which each output mode is measured by a separate photodetector, with efficiency η_j:

$$d\rho^{(c)} = -i[\hat{H}, \rho^{(c)}]dt + \sum_j \left((1-\eta_j)\mathcal{D}[\hat{c}_j]\varrho^{(c)} - \frac{\eta_j}{2}(\hat{c}_j^\dagger \hat{c}_j \rho^{(c)} + \rho^{(c)}\hat{c}_j^\dagger \hat{c}_j) + \eta_j \mathrm{Tr}[\rho^{(c)}\hat{c}_j^\dagger \hat{c}_j]\rho^{(c)} \right) dt$$
$$+ \sum_j \left(\frac{\hat{c}_j \rho^{(c)} \hat{c}_j^\dagger}{\mathrm{Tr}[\rho^{(c)}\hat{c}_j^\dagger c_j]} - \rho^{(c)} \right) dN_j \,, \tag{2.33}$$

instead of a single Poisson process there are N processes, the average value of each process is $\mathbb{E}[dN_j] = \eta_j \mathrm{Tr}[\hat{c}_j^\dagger \hat{c}_j \rho^{(c)}]\, dt$.

Likewise, for time-continuous homodyne detection on each output, the stochastic master equation reads

$$d\rho^{(c)} = -i[\hat{H}, \rho^{(c)}]\, dt + \sum_j \mathcal{D}[\hat{c}_j]\rho^{(c)}\, dt + \sum_j \sqrt{\eta_j}\mathcal{H}[\hat{c}_j]\rho^{(c)}\, dw_j \,, \tag{2.34}$$

where $dw_j = dy_j - \sqrt{\eta_j}\mathrm{Tr}[\varrho^{(c)}(\hat{c}_j + \hat{c}_j^\dagger)]$ represent independent Wiener increments (satisfying $dw_j dw_k = \delta_{jk} dt$).

2.3.1 Completely positive infinitesimal evolution

The most natural approach for solving SMEs is to write down a system of coupled stochastic differential equations for the matrix elements of the density operator and then use existing numerical methods. It might also be useful to consider the Bloch form of the equation, obtained by expanding the density matrix on a basis of Hermitian operators, instead of the matrix elements in the canonical basis, so that all the coefficients are real. Unfortunately, due to the stochastic nature of the problem there is no guarantee that the evolved state is always perfectly positive, even when using rather advanced numerical methods. In particular, such instabilities appear to seriously undermine the computation of the effective QFI [98].

For these reasons it is very useful to employ a numerical method that completely preserves the positivity of the conditional state. In this way it is also possible to get sensible results without the need of advanced numerical solvers. The approach that we present was introduced by Rouchon and Ralph [245]; their aim was to achieve stability

and speed, in order to enable *real-time* tracking of monitored systems during actual experiments.

The main insight of this method is to notice that the evolution of the conditional state in an infinitesimal time step dt can always be written as the action of a CP map. This point of view comes naturally from the perspective of quantum instruments and we have already shown that we can model each infinitesimal evolution with Kraus operators for photo-detection, see Eqs. (1.39) and (1.40).

In the case of a diffusive evolution the situation is less straight forward, however it turns out that we can write the infinitesimal evolution in this form

$$\rho^{(c)}_{t+dt} = \frac{\hat{M}_{\boldsymbol{dy}}\rho^{(c)}_t\hat{M}^\dagger_{\boldsymbol{dy}} + \sum_{j=1}^N(1-\eta_j)\hat{c}_j\rho^{(c)}_t\hat{c}^\dagger_j\,dt}{\mathrm{Tr}[\hat{M}_{\boldsymbol{dy}}\rho^{(c)}_t\hat{M}^\dagger_{\boldsymbol{dy}} + \sum_{j=1}^N(1-\eta_j)\hat{c}_j\rho^{(c)}_t\hat{c}^\dagger_j\,dt]}\,, \tag{2.35}$$

where we have explicitly put the time dependence of the density operators and we have defined the following Kraus operator

$$\hat{M}_{\boldsymbol{dy}} = \mathbb{1} - i\hat{H}_\lambda\,dt - \frac{1}{2}\sum_{j=1}^N\hat{c}^\dagger_j\hat{c}_j\,dt + \sum_{j=1}^N\sqrt{\eta}\hat{c}_j\,dy_j\,, \tag{2.36}$$

with $\boldsymbol{dy} = \{dy_j\}$ being a vector of measurement results, corresponding to each output channel,

$$dy_j = \sqrt{\eta_j}\,\mathrm{Tr}[\varrho^{(c)}_t(\hat{c}_j + \hat{c}^\dagger_j)]\,dt + dw_j. \tag{2.37}$$

Equation (2.35) can be used for numerical purposes by replacing the infinitesimal increment dt with a finite time step Δt, the Wiener increments dw_j are then replaced by Gaussian random variables Δw_j centered in zero and with variance equal to Δt. Moreover one can also implement the second order Euler-Milstein corrections. The (numerical) Kraus operators in this case read

$$\hat{M}_{\boldsymbol{\Delta y}} = \mathbb{1} - i\hat{H}_\omega\,\Delta t - \frac{1}{2}\sum_{j=1}^N\hat{c}^\dagger_j\hat{c}_j\,\Delta t + \sum_{j=1}^N\sqrt{\eta_j}\,\hat{c}_j\,\Delta y_j + \sum_{j,k}^N\frac{\eta}{2}\hat{c}_j\hat{c}_k(\Delta y_j\Delta y_k - \delta_{j,k}\Delta t)\,, \tag{2.38}$$

with

$$\Delta y_j = \sqrt{\eta_j}\,\mathrm{Tr}[\varrho^{(c)}_t(\hat{c}^\dagger_j + \hat{c}_j)]\,\Delta t + \Delta w_j\,, \tag{2.39}$$

denoting the (finite) increments of the measurement records.

One can appreciate that in the case of unit efficiency $\eta_j = 1$ the evolution is given by a single rank one Kraus operator, but when we have finite efficiency the map applied to $\rho^{(c)}_t$ is a CP map. As a matter of fact the numerator of (2.35) is in Kraus form, i.e. it is a sum of operators acting on the left with their conjugates acting on the right. Therefore, even for finite Δt the evolved state at $t + \Delta t$ is always positive.

For photodetection the Kraus operators in (1.35) and (1.36) are generalized as follows

$$\hat{M}_0 = \mathbb{1} - i\hat{H}\,dt - \frac{1}{2}\sum_j^N\hat{c}^\dagger_j\hat{c}_j\,dt\,, \tag{2.40}$$

$$\hat{M}_{1,j} = \sqrt{\eta_j}\hat{c}_j\,\sqrt{dt}\,, \tag{2.41}$$

where now we have one operator M_0 corresponding to the "no detector click" event and N different operators each corresponding to a click on a different detector. At each time step, each $\hat{M}_{1,j}$ has to be applied with probabilities $p_1^{(j)} = \eta_j \mathrm{Tr}[\rho_t^{(c)} \hat{c}_j^\dagger \hat{c}_j]\, dt$ and, correspondingly, the Kraus operator M_0 has to be applied with probability $p_0 = 1 - \sum_j p_1^{(j)}$. From a physical point of view, this update rule means that we are disregarding the possibility of two independent detections in the same infinitesimal time dt [298].

Even in this case the numerical algorithm is obtained by simply replacing dt with a finite Δt and the evolution applied at each step is a CP map preserving the positivity of the state.

2.3.2 Algorithm for the effective quantum Fisher information

In the following we are going to show how this approach can be applied to get an efficient and numerically stable calculation of both $\mathcal{F}[p_{\mathsf{traj}}]$ and $\mathcal{Q}[\rho^{(c)}]$. We are going to prove everything in terms of the "infinitesimal" Kraus operators, that have to be replaced by Eq. (2.38) when implementing the numerical algorithm. We start by showing the results for the most general case of SME and inefficient detection; we then describe the more efficient algorithm that can be implemented in the case of perfect detection ($\eta_j = 1$), i.e. when the dynamics can be described by a stochastic Schrödinger equation.

Non-unit efficiency detection (stochastic master equation)

We start by observing that the evolution of the unnormalized conditional state and of its derivative can be written in terms of the Kraus operators (we omit the superscript (c) used to denote conditional states):

$$\begin{aligned} \tilde{\rho}_{t+dt} &= \hat{M}_{\boldsymbol{dy}} \tilde{\rho}_t \hat{M}_{\boldsymbol{dy}}^\dagger + \sum_j (1-\eta_j) \hat{c}_j \tilde{\rho}_t \hat{c}_j^\dagger \, dt \,, \\ \partial_\lambda \tilde{\rho}_{t+dt} &= \hat{M}_{\boldsymbol{dy}} (\partial_\lambda \tilde{\rho}_t) \hat{M}_{\boldsymbol{dy}}^\dagger + (\partial_\lambda \hat{M}_{\boldsymbol{dy}}) \tilde{\rho}_t \hat{M}_{\boldsymbol{dy}}^\dagger + \hat{M}_{\boldsymbol{dy}} \tilde{\rho}_t (\partial_\lambda \hat{M}_{\boldsymbol{dy}}^\dagger) + \sum_j (1-\eta_j) \hat{c}_j (\partial_\lambda \tilde{\rho}_t) \hat{c}_j^\dagger \, dt \,, \end{aligned} \tag{2.42}$$

where $\partial_\lambda \hat{M}_{\boldsymbol{dy}} = -i(\partial_\lambda \hat{H}_\lambda)\, dt$, since we are considering an Hamiltonian parameter.

The trace of the unnormalized state reads

$$\begin{aligned} \mathrm{Tr}[\tilde{\rho}_{t+dt}] &= \mathrm{Tr}[\hat{M}_{\boldsymbol{dy}} \tilde{\rho}_t \hat{M}_{\boldsymbol{dy}}^\dagger + \sum_j (1-\eta_j) \hat{c}_j \tilde{\rho}_t \hat{c}_j^\dagger \, dt] \\ &= \mathrm{Tr}[\tilde{\rho}_t] \mathrm{Tr}[\hat{M}_{\boldsymbol{dy}} \rho_t \hat{M}_{\boldsymbol{dy}}^\dagger + \sum_j (1-\eta_j) \hat{c}_j \rho_t \hat{c}_j^\dagger \, dt] \,, \end{aligned} \tag{2.43}$$

where we have used the relation $\rho_t = \tilde{\rho}_t / \mathrm{Tr}[\tilde{\rho}_t]$. We can now use these formulas to obtain the evolution for the operator τ_{t+dt} just in terms of the operators ρ_t and τ_t at the previous time step:

$$\tau_{t+dt} = \frac{1}{\mathrm{Tr}[\tilde{\rho}_{t+dt}]}\left[(\partial_\lambda \hat{M}_{\boldsymbol{dy}})\tilde{\rho}_t \hat{M}^\dagger_{\boldsymbol{dy}} + \hat{M}_{\boldsymbol{dy}}(\partial_\lambda \tilde{\rho}_t)\hat{M}^\dagger_{\boldsymbol{dy}} + \hat{M}_{\boldsymbol{dy}}\tilde{\rho}_t(\partial_\lambda \hat{M}^\dagger_{\boldsymbol{dy}}) + \sum_j (1-\eta_j)\hat{c}_j(\partial_\lambda \tilde{\rho}_t)\hat{c}_j^\dagger\, dt\right]$$
$$= \frac{(\partial_\lambda \hat{M}_{\boldsymbol{dy}})\rho_t \hat{M}^\dagger_{\boldsymbol{dy}} + \hat{M}_{\boldsymbol{dy}}\tau_t \hat{M}^\dagger_{\boldsymbol{dy}} + \hat{M}_{\boldsymbol{dy}}\rho_t(\partial_\lambda \hat{M}^\dagger_{\boldsymbol{dy}}) + \sum_j (1-\eta_j)\hat{c}_j\tau_t\hat{c}_j^\dagger\, dt}{\mathrm{Tr}\left[\hat{M}_{\boldsymbol{dy}}\rho_t\hat{M}^\dagger_{\boldsymbol{dy}} + \sum_j(1-\eta_j)\hat{c}_j\rho_t\hat{c}_j^\dagger\, dt\right]}\,. \tag{2.44}$$

One can thus evaluate the trace of this operator at each time t, and evaluate accordingly the classical Fisher information $\mathcal{F}[p_{\mathrm{traj}}]$ as in Eq. (2.22).

Notice that the evolution for the derivative operator $\partial_\lambda \rho_t$ can now be written in terms of the renormalized operators ρ_t and τ_t:

$$\partial_\lambda \rho_t = \frac{\partial_\lambda \tilde{\rho}_t}{\mathrm{Tr}[\tilde{\rho}_t]} - \frac{\mathrm{Tr}[\partial_\lambda \tilde{\rho}_t]}{\mathrm{Tr}[\tilde{\rho}_t]^2}\tilde{\rho}_t = \tau_t - \mathrm{Tr}[\tau_t]\rho_t\,. \tag{2.45}$$

The QFI $\mathcal{Q}[\rho_t]$ can then be evaluated at each time t by numerically diagonalising the state and applying the generic formula for the QFI .

Let us review again the key features of this numerical method. The relevant figures of merit could naively be derived from the evolution of the unnormalized conditional state $\tilde{\rho}_t^{(c)}$, described in Eq. (2.42). However, $\mathrm{Tr}[\tilde{\rho}_t]$ becomes very small during the evolution, leading to numerical instabilities in the evaluation of $\mathcal{F}[p_{\mathrm{traj}}]$. Thanks to Eqs. (2.44) and (2.45) we can express all the quantities in terms of the numerically stable operators ϱ_t and τ_t. Besides, the formulation in terms of Kraus operators, following [244, 245], ensures that the density operator remains positive, as opposed to standard numerical integration of the SME.

Unit efficiency detection (stochastic Schrödinger equation)

The above calculations are greatly simplified when the dynamics starts with a pure initial state and the efficiency parameters are equal to one, $\eta_j = 1$. In this instance, the quantum conditional state $|\psi_t\rangle$ remains pure during the whole evolution and the dynamics is described by a stochastic Schrödinger equation. We can thus work with state vectors, instead of density matrices, with a consequent reduction of complexity of the numerical simulation, that allows to reach higher values of N with a given amount of memory.

In terms of Kraus operators, the unnormalized and normalized conditional states are obtained respectively as:

$$|\widetilde{\psi}_{t+dt}\rangle = \hat{M}_{\boldsymbol{dy}}|\widetilde{\psi}_t\rangle\,, \tag{2.46}$$

$$|\psi_{t+dt}\rangle = \frac{\hat{M}_{\boldsymbol{dy}}|\psi_t\rangle}{\sqrt{\langle\psi_t|M^\dagger_{\boldsymbol{dy}}M_{\boldsymbol{dy}}|\psi_t\rangle}} = \frac{\hat{M}_{\boldsymbol{dy}}|\widetilde{\psi}_t\rangle}{\sqrt{\langle\widetilde{\psi}_t|M^\dagger_{\boldsymbol{dy}}M_{\boldsymbol{dy}}|\widetilde{\psi}_t\rangle}}\,. \tag{2.47}$$

The operator τ_t in this case can be written as

$$\tau_t = \frac{\partial_\lambda(|\widetilde{\psi}_t\rangle\langle\widetilde{\psi}_t|)}{\langle\widetilde{\psi}_t|\widetilde{\psi}_t\rangle} = \frac{|\partial_\lambda\widetilde{\psi}_t\rangle\langle\widetilde{\psi}_t| + |\widetilde{\psi}_t\rangle\langle\partial_\lambda\widetilde{\psi}_t|}{\langle\widetilde{\psi}_t|\widetilde{\psi}_t\rangle}\,, \tag{2.48}$$

and its trace is equal to

$$\mathrm{Tr}[\tau_t] = \frac{\langle\widetilde{\psi}_t|\partial_\lambda\widetilde{\psi}_t\rangle + \mathrm{h.c.}}{\langle\widetilde{\psi}_t|\widetilde{\psi}_t\rangle} = \langle\psi_t|\phi_t\rangle + \langle\phi_t|\psi_t\rangle\,. \tag{2.49}$$

In the last equation we have introduced the vector

$$|\phi_t\rangle = \frac{|\partial_\lambda\widetilde{\psi}_t\rangle}{\sqrt{\langle\widetilde{\psi}_t|\widetilde{\psi}_t\rangle}}\,. \tag{2.50}$$

At time $t+dt$, the vector $|\phi_{t+dt}\rangle$ can be obtained as

$$|\phi_{t+dt}\rangle = \frac{(\partial_\lambda\hat{M}_{\boldsymbol{dy}})|\widetilde{\psi}_t\rangle + \hat{M}_{\boldsymbol{dy}}|\partial_\lambda\widetilde{\psi}_t\rangle}{\sqrt{\langle\widetilde{\psi}_t|\hat{M}^\dagger_{\boldsymbol{dy}}\hat{M}_{\boldsymbol{dy}}|\widetilde{\psi}_t\rangle}} = \frac{(\partial_\lambda\hat{M}_{\boldsymbol{dy}})|\psi_t\rangle + \hat{M}_{\boldsymbol{dy}}|\phi_t\rangle}{\sqrt{\langle\psi_t|\hat{M}^\dagger_{\boldsymbol{dy}}\hat{M}_{\boldsymbol{dy}}|\psi_t\rangle}}\,, \tag{2.51}$$

where we have exploited the identity $\langle\widetilde{\psi}_t|\hat{M}^\dagger_{\boldsymbol{dy}}\hat{M}_{\boldsymbol{dy}}|\widetilde{\psi}_t\rangle = \langle\widetilde{\psi}_t|\widetilde{\psi}_t\rangle\langle\psi_t|\hat{M}^\dagger_{\boldsymbol{dy}}\hat{M}_{\boldsymbol{dy}}|\psi_t\rangle$.

We notice that as in Eq. (2.44), the evolution equation for the vector $|\phi_{t+dt}\rangle$ depends only on the vectors $|\psi_t\rangle$ and $|\phi_t\rangle$ and not on the unnormalized state $|\widetilde{\psi}_t\rangle$, and one can readily evaluate the classical Fisher information in terms of these two vectors via Eqs. (2.49) and (2.22).

Concerning the QFI of the conditional state, we first observe that

$$|\partial_\lambda\psi_t\rangle = \frac{|\partial_\lambda\widetilde{\psi}_t\rangle}{\sqrt{\langle\widetilde{\psi}_t|\widetilde{\psi}_t\rangle}} - \frac{\langle\widetilde{\psi}_t|\partial_\lambda\widetilde{\psi}_t\rangle + \langle\partial_\lambda\widetilde{\psi}_t|\widetilde{\psi}_t\rangle|\widetilde{\psi}_t\rangle}{2\langle\widetilde{\psi}_t|\widetilde{\psi}_t\rangle^{3/2}} = |\phi_t\rangle - \frac{\langle\psi_t|\phi_t\rangle + \langle\phi_t|\psi_t\rangle}{2}|\psi_t\rangle\,. \tag{2.52}$$

As we are dealing with pure states, the QFI of the conditional state does not require a diagonalization and only boils down to computing the overlaps $\langle\partial_\lambda\psi_t|\partial_\lambda\psi_t\rangle$ and $\langle\partial_\lambda\psi_t|\psi_t\rangle$ as presribed by Eq. (1.84)

The algorithms above have been derived for the case of time-continuous homodyne detection, but they can readily be adapted to photo-detection replacing $\hat{M}_{\boldsymbol{dy}}$ at each time step with on of Kraus operators (2.40) and (2.41).

2.4 The fundamental quantum limit for continuous measurements

The estimation scheme we outlined in the previous section involves a conditional evolution of the system of interest and then a final measurement on it. The conditional evolution can be understood abstractly in terms of CP maps or dynamically in the case of continuous measurements, where the conditional state undergoes an evolution governed by some stochastic process. As we explained in Section 1.1.3 any quantum instrument can always be understood as the result of a unitary interaction of the main system with an ancillary one in a fixed pure state, which is then measured. For continuous measurements there is an infinite number of independent ancillary systems, each interacting with the main system for a vanishingly small time.

It is easy to understand that, by having access to a purification of the conditional evolution, more information can be retrieved. This condition can be hard to satisfy in practice, but from a theoretical perspective it allows us to derive a fundamental bound.

Another problem is that in the realistic case of continuous measurements the global state of system and environment after the interaction is a multipartite entangled state living in a exceedingly big Hilbert space, thus rendering a direct calculation quite hard. However, it is quite remarkable that, in the Markovian case we are considering, it is possible to have access to some properties of the global state by working in the reduced Hilbert space of the system and knowing only the unconditional dynamics of the system.

As far as an estimation problem is concerned, we are interested to obtain the QFI of the global state after the interaction. This quantity is optimized over all possible measurements on the global state, including non-separable measurements (i.e. projections on entangled states) over the system and all the output modes at different times. Even though in principle it could be possible to implement such measurements, e.g. by using delay lines or some kind of quantum memory, in general it is very hard to saturate the corresponding Cramér-Rao inequality. Nonetheless, we are going to show in Chapters 3 and 4 that, at least in some interesting cases, this ultimate bound can be saturated by a sequential estimation scheme, for which the precision is quantified by the effective QFI just introduced.

2.4.1 Ultimate quantum Fisher information

Let us see how to compute the QFI of the global state, as shown in [93, 178], see also [121]. The derivation of a computable formula is based on the assumption that the initial state of the system is pure. This assumption makes the result less general, but it is justified by the fact that the optimal state for estimation is pure, due to the convexity of the QFI.

Let us start from the Lindblad master equation governing the unconditional evolution, which was introduced in Section 1.2.1:

$$\frac{d\rho}{dt} = \mathcal{L}_\lambda \rho = -i\big[\hat{H}_\lambda, \rho\big] + \sum_i \mathcal{D}[\hat{c}_{i,\lambda}] \, ; \tag{2.53}$$

now we hilight the fact that both the system Hamiltonian and the collapse operators (which include also multiplicative numerical constants) can depend on a parameter λ.

For clarity we discretize time as done in the previous section and we consider the unitary evolution for an infinitesimal step dt (1.26) as acting for a finite time Δt. The unitary acting for each time step Δt is denoted ad $\hat{U}_{t_j} = \hat{U}(t_j, t_j + \Delta t)$. If the pure initial state of the system is $|\psi_0\rangle$, the global state of system and environment at the final time T can be written as

$$|\Psi_\lambda(T)\rangle = \hat{U}_{t_{N-1}} \dots \hat{U}_{t_0} \Big(|\psi_0\rangle \otimes |0\rangle_{t_0} \otimes \dots \otimes |0\rangle_{t_N} \Big) \, . \tag{2.54}$$

In the limit $\Delta t \to 0$, the partial trace over the environment of this global state gives the density matrix of system obtained by solving the master equation, i.e. $\mathrm{Tr}_{\mathrm{env}}[|\Psi_\lambda(T)\rangle\langle\Psi_\lambda(T)|] = e^{T\mathcal{L}_\lambda}|\psi_0\rangle\langle\psi_0|$.

In order to compute the QFI of the global state, the object we really need is the overlap for different values of the parameter λ, as per Eq. (1.90). We can in general always compute this overlap from an effective operator living in the system Hilbert space, because of the following identity

$$\langle\Psi_{\lambda_1}(T)|\Psi_{\lambda_2}(T)\rangle = \mathrm{Tr}_{\mathrm{syst,env}}\big[|\Psi_{\lambda_1}(T)\rangle\langle\Psi_{\lambda_2}(T)|\big] = \mathrm{Tr}_{\mathrm{syst}}\big[\bar{\rho}_{\lambda_1,\lambda_2}(T)\big] \, , \tag{2.55}$$

where $\bar{\rho}$ is an operator on $\mathcal{H}_{\text{syst}}$, which is neither normalized nor positive, since the overlap is a complex number.

Now the non-trivial fact: it is possible to write down an evolution equation for this operator $\bar{\rho}$, in terms of the operators entering in the Lindblad equation (2.53). This equation governing the evolution is still linear in $\bar{\rho}$, but different operators act on the left and on the right, we call it a *generalized* Lindblad master equation[2]:

$$\begin{aligned}\frac{d\bar{\rho}_{\lambda_1,\lambda_2}}{dt} &= \bar{\mathcal{L}}_{\lambda_1,\lambda_2}\bar{\rho}_{\lambda_1,\lambda_2} \;= \\ &= -i\hat{H}_{\lambda_1}\bar{\rho} + i\bar{\rho}\hat{H}_{\lambda_2} + \sum_i \hat{c}_{i,\lambda_1}\bar{\rho}\hat{c}^\dagger_{i,\lambda_2} - \frac{1}{2}\left(\hat{c}^\dagger_{i,\lambda_1}\hat{c}_{i,\lambda_1}\bar{\rho} + \bar{\rho}\hat{c}^\dagger_{i,\lambda_2}\hat{c}_{i,\lambda_2}\right),\end{aligned} \tag{2.56}$$

for readability we suppressed the dependence on time of the operator $\bar{\rho}$ and also on the parameters λ_1 and λ_2 in the second line. In the following applications we restrict ourselves to the estimation of a parameter in the Hamiltonian, so that Eq. (2.56) takes a simpler form:

$$\frac{d\bar{\rho}}{dt} = -i\big(\hat{H}_{\lambda_1}\bar{\rho} - \bar{\rho}\hat{H}_{\lambda_2}\big) + \sum_i \mathcal{D}[\hat{c}_i]\bar{\rho}\,; \tag{2.57}$$

however the results of this Chapter are valid in the more general setting.

The modified Lindbladian $\mathcal{L}_{\lambda_1,\lambda_2}$ is still a linear time-independent superoperator, thus the formal solution can be given by exponentiation as

$$\langle\Psi_{\lambda_1}(T)|\Psi_{\lambda_2}(T)\rangle = \text{Tr}_{\text{syst}}\left[e^{T\bar{\mathcal{L}}_{\lambda_1,\lambda_2}}|\psi_0\rangle\langle\psi_0|\right]; \tag{2.58}$$

the map $e^{T\mathcal{L}_{\lambda_1,\lambda_2}}$ is linear but neither trace-preserving nor positive.

Recalling the formula for the QFI (1.90) it is now trivial to write down the QFI of the global state. In the context of continuous measurements we call this quantity the *ultimate* QFI and it is denoted by a bar:

$$\overline{\mathcal{Q}}_{\mathcal{L}_\lambda} = 4\partial_{\lambda_1}\partial_{\lambda_2}\log|\text{Tr}[\bar{\rho}]|\,\Big|_{\lambda_1=\lambda_2=\lambda}, \tag{2.59}$$

we make the dependence on the Lindbladian explicit, to stress the difference from the effective QFI which depends also on the specific Markovian unravelling.

We thus can write the following chain of inequalities for the QFI of the unconditional state $\mathcal{Q}[\rho_{\text{unc}}]$, the effective QFI $\tilde{\mathcal{Q}}_{\text{unr}}$ (depending on the particular sequential measurement strategy) and the ultimate QFI $\overline{\mathcal{Q}}_{\mathcal{L}_\lambda}$:

$$\mathcal{Q}[\rho_{\text{unc}}] \leq \tilde{\mathcal{Q}}_{\text{unr}} \leq \overline{\mathcal{Q}}_{\mathcal{L}_\lambda}\,; \tag{2.60}$$

the first inequality is due to the extended convexity and the second is due to the very definition of the QFI as an optimization over all possible measurements.

The effective QFI also depends on the efficiency of the monitoring, indeed for $\eta_j = 0 \quad \forall j$ in Eqs. (2.33) and (2.34), we get back to the unconditional dynamics and thus

[2]Generalized master equations similar to (2.56) appear also in other contexts, such non-Markovian open quantum systems and full-counting statistics, see [139] and references therein.

$\widetilde{\mathcal{Q}}_{\mathsf{unr},\eta=0} = \mathcal{Q}[\rho_{\mathrm{unc}}]$. We conjecture that, for a fixed unravelling, and for fixed efficiency on all the output channels (i.e. for $\eta_j = \eta\ \forall j$), the effective QFI is monotonic with respect to the efficiency parameter, that is:

$$\widetilde{\mathcal{Q}}_{\mathsf{unr},\eta} \leq \widetilde{\mathcal{Q}}_{\mathsf{unr},\eta'} \quad \Longleftrightarrow \quad \eta \leq \eta' \qquad \text{(conjecture)}\,. \tag{2.61}$$

We are going to see that this conjecture is satisfied in all the examples we consider. Even though it is a rather intuitive statement, we are still lacking a general proof.

Simple derivation

The generalized master equation (2.56) can be derived in different ways, see [93, 178]. However, we want to present the more intuitive argument given in [198], where the overlap (2.55) is used for hypothesis testing.

Let us consider an additionally ancillary qubit so that the full Hamiltonian of system, environment and ancilla reads

$$\hat{H}_{\mathrm{ASE}} = (|0\rangle\langle 0|)_{\mathrm{A}} \otimes \hat{H}^{\lambda_1}_{\mathrm{int}}(t) + (|1\rangle\langle 1|)_{\mathrm{A}} \otimes \hat{H}^{\lambda_2}_{\mathrm{int}}(t)\,, \tag{2.62}$$

where the interaction Hamiltonian is the one considered in (1.20). We stress that the ancillary qubit is introduced as a theoretical construction to conveniently represent alternative values of the parameter. The initial pure state of ancilla, system and environment is $(|0\rangle_{\mathrm{A}} + |1\rangle_{\mathrm{A}})/\sqrt{2} \otimes |\Psi(t=0)\rangle$, where the joint system-environment state is given by (2.54); it is initially factorized for $t = 0$ and independent from λ.

The evolution according the total Hamiltonian $\hat{H}_{\mathrm{ASE}}$ gives the pure state

$$|\phi(t)\rangle = \frac{1}{\sqrt{2}}\left[|0\rangle_{\mathrm{A}} \otimes |\Psi_{\lambda_1}(t)\rangle + |1\rangle_{\mathrm{A}} \otimes |\Psi_{\lambda_2}(t)\rangle\right]\,, \tag{2.63}$$

i.e. the ancillary qubit makes it possible to evolve in parallel the global system for two different values of the parameter. The raising operator on the ancillary system $\sigma^+_{\mathrm{A}} = (|1\rangle\langle 0|)_{\mathrm{A}}$ can be used to obtain the overlap that we are looking for:

$$\langle\Psi_{\lambda_1}(t)|\Psi_{\lambda_2}(t)\rangle = 2\mathrm{Tr}_{\mathrm{ASE}}\left[\sigma^+_{\mathrm{A}} \otimes \mathbb{1}_{\mathrm{SE}}\right]\,. \tag{2.64}$$

Now one can make the Born-Markov approximation for the system environment interaction and reproduce the steps to obtain a Lindblad master equation, as explained in Section 1.2.1 and trace out the degrees of freedom of the environment. The reduced state of ancilla plus system can be represented in block form as

$$\rho^{\mathrm{AS}}(t) = \frac{1}{2}\begin{pmatrix}\rho_{00}(t) & \rho_{01}(t)\\ \rho_{10}(t) & \rho_{11}(t)\end{pmatrix}\,, \tag{2.65}$$

where each operator ρ_{ij} is an operator on the Hilbert space of the system. At the beginning there are no correlations between the two subspaces and the initial reduced operators are equal to the pure initial state of the system $|\psi_0\rangle$

$$\rho^{\mathrm{AS}}(0) = \frac{1}{2}\begin{pmatrix}|\psi_0\rangle\langle\psi_0| & 0\\ 0 & |\psi_0\rangle\langle\psi_0|\end{pmatrix}\,. \tag{2.66}$$

The evolution of $\rho_{\mathrm{AS}}(t)$ has a Lindblad form, i.e.

$$\frac{d\rho^{\mathrm{AS}}}{d} = -i\left[\hat{H}^{\mathrm{AS}}, \rho^{\mathrm{AS}}\right] + \sum_k \mathcal{D}\left[\hat{c}_k^{\mathrm{AS}}\right]\rho^{\mathrm{AS}}\,, \tag{2.67}$$

and both the collapse operators and the Hamiltonian have a direct sum structure

$$\hat{H}^{\mathrm{AS}} = \begin{pmatrix} \hat{H}_{\lambda_1} & 0 \\ 0 & \hat{H}_{\lambda_2} \end{pmatrix} \quad \text{and} \quad \hat{c}_k^{\mathrm{AS}} = \begin{pmatrix} \hat{c}_{k,\lambda_1} & 0 \\ 0 & \hat{c}_{k,\lambda_2} \end{pmatrix}. \tag{2.68}$$

The overlap (2.64) that we are seeking can now be written as the trace of the off-diagonal operator ρ_{01}, i.e. $\langle \Psi_{\lambda_1}(t)|\Psi_{\lambda_2}(t)\rangle = \mathrm{Tr}_{\mathrm{S}}[\rho_{01}]$. From the direct sum structure of the operators appearing in the Lindblad equation, it easy to obtain the evolution equation only for the off-diagonal operator ρ_{01}, where operators pertaining to λ_1 (λ_2) act only the left (right). The result is exactly the generalized master equation (2.56); the only difference is in notation and it is fixed by recognizing that ρ_{01} corresponds to $\bar{\rho}_{\lambda_1,\lambda_2}$.

This derivation also shows that it is possible to solve the generalized master equation (2.56) by enlarging the Hilbert space to include the ancillary qubit and then solve a standard Lindblad master equation for the composite system. This method has been further generalized in [139].

Summary

- When a quantum systems is subjected to a Markovian continuous measurement the correct figure of merit to quantify the achievable precision in the estimation of some parameter is given by the *effective* quantum Fisher information. This quantity is the classical Fisher information pertaining to the distribution of the (continuous in time) measurement outcomes plus the average quantum Fisher information of the possible conditional states.
- The classical Fisher information for a continuous measurement can be obtained by sampling trajectories from the stochastic master equation, via an auxiliary operator encoding the likelihood, which is also dependent on the sampled trajectories. For Gaussian systems the problem can be simplified and recast in terms of density matrices and first moment vectors.
- The effective quantum Fisher information for time-continuous measurements can be efficiently computed numerically. This is achieved by writing the evolution at each discrete time step as a CP map, which guarantees the positivity of the density operator.
- An ultimate bound to the estimation precision achievable by continuous measurements can be obtained by assuming to have access to all the environmental degrees of freedom after they interacted with the system. Such a bound is given by the QFI of the joint state of system and environment, we dub this quantity *ultimate* QFI. One can compute such a quantity by solving a generalized master equation for an operator (which is not a density matrix) acting the system Hilbert space only, without the need of a full description of the joint state.

CHAPTER 3

Magnetometry with large ensembles of two-level atoms

It is now time to apply the tools we have introduced in the previous Chapter to a concrete problem. In this Chapter we study the estimation of the intensity of a magnetic field by continuous measurement of the collective spin of a large ensemble of two-level atoms. The results presented in this chapter have been published in [12, 13].

Magnetometry is a paradigmatic example of quantum metrology and under some conditions it can be mapped to the problem of estimating a frequency. Even though the two problems are intimately connected, we keep the two topics separated. Frequency estimation is going to be the subject of the next chapter.

When the initial state of an atomic ensemble of N atoms is an uncorrelated spin coherent state, the mean-squared error in the estimation of the magnetic field scales, in terms of the total spin number $J = N/2$, as $1/J$, which is usually referred to as the standard quantum limit (SQL) to precision. If quantum resources, such as spin squeezing or entanglement between the atoms, are exploited, it is possible to achieve a quadratic enhancement, the so-called *Heisenberg scaling*, i.e. $1/J^2$ [31, 294]. We will see in the next Chapter that when the evolution is not unitary, it gets very difficult to achieve Heisenberg scaling.

In this Chapter we consider an alternative approach. We start with a *classical* initial state that is continuously monitored via the interaction with an external travelling field. In this case we think of the input modes as a "probe" rather than an environment; there is no difference in the mathematical description, which is the one presented in Section 1.2 and 1.4.2.

The crucial assumption behind these results is that the atoms are *collectively* coupled with the input field. By properly engineering this interaction one can then exploit the back action of the measurement to drive the system into more sensitive and entangled conditional states. At the same time one can also take advantage of the information acquired through the continuous weak measurement; for this reason our approach is not merely a state preparation protocol.

A similar setup for magnetometry has been considered in previous literature [23, 51, 108, 179, 199, 268]. Our contribution is to rigorously address the performance of these protocols using the quantum estimation methods introduced in Chapter 2. In this way, we can coherently take into account both the information obtained via the time-continuous non-demolition measurement, as well as the information obtained by a strong measurement on the conditional state of the system.

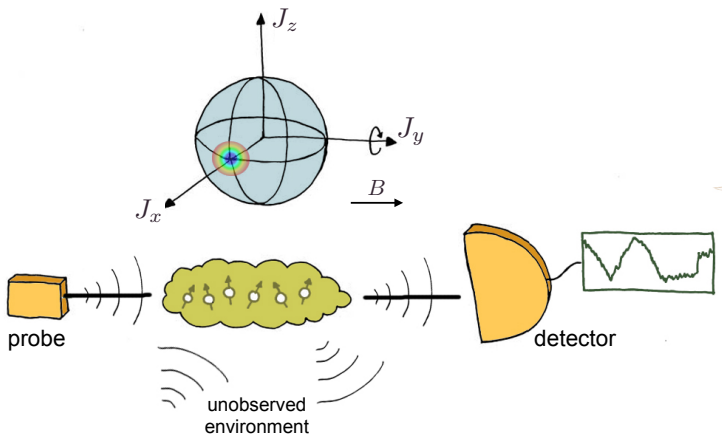

Figure 3.1: Pictorial representation of the metrological scheme. An atomic ensemble, prepared in a spin coherent state aligned to the x-direction and placed in a constant magnetic field B in the y-direction. In the upper figure the spin coherent state is represented as a circle in the Bloch sphere; the circle represents the fact that its fluctuations are equal in all directions. The ensemble is coupled to train of probing fields that are continuously monitored via homodyne detection after the interaction with the sample (bottom figure).

We study this problem in the limit of large spin, so that the system behaves as a continuous variable one. In this approximation we can derive an analytical formula for the ultimate bound on the mean-squared error of any unbiased estimator, and conclusively show that, for experimentally relevant values of the dynamical parameters, one can observe a Heisenberg-like scaling.
We can also analytically prove that the ultimate quantum limit is in fact saturated by the sequential strategy and one does not need to implement more involved measurements.

3.1 Physical model

We address the estimation of the intensity of a static and constant magnetic field B acting on a ensemble of N two-level atoms that are continuously monitored [23, 108, 199, 268], as depicted in Fig. 3.1. The atomic ensemble can be described as a system with total spin $J = N/2$ with collective spin operators defined as

$$\hat{J}_\alpha = \frac{1}{2}\sum_{i=0}^{N} \sigma_\alpha^{(i)}, \qquad \alpha = x, y, z, \tag{3.1}$$

and $\sigma_\alpha^{(i)}$ denotes Pauli matrices acting on the i-th spin. More explicitly, the total Hilbert space of the system is $\mathcal{H}_N = \otimes_{i=1}^{N} \mathbb{C}_2$ and has dimension 2^N; the single atom operators are obtained by tensor products with identities on all the other subsystems

$$\sigma_\alpha^{(i)} = \underbrace{\mathbb{1} \otimes \cdots \otimes \mathbb{1}}_{i-1} \otimes \sigma_\alpha \otimes \underbrace{\mathbb{1} \otimes \cdots \otimes \mathbb{1}}_{N-i} . \tag{3.2}$$

The collective operators obey the usual su(2) angular momentum commutation rules $[\hat{J}_i, \hat{J}_j] = i\varepsilon_{ijk}\hat{J}_k$, where ε_{ijk} is the Levi-Civita symbol. We remark again that we choose units such that $\hbar = 1$.

We assume that the atomic sample is coupled to a train of electromagnetic modes $\hat{b}_{\text{in}}(t)$. There are mainly two physical scenarios where this description can be used. In the first case the ensemble of atoms is placed inside a strongly driven and heavily damped cavity, and the input mode can be used to represent the cavity mode, this approach is described in [277]. The mode $\hat{b}_{\text{in}}(t)$ can also represent a far-detuned travelling light field passing through the ensemble and interacting via Faraday effect [199].

In either case we can consider an interaction Hamiltonian of the form $\hat{H}_{\text{int}} = \sqrt{\kappa}\hat{J}_z(\hat{b}_{\text{in}}(t) + \hat{b}^\dagger_{\text{in}}(t))$. If these *environmental* light modes are left unmeasured, the evolution of the system is expressed by a master equation with a single Hermitian collapse operator, which in this case corresponds to a collective transverse noise on the atomic sample,

$$\frac{d\rho}{dt} = \mathcal{L}_{\text{coll}}\,\rho = -i\gamma B\left[\hat{J}_y, \rho\right] + \kappa\mathcal{D}[\hat{J}_z]\rho, \tag{3.3}$$

where the parameter γ represents the strength of the coupling with the magnetic field that is directed along the y-axis and thus perpendicular to the noise generator.

At $t = 0$ we consider the system prepared in a spin coherent state, i.e. a tensor product of single spin states (qubits) directed in the positive x direction,

$$|\psi(0)\rangle = \bigotimes_{k=0}^{N} |+\rangle_k = |J\rangle_x, \tag{3.4}$$

where $|+\rangle$ is the eigenstate of σ_x with eigenvalue $+1$. We thus have that the spin component on the x direction attains the macroscopic value $\langle \hat{J}_x(0)\rangle = J$. The unconditional dynamics of $\langle \hat{J}_x\rangle$ is given by the following equation describing damped oscillations

$$\frac{d\langle \hat{J}_x(t)\rangle}{dt} = \gamma B\langle \hat{J}_z(t)\rangle - \frac{\kappa}{2}\langle \hat{J}_x(t)\rangle\,, \tag{3.5}$$

where we observe how the the dissipative and unitary parts of the dynamics are respectively shrinking the spin vector $\langle \hat{\boldsymbol{J}}\rangle$ and causing its Larmor precession around the y-axis. In the following we assume to measure *small* magnetic fields, such that $\gamma Bt \ll 1$ and we can approximate the solution of the previous equation as

$$\langle \hat{J}_x(t)\rangle \approx \langle \hat{J}_x(0)\rangle e^{-\kappa t/2} = Je^{-\kappa t/2}\,. \tag{3.6}$$

If the light modes are continuously monitored via homodyne measurements at the appropriate phase, one can perform a continuous measurement of $\hat{J}_z$ [1]; the corresponding stochastic master equation for finite monitoring efficiency η reads

$$d\rho^{(c)} = -i\gamma B[\hat{J}_y, \rho^{(c)}]\mathrm{d}t + \kappa\mathcal{D}[\hat{J}_z]\rho^{(c)}dt + \sqrt{\eta\kappa}\mathcal{H}[\hat{J}_z]\rho^{(c)}dw_t\,, \tag{3.7}$$

[1] We also call this a *weak* or *non-demolition* measurement of $\hat{J}_z$, because the instantaneous disturbance on the system is small. Note that these terms are somtimes used with other more specific meanings.

while the measurement result at time t corresponds to an infinitesimal photocurrent

$$dy_t = 2\sqrt{\eta\kappa}\,\mathrm{Tr}[\rho^{(c)}\hat{J}_z]dt + dw_t\,; \tag{3.8}$$

these equations correspond to Eqs. (1.56) and (1.54) with the choice[2] $\hat{c} = \hat{J}_z$.

We remark that this kind of collective noise in the master equation (3.3) describes the dynamics also in experimental situations where the coupling to the atomic ensemble is not explicitly engineered for continuous monitoring [64, 72, 234]. In this respect, assuming a non-unit efficiency η corresponds to considering both homodyne detectors that are not able to capture all the photons that have interacted with the spin, and environmental degrees of freedom, causing the same kind of noisy dynamics, that cannot be measured during the experiment.

3.1.1 Gaussian approximation for large spin

Let us now consider the limit of large spin $J \gg 1$. In this case, the dynamics may be effectively described with the Gaussian formalism as long as $\langle \hat{J}_x(t)\rangle \approx J$, i.e. $\kappa t \lesssim 1$. We define the effective quadrature operators of the atomic sample, satisfying the canonical commutation relation $[\hat{X}, \hat{P}] = i$, as [179, 199]

$$\hat{X} = \hat{J}_y/\sqrt{\bar{J}_t} \qquad \hat{P} = \hat{J}_z/\sqrt{\bar{J}_t}\,, \tag{3.9}$$

where $\bar{J}_t \equiv |\langle \hat{J}_x(t)\rangle|$ Notice that in the limit of large spin J we are assuming that we can safely consider the unconditional average value $\langle \hat{J}_x(t)\rangle$ only, since the stochastic correction obtained via (3.7) would be negligible.

In the Gaussian description the initial state $|\psi(0)\rangle$ corresponds to the vacuum state $(\hat{X} + i\hat{P})|0\rangle = |0\rangle$, which is Gaussian. With this approach, the stochastic master equation (3.7) becomes quadratic in the canonical operators (and thus preserves the Gaussian character of states)

$$d\rho^{(c)} = -i\gamma B\sqrt{\bar{J}_t}\left[\hat{X}, \rho^{(c)}\right]dt + \kappa\bar{J}_t\mathcal{D}[\hat{P}]\,\rho^{(c)}dt + \sqrt{\bar{J}_t\eta\kappa}\,\mathcal{H}[\hat{P}]\,\rho^{(c)}dw_t\,. \tag{3.10}$$

Let us briefly comment this equation. Crucially, the effect of the magnetic field becomes a displacement of the P quadrature. Moreover, strictly speaking this equation is not in Lindblad form (1.31), since the coefficients are time dependent. This time dependence could be avoided by choosing $\bar{J}_t \approx J$, i.e. neglecting the decay of the spin, which is still a good approximation for $J \gg 1$ and $\gamma Bt \ll 1$. However, such a crude approximation does not completely capture the dynamics of the system and we prefer to work in the more general case. Since all the coefficients in (3.10) are positive, we are still allowed to apply all the quantum trajectories approach, see also [108, 179]. The dynamics is still Markovian, but it is not time homogeneous, i.e. we lose the semigroup property of the unconditional dynamics.

Being quadratic, the whole dynamics can be equivalently rewritten in terms of first and second moments, i.e. the first moments vector $\boldsymbol{r}$ and the covariance matrix σ of the

[2] Note also that γ in Eqs. (1.56) and (1.54) corresponds here to κ and has nothing to do with the γ of Eq. (3.3).

quantum state $\rho^{(c)}$. As explained in Section 1.4.2, one can derive the following equations:

$$d\boldsymbol{r}_t = \boldsymbol{u}_t\, dt + \frac{\boldsymbol{\sigma}_t M_t\, d\boldsymbol{w}}{\sqrt{2}}\,, \tag{3.11}$$

$$\frac{d\boldsymbol{\sigma}_t}{dt} = D_t - \boldsymbol{\sigma}_t M_t M_t^{\mathsf{T}} \boldsymbol{\sigma}_t\,, \tag{3.12}$$

where

$$D_t = \begin{pmatrix} 2\kappa J e^{-\kappa t/2} & 0 \\ 0 & 0 \end{pmatrix}, \qquad M_t = \begin{pmatrix} 0 & 0 \\ \sqrt{2\eta\kappa J e^{-\kappa t/2}} & 0 \end{pmatrix}, \qquad \boldsymbol{u}_t = \begin{pmatrix} 0 \\ -\gamma B\sqrt{J e^{-\kappa t/2}} \end{pmatrix}, \tag{3.13}$$

and $d\boldsymbol{w}$ is a vector of Wiener increments such that $dw_j\, dw_k = \delta_{jk} dt$, related to the photocurrent via the equation

$$d\boldsymbol{y}_t = -\sqrt{2} M_t^{\mathsf{T}} \boldsymbol{r}_t\, dt + d\boldsymbol{w}\,, \tag{3.14}$$

but since we are considering homodyne measurements of a single mode the current is clearly not a vector (this is due to the singular matrix M_t):

$$dy_t = -\sqrt{2\eta\kappa J e^{-\frac{\kappa t}{2}}}\,\langle \hat{P}(t)\rangle_c \mathrm{d}t + dw_t = 2\gamma B J e^{-\kappa t/2}\sqrt{\kappa\eta}\, dt + dw_t\,. \tag{3.15}$$

As it will be clear in the following, for the estimation of B, we only need to retain the evolution of the mean and the variance of the atomic momentum quadrature $\hat{P}$ calculated on the conditional state $\rho^{(c)}$. Remembering that with our definitions $\sigma_{22} = 2\mathrm{Var}_c[\hat{P}(t)]$ the equations we are seeking are the following

$$d\langle \hat{P}(t)\rangle_c = -B\gamma\sqrt{J e^{-\frac{\kappa t}{2}}}\, dt + 2\mathrm{Var}_c[\hat{P}(t)]\sqrt{\eta\kappa J e^{-\frac{\kappa t}{2}}}\, dw_t\,, \tag{3.16}$$

$$\frac{d\mathrm{Var}_c[\hat{P}(t)]}{dt} = -4\eta\kappa J e^{-\frac{\kappa t}{2}} \left(\mathrm{Var}_c[\hat{P}(t)]\right)^2. \tag{3.17}$$

The differential equation for the conditional second moment is deterministic and can be solved analytically. For an initial coherent spin state, in this CV description a vacuum state with $\mathrm{Var}[\hat{P}(0)] = \frac{1}{2}$, we obtain the following solution

$$\mathrm{Var}_c[\hat{P}(t)] = \frac{1}{8\eta J\left(1 - e^{-\frac{\kappa t}{2}}\right) + 2}\,. \tag{3.18}$$

This expression shows that the conditional state of the atomic sample is deterministically driven by the dynamics into a spin-squeezed state. For our discussion spin-squeezing simply means that $\mathrm{Var}\left[\hat{J}_z\right]/|\langle \hat{J}_x\rangle|^2 = \mathrm{Var}[\hat{P}(t)] \leq 1/2$[3], which in turn implies that quantum correlations between the individual atoms are formed, see [175, 290] for more details.

The value of the squeezing depends on the efficiency η, as expected the state is not squeezed at all when it is not monitored (for $\eta = 0$), and it is inversely proportional to the total spin J. We can also appreciate that, due to the decay of the spin amplitude $\langle \hat{J}_x(t)\rangle$, the variance does not tend to zero for long times, but tends to the asymptotic value $1/2 \cdot (1 + 4\eta J)^{-1}$.

[3]We recall that the uncertainty relation coming from the su(2) commutation rules is $\mathrm{Var}\left[\hat{J}_z\right]\mathrm{Var}\left[\hat{J}_y\right] \leq |\langle \hat{J}_x\rangle|^2/4$.

3.2 Analytical results

Here we present our main results: the derivation of ultimate quantum limits on noisy magnetometry via time-continuous measurements of the atomic sample. We first evaluate the classical Fisher information $\mathcal{F}[y_t]$ corresponding to the information obtainable from the photocurrent. Then evaluate the second term appearing in the bound, corresponding to the information obtainable via a *strong* measurement on the conditional state of the atomic sample. This allow us to discuss the ultimate limit on the estimation strategy via the effective quantum Fisher information: we focus on the scaling with the relevant parameters of the experiment, i.e. with the total spin number J and the monitoring time characterizing each experimental run t, and we address the role of the detector efficiency η. Finally, we discuss the optimality of our measurement scheme, evaluating the ultimate limits on the precision given the noisy dynamics we are considering, using the tools presented in Section 2.4.

3.2.1 Effective quantum Cramér-Rao bound

Fisher information for the time-continuous photocurrent

As discussed before, the measured photocurrent y_t obtained via continuous homodyne detection can be used to extract information about the system and to estimate parameters which appear in the dynamics. The ultimate limit on the precision of this estimate is quantified by the FI $\mathcal{F}[p(y_t)]$. Given the Gaussian nature and the simple dynamics of the problem we can compute it analytically in closed form, by applying the results described in 2.2.3.

In this case the parameter is encoded only in the first moments of the conditional state, therefore one has to evaluate only this formula

$$\mathcal{F}[p(y_t)] = \mathbb{E}_{p(y_t)}\left[2(\partial_B \boldsymbol{r}_t)^{\mathsf{T}} M_t M_t^{\mathsf{T}} (\partial_B \boldsymbol{r}_t)\right]. \tag{3.19}$$

By noticing that the only non-zero entry of the vector $\partial_B \boldsymbol{r}_t$ is the one corresponding to $\langle \hat{P}(t)\rangle_c$, we thus obtain the formula

$$\mathcal{F}[p(y_t)] = 2\eta\kappa J e^{-\kappa t/2}\, \mathbb{E}_{p(y_t)}\left[\left(\partial_B \langle \hat{P}(t)\rangle_c\right)^2\right]. \tag{3.20}$$

By considering (3.16) and remembering Eq. (3.15), the time evolution of the derivative of the conditional first moment $\langle \hat{P}(t)\rangle_c$ w.r.t. the parameter B can be written as

$$\frac{d\left(\partial_B \langle \hat{P}(t)\rangle_c\right)}{dt} = -\gamma\sqrt{J e^{-\kappa t/2}} - 4\mathrm{Var}_c[\hat{P}(t)]\eta\kappa J e^{-\kappa t/2}\left(\partial_B \langle \hat{P}(t)\rangle_c\right). \tag{3.21}$$

where $\mathrm{Var}_c[\hat{P}(t)]$ is given by Eq. (3.18). The evolution of this quantity is deterministic and the equation can easily be solved. It follows that the average over the trajectories in Eq. (3.20) is not needed and we readily obtain the following closed expression for the FI

$$\mathcal{F}[p(y_t)] = \frac{64\gamma^2\eta J^2 e^{-\kappa t}\left(e^{\frac{\kappa t}{4}}-1\right)^3\left[-4\eta J - 12\eta J e^{\frac{\kappa t}{4}} + 3(4\eta J+3)e^{\frac{\kappa t}{2}} + (4\eta J+3)e^{\frac{3\kappa t}{4}}\right]}{9\kappa^2\left[(4\eta J+1)e^{\frac{\kappa t}{2}} - 4\eta J\right]}. \tag{3.22}$$

In Section 3.3 we show that a Bayesian estimator can indeed easily saturate the lower bound given by this Fisher information.

Average quantum Fisher information

In order to evaluate the effective quantum Cramér-Rao bound defined in Eq. (2.14) we now consider the second term $\mathbb{E}_{p(y_t)}\left[\mathcal{Q}[\rho^{(c)}]\right]$, that represents the information obtained via strong quantum measurement on the conditional states.

The conditional state $\rho^{(c)}$ is Gaussian and carries a dependence on the parameter B only in the first moments. As shown e.g. in [232, 256], the QFI of a parameter in the first moments of a Gaussian state is equal to the FI of a classical Gaussian probability distribution:

$$\mathcal{Q}[\rho^{(c)}] = 2\left(\partial_B \boldsymbol{r}_t\right)^{\mathsf{T}} \boldsymbol{\sigma}_t^{-1}\left(\partial_B \boldsymbol{r}_t\right); \tag{3.23}$$

which in the present case can be expressed as

$$\mathcal{Q}[\rho^{(c)}] = \frac{\left(\partial_B \langle \hat{P}(t)\rangle_c\right)^2}{\mathrm{Var}_c[\hat{P}(t)]}. \tag{3.24}$$

Since, as we proved before, the evolution of both $\partial_B\langle \hat{P}(t)\rangle_c$ and $\mathrm{Var}_c[\hat{P}(t)]$ is deterministic, the average over all possible trajectories is trivial and we have $\mathbb{E}_{p(y_T)}\left[\mathcal{Q}[\rho^{(c)}]\right] = \mathcal{Q}[\rho^{(c)}]$. By exploiting the analytical solution for both quantities, the QFI reads

$$\mathcal{Q}[\rho^{(c)}] = \frac{32\gamma^2 J\left(12\eta J - 4\eta J e^{-\frac{\kappa t}{2}} + (-8\eta J - 3)e^{\frac{\kappa t}{4}} + 3\right)^2}{9\kappa^2\left[(4\eta J + 1)e^{\frac{\kappa t}{2}} - 4\eta J\right]}. \tag{3.25}$$

As expected, when the monitoring of the environment is switched off ($\eta = 0$), one gets a SQL scaling $\mathcal{Q}[\rho^{(c)}] \sim J$, since no entanglement is created by the back-action of the measurement and the initial state is classical. We also remark that the QFI is equal to the classical FI for a measurement of the quadrature $\hat{P}$, thus showing that a strong measurement of the operator $\hat{J}_z$ on the conditional state of the atomic sample is the optimal measurement saturating the corresponding quantum Cramér-Rao bound.

Effective quantum Fisher information

By combining Eqs. (3.22) and (3.25), we can now finally compute the *effective* quantum Fisher information (2.15), which in this case reads

$$\widetilde{\mathcal{Q}} = \mathcal{F}[p(y_t)] + \mathbb{E}_{p(y_t)}\left[\mathcal{Q}[\rho^{(c)}]\right] = \mathcal{F}[p(y_t)] + \mathcal{Q}[\rho^{(c)}], \tag{3.26}$$

we recall that this quantity represents the inverse of the best achievable variance of an unbiased estimator, according to the quantum Cramér-Rao bound (2.14). The resulting expression can be simplified to get to a remarkably simple analytical formula

$$\tilde{\mathcal{Q}}_\eta = K_1 J + \eta K_2 J^2 \tag{3.27}$$

where the two coefficents are

$$K_1 = 32\frac{\gamma^2}{\kappa^2}\left(1 - e^{-\kappa t/4}\right)^2 \qquad K_2 = 64\frac{\gamma^2}{\kappa^2}\left(1 - \frac{8}{3}e^{-\kappa t/4} + 2e^{-\kappa t/2} - \frac{1}{3}e^{-\kappa t}\right). \tag{3.28}$$

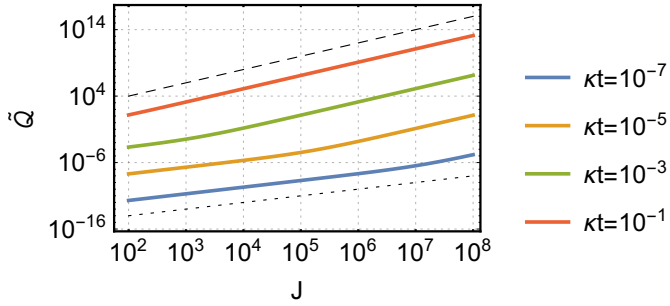

Figure 3.2: **J scaling** - effective QFI $\widetilde{\mathcal{Q}}$ as a function of J for different vales of κt, for unit efficiency η and effective coupling strength $\gamma/\kappa = 1\,\mathrm{G}^{-1}$; axes are in logarithmic scale. The solid curves are for increasing values of κt (shown in the legend) from top to bottom. The two regimes appearing in the plots are $\sim J^2$ (steeper slope) for higher values of κt and higher values of J and $\sim J$ (gentler slope) for the opposite parameters' regions. For visual comparison we show a dashed line at the top $\propto J^2$ and a dotted line at the bottom $\propto J$.

We start by studying how this quantity scales with the total spin: in Fig. 3.2 we plot $\widetilde{\mathcal{Q}}$ as a function of J in the appropriate regions of parameters. We remark that the plots are presented choosing $1/\kappa$ as the time unit so that the strength of the interaction becomes γ/κ and is always fixed to $1\,\mathrm{G}^{-1}$ in the following. We observe that, within the validity of our approximation ($\kappa t \lesssim 1$), it is possible to obtain the Heisenberg scaling J^2 for the effective QFI. There is a transition between SQL-like scaling and Heisenberg scaling depending on the relationship between J and κt, showing how the quantum enhancement is observed for $J \gg 1/\kappa t$.

The same conclusions are drawn if we look at the behaviour of $\widetilde{\mathcal{Q}}$ as a function of the interrogation time t, plotted in Fig. 3.3: a transition from a t^2-scaling to a quantum-enhanced t^3-scaling is observed for $J \gg 1/\kappa t$.

The previous results were both shown by considering the case of perfect monitoring of the environment, i.e. for homodyne detectors with unit efficiency η. In Fig. 3.4 we plot the behaviours of $\widetilde{\mathcal{Q}}$ as a function of J and t, varying the detector efficiency η; we observe that the quantum enhancements can be obtained for all non-zero values of η. With a non-unit monitoring efficiency the transition from SQL to Heisenberg-scaling is obtained for larger values of J. Clearly, the effective QFI (3.26) satisfies our previous conjecture (2.61): it is monotonically increasing (linearly) in η.

We finally remark that if we consider only the classical FI $\mathcal{F}[p(y_t)]$, the Heisenberg scaling in terms of J and t^3-scaling are *always* obtained for $\kappa t \lesssim 1$ and for every η. However, when the contribution of the term quadratic in J is too small then the QFI of the unconditional state, i.e. (3.25) with $\eta = 0$, dominates and we observe SQL scaling for $\tilde{\mathcal{Q}}$. This idea can be used to pinpoint more clearly the transition between the two regimes.

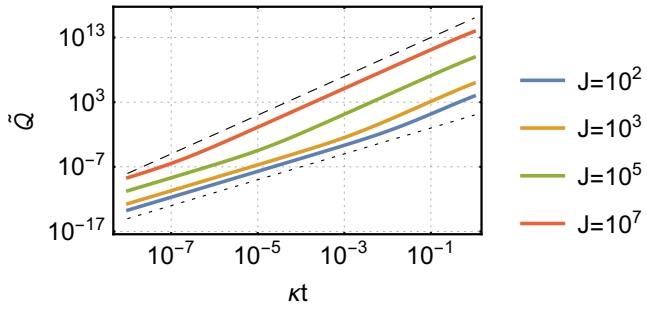

Figure 3.3: **Time scaling** - effective QFI $\widetilde{\mathcal{Q}}$ as a function of κt for different values of J, for unit efficiency η and effective coupling strength $\gamma/\kappa = 1\,\mathrm{G}^{-1}$; axes are in logarithmic scale. The solid curves are for increasing values of J (shown in the legend) from top to bottom. The two regimes appearing in the plots are $\sim (\kappa t)^3$ (steeper slope) for higher values of κt and higher values of J and $\sim (\kappa t)^2$ (gentler slope) for the opposite parameters' regions. For visual comparison we show a dashed line at the top $\propto (\kappa t)^3$ and a dotted line at the bottom $\propto (\kappa t)^2$.

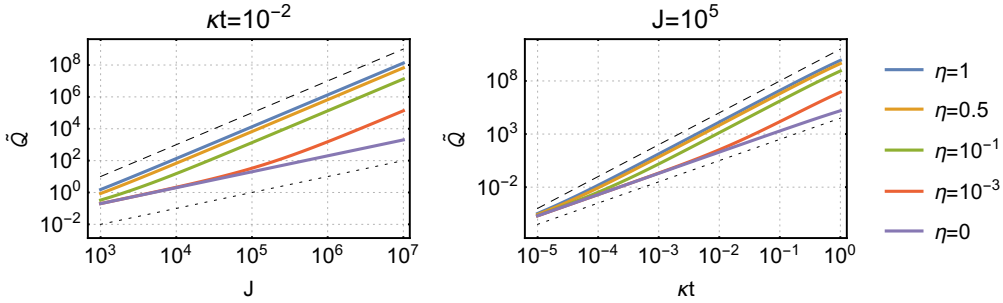

Figure 3.4: **Effect of non unit efficiency** - effective QFI $\widetilde{\mathcal{Q}}$ as a function of J (top panel) and κt (bottom panel) for different values of η and effective coupling strength $\gamma/\kappa = 1\,\mathrm{G}^{-1}$. The two regimes appearing in the plots are $\sim J^2$ (top panel) and $\sim (\kappa t)^3$ (bottom panel) for higher values of κt and higher values of J while $\sim J^2$ (top panel) and $\sim (\kappa t)^2$ (bottom panel) for the opposite parameters' regions. For visual comparison we show a dashed line at the top $\propto J^2$ (top panel) and $\propto (\kappa t)^3$ (bottom panel) and also a dotted line at the bottom $\propto J$ (top panel) and $\propto (\kappa t)^2$ (bottom panel).

Threshold on the number of atoms to observe Heisenberg scaling

The formula reported in Eq. (3.27) is particularly illuminating, specifically it allows us to discuss in more detail the role played by the two parameters describing the protocol: the (dimensionless) monitoring time κt and the monitoring efficiency η.

We start by observing that the effective QFI is the sum of two terms, one linear in J (SQL scaling) and one quadratic (Heisenberg scaling). The latter one depends linearly on the monitoring efficiency η and correctly goes to zero for $\eta \to 0$, i.e. when no monitoring is performed and the SQL-scaling is the expected result for an initial spin-coherent state. The observation that Heisenberg scaling can be obtained when $J \gg 1/\kappa t$ can be rigorously studied by looking more carefully at Eqs.(3.27) and (3.28). We define the condition to

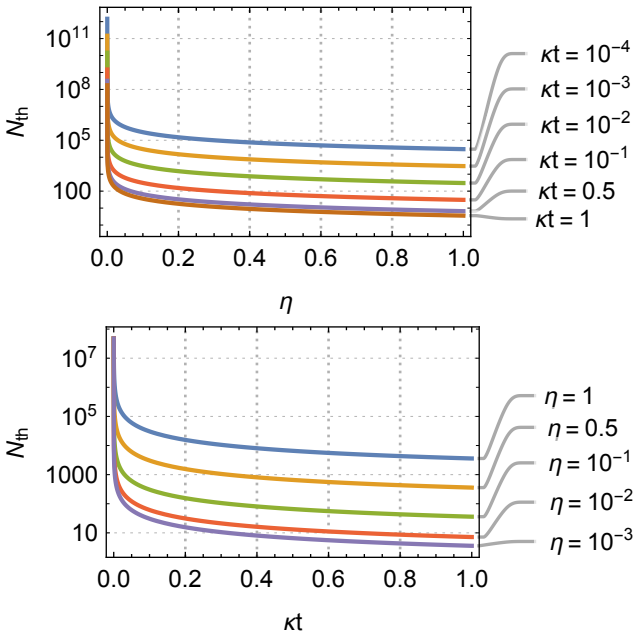

Figure 3.5: The minimum number N_{th} of atoms in the ensemble needed to to observe Heisenberg scaling for the effective QFI $\widetilde{\mathcal{Q}}$. In the upper panel we plot N_{th} as a function of η for different values of κt (increasing going from top to bottom), there is an inverse proportionality relationship. In the right panel we plot the same quantity as a function of κt for different values of η (increasing going from top to bottom), in this case the relationship is only approximately inversely proportional.

observe Heisenberg scaling as

$$\text{Heisenberg scaling} \iff \eta K_2 J > K_1 \tag{3.29}$$

i.e. when the quadratic contribution is greater than the linear one. This implies that we have a threshold value for the total spin,

$$J_{\text{th}} = \frac{K_1}{\eta K_2}, \tag{3.30}$$

and obviously, in terms of the total number of atoms, $N_{\text{th}} = 2J_{\text{th}}$. If we plug in the coefficients from (3.28), we get this simple expression

$$N_{\text{th}} = \frac{1}{\eta\left(1 - \frac{1}{3}e^{-\kappa t/2} - \frac{2}{3}e^{-\kappa t/4}\right)}, \tag{3.31}$$

which can be approximated as $N_{\text{th}} \approx \frac{3}{\eta\kappa t}$ when $\kappa t \ll 1$. The expected inverse relationship between the threshold number of atoms and both the monitoring time κt and the efficiency η, can be explicitly observed in Fig. 3.5, where we plot N_{th} as a function of both experimental parameters characterizing the protocol.

3.2.2 Optimality of the sequential strategy

The ultimate limit for quantum magnetometry, in the presence of Markovian collective transversal noise as the one described by the master equation (3.3), is given by the QFI $\overline{\mathcal{Q}}_{\mathcal{L}_{\rm coll}}$, previosuly introduced in Eq. (2.59). In this section we show that the effective FI $\tilde{\mathcal{Q}}$ actually corresponds to the ultimate bound given by $\overline{\mathcal{Q}}_{\mathcal{L}_{\rm coll}}$, thus proving that homodyne monitoring of the light interacting with the system is the optimal strategy to extract information about the magnetic field.

The generalized master equation (2.57) in this case (considering the large-spin approximation) reads

$$\frac{d\bar{\rho}}{dt} = -i\gamma\sqrt{\bar{J}_t}\left(B_1\hat{X}\bar{\rho} - B_2\bar{\rho}\hat{X}\right) + \kappa\bar{J}_t\mathcal{D}\left[\hat{P}\right]\bar{\rho}\,. \tag{3.32}$$

This equation can readily be solved in a phase space picture, since the terms in $\hat{X}$ and $\hat{P}$ are at most quadratic the Gaussian character of the operator $\bar{\rho}$ is preserved. Let us explicitly show how to solve Eq. (3.32).

The characteristic function can be defined for a generic operator $\hat{O}$ as $\chi[\hat{O}](\boldsymbol{s}) = \mathrm{Tr}\left[\hat{D}_{-\boldsymbol{s}}\hat{O}\right]$, in accordance with (1.104). In particular we work in the phase space of a single mode system, so that $\hat{\boldsymbol{r}}^\top = (\hat{X}, \hat{P})$ is the vector of quadrature operators and $\boldsymbol{s}^\mathsf{T} = (x, p)$ is the vector of phase space coordinates. Crucially, the action of operators in the Hilbert space corresponds to differential operators acting on the characteristic function via the following mapping [27, 100]

$$\hat{X}\rho \leftrightarrow \left(-i\partial_p - \frac{x}{2}\right)\chi(\boldsymbol{s}) \tag{3.33}$$

$$\rho\hat{X} \leftrightarrow \left(-i\partial_p + \frac{x}{2}\right)\chi(\boldsymbol{s}) \tag{3.34}$$

$$\hat{P}\rho \leftrightarrow \left(i\partial_x - \frac{p}{2}\right)\chi(\boldsymbol{s}) \tag{3.35}$$

$$\rho\hat{P} \leftrightarrow \left(i\partial_x + \frac{p}{2}\right)\chi(\boldsymbol{s}). \tag{3.36}$$

We can now introduce the characteristic function associated to the operator $\bar{\rho}$ appearing in Eq. (2.57)

$$\bar{\chi}(\boldsymbol{s}, t) \equiv \chi[\bar{\rho}](\boldsymbol{s}). \tag{3.37}$$

The only quantity of interest in order to compute the QFI is the the trace of this operator, which corresponds to the characteristic function evaluated in the origin of the phase space, i.e. $\mathrm{Tr}\bar{\rho} = \bar{\chi}(\boldsymbol{0}, t)$. This can readily be checked from the definition (1.104); for normalized quantum states this quantity is always one.

By applying the phase space mapping, from the generalized master equation (3.32) we get to the following partial differential equation for the characteristic function

$$\frac{\partial\bar{\chi}(\boldsymbol{s}, t)}{\partial t} = \left[i\gamma\sqrt{\bar{J}_t}\frac{B_1 + B_2}{2}x - \frac{\kappa\bar{J}_t}{2}p^2 - \gamma\sqrt{\bar{J}_t}(B_1 - B_2)\partial_p\right]\bar{\chi}(\boldsymbol{s}, t). \tag{3.38}$$

This equation can be solved by performing a Gaussian ansatz; we assume that at every

time the characteristic function can be written in the following form[4]

$$\bar{\chi}(\boldsymbol{s},t) = C(t)\exp\left[-\frac{1}{4}\boldsymbol{s}^\top\Omega^\top\boldsymbol{\sigma}(t)\Omega\,\boldsymbol{s} + i\boldsymbol{s}^\top\Omega^\top\boldsymbol{s}_m(t)\right]. \tag{3.39}$$

The dependence on time and on the parameters $B_{1/2}$ is completely contained in the covariance matrix $\boldsymbol{\sigma}(t)$, in the first moment vector $\boldsymbol{s}_m(t)^\top = (x_m(t), p_m(t))$ and in the function $C(t) = \bar{\chi}(0,t)$, which is exactly the final result we are seeking.

By plugging (3.39) into (3.38) and equating the coefficients for different powers of x and p, one obtains a system of differential equations. The relevant equations come from the coefficients of order one, and the coefficients of terms in p and p^2:

$$\frac{d\boldsymbol{\sigma}_{1,1}(t)}{dt} = 2\kappa J e^{-\frac{\kappa t}{2}} \tag{3.40}$$

$$\frac{dx_m(t)}{dt} = -i\frac{\gamma}{2}\sqrt{Je^{-\frac{\kappa t}{2}}}(B_1 - B_2)\boldsymbol{\sigma}_{1,1}(t) \tag{3.41}$$

$$\frac{dC(t)}{dt} = -i\gamma\sqrt{Je^{-\frac{\kappa t}{2}}}(B_1 - B_2)x_m(t)C(t)\,. \tag{3.42}$$

These equations are solved analytically with the initial conditions $\boldsymbol{\sigma}_{1,1}(0) = 1$, $x_m(0) = 0$ and $C(0) = 1$. These conditions express the fact that for $t = 0$ the operator $\bar{\rho}$ is exactly to the initial state of the system $|0\rangle\langle 0|$. The solution has the following form

$$C(t) = \exp\left[-\frac{4\gamma^2}{3\kappa^2}J(B_1 - B_2)^2 e^{-\kappa t}\left(e^{\frac{\kappa t}{4}} - 1\right)^2\left(-4Je^{\frac{\kappa t}{4}} + (6J+3)e^{\frac{\kappa t}{2}} - 2J\right)\right]. \tag{3.43}$$

Now, the ultimate QFI is given by Eq. (2.59), which in this case reads

$$\overline{\mathcal{Q}}_{\mathcal{L}_{\text{coll}}} = 4\partial_{B_1}\partial_{B_2}\log|C(t)|\,\big|_{B_1=B_2=B}\,. \tag{3.44}$$

It is a matter of simple algebra to get to the following final result

$$\overline{\mathcal{Q}}_{\mathcal{L}_{\text{coll}}} = \tilde{\mathcal{Q}}_{\eta=1} = \frac{32\gamma^2 J e^{-\kappa t}\left(e^{\frac{\kappa t}{4}} - 1\right)^2\left(-4Je^{\frac{\kappa t}{4}} + (6J+3)e^{\frac{\kappa t}{2}} - 2J\right)}{3\kappa^2}; \tag{3.45}$$

remarkably it coincides with the effective QFI $\tilde{\mathcal{Q}}$ in (3.26) for unit efficiency $\eta = 1$.

This result proves that our strategy, not only allows to obtain the Heisenberg limit, but also corresponds to the optimal one, given the unconditional master equation (3.3) with collective transversal noise and for perfectly efficient detectors. Indeed, any other more experimentally complicated strategy, based on entangled and non-local in time measurements of the output modes and the system, would not give better results in the estimation of the magnetic field B.

3.3 Bayesian estimator

In this section we concretely show that it is possible to achieve the classical Cramér-Rao bound from the time-continuous measurement outcomes by explicitly building a Bayesian

[4] This approach to solve a generalized master equation in phase space with a Gaussian ansatz is analogous to the one used in [119] in the context of full-counting statistics.

estimator, implementing what we explained in Section 1.3.1. We also point out that a Bayesian approach has already proven to be very useful for parameter estimation with continuously monitored quantum systems [51, 61, 92, 153, 154].

The goal is to reconstruct the posterior distribution of B given the observed current y_t, by Bayes rule:

$$p(B|y_t) = \frac{p(y_t|B)p(B)}{p(y_t)}, \tag{3.46}$$

where $p(B)$ is the prior distribution, $p(y_t|B)$ is the likelihood and $p(y_t)$ serves as a normalization factor. As a Bayesian estimator we choose the mean of the posterior distribution $\hat{B}(y_t) = \mathbb{E}_{p(B|y_t)}[B]$; the corresponding variance $\mathrm{Var}_{\hat{B}}(B) = \mathbb{E}_{p(B|y_t)}[B^2] - (\mathbb{E}_{p(B|y_t)}[B])^2$ is asymptotically optimal and tends to saturate the Cramér-Rao bound when the length of the vector y_T is large.

The simulated experimental run is obtained by numerically integrating the stochastic differential equation (3.16) with the Euler-Maruyama method for the "true" value of the parameter B_{true}. Time is discretized with steps of length Δt, i.e. to get from time 0 to time T we perform $n_T = T/\Delta t$ steps. Experimental data is represented by the observed measurement current $y_T = (\Delta y_{t_1}, \ldots, \Delta y_{t_{n_T}})^{\mathsf{T}}$, which corresponds to an n_T-dimensional vector. The outcome at every time step Δy_{t_i} is sampled from a Gaussian distribution with variance Δt and mean $\overline{\Delta y_{t_i}}(B) = \sqrt{2\eta\kappa J e^{-\frac{\kappa t}{2}}}\langle \hat{P}(t_i)\rangle_c \Delta t$. Notice that $\overline{\Delta y_{t_i}}(B)$ depends explicitly on the parameter B via the quantum expectation value $\langle \hat{P}(t_i)\rangle_c$ on the conditional state.

Since we are estimating only one parameter the posterior can be obtained on a grid on the parameter space; for more complicated problems Markov chain Monte Carlo methods might be needed to sample from the posterior [92]. In practical terms we need to solve Eqs. (3.16) and (3.17) for every value of the parameter B on the grid, assuming to perfectly know all the other parameters; then we need to calculate the likelihood for each value via

$$p(y_t|B) \propto \prod_{i=0}^{n_T} \exp\left[-\frac{\left(\Delta y_{t_i} - \overline{\Delta y_{t_i}}(B)\right)^2}{2\,\Delta t}\right], \tag{3.47}$$

by considering the outcomes as independent random variables, i.e. multiplying the corresponding probabilities. We then apply Bayes rule, Eq. (3.46), assuming a flat prior distribution $p(B)$ on a finite interval. The same analysis is trivially applied to more than one experiment by simply multiplying the likelihood obtained for every different observed measurement current.

In Figure 3.6 we indeed show the posterior distribution as a function of time for a single experimental run, obtained after a Bayesian analysis. We observe how the distribution gets narrower in time around the true value and we also explicitly show that its standard deviation $\sigma_{\mathrm{est}} = \sqrt{\mathrm{Var}_{\hat{B}}(B)}$ converges to the one predicted by the Cramér-Rao bound $\sigma_{\mathrm{CR}}(t) = \mathcal{F}[p(y_t)]^{-1/2}$.

Notice that in the initial part of the dynamics the values of σ_{est} are smaller than the corresponding σ_{CR}. This behaviour is due to the choice of the prior distribution, which is narrower than the likelihood and thus implies some initial knowledge on the parameter.

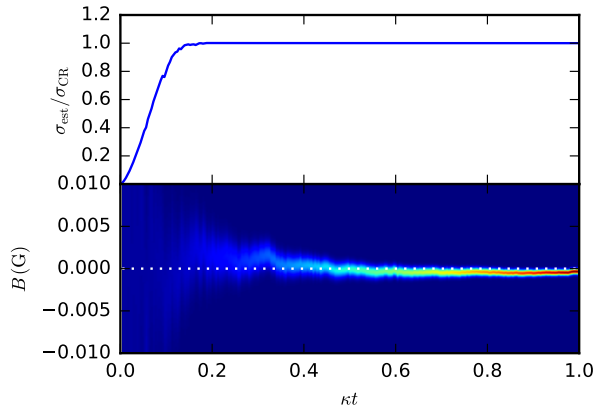

Figure 3.6: **Bayesian estimation of B from a single simulated experiment** - the data shown in the plots are obtained as a function of κt, for $\gamma/\kappa = 1\,\mathrm{G}^{-1}$, $J = 10^4$ and $\eta = 1$; the prior distribution of the parameter B is uniform in the interval $[-0.01, 0.01]\,\mathrm{G}$, and the true value is $B_{\rm true} = 0\,\mathrm{G}$. In the top panel we show the ratio between the standard deviation of the posterior distribution and the standard deviation predicted by the Cramér-Rao bound. In the bottom panel we show the posterior distribution as a function of time, the constant white dashed line marks the value $B_{\rm true}$.

This knowledge coming from the prior is larger than the information obtainable for small monitoring times and thus the variance is below the value obtained from the Cramér-Rao bound. It is important to remember that the FI $\mathcal{F}[p(y_t)]$ is monotonically increasing with time t, so the information gained by the currents increases with time, as one could expect.

Summary

- An ensemble of two-level atoms can be used to estimate the strength of a constant magnetic field. A travelling field interacting collectively with all the atoms is measured with homodyne-detection after the interaction with the sample. The evolution is described by a stochastic master equation. In the limit of a large number of atoms (equivalently large total spin of the system) an effective Gaussian description is sufficient. The back-action of the measurement due to the continuous monitoring induces spin-squeezing on the state of the atomic ensemble.

- The metrological scheme consists in using the information from the continuous measurement and a final measurement on the conditional state. The precision is quantified by the effective quantum Fisher information, which can be computed analytically. The effective QFI is Heisenberg limited, i.e. it shows a quadratic scaling in the number of atoms, even when the initial state is completely uncorrelated. Inefficient homodyne detection does not destroy the scaling, but only increases the number of atoms required to witness it.

- The scheme based on sequential continuous measurements is optimal for perfect detection efficiency. In this case the ultimate quantum Fisher information (optimized

over all possible measurement on the joint system-environment state) is equal to the effective Fisher information for the considered strategy.

- We explicitly show that a Bayesian estimator rapidly saturates the classical Cramér-Rao bound given by the Fisher information of the continuous measurement.
- In conclusion, time continuous measurement of a collective spin observable is a precious resource for magnetometry, since it allows both to directly extract information about the parameter and to prepare very sensitive conditional states.

CHAPTER 4

Restoring Heisenberg scaling in frequency estimation

In the previous Chapter we studied the effect of the continuous measurement of a *collective* observable of a system of two-level atoms. We have shown that the spin-squeezing (and thus the entanglement) generated by the continuous monitoring is sufficient to achieve Heisenberg scaling even with a factorized initial state, i.e. with completely uncorrelated atoms. In this situation the continuous nondemolition measurement of the collective spin observable is the resource for quantum metrology. The external light field coupled to the system has to be considered as a useful *probe* rather than an unwanted *environment*.

In this chapter we flip the point of view and we consider a complementary scenario, where the metrological resource is an *initially entangled* state. In general, when noisy open quantum dynamics is added on top of the encoding Hamiltonian, the advantage given by the initial quantum correlations is easily lost. In this situation, we show that, by having full or partial access to the environment causing the noisy dynamics, it is possible to restore the advantage.

Even if the Hamiltonian encoding the parameter is basically the same as in the previous section[1], we look at the problem with a slightly different point of view and we now talk about frequency estimation, rather then magnetometry. As we explain in Sec. 4.1 the main difference is that it is customary to consider the total time of an experiment as a valuable resource and not only the number of probes. This leads to consider a figure of merit which is optimized over the interaction time of a single run.

In this Chapter we start from an unconditional evolution described by a Markovian master equation, see Section 1.2. In particular, we focus on *independent* noise acting on each different two-level system, either parallel or transverse to the generator of the phase rotation to be estimated. In the former case, which corresponds to the so-called pure dephasing, the unconditional Lindblad dynamics leads to a standard quantum limited precision, even for an infinitesimal amount of noise [69]. In the case of transverse noise, it was shown that, by optimizing over the evolution time, it is possible to restore a super-classical scaling between SQL and HL [35, 53]; see also [123] for a recent review about quantum metrology with open quantum systems.

Our goal is to study whether time-continuous monitoring allows one to restore the HL, and to analyze in detail the effect of the monitoring efficiency on the performance

[1] In order to adhere to the standards used in previous literature on the topic, we change the axis of the Hamiltonian from y to z; this change is inconsequential for the physics of the problem.

of the estimation schemes. We derive both the ultimate limit on estimation precision (introduced in Section 2.4) and the effective bound for sequential strategies (introduced in Section 2.1). At variance with the previous chapter, we consider not only time-continuous homodyne-detection, but also photo-detection.

It is important to remark that the use of continuous measurements and feedback techniques has long been recognized as a useful tool for fighting decoherence [6–8, 94, 101, 107, 271]. Our metrological scheme follows this line of thought, but with the great advantage that it is based on continuous monitoring only, without error correction steps (or feedback), differently from other recent approaches in noisy quantum metrology [95, 236].

We stress that a great deal of effort has been also devoted to study the asymptotic properties of estimation via repeated/continuous measurements [43, 47, 122]. In this approach one is usually interested in performing a single run of the experiment and thus the system is observed for a long time. Our point of view is radically different and rooted in previous works on quantum frequency estimation. We are interested in the initial part of the dynamics, long before reaching the steady state. For this reason the asymptotic regime of the statistical model is reached by running the experiment many times, instead of observing the system for a long time.

Moreover, while most of the literature on parameter estimation with continuous measurements only deals with the information gained from the continuous signal only, the crucial part that makes our protocol able to recover Heisenberg scaling is the final strong measurement on the conditional state.

Finally, we point out a couple of works connected to the one presented in this chapter. An estimation problem closely related to the present one is studied in [48]; the setup is similar and the authors consider the same figure of merit, but the analysis is not performed in the context of continuous measurements. Very recently, after the appearance of our manuscript [14], another group independently obtained similar results [176]. In this work the authors only consider ideal jump-like evolution and they mainly focus on a single qubit probe; on the other hand they are able to generalize results to different interactions, initial states and parameters to be estimated.

4.1 Noisy frequency estimation

We consider a system of N qubits, described by an Hamiltonian $\hat{H}_\omega = \omega \hat{J}_z = (\omega/2)\sum_{j=1}^{N} \sigma_z^{(j)}$, where ω is the unknown frequency to be estimated, and $\sigma_z^{(j)}$ is the Pauli-z operator acting on the j-th qubit, as explicitly reported in (3.2).

The system is interacting also with a Markovian environment, so that the evolution is described by the master equation

$$\frac{d\rho}{dt} = \mathcal{L}_\omega \rho = -i\left[\hat{H}_\omega, \rho\right] + \frac{\kappa}{2}\sum_{j=1}^{N} \mathcal{D}\left[\sigma_\alpha^{(j)}\right]\rho = -i\frac{\omega}{2}\sum_j \left[\sigma_z^{(j)}, \rho\right] + \frac{\kappa}{2}\left(\sum_{j=1}^{N} \sigma_\alpha^{(j)} \rho \sigma_\alpha^{(j)} - N\rho\right). \tag{4.1}$$

We consider two possible geometries for the noise: we refer to $\alpha = z$ as *parallel* noise, while $\alpha = z$ is transverse noise, since the collapse operators are respectively parallel or

transverse to the Hamiltonian. The form of the Lindblad master equation is particularly simple due to the fact that the operators σ_α are both *hermitian* $\sigma_\alpha^\dagger = \sigma_\alpha$ and *unitary* $\sigma_\alpha\sigma_\alpha = \mathbb{1}$. The master equation (4.1) is in Lindblad form, given by (1.31). The equivalence with the results of Chapter 2 can be seen by considering the noise operators[2]

$$\hat{c}_j = \sqrt{\kappa/2}\sigma_\alpha^{(j)} \,. \tag{4.2}$$

In quantum frequency estimation strategies, one considers the number of qubits N and the total time of the experiment T as the resources of the protocol. The quantum Cramér-Rao bound is usually rewritten as

$$\delta\omega\sqrt{T} \geq \frac{1}{\sqrt{\mathcal{Q}/t}} \geq \frac{1}{\sqrt{\max_t[\mathcal{Q}/t]}} \tag{4.3}$$

where $t = T/M$ corresponds to the duration of each round, over which one can perform a further optimization, and where $\mathcal{Q}$ corresponds here to the QFI charaterizing the particular estimation strategy considered. The error on the estimate is the standard deviation of the estimator $\delta\omega \equiv \sqrt{\mathrm{Var}[\hat{\omega}]}$.

A particularly important class of states for this estimation problem is represented by the N-qubits GHZ states

$$|\psi_{\mathsf{GHZ}}\rangle = (|0\rangle^{\otimes N} + |1\rangle^{\otimes N})/\sqrt{2}\,; \tag{4.4}$$

in most of the following we consider a GHZ initial state. This is a strong assumption, since GHZ states are very fragile and difficult to prepare, however this choice simplifies calculations and leads to analytical results.

It is well known (and easy to check) that in the noiseless case, i.e. for $\kappa = 0$, an initial GHZ state is optimal and the QFI is Heisenberg limited, $\mathcal{Q}_{\mathsf{HL}} = N^2t^2$. This leads to a quadratic enhancement w.r.t. the "standard quantum limited" QFI, $\mathcal{Q}_{\mathsf{SQL}} = Nt^2$, which is obtained in the case of an initial factorized spin coherent state $|\psi_{\mathsf{coh}}\rangle = [(|0\rangle + |1\rangle)/\sqrt{2}]^{\otimes N}$. Let us remark that both the t^2 scaling in time and the N^2 scaling in the number of qubits are called "Heisenberg" scaling in the literature; we reserve the phrase for the scaling in N exclusively. In what follows, we are going to consider the noisy case ($\kappa > 0$); the generic QFI $\mathcal{Q}$ in Eq. (4.3) corresponds to either: i) the QFI of the unconditional state $\mathcal{Q}[\rho_{\mathrm{unc}}]$ corresponding to the master equation (4.1); ii) the ultimate QFI $\overline{\mathcal{Q}}_{\mathcal{L}_\omega}$ obtained optimizing over all the possible measurements on system and environmental outputs; iii) the effective QFI $\widetilde{\mathcal{Q}}_{\mathrm{unr},\eta}$ corresponding to a specific time-continuous (sequential) measurement of the output modes and a final strong measurement on the conditional state of the system.

In particular we are going to focus on time-continuous photo-detection and homodyne detection; the respective SMEs are given by (2.33) and (2.34), by applying the substitution (4.2) and considering a single measurement efficiency $\eta_j = \eta$ for every output channel. The two effective QFIs are respectively labeled as $\widetilde{\mathcal{Q}}_{\mathsf{pd},\eta}$ and $\widetilde{\mathcal{Q}}_{\mathsf{hom},\eta}$, where we also keep the dependence on the efficiency explicit.

[2] Again, we use the parameter κ for the coupling with the environment, instead of γ used in Chapter 2.

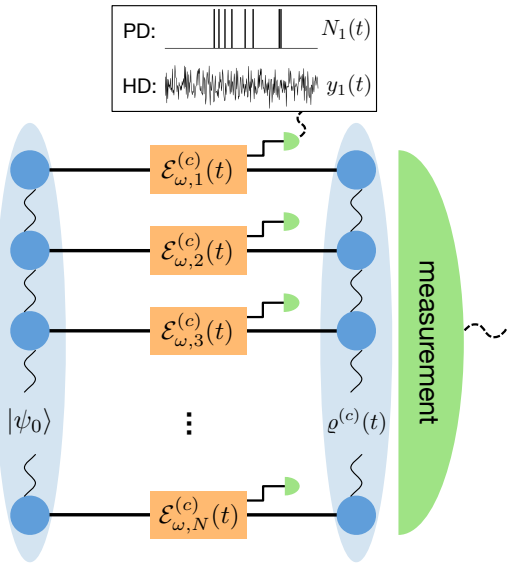

Figure 4.1: **Schematic representation of the metrological scheme.** A N-qubit input state $|\psi_0\rangle$ interacts with N independent environments which are monitored by N detectors, either by photo-detection (PD) or homodyne detection (HD). In the former case each output is a binary valued detection record $N_j(t)$, in the latter a real valued photo-current $y_j(t)$. The map $\mathcal{E}^{(c)}_{\omega,j}(t)$ represents the corresponding conditional dynamics acting on the j-th qubit only, and it depends on the measurement output $N_j(t)$ or $y_j(t)$. The N-qubit quantum state $\rho^{(c)}(t)$, conditioned on all the measurement outcomes acquired during the evolution, is collectively measured at the end of the conditional dynamics.

The metrological scheme corresponding to the effective QFI is schematically shown in Fig. 4.1, where we graphically stress that the evolution of every qubit is independent from the others: we assume that N different (homodyne or photo-) detectors are monitoring each environment. However there are instances where these assumptions may be relaxed, due to the symmetry of the initial state.

In the next sections we address separately the two different cases of parallel and transverse noise. For each case we start by reviewing known results for the QFI of the unconditional states. Then we present original results, regarding the ultimate QFI $\overline{\mathcal{Q}}_{\mathcal{L}_\omega}$ and the effective QFIs $\widetilde{\mathcal{Q}}_{\mathsf{pd},\eta}$ and $\widetilde{\mathcal{Q}}_{\mathsf{hom},\eta}$. For parallel noise we can compute everything analytically, while for the transverse case only the ultimate QFI for a GHZ state can be computed analytically and we make use of the algorithm presented in Section 2.3 for the effective QFI.

4.2 Parallel noise

Parallel noise, corresponding to the master equation (4.1) with $\sigma^{(j)}_\alpha = \sigma^{(j)}_z$, is typically considered the most detrimental noise for frequency estimation since the evolution induces dephasing in the same eigenbasis of the Hamiltonian $\hat{H}_\omega$. For an initial GHZ

state, the QFI of the unconditional state can be evaluated analytically [15, 137], obtaining

$$\mathcal{Q}\left[\rho^{\parallel}_{\mathsf{unc}}\right] = N^2 t^2 e^{-2\kappa N t} \,. \tag{4.5}$$

By optimizing over the single-shot duration t, one obtains that the optimal QFI is standard quantum limited,

$$\max_t \left[\frac{\mathcal{Q}\left[\rho^{\parallel}_{\mathsf{unc}}\right]}{t}\right] = \frac{N}{2e\kappa}\,; \tag{4.6}$$

this result is exactly the same obtained with a factorized initial state $|\psi_{\mathsf{coh}}\rangle$. If one can optimize over the initial entangled states a better precision can be achieved, but only a constant enhancement can in fact be gained [137]. Some general bounds on the precision of parameter estimation with noisy dynamics have been derived [69, 75] and the result is that as soon as some parallel noise is present in the dynamics, the ultimate precision is standard quantum limited.

4.2.1 Analytical results

We present result about frequency estimation with parallel noise; part of these results are valid more in general. We discuss more explicitly the case frequency estimation with an initial GHZ state at the end of the section.

Ultimate QFI for noise commuting with the Hamiltonian

In this section we show that, whenever the collapse operators $\hat{c}_j$ commute with the free Hamiltonian $\hat{H}_\omega$, the ultimate QFI $\overline{\mathcal{Q}}_{\mathcal{L}_\omega}$ is always equal to the QFI of the state evolving under the unitary dynamics generated by $\hat{H}_\omega$.

The master equation and the stochastic master equations are obtained by considering the following interaction Hamiltonian between the system and the input modes: $\hat{H}_{\mathsf{int}}(t) = \sum_{j=1}^{N}\left(\hat{c}_j \hat{b}^{(j)\dagger}_{\mathsf{in}}(t) + \hat{c}^\dagger_j \hat{b}^{(j)}_{\mathsf{in}}(t)\right)$. We remind that t enters the Hamiltonian as a parameter that labels which mode interacts with the system at time t and for each t we have a different operator acting on a different Hilbert space, see Section 1.2 for more details. The total time-dependent Hamiltonian for the system and environment is thus $\hat{H}_{\mathsf{SE}}(t) = \hat{H}_\omega + \hat{H}_{\mathsf{int}}(t)$ and each input mode interacts with the main system for an infinitesimal time dt.

For the sake of clarity, we consider a discretization with a finite interaction time δt, so that the evolution over a total time $T = M\delta t$ involves a finite number M of input modes. As we did in Section 1.2.1 we assume that the state of the input modes is the vacuum $|0\rangle$ and that the initial state of the system $|\psi_0\rangle$ is pure. The result holds also in the limit $\delta t \to 0$.

Under these assumptions the joint state of system and environment evolves as

$$|\psi_{\mathsf{SE}}(\omega)\rangle = \hat{U}_{t_M} \ldots \hat{U}_{t_2} \hat{U}_{t_1}\left(|\psi_0\rangle \otimes |0\rangle^{\otimes M}\right), \tag{4.7}$$

where $t_j = j \cdot \delta t$ and $\hat{U}_{t_j} = \exp\left[-i\delta t\left(\hat{H}_\omega + \hat{H}_{\mathsf{int}}(t_j)\right)\right]$. The object we need to evaluate the QFI is the overlap for two different values of the parameter, i.e.

$$\langle \psi_{\mathsf{SE}}(\omega_1)|\psi_{\mathsf{SE}}(\omega_2)\rangle = \mathrm{Tr}[\bar{\rho}]\,, \tag{4.8}$$

where the operator $\bar{\rho}$ is the one appearing in Eq. (2.57), as explained in Section 2.4.

When all the collapse operators $\hat{c}_j$ commute with the free Hamiltonian $\hat{H}_\omega$, the interaction Hamiltonian $\hat{H}_{\mathsf{int}}$ also commutes and we have

$$\hat{U}_{t_i} = \exp\left[-i\delta t\hat{H}_{\mathsf{int}}(t_i)\right] \cdot \exp\left[-i\delta t\hat{H}_\omega\right]. \tag{4.9}$$

Therefore, in the computation of the overlap (4.8) the terms due to the interaction cancel out and we have

$$\langle \psi_{\mathsf{SE}}(\omega_1)|\psi_{\mathsf{SE}}(\omega_2)\rangle = \langle\psi_0|\exp[-iT(H_{\omega_2} - H_{\omega_1})]|\psi_0\rangle,$$

so that Eq. (2.59) gives the QFI of the unitary case. This result is valid for any Hamiltonian parameter [218] and any commuting collapse operator.

In particular, this is true for the Hamiltonian $\hat{H}_\omega = \omega\hat{J}_z$ with parallel noise $\hat{c}_j = \sqrt{k/2}\sigma_z^{(j)}$; for any pure initial state of the system $|\psi_0\rangle$ we have

$$\overline{\mathcal{Q}}^{\parallel}_{\mathcal{L}_\omega} = \mathcal{Q}\left[e^{-i\hat{H}_\omega t}|\psi_0\rangle\langle\psi_0|e^{i\hat{H}_\omega t}\right] = 4\left[\langle\psi_0|\hat{J}_z^2|\psi_0\rangle - \langle\psi_0|\hat{J}_z|\psi_0\rangle^2\right]. \tag{4.10}$$

This result shows that, by measuring the output modes, it is in principle possible to recover not only a Heisenberg scaling for the error $\delta\omega$, but also the whole information on the parameter.

Effective quantum Fisher information for Hermitian and unitary collapse operators

In this section we show that the effective QFI $\tilde{\mathcal{Q}}_{\mathsf{unr},\eta}$ for $\eta = 1$ can be equal to the QFI of the noiseless unitary dynamics, thus saturating the ultimate bound $\overline{\mathcal{Q}}_{\mathcal{L}_\omega}$; on the other hand for $\eta < 1$ the result is the same as for the unconditional dynamics, but with a rescaled coupling constant $\kappa(1-\eta)$. In general, when the collapse operators $\hat{c}_j$ commute with the Hamiltonian and are also unitary and Hermitian (in this case the Pauli matrices σ_z) it is always possible to recast the evolution due to the SME as a random unitary transformation followed by the unconditional CPT cap.

For photo-detection we have the following SME, starting from the general one in Eq. (2.33):

$$d\rho_t = -i\omega\left[\hat{J}_z, \rho_t\right]dt + (1-\eta)\frac{\kappa}{2}\sum_j \mathcal{D}\left[\sigma_z^{(j)}\right]\rho_t\, dt + \sum_j\left(\sigma_z^{(j)}\rho_t\sigma_z^{(j)} - \rho_t\right)dN_j\,; \tag{4.11}$$

now, due to the unitarity of σ_z, the statistics of the Poisson processes is independent from the state of the system $\mathbb{E}\left[dN_j\right] = \eta\frac{\kappa}{2}dt$. This means that the measurement records $N_j(t)$ contain "only noise" and no information on the state of the system and thus they give zero information about the parameter, i.e. $\mathcal{F}\left[p_{\mathrm{traj}}\right] = 0$.

We can now exploit the following identity for Poisson processes [144]:

$$1 + A dN = e^{\log(1+A) dN} = (A+1)^{dN} , \tag{4.12}$$

which stems from the fact that $dN^2 = dN$. This identity holds not only for scalars but also when A is an operator or a superoperator, the only crucial property is that the exponential is defined as a power series (and in this case 1 represents the identity operator/superoperator).

In Eq. (4.11) all the terms multiplying the Poisson increments are given by a superoperator with the action $\bullet \to \sigma_z \bullet \sigma_z$, minus the identity superoperator. By using this observation in conjunction with the identity (4.12) and by exploiting the properties of independent Poisson increments, $dt dN_j = 0$ and $dN_j dN_k = \delta_{jk} dN_j$, we can finally write the infinitesimal evolution of the density operator as

$$\rho_{t+dt} = e^{dt(1-\eta)\frac{\kappa}{2}\sum_j \mathcal{D}[\sigma_z^{(j)}]} \left[\left(\prod_j \sigma_z^{(j)\, dN_j} \right) \left(e^{-i\omega \hat{J}_z\, dt} \rho_t\, e^{i\omega \hat{J}_z\, dt} \right) \left(\prod_j \sigma_z^{(j)\, dN_j} \right) \right] . \tag{4.13}$$

This identity is true up to order dt and we see that the Hamiltonian part is followed by random "spin-flips" and by the dissipative part with a rescaled coupling $\kappa(1-\eta)$.

Since everything commutes, the solution is trivial and iterating the infinitesimal evolution amounts to integrating the various exponents separately, therefore we get to

$$\begin{aligned} \rho_t &= e^{(1-\eta)\frac{\kappa}{2}\sum_j \mathcal{D}\left[\sigma_z^{(j)}\right] t} \left[\left(\prod_j \sigma_z^{(j)\, N_j(t)} \right) \left(e^{-i\omega \hat{J}_z\, t} \rho_0\, e^{i\omega \hat{J}_z\, t} \right) \left(\prod_j \sigma_z^{(j)\, N_j(t)} \right) \right] \\ &= e^{(1-\eta)\frac{\kappa}{2}\sum_j \mathcal{D}\left[\sigma_z^{(j)}\right] t} \left[e^{-i\frac{\pi}{2}\sum_j \sigma_z^{(j)} N_j(t)} \left(e^{-i\omega \hat{J}_z\, t} \rho_0\, e^{i\omega \hat{J}_z\, t} \right) e^{i\frac{\pi}{2}\sum_j \sigma_z^{(j)} N_j(t)} \right] , \end{aligned} \tag{4.14}$$

where the random variable $N_j(t) = \int_0^t dN_j$ counts the number of detections at the j-th detector. Now, since the spin-flips depending on the random Poisson processes are unitary operations they leave the QFI invariant. From this argument, it follows that the QFI of each conditional state is exactly equal to the QFI of the unconditional but with a rescaled coupling $\kappa \mapsto \kappa(1-\eta)$. For $\eta = 1$ the QFI of each conditional state (and thus also the average QFI) is equal to the noiseless case and saturates the ultimate bound $\overline{\mathcal{Q}}_{\mathcal{L}_\omega}$. This last result was only proven numerically in [14].

For homodyne detection the "trick" is to choose the appropriate quadrature to measure, which amounts to changing the angle θ which decides which collapse operators $\hat{c}_j e^{i\theta}$ enter into the SME. By choosing $\theta = \pi/2$ we have the expectation value $\mathrm{Tr}\left[\rho(i\hat{c} - i\hat{c}^\dagger)\right]$, which clearly is zero for Hermitian $\hat{c}$, e.g. Pauli matrices. This means that the observed photocurrent is again only noise and no signal, i.e. $dy_t = dw_t$ and again the corresponding FI vanishes. The corresponding SME has the following form

$$d\rho_t = \left(-i\omega \left[\hat{J}_z, \rho_t \right] + \frac{\kappa}{2} \sum_j \mathcal{D}\left[\sigma_z^{(j)} \right] \rho_t \right) dt + i \sqrt{\frac{\eta\kappa}{2}} \sum_j \left[\sigma_z^{(j)}, \rho_t \right] dw_j \, . \tag{4.15}$$

For $\eta = 1$[3] it is not difficult to write the final state as (for more details see Section 3.2

[3] In order to take into consideration finite efficiency for the homodyne case a more complicated approach is needed, see for example [54]. We leave this general case for future studies.

of [144]):

$$\rho_t = e^{i\sqrt{\frac{\kappa}{2}}\sum_j W_j(t)\sigma_z^{(j)}} \left(e^{-i\omega \hat{J}_z t} \rho_0 \, e^{i\omega \hat{J}_z t} \right) e^{-i\sqrt{\frac{\kappa}{2}}\sum_j W_j(t)\sigma_z^{(j)}} , \tag{4.16}$$

where the random variables $W_j(t) = \int_0^t dw_j$ are Gaussianly distributed with mean 0 and variance t. We can see again that each conditional state differs from a purely Hamiltonian evolution only by a random unitary transformation. The QFI of each conditional state (and thus also the average QFI) is equal to the noiseless case and therefore we can saturate the ultimate bound even with homodyne monitoring. If one monitors a different quadrature, i.e. $\theta = 0$, the classical FI is not zero, but the effective QFI does not saturate the ultimate bound, as numerically observed [14].

Interestingly, this way of monitoring the environment, where only noise is measured and no information about the state of the system is gained, can be used to reduce decoherence by a factor $(1-\eta)$ by implementing a Markovian feedback [271]. We stress that our approach is different because it is not necessary to apply any feedback to take advantage of the improved metrological power of the conditional states, even though this strategy works only for parallel noise, while the feedback scheme works for any Hermitian collapse operator.

Initial GHZ state

Applying the results of the previous sections, for an initial GHZ state we have

$$\overline{\mathcal{Q}}^{\parallel}_{\mathcal{L}_\omega} = \widetilde{\mathcal{Q}}^{\parallel}_{\eta=1} = \mathcal{Q}_{\mathsf{HL}} = N^2 t^2 . \tag{4.17}$$

Therefore we verify that the strategies based on time-continuous photo-detection and homodyne detection (for $\theta = \pi/2$) with perfect efficiency $\eta = 1$ are indeed optimal, showing that the noiseless Heisenberg-limited result can be recovered, without the need to perform complicated (non-local in time) measurement strategies on system and environment.

For both time-continuous homodyne and photo-detection, the evolution of an initial GHZ state, under parallel noise and conditioned on the measurement results, is restricted to a two-dimensional Hilbert space. As a consequence, the results obtained for $N = 1$ qubit can be readily used to infer the results for generic N qubits, by simply rescaling the evolution time $t \to Nt$ and considering the random processes $dM = \sum_j dN_j$ and $dW = \sum_k dw_j$. The reason is that every operator $\sigma_z^{(j)}$ has the same action on the GHZ state, because of its special symmetric form.

Therefore, starting from (4.14) with $\eta = 1$, it is easy to see that, for an initial GHZ state, after a time t the conditional state for photo-detection reads (up to an irrelevant global phase):

$$|\psi_t\rangle = \frac{1}{\sqrt{2}} \left(|0\rangle^{\otimes N} + e^{i(N\omega t + M(t)\pi)} |1\rangle^{\otimes N} \right) , \tag{4.18}$$

where the Poissonian random variable $M(t) = \sum_j N_j(t)$ counts the *total* number of photo-detections on all the detectors up to time t. Thanks to the permutational symmetry of the

GHZ state, and given that only one jump may occur at each time[4], it is not necessary to know exactly from which qubit channel the photon has been detected. One may obtain the same result by using a single perfect photo-detector monitoring jointly all the N output modes and thus having only the result $M(t)$ instead of all the $N_j(t)$. Once the number of detected photons $M(t)$ is known, and the corresponding "GHZ-equivalent" conditional state is prepared, it is possible estimate the frequency ω at the Heisenberg limit.

As we explained, as soon as the photo-detection monitoring is not perfectly efficient, Heisenberg scaling is immediately lost and the effective QFI is equal to $\widetilde{\mathcal{Q}}^{\parallel}_{\mathsf{pd},\eta} = N^2 t^2 e^{-2\kappa(1-\eta)Nt}$; optimizing over time we have:

$$\max_t \left[\frac{\widetilde{\mathcal{Q}}^{\parallel}_{\mathsf{pd},\eta}}{t} \right] = \frac{N}{2e\kappa(1-\eta)} \,. \tag{4.19}$$

However, thanks to the permutational symmetry the overall efficiency parameter η corresponds to the product between the factual efficiency of the detectors and the fraction of qubits that are actually monitored.

We have already noticed that, for every value of ω, all the information is contained in the conditional quantum states and the classical Fisher information $\mathcal{F}[p_{\mathsf{traj}}]$ is in fact identically equal to zero. Nevertheless, we remark that the output from the photo-detection measurement is essential to know the corresponding conditional state, and thus to extract the whole information on ω via the final strong measurement.

4.3 Transverse noise

Transverse noise, corresponding to $\sigma^{(j)}_{\alpha} = \sigma^{(j)}_{x}$ is much harder to handle than parallel noise, due to the noncommutativity. However, thanks to the particular symmetry of the GHZ state, the QFI for the unconditional dynamics with arbitrary collapse operators can be obtained without the need to diagonalize the full density matrix [53]. The corresponding optimized QFI can be then numerically obtained and the scaling is found to be intermediate between SQL and Heisenberg: $\max_t \left[\mathcal{Q}\left[\rho^{\perp}_{\mathsf{unc}}\right]/t \right] \approx N^{5/3}$, for $N \gg 1$. The optimal time decreases to zero as the number of qubit increases: $\lim_{N\to\infty} t_{\mathrm{opt}} = 0$. However, for $\omega \to 0$ we show in Subsection 4.3.3 that the unconditional QFI can be computed analytically and it scales quadratically in N.

In the following sections we first present analytical results on the ultimate QFI, obtained by solving the generalized master equation (2.56) and then numerical results on the effective QFI, obtained by using the numerical methods introduced in Section 2.3.

[4]This can be justified on physical grounds: the probability of a photon-detection in an infinitesimal time is vanishingly small (being proportional to dt), therefore the probability of two or more detections at the same time can be disregarded [298]. Mathematically this is equivalent to working with *independent* Poission processes, satisfying the rule $dN_j dN_k = \delta_{jk} dN_j$.

4.3.1 Analytical results on the ultimate bound

When the noise and the Hamiltonian parameter do not commute it is harder to obtain general analytical results; for this reason we restrict only to an initial GHZ state, which makes it possible to get a closed formula for the effective QFI.

Ultimate quantum Fisher information for GHZ state

The choice of an identical and independent noise acting on each qubit is very important to work out an expression for the ultimate QFI. The modified master equation Eq. (2.57) is linear in the operator $\bar{\rho}$ and the coefficients are time-independent, therefore it is possible write the solution as a linear map, formally $\bar{\mathcal{E}}_{\omega_1,\omega_2}(t) = \exp\left(t\bar{\mathcal{L}}_{\omega_1,\omega_2}\right)$. This map is only guaranteed to be linear and in general it is not even positive.

Since the map acts independently on each qubit, we can still write the global action on the N-qubit state as the tensor product $\bar{\mathcal{E}}^N_{\omega_1,\omega_2}(t) = \bar{\mathcal{E}}_{\omega_2,\omega_2}(t)^{\otimes N}$, where $\bar{\mathcal{E}}_{\omega_2,\omega_2}(t)$ is the single-qubit solution. The ultimate bound is thus obtained as

$$\overline{\mathcal{Q}}_{\mathcal{L}_\omega}[|\psi_0\rangle] = 4\,\partial_{\omega_1}\partial_{\omega_2}\log \mathrm{Tr}[\bar{\mathcal{E}}^N_{\omega_1,\omega_2}(t)\,\rho_0]\Big|_{\omega_1=\omega_2=\omega}, \tag{4.20}$$

where ρ_0 is the initial pure state. Given our choice $\rho_0 = |\psi_{\mathsf{GHZ}}\rangle\langle\psi_{\mathsf{GHZ}}|$, the computation can be greatly simplified. We find that

$$\begin{aligned}\bar{\mathcal{E}}^N_{\omega_1,\omega_2}(t)\,|\psi_{\mathsf{GHZ}}\rangle\langle\psi_{\mathsf{GHZ}}| =& \frac{1}{2}\Big[\left(\bar{\mathcal{E}}_{\omega_1,\omega_2}(t)\,|0\rangle\langle 0|\right)^{\otimes N} + \left(\bar{\mathcal{E}}_{\omega_1,\omega_2}(t)\,|1\rangle\langle 1|\right)^{\otimes N} \\ &+ \left(\bar{\mathcal{E}}_{\omega_1,\omega_2}(t)\,|0\rangle\langle 1|\right)^{\otimes N} + \left(\bar{\mathcal{E}}_{\omega_1,\omega_2}(t)\,|1\rangle\langle 0|\right)^{\otimes N}\Big]\end{aligned} \tag{4.21}$$

and now we need to find the expression for the single qubit map.

For transverse noise and for a single qubit, the equation to be solved in order to compute $\overline{\mathcal{Q}}$ is the following

$$\frac{\mathrm{d}\bar{\rho}}{\mathrm{d}t} = \bar{\mathcal{L}}^{\perp}_{\omega_1,\omega_2}\bar{\rho} = -\frac{i}{2}(\omega_1\sigma_z\bar{\rho} - \omega_2\bar{\rho}\sigma_z) + \frac{\kappa}{2}(\sigma_x\bar{\rho}\sigma_x - \bar{\rho}).$$

The solution to this equation can be obtained by choosing a basis of operators and using a matrix representation of superoperators [20] (see also the Supplementary Material of [93]). This is a standard technique also for canonical master equations. We choose to use the normalized Pauli operators $\tilde{\sigma}_i = \sigma_i/\sqrt{2}$ (where $\sigma_0 = \mathbb{1}$), so that $\mathrm{Tr}\left[\tilde{\sigma}_i\tilde{\sigma}_j\right] = \delta_{ij}$ The matrix associated to the single qubit map in this basis can then be obtained by matrix exponentiation.

We can write the generalized density operator $\bar{\rho}$ in Bloch form as

$$\bar{\rho} = \frac{1}{\sqrt{2}}(a_0\tilde{\sigma}_0 + \boldsymbol{a}\cdot\tilde{\boldsymbol{\sigma}}) \tag{4.22}$$

such that its trace is simply $\mathrm{Tr}[\bar{\rho}] = a_0$, since the basis operators are traceless. In this notation, the initial states $|0\rangle\langle 0|$ and $|1\rangle\langle 1|$ correspond to the vectors $e_{00} = \frac{1}{\sqrt{2}}(1,0,0,1)^{\mathsf{T}}$ and $e_{11} = \frac{1}{\sqrt{2}}(1,0,0,-1)^{\mathsf{T}}$, while the off-diagonal elements are $e_{01/10} = \frac{1}{\sqrt{2}}(0,1,\pm i,0)^{\mathsf{T}}$.

For our purposes we need the coefficient a_0, therefore we only need the first row of the matrix representation of $\bar{\mathcal{E}}^{\perp}_{\omega_1,\omega_2}(t)$, which turns out to be

$$\left[\bar{\mathcal{E}}^{\perp}_{\omega_2,\omega_2}(t)\right]_{0,*} = e^{-\frac{\kappa t}{2}} \begin{pmatrix} \cosh\left(\frac{t}{2}\sqrt{\kappa^2-(\omega_1-\omega_2)^2}\right) + \frac{\kappa \sinh\left(\frac{t}{2}\sqrt{\kappa^2-(\omega_1-\omega_2)^2}\right)}{2\sqrt{\kappa^2-(\omega_1-\omega_2)^2}} \\ 0 \\ 0 \\ \frac{i(\omega_2-\omega_1)\sinh\left(\frac{t}{2}\sqrt{\kappa^2-(\omega_1-\omega_2)^2}\right)}{\sqrt{\kappa^2-(\omega_1-\omega_2)^2}} \end{pmatrix}^{\mathsf{T}}. \tag{4.23}$$

From the two zeros in this vector we can see that the off-diagonal terms do not contribute to the trace and we can further simplify the calculation as

$$\begin{aligned} \mathrm{Tr}\left[\bar{\mathcal{E}}^{\perp N}_{\omega_1,\omega_2}(t)|\psi_{\mathsf{GHZ}}\rangle\langle\psi_{\mathsf{GHZ}}|\right] &= \frac{1}{2}\left(\mathrm{Tr}\left[\bar{\mathcal{E}}^{\perp}_{\omega_1,\omega_2}(t)|0\rangle\langle 0|\right]^N + \mathrm{Tr}\left[\bar{\mathcal{E}}^{\perp}_{\omega_1,\omega_2}(t)|1\rangle\langle 1|\right]^N\right) \\ &= \frac{1}{\sqrt{2}}\left\{\left([\bar{\mathcal{E}}^{\perp}_{\omega_1,\omega_2}(t)]_{0,*}\cdot e_{00}\right)^N + \left([\bar{\mathcal{E}}^{\perp}_{\omega_1,\omega_2}(t)]_{0,*}\cdot e_{11}\right)^N\right\}. \end{aligned} \tag{4.24}$$

After some algebra we can plug the result into (4.20) and finally obtain:

$$\overline{\mathcal{Q}}^{\perp}_{\mathcal{L}_\omega} = \frac{N^2\left(1-e^{-\kappa t}\right)^2 + N\left[2\kappa t + 1 - \left(2-e^{-\kappa t}\right)^2\right]}{\kappa^2}. \tag{4.25}$$

We immediately observe that $\overline{\mathcal{Q}}^{\perp}_{\mathcal{L}_\omega}$ depends on the noise parameter κ and is always smaller than the noiseless QFI $\mathcal{Q}_{\mathsf{HL}} = N^2t^2$, as expected because of the chained inequalities (2.60).

Furthermore this results shows that, as opposed to the parallel noise case, part of the information leaking into the environment is irretrievably lost, and cannot be recovered even if one has at disposal all the environmental degrees of freedom. On the other hand this expression does explicitly show Heisenberg scaling, and can be further optimized over the evolution time t. The optimal time $t_{\mathsf{opt}}(N)$ does not go to zero for $N \to \infty$, as it happens for the unconditional dynamics, instead it tends to a constant: $\lim_{N\to\infty} t_{\mathsf{opt}}(N) = c/\kappa$, where $c \approx 1.26$.

Curiously, the very same result is obtained by computing the unconditional QFI in the limit $\omega \to 0$, i.e.

$$\overline{\mathcal{Q}}^{\perp}_{\mathcal{L}_\omega} = \lim_{\omega\to 0} \mathcal{Q}\left[\rho^{\perp}_{\mathsf{unc}}\right], \tag{4.26}$$

the explicit proof of this fact is given in Section 4.3.3.

4.3.2 Numerical results on the effective bound

Having an analytical expression for the ultimate QFI, we want to check the performance of the realistic sequential scheme previously described, as quantified by the effective QFI. We compute this figure of merit both for photo-detection and homodyne detection via

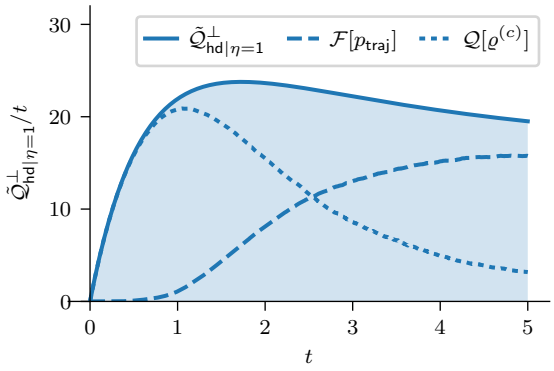

Figure 4.2: Contributions of the classical FI $\mathcal{F}[p_{\mathsf{traj}}]$ and the QFI of the final strong measurement $\mathcal{Q}[\rho^{(c)}]$ to the effective QFI $\tilde{\mathcal{Q}}_{\mathsf{hd}|\mathrm{J}=1}$ for homodyne with $N = 7$ and $\omega = 1$, in the transverse noise case.

the numerical methods presented in Sec. 2.3. Remarkably, from our results we observe that for unit efficiency $\eta = 1$ the effective QFI saturates the ultimate bound in both cases

$$\widetilde{\mathcal{Q}}^{\perp}_{\mathsf{hd},\eta=1} = \widetilde{\mathcal{Q}}^{\perp}_{\mathsf{pd},\eta=1} = \overline{\mathcal{Q}}^{\perp}_{\mathcal{L}_\omega}. \tag{4.27}$$

This has been checked up to $N = 14$, but we conjecture that this equality holds in general.

The two terms that contribute to $\widetilde{\mathcal{Q}}^{\perp}_{\mathsf{hd},\eta=1}$ always sum up to $\overline{\mathcal{Q}}^{\perp}_{\mathcal{L}_\omega}$ but with ω-dependent behaviors. This is shown for a particular set of parameters in Fig. 4.2. On the other hand, as explained before for the parallel case, $\widetilde{\mathcal{Q}}^{\perp}_{\mathsf{pd},\eta=1}$ is only equal to the average QFI of the conditional states. The classical FI $\mathcal{F}[p_{\mathsf{traj}}]$ is always identical to zero because the collapse operator $\sigma_x^{(j)}$ are unitary.

If we turn to the case of imperfect detection $\eta < 1$, we observe that the effective QFI lies between the unconditional QFI and the ultimate QFI, for both detection measurement strategies. This is expected because of the chained inequalities (2.60) and also confirms the conjecture (2.61) regarding the monotonicity with the efficiency η.

As an example, in Fig. 4.3 we plot the effective QFI over time for photo-detection and homodyne detection at different efficiencies, for three different values of N. We can see that at lower efficiencies the curves tend to the unconditional QFI $\mathcal{Q}[\rho^{\perp}_{\mathsf{unc}}]$, while for perfect efficiency they coincide with $\overline{\mathcal{Q}}_{\mathcal{L}_\omega}$. Notice that in general one cannot define a hierarchy between the two strategies, and that in particular, in the case of homodyne, the curves become constant at large t, due to the non-vanishing contribution of the classical Fisher information $\mathcal{F}[p_{\mathsf{traj}}]$ that is linear in t.

Since the numerical method for non-unit efficiency requires using the full Hilbert space, the complexity of the algorithm is exponential in N and we have been able to obtain results only up to $N = 7$. Consequently, we cannot explicitly witness a different scaling from the unconditional case. As a matter of fact the difference between $\max_t \left[\overline{\mathcal{Q}}^{\perp}_{\mathcal{L}_\omega}/t\right]$ and $\max_t \left[\mathcal{Q}\left[\rho^{\perp}_{\mathsf{unc}}\right]/t\right]$ is not very significant for $N \leq 7$. This is shown in Fig. 4.4 for

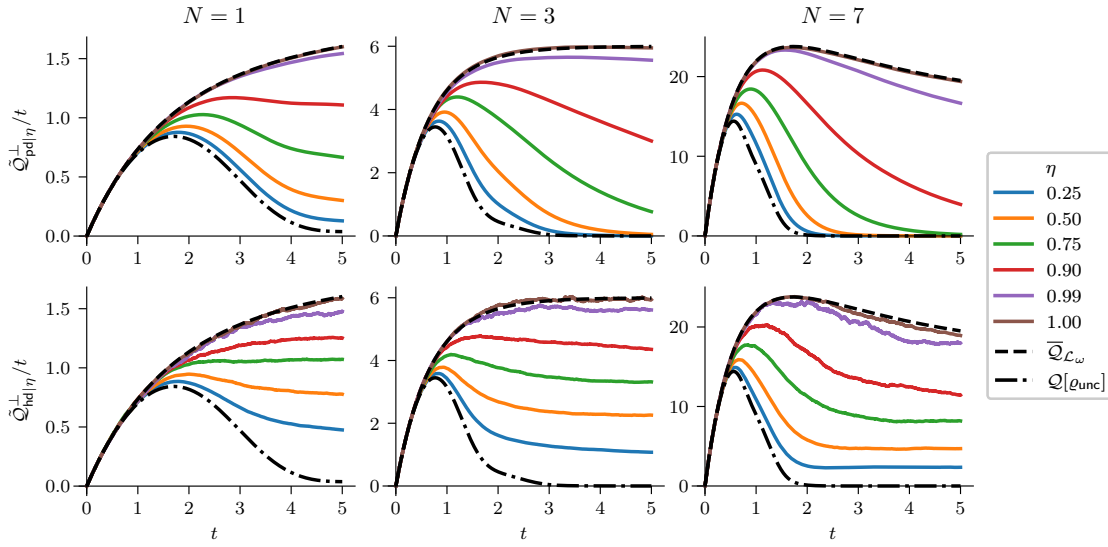

Figure 4.3: The figure shows the effective QFI for photo-detection $\widetilde{\mathcal{Q}}^{\perp}_{\mathsf{pd},\eta}/t$ (top row) and for homodyne detection $\widetilde{\mathcal{Q}}^{\perp}_{\mathsf{ph},\eta}/t$ (bottom row) with transverse noise over time, for different efficiencies η and for different values of N. The effective QFI is compared with the ultimate bound $\overline{\mathcal{Q}}^{\perp}_{\mathcal{L}_\omega}$ (black dashed line), and the QFI for the unconditional evolution $\mathcal{Q}[\rho^{\perp}_{\mathsf{unc}}]$ (black dot-dashed line). Here we take $\omega = \kappa$. The colored curves are obtained numerically as explained in Sec. 2.3, by simulating a large number $> 10\,k$ trajectories.

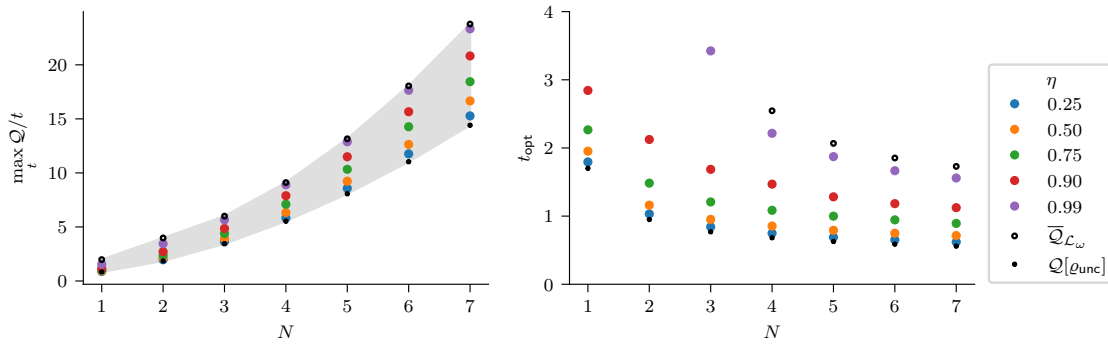

Figure 4.4: The maximum over time of the quantity $\mathcal{Q}/t$ (left panel) and the corresponding optimal time (right panel) for $\omega = \kappa$, where $\mathcal{Q} = \widetilde{\mathcal{Q}}^{\perp}_{\mathsf{pd}|\mathsf{J}}$ for various values of η for the colored dots, $\mathcal{Q} = \overline{\mathcal{Q}}^{\perp}_{\mathcal{L}_\omega}$ for the black circles, and $\mathcal{Q} = \mathcal{Q}[\rho_{\mathsf{unc}}]$ for the black stars. The gray shade shows the region individuated by the bounds in Eq. (2.60). Notice that $\overline{\mathcal{Q}}^{\perp}_{\mathcal{L}_\omega}/t$ is monotonically increasing for $N \leq 3$, and it reaches its maximum value for $t \to \infty$, and that the optimal measurement time $N \leq 2$ for $\eta = 0.99$ is out of scale.

photo-detection, in the case $\omega = \kappa$. As we can see, the two quantities have a similar scaling in this range of N, with the effective QFI lying between them with optimal values that are monotonous with η. The optimal measurement time decreases with N, and it increases with increasing η.

4.3.3 Unconditional quantum Fisher information for vanishing frequency

We are now going to present an explicit proof of the fact that the ultimate QFI for transverse noise is equal to the unconditional QFI for $\omega \to 0$. This fact is not fundamental for our previous results, but as far as we know this result is not present elsewhere in the literature. Since the way to obtain the final formula is not completely trivial, for completeness we decided to include the proof in this Thesis. The result is only mentioned, but not included in the paper [14]. We remark that frequency estimation with transverse noise and a vanishing parameter was considered in Appendix D of [35], where the authors highlight Heisenberg scaling can be recovered for $N \to \infty$. On the other hand, we are able to obtain the general result for any value of N.

Unconditional evolution of a GHZ state in transverse noise

A GHZ state evolving in time according to Eq. (4.1) becomes a mixture of states of the form $|s\rangle \pm |\bar{s}\rangle$, where s is a binary string and $\bar{s}$ is its bitwise negation, e.g $|s\rangle = |00101\rangle$ and $|\bar{s}\rangle = |11010\rangle$. In the computational basis the density matrix maintains a cross-diagonal form.

It is clever to parametrise the matrix elements with an index $m \in [0, N]$ (as usual N is the number of qubits), which counts how many 1s appear in the binary string s, i.e. the sum of the binary elements of s. Since we have N qubits there are 2^N different possible strings, and there are $\binom{N}{m}$ different binary strings that sum to the value m, so that $\sum_{m=0}^{N} \binom{N}{m} = 2^N$. It turns out that the matrix elements of an evolved GHZ state only depend the value m.

With this parametrization we have the following matrix elements [53]

$$\begin{aligned} \rho_{m,m} &= \frac{1}{2}\left[d^m a^{N-m} + d^{N-m} a^m\right] \\ \rho_{m,N-m} &= \frac{1}{2}\left[f^m (b - ic)^{N-m} + f^{N-m}(b + ic)^m\right], \end{aligned} \tag{4.28}$$

where we can further notice the symmetry of the diagonal terms under the exchange $m \to N - m$. The coefficients appearing in the expression are given by

$$\begin{aligned} a &= \frac{1}{2}\left(1 + e^{-\kappa t}\right) \qquad d = \frac{1}{2}\left(1 - e^{-\kappa t}\right) \qquad b = e^{-\frac{\kappa t}{2}} \cosh\left(\frac{t}{2}\sqrt{\kappa^2 - 4\omega^2}\right) \\ f &= \kappa \frac{e^{-\frac{\kappa t}{2}} \sinh\left(\frac{t}{2}\sqrt{\kappa^2 - 4\omega^2}\right)}{\sqrt{\kappa^2 - 4\omega^2}} \qquad c = 2\omega \frac{e^{-\frac{\kappa t}{2}} \sinh\left(\frac{t}{2}\sqrt{\kappa^2 - 4\omega^2}\right)}{\sqrt{\kappa^2 - 4\omega^2}}. \end{aligned} \tag{4.29}$$

All these coefficients are real as long as $\omega < \frac{\kappa}{2}$, which is the case we are interested in, since we want to take the limit $\omega \to 0$.

Piecewise QFI for a qubit

The QFI for qubit states can be very conveniently written via Bloch representation [310]; by writing the state in Bloch form

$$\rho = \frac{1}{2}(\mathbb{1} + \boldsymbol{v}\cdot\boldsymbol{\sigma}), \tag{4.30}$$

the QFI reads

$$\mathcal{Q}_\lambda[\rho] = \begin{cases} |\partial_\lambda \boldsymbol{v}|^2 + \frac{|\partial_\lambda \boldsymbol{v}\cdot\boldsymbol{v}|^2}{1-|\boldsymbol{v}|^2} & |\boldsymbol{v}| < 1 \\ |\partial_\lambda \boldsymbol{v}|^2 & |\boldsymbol{v}| = 1; \end{cases} \tag{4.31}$$

we note that this piecewise definition can give rise to discontinuities in the QFI. This is not an accident of this formula, but it is a general behaviour of the QFI when the density matrix changes its rank by varying the value of the estimated parameter [247][5]

In particular, for a qubit the only possible change of rank is that for λ_0 the state becomes pure, i.e. $|\boldsymbol{v}| = 1$ and so the $\lim_{\lambda\to\lambda_0}$ gives rise to a $\frac{0}{0}$ indeterminate form; we can then use L'Hôpital's rule and get

$$\lim_{\lambda\to\lambda_0} \mathcal{Q}_\lambda[\rho] = -\boldsymbol{v}\cdot\partial_\lambda^2\boldsymbol{v}|_{\lambda=\lambda_0}. \tag{4.32}$$

It is easy to see that this example is relevant for frequency estimation with transversal noise. If we choose an autostate of σ_x as the initial state and then evolve it with the dynamics given by (4.1) for $\alpha = x$ and $N = 1$, when $\omega = 0$ the evolved state remains pure, since the initial state is an eigenstate of the Liouvillian. A similar argument can be applied when dealing with an initial GHZ state, as we now proceed to show.

Final result

It is important to notice the QFI of a GHZ state evolving with the dynamics given by the master equation (4.1) for $\alpha = x$ can be computed by summing up with the appropriate weights the QFIs of $\lfloor N/2+1\rfloor$ qubits.

Given the cross structure of the evolved density matrix and the symmetry of the elements (4.28), we can reshuffle (swapping columns and rows) the $2^N \times 2^N$ matrix and write it as the direct sum of 2×2 matrices defined as follows

$$\varsigma_m = \begin{pmatrix} \rho_{m,m} & \rho_{m,N-m} \\ \rho^*_{m,N-m} & \rho_{m,m} \end{pmatrix}, \tag{4.33}$$

where now we need only half the values of the index $m = 0,\ldots,\lfloor N/2\rfloor$. In the reshuffled total state each of these ς_m is repeated $\binom{N}{m}$ times, except the last matrix for $m = \lfloor N/2\rfloor$ that appears $\frac{1}{2}\binom{N}{m}$ times if N is even and $\binom{N}{m}$ times if N is odd. We remark that this reshuffling is a unitary operation and it does not change the QFI.

[5] It is not widely known in the quantum metrology community that this behaviour is not peculiar of quantum mechanics. The *classical* statistical model corresponding to the optimal measurement is not regular around the critical value of the parameter. Since the support of the random variable changes by changing the parameter the *classical* Cramér-Rao bound is not well defined. This issue will we addressed in a forthcoming communication [258].

Each matrix ς_m is defined by three distinct real numbers, while their partial derivative, has only two non-zero real elements

$$\partial_\omega \varsigma_m = \begin{pmatrix} 0 & \partial_\omega \rho_{m,N-m} \\ (\partial_\omega \rho_{m,N-m})^* & 0 \end{pmatrix}. \tag{4.34}$$

To compute the QFI it is not necessary to diagonalize the whole density matrix but we can do it block by block and we get to

$$\mathcal{Q}[\rho_t] = \frac{1}{2} \sum_{m=0}^{N} \binom{N}{m} \mathcal{Q}[\varsigma_m], \tag{4.35}$$

where we have extended the sum to N again since we have that $\varsigma_m = \varsigma_{N-m}$ for the simmetry of the coefficients. Even if the matrices ς_m are not properly normalized density matrices, the function $\mathcal{Q}$ is the same function used to computed the QFI on a normalized state. If we renormalize the matrices as follows

$$\tilde{\varsigma}_m = \frac{1}{2} \begin{pmatrix} 1 & \frac{\rho_{m,N-m}}{\rho_{m,m}} \\ \frac{\rho^*_{m,N-m}}{\rho_{m,m}} & 1 \end{pmatrix} \qquad \partial_\omega \tilde{\varsigma}_m = \frac{1}{2} \begin{pmatrix} 0 & \frac{\partial_\omega \rho_{m,N-m}}{\rho_{m,m}} \\ \frac{(\partial_\omega \rho_{m,N-m})^*}{\rho_{m,m}} & 0 \end{pmatrix}, \tag{4.36}$$

the corresponding term in the total QFI is then the rescaled QFI of the normalized matrix:

$$\mathcal{Q}[\varsigma_m] = 2\rho_{m,m} \mathcal{Q}[\tilde{\varsigma}_m]. \tag{4.37}$$

For $\omega \to 0$ we have that $|\rho_{m,N-m}| = \rho_{m,m}$, therefore the normalized qubit states are pure and to get the limiting QFI we need to use the previously introduced formula (4.32). The global N qubit state does not become pure for $\omega \to 0$, but the density matrix goes from full rank, i.e. 2^N nonzero eigenvalues, to having rank 2^{N-1} half the eigenvalues go to zero for $\omega \to 0$. In this case it is possible to compute the sum (4.35) explicitly

$$\lim_{\omega \to 0} \mathcal{Q}\left[\rho^N_{\mathrm{GHZ}}, \mathcal{L}_\omega, t\right] = \frac{1}{2} \sum_{m=0}^{N} \binom{N}{m} \left(\frac{-2\rho_{m,N-m} \cdot \partial^2_\omega \rho_{m,N-m}}{\rho_{m,m}} \right) \Bigg|_{\omega=0}, \tag{4.38}$$

the formula for the qubit QFI is simplified because the off-diagonal terms are real for $\omega = 0$. The final result is the following

$$\lim_{\omega \to 0} \mathcal{Q}\left[\rho^N_{\mathrm{GHZ}}, \mathcal{L}_\omega, t\right] = \frac{N^2 \left(1 - e^{-\kappa t}\right)^2 + N\left[2\kappa t + 1 - \left(2 - e^{-\kappa t}\right)^2\right]}{\kappa^2} = \overline{\mathcal{Q}}^{\perp}_{\mathcal{L}_\omega} \tag{4.39}$$

and it is equal to the ultimate QFI as previously anticipated. This means that for $\omega \to 0$ the hierarchy of inequalities (2.60) collapses and the three QFIs (unconditional, effective and ultimate) have the same value. It is not clear if there is a deeper physical meaning behind this result.

Summary

- A system of N qubits is used to estimate the frequency of rotation around a certain axis. When the evolution is only given by the Hamiltonian and the system is

prepared in the optimal GHZ state the QFI scales as N^2 (Heisenberg limit). When the same noise acts independently on each qubit this scaling is lost. For noise parallel to the Hamiltonian imprinting the rotation, the scaling gets linear in N (standard quantum limit). When the noise is transverse there is an intermediate asymptotic scaling.

- We consider an initial GHZ state, which is optimal in the noiseless case. For both geometries, by continuously monitoring the noise channel of each qubit, Heisenberg scaling can be restored when detection is perfectly efficient, without the need of any feedback operation.

- For parallel noise the ultimate achievable precision is equal to that obtainable in the purely Hamiltonian case. This precision can be achieved both by photo-detection and homodyne detection in the limit of perfect efficiency, thus all the original information can be retrieved. When the efficiency is not one, the scaling is standard quantum limited, but the constant is rescaled by a factor dependent on the efficiency. Moreover, for an initial GHZ state it is not necessary to monitor all the qubits separately; due to the symmetry of the state, a single efficient photo-detector monitoring all the output fields is enough.

- For transverse noise the non-commutative nature of the dynamics makes the ultimate quantum Fisher information smaller than the purely Hamiltonian case. This ultimate bound can be saturated both by photo-detection and homodyne detection, as numerically shown. There are no conclusive result on the scaling for inefficient monitoring.

- When the true value of the frequency is zero (more precisely it *tends* to zero) the unconditional, effective and ultimate quantum Fisher informations are all equal, and thus continuous monitoring is not necessary.

Part II

Nonclassical continuous variables quantum states

CHAPTER 5

Kerr nonlinearity for enhanced loss estimation

This chapter is the first one dealing with continuous variable states and their nonclassical properties, but the topic is still closely related to the first part of this thesis. Previously, we have shown how continuous measurements are useful to obtain an improved metrological precision. Here, we explore the effect of a nonlinear Hamiltonian acting on a continuous variable system and we show that, in the estimation problem under consideration, such a nonlinearity can again be considered a metrological resource.

In the following analysis, the quantum estimation framework is more straight-forward and we now concentrate only on the unconditional Lindblad dynamics of the system; the relevant figure of merit is the QFI of the unconditional state. However, the metrological problem is quite different; we are not interested in the estimation of a Hamiltonian parameter, but of the strength of the coupling with the external environment, which represents the *loss rate*.

Characterizing lossy channels in continuous variable systems is crucial to quantify decoherence [257], to assess quantum illumination protocols [40, 120, 273, 306] and to realize quantum reading of classical memories [233]. In some specific cases, the task is simply to discriminate between the presence or the absence of losses [140, 220, 253], whereas, in general, a strategy to estimate the exact value of the loss is needed.

In the last decades, much attention has been devoted to the estimation of loss with different initial preparations of the probes. Optimization over Gaussian input states has been performed [200], showing that ultimate precision may be achieved using photon counting and Gaussian operations at the output. Fock states have also been shown to saturate the ultimate bound on precision [1, 252] and also the performance of thermal states was addressed [91]. Very recently, the more general problem of estimating multiple loss parameters under energy constraints has been solved in full generality [204].

All these works are focused on Gaussian lossy channels, where dissipation is due to linear coupling of a radiation mode to the environment, modeled as a bath of external oscillators in the vacuum state. On the other hand, optical media where light propagates, such as gasses, biological samples or optical fibers, may be characterized also by a (usually small) non-linear response to the electromagnetic field. This motivates us to consider systems where, besides the dissipation due to linear coupling to the environment, a nonlinear Hamiltonian is present.

For this analysis, we focus on self-Kerr interaction [32], naturally occurring during propagation of radiation in a nonlinear medium with non negligible cubic nonlinearity.

The dissipative evolution in the presence of self-Kerr effect has been widely studied in quantum optics, either at zero [193] or at finite temperature [267]. This effect can be used to generate Schrödinger cat-like states [148, 196, 219, 307, 308]. Even though cubic nonlinearities of optical media are too small to witness these states, they have been observed with an artificial Kerr medium in circuit quantum electrodynamics [157]. The appeareance of nonclassical states is a general feature of nonlinear Hamiltonians; we are going to explore this topic with a different kind of systems in Chapter 6.

In quantum metrology, the presence of non-linear effects has been already recognized as a resource. Intuitively, it allows one to achieve high precision by using robust classical probe states, instead of fragile nonclassical states [170, 171, 242], because the nonclassicality is dynamically generated during the encoding of the parameter. This is in some way similar to what we saw in Chapter 3, in that case the nonclassicality was represented by the conditional spin squeezing. In particular, a Kerr-type nonlinearity has been studied for estimation of squeezing and displacement of a Gaussian state [99] and to improve Michaelson interferometry [172].

We analyse in detail the estimation of loss in the presence of Kerr nonlinearity. We mostly focus on estimation strategies based on Gaussian probes (coherent and squeezed vacuum states), while also briefly examining the use of few-photon probes, the simplest nontrivial ones being optical qutrits. Overall, our results indicate that the presence of Kerr nonlinearity always enhances estimation, improving precision compared to the pure linear case. This kind of nonlinearity is present in optical fibers, but it can have a negative impact on other tasks beyond estimation, for example it degrades the capacity of the channel [76].

The work we present here has a slightly different approach than most of the previous works on loss estimation in the linear case. Nearly all of the literatures is focused on the estimation of the overall loss, which includes also the interaction time and not only the loss *rate*. On the other hand, we focus on the loss rate parameter itself, thus making the time dependence explicit. This point is relevant in our analysis, because dissipation and nonlinearity set two different time scales in the evolution of the probe state. We address the estimation precision in two regimes of "short" and "long" interaction times. We show that in principle nonlinearity always improves estimation, even though the optimal measurement might be complicated. However, for a short interaction time, i.e. for media of moderate size, the enhancement of precision may be substantial and it can also be relevant for conventional detection schemes, such as homodyning.

5.1 The interaction model

In this work we consider a lossy bosonic channel with a loss rate parameter γ, which is the quantity that we want to estimate, where non-linear Kerr effect with coupling $\tilde{\lambda}$ is present. In the absence of any non-linear effect and working in the interaction picture, the density operator ρ for a single bosonic mode in the channel satisfies a Lindblad master equation of the form

$$\frac{d\rho}{dt} = \frac{\gamma}{2}\mathcal{D}[\hat{a}]\rho = \gamma(\hat{a}\rho a^\dagger - \frac{1}{2}\hat{a}^\dagger\hat{a}\rho - \frac{1}{2}\rho\hat{a}^\dagger\hat{a}), \tag{5.1}$$

where $\hat{a}$ is the annihilation operator in the Fock space of the bosonic mode and $\mathcal{D}$ is the usual Lindblad dissipation superoperator. This equation can be obtained from the methods of Section 1.2, by specifying an interaction Hamiltonian between the input modes of the form $\hat{a}^\dagger \hat{b}_{\rm in}(t) + \hat{a}\hat{b}_{\rm in}(t)^\dagger$ and by choosing the vacuum as initial state of the input modes. This equation can also be recast in terms of covariance matrix and first-moments, as shown in Section 1.4.3; we do not make use of that description, because it is not very helpful when adding a nonlinear Hamiltonian term.

The Kerr interaction is described by a term in the Hamiltonian of the system, which is more than quadratic in the creation and destruction operators, namely

$$\hat{H}_{\rm K} = \tilde{\lambda}(\hat{a}^\dagger \hat{a})^2. \tag{5.2}$$

To take into account this effect, the master equation in Eq. (5.1) now becomes

$$\frac{d\rho}{dt} = -i[\hat{H}_{\rm K}, \rho] + \frac{\gamma}{2}\mathcal{D}[\hat{a}]\rho. \tag{5.3}$$

Upon rescaling the quantities with respect to the loss parameter γ

$$\tau = \gamma t, \qquad \lambda = \tilde{\lambda}/\gamma, \tag{5.4}$$

we arrive at

$$\frac{d\rho}{d\tau} = -i\lambda[(\hat{a}^\dagger \hat{a})^2, \rho] + \hat{a}\rho\hat{a}^\dagger - \frac{1}{2}\hat{a}^\dagger\hat{a}\rho - \frac{1}{2}\rho\hat{a}^\dagger\hat{a}, \tag{5.5}$$

which corresponds to the following system of equations for the matrix elements $\rho_{p,q} = \langle p|\rho|q\rangle$ in the Fock basis:

$$\frac{d\rho_{p,q}}{d\tau} = -\left[i\lambda(p^2 - q^2) + \frac{1}{2}(p+q)\right]\rho_{p,q} + \sqrt{(1+p)(1+q)}\rho_{p+1,q+1}. \tag{5.6}$$

The solution for the $\rho_{p,q}$ has a nice form when the initial state is a coherent state, $\rho_0 = |\alpha\rangle\langle\alpha|$ [219]. It reads

$$\rho_{p,q}(\tau) = \frac{\alpha^p \overline{\alpha}^q}{\sqrt{p!q!}} \exp\left\{-\frac{1}{2}(p+q)\Delta\tau - |\alpha|^2\left[1 - \frac{1-e^{-\Delta\tau}}{\Delta}\right]\right\}, \tag{5.7}$$

where $\Delta = 1 + 2i\lambda(p-q)$.

We also consider the case of a squeezed vacuum initial state $\rho_0 = |r\rangle\langle r|$; for convenience, but without loss of generality we restrict to a real squeezing parameter r, so that the squeezing operator reads $\hat{S}(r) = \exp\left(\frac{1}{2}r^2(\hat{a}^{\dagger 2} - \hat{a}^2)\right)$. The explicit analytical expression of the matrix elements of the solution with this initial state can be found in Refs. [192, 229]. The matrix elements are known also for arbitrary initial states [52, 230]. Notice that for the lossy channel (i.e. a thermal bath at zero temperature) these analytical expressions of the matrix elements are suitable for a numerical computation of the values of the relevant observables. As a matter of fact it is possible to work in a truncated Hilbert space in the Fock basis, since the loss only drives the system into smaller subspaces; this would not be possible if we considered both loss and noise (i.e. a bath with finite temperature). Notice also that $\rho(\tau)$ is in general a mixed state and cannot be diagonalized

explicitly, such that an analytic expression for the quantum Fisher information is not available.

We start our analysis by reviewing the analytic solutions when the Kerr effect is not present (i.e. $\lambda = 0$), and then discuss approximate and numerical solutions for the general case of $\lambda \neq 0$. Before proceeding, a quick remark about the notation. In order to conform with the notation of the original paper [243], we employ the following notation for the QFI of the evolved state:

$$H_\gamma(\tau) \equiv \mathcal{Q}[\rho_\gamma(\tau)] \tag{5.8}$$

and we denote the same quantity obtained for different initial states with superscripts.

5.2 Solution in the absence of non-linear effects

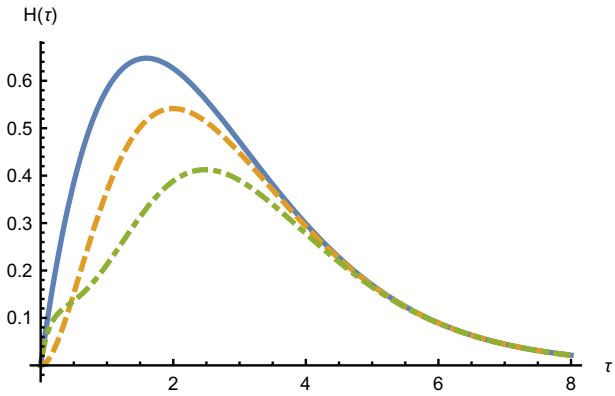

Figure 5.1: Plot of the QFI in the absence of non-linearity as a function of the rescaled time τ for different probe states at the fixed mean input energy $\bar{n} = 1$. The solid blue line represents the optimal Fock state $|1\rangle$, the dashed orange line represent a coherent state, while the dot-dashed green line represent the squeezed vacuum. The graph reflects the general fact that a Fock state is always optimal and for $\tau \to 0$ the optimal Gaussian state is the squeezed vacuum, while for greater values a coherent state allows for a better estimation.

When $\lambda = 0$, i.e. the non-linear effects are absent, the channel is Gaussian and an initial coherent state remains coherent and decreases its amplitude during the evolution:

$$|\psi_\gamma(\tau)\rangle = |\alpha e^{-\frac{1}{2}\tau}\rangle\,. \tag{5.9}$$

An analytic expression for the QFI is easily obtained using the formula for pure states (1.84):

$$H_\gamma^{\mathrm{c}}(\tau) = \frac{\bar{n}}{\gamma^2}\tau^2 e^{-\tau}, \tag{5.10}$$

while for the squeezed vacuum the solution is [200]:

$$H_\gamma^{\mathrm{sv}}(\tau) = \frac{\left(-2e^\tau + e^{2\tau} + 2\right)\tau^2\bar{n}}{\gamma^2(e^\tau - 1)(2e^\tau\bar{n} - 2\bar{n} + e^{2\tau})}, \tag{5.11}$$

where $\bar{n} = \mathrm{Tr}\left[\rho_0 \hat{a}^\dagger \hat{a}\right]$ is the mean photon-number of the initial state; we have $\bar{n} = |\alpha|^2$ for the coherent state and $\bar{n} = \sinh^2 r$ for the squeezed vacuum. We also report the QFI for Fock probe states $|n\rangle$, which is optimal when the mean energy is an integer ($\bar{n} = n$):

$$H_\gamma^{\mathrm{F}}(\tau) = \frac{\bar{n}\tau^2}{\gamma^2(e^\tau - 1)}. \tag{5.12}$$

In Figure 5.1 we represent the plots of the QFI for the three probe states; this also sums up previous results [1, 200] by showing that for small losses the optimal Gaussian state is the squeezed vacuum, for higher losses a coherent state is better, while a Fock state is optimal for every τ. Moreover, we observe that in general $H_\gamma(\tau)$ vanishes for $\tau \gg 1$ and has a global maximum at a certain time $\overline{\tau}$. This means that if one is able to control the interaction time in an experiment, setting it to $\overline{\tau}$ allows for optimal estimation of γ. In particular for the coherent state the optimal time is $\overline{\tau} = 2$, with the following optimal value (we use a bar to denote quantities optimized over the interaction time τ):

$$\overline{H}_\gamma^{\mathrm{c}} = \frac{4|\alpha|^2}{e^2\gamma^2}. \tag{5.13}$$

Furthermore, for coherent states the QFI is saturated by photon-number and a quadrature measurement; more complicated measurements are needed to saturate the QFI of the squeezed vacuum.

5.3 Solution in the presence of Kerr effect

As stated in Section 5.1, with $\lambda \neq 0$ the state $\rho(\tau)$ is a mixed state and not explicitly diagonalizable. In the following, we present an approximate solution for the coherent probe state, valid in the regime of small λ and τ, in which the state of the system remains pure and it is thus possible to get an analytical expression for the QFI. Then we show numerical results obtained from a truncation of the Fock space for both coherent and squeezed vacuum probe states. The results are presented both for the optimal time and small time cases; at optimal time only the coherent input is considered since the optimal value of the QFI is always greater than the optimal value of the squeezed vacuum QFI. This fact can be seen in Fig. 5.2, where we show the behaviour of the QFI with and without Kerr interaction for both the Gaussian probes we are considering. From the particular choice of parameters in Fig. 5.2 we see that the QFI with nonlinear interaction always has a greater value: we are going to show that this is true in general.

5.3.1 Pure state approximation

When we work with a coherent input state and the non-linear effect is small compared to the loss parameter, i.e. when $\lambda \ll 1$, the state of the system can still be approximated with a pure state for small τ. Expansion of the exponent of e in Eq. (5.7) to the first order in λ and then expansion to the second order of τ yields

$$\rho_{p,q}(\tau) = \frac{\alpha^p \bar{\alpha}^q}{\sqrt{p!q!}} \exp\left[-\frac{1}{2}(p+q)\tau - e^{-\tau}|\alpha|^2 - i\lambda(p^2 - q^2)\tau - i\lambda|\alpha|^2(p-q)\tau^2\right]. \tag{5.14}$$

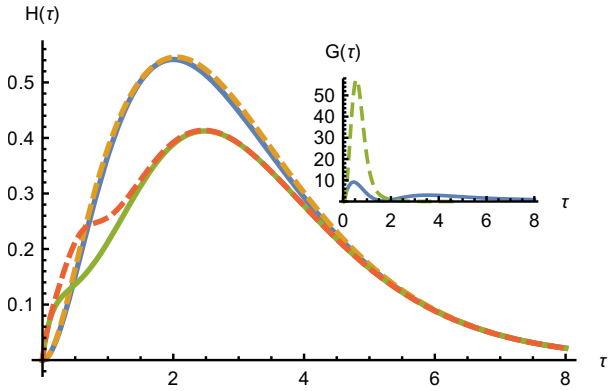

Figure 5.2: Plot of the QFI as a function of the rescaled time τ for different probe states at the fixed mean input energy $\bar{n} = 1$. The solid curves are obtained in the absence of nonlinearity, while the dashed curves are obtained in the presence of Kerr nonlinearity (with $\lambda = 0.5$). The solid blue and dashed oranges curves which lie on top in the region $\tau \approx 2$ refer to the coherent state probe, while the solid green and dashed orange curves which lie on top in the region $\tau \approx 0$ refer to the squeezed vacuum probe. In the inset panel we represent the relative gain $G(\tau) \equiv H_{\lambda,\gamma}(\tau)/H_{\gamma}(\tau) - 1$ of the QFI in the presence of non-linearity over the QFI without Kerr effect, shown in percentage. The solid blue line represents the coherent probe, while the dashed green line represents the squeezed vacuum. In both cases there is a peak in gain at $\tau \lesssim 1$, much more pronounced for the squeezed vacuum state. The gain vanishes for increasing τ, but a second, smaller peak can be observed for the coherent state.

This is the lowest order of expansion for which we obtain a correction to the QFI of Eq. (5.10).

The QFI computed for $\rho_{p,q}(\tau)$ of Eq. (5.14) is

$$H^{c}_{\lambda,\gamma}(\tau) = \frac{|\alpha|^2}{\gamma^2}\tau^2 e^{-\tau}\left(1 + 4\lambda^2\tau^2|\alpha|^4\right) + O(\lambda^3). \tag{5.15}$$

We notice that $H^{c}_{\lambda,\gamma}(t)$ adds a correction of second order in λ and in τ to $H^{c}_{\gamma}(\tau)$ of Eq. (5.10). We define a new figure of merit: the *relative gain* in the estimation of γ, as follows

$$G_{\lambda}(\tau) \equiv H_{\lambda,\gamma}(\tau)/H_{\gamma}(\tau) - 1\,, \tag{5.16}$$

then using the pure state approximation it reads:

$$G^{c}_{\lambda}(\tau) = 4\lambda^2\tau^2|\alpha|^4 + O(\lambda^3). \tag{5.17}$$

The optimal time, up to the second order in λ, is

$$\overline{\tau}(\lambda) = 2 + 32\lambda^2|\alpha|^4 + O(\lambda^3) \tag{5.18}$$

and the corresponding optimal QFI is

$$\overline{H}^{c}_{\gamma}(\lambda) = \frac{4|\alpha|^2}{e^2\gamma^2}(1 + 16\lambda^2|\alpha|^4) + O(\lambda^3); \tag{5.19}$$

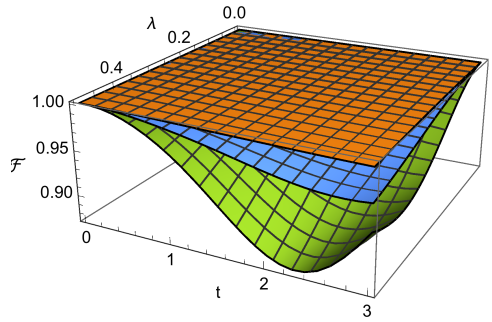

Figure 5.3: Fidelity between the pure state of Eq. (5.14) and the exact state (truncation at 10 photons), for $\alpha = 0.5$ (orange), $\alpha = 0.75$ (blue) and $\alpha = 1$ (green). The fidelity decreases with increasing λ and α. It temporarily decreases with time, but it tends asymptotically to one as the system reaches the state $|0\rangle$. For small values of α and λ the pure state approximation has fidelity above 0.99, which then decreases as the energy of the state increases.

so the *optimal relative gain* $\overline{G}_\lambda \equiv \overline{H}_{\lambda,\gamma}/\overline{H}_\gamma - 1$ is

$$\overline{G}^{\mathrm{c}}_\lambda = 16\lambda^2|\alpha|^4 + O(\lambda^3). \tag{5.20}$$

Equations (5.17) and (5.20) show that the correction to the QFI due to the presence of a small non-linear effect is positive and increases with λ^2. This means that the nonlinearity of the dispersive medium can be a resource in the estimation of the loss parameter.

The fidelity of the approximate state of Eq. (5.14) to the exact state (after a truncation of the density matrix) is shown in Fig. 5.3 as a function of τ and λ, for two values of $|\alpha|$. The pure state approximation is good for a wide range of parameters only if the energy of the initial state is not too big, so that fidelity is close to one. This means that the analytical expression of the optimal relative gain (5.20) is good only for small energies, while at a fixed small time $\tau \ll 1$ the relative gain (5.17) is a good approximation even for higher input energies.

In Subsection 5.3.2 we calculate the QFI numerically for general values of λ and α, in order to verify the increase of the QFI also for regions where the pure-state approximation does not hold.

5.3.2 Numerical results

As the density matrix cannot be diagonalized in general and the Fock space is infinite-dimensional, in order to evaluate the QFI we resort to numerical diagonalization of the density matrix in a truncated Fock space. The truncation size, which depends on the input energy, is chosen in such a way that the difference between the analytical and the numerical QFI for $\lambda = 0$ must be less than 0.001%.

Optimal QFI

The behaviour of the QFI as a function of time for fixed λ and α is shown in Fig. 5.2. The QFI starts from zero and reaches a maximum, then vanishes as τ increases and the system

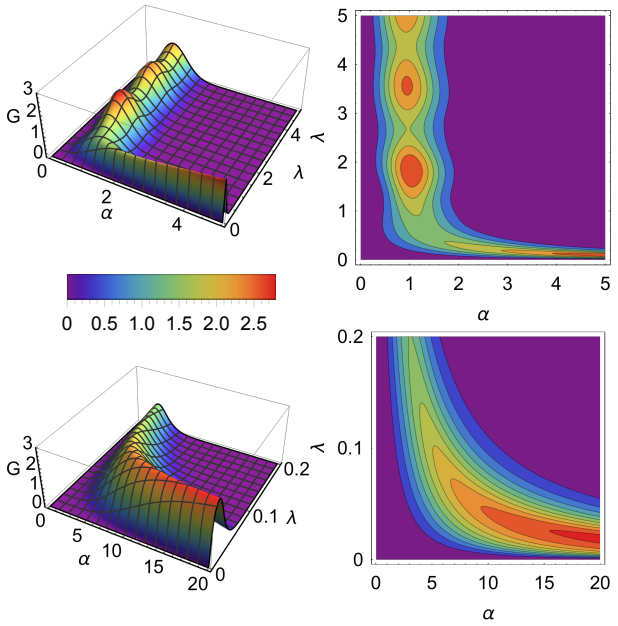

Figure 5.4: Optimal relative gain $\overline{G} \equiv \overline{H}_{\lambda,\gamma}/\overline{H}_{\gamma} - 1$ of the optimal QFI in presence of non-linearity over the optimal QFI without Kerr effect for different regions of α and λ, shown in percentage. On the left, a 3D plot, on the right the corresponding contour plot. We can see that the gain is always greater than zero, vanishing for large λ and α. We can identify two regimes: the first regime, visible in the upper panels when $\alpha \lesssim 2$ is characterized by the presence of local maxima of the gain, which reaches values of about 2%. For large λ the improvement reaches a non-vanishing asymptotic value. In the second regime, visible in the lower panels, at fixed α the gain has a single maximum with respect to λ. As α increases, the maximum moves to smaller values of λ, but G increases.

reaches the zero-photon state $|0\rangle$. Assuming that we are able to control the interaction time of the probe with the channel, we can consider as a figure of merit the optimal QFI, i.e. the maximum of $H_{\lambda,\gamma}(t)$ over time.

In Fig. 5.4 we show the optimal relative gain in the estimation of γ. The first notable result is the confirmation of the results obtained in the pure state approximation: the optimal QFI in presence of non-linearity is always greater than without Kerr effect, i.e. the optimal relative gain is always greater than zero. It vanishes for increasing α and λ and for $\alpha \to 0$.

By looking at the panels of Fig. 5.4, we can identify two regimes. The first regime, for $\alpha \lesssim 2$, is characterized by the presence of local maxima of the gain. At fixed α, the maxima occur periodically, with G reaching an asymptotic value for $\lambda \to \infty$. In the second regime, for $\alpha \gtrsim 2$, there is a single local maximum for the gain at fixed α. For increasing α, the optimal λ decreases, but G increases. It is not clear if there is a local maximum for α greater than the values under investigation or if this behaviour will persist for $\alpha \to \infty$, and, in the latter case, if G increases indefinitely or saturates with α.

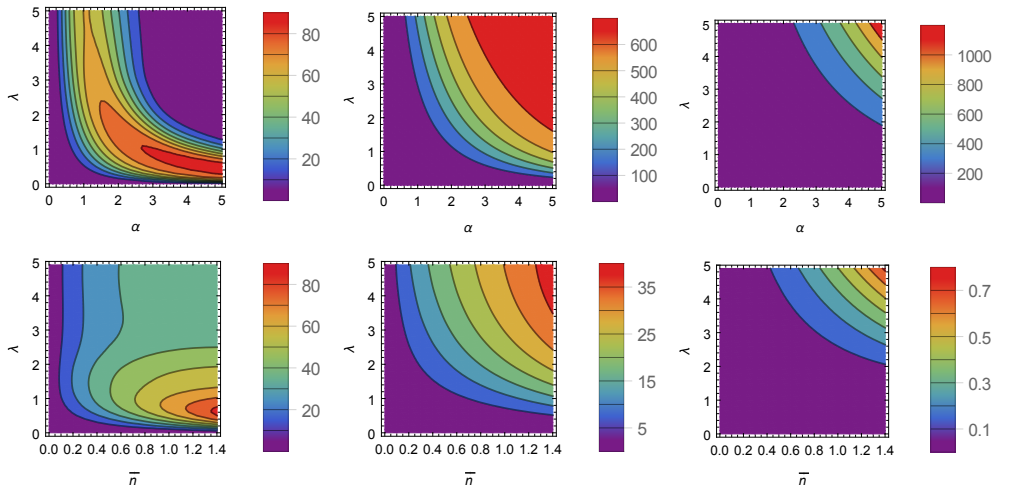

Figure 5.5: Relative gain $G(\tau) \equiv H_{\lambda,\gamma}(\tau)/H_{\gamma}(\tau) - 1$ of the QFI in presence of non-linearity over the QFI without Kerr effect at fixed time for a coherent probe state (top) and for a squeezed vacuum probe state (bottom), shown in percentage. From left to right we have the results for $\tau = 0.5$, 0.1, 0.01. For coherent states we can see a structure similar to that of Fig. 5.4: the relative gain increases with α and λ until it reaches a maximal value, but at small τ the relative gain is much higher than at the optimal time. For the squeezed vacuum state the gain is smaller as τ gets smaller (cfr. Fig. 5.2).

Small time QFI

Now instead of studying the QFI maximized over time we look at the behaviour at a fixed time, in particular we focus on times smaller than the characteristic time of the loss, i.e. $\tau < 1$, as an example we study three cases $\tau = 0.5, 0.1, 0.01$. This regime is of interest for media of moderate size, such as biological samples.

In this setting the improvement brought by the nonlinear interaction can be substantial. In Fig. 5.5 we show the results for a coherent probe state (top row) and for a squeezed vacuum probe state (bottom row). For the squeezed probe we restricted the computation to a smaller range of mean input energies, as the dimension of the truncated Hilbert space needed to obtain a good approximation grows much more rapidly.

By looking at the top-left panel in Fig. 5.5, the one for $\tau = 0.5$, we notice a similar structure to the one in Fig. 5.4, albeit rescaled. We found that fixing the time parameter τ changes the scaling in the $\alpha - \lambda$ (or $\bar{n} - \lambda$) plane; however, it was not possible to explicitly see this scaling from the analytical expressions of the states.

The improvement due to the Kerr nonlinearity is much more relevant at times which do not correspond to the optimal time, indeed in Fig. 5.2 we see that the maxima of the graph in the inset panel do not correspond to the ones in the main graph. Moreover, even if the behaviour of different input states is slightly different, the most relevant improvement is always obtained for $\tau < 1$, this is due to the fact that the value of the QFI at those times is smaller, so that a slight improvement in the absolute value brings a great relative gain.

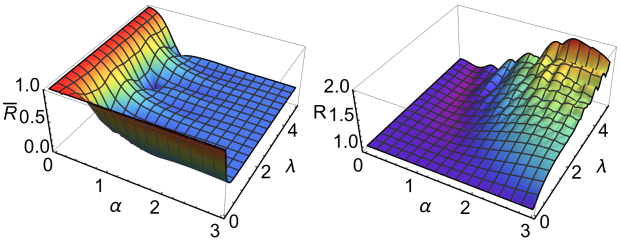

Figure 5.6: In the left panel we show the ratio $\overline{R} = F_x(\overline{\tau})/\overline{H}^c_\gamma(\lambda)$ between the FI of the quadrature at the time $\overline{\tau}$, $F_x(\overline{\tau})$, after an optimization over the quadrature phase and the optimal QFI $\overline{H}_\gamma(\lambda)$, for various values of λ and α. The quadrature measurement is optimal only for $\lambda = 0$ and for vanishing energy of the probe ($\alpha \to 0$). For $\alpha \lesssim 2$ the ratio oscillates with λ. For large α and λ the ratio reaches asymptotically the value of $1/3$. In the right panel we show the ratio $R = F_x(\tau)/H^c_\gamma(\tau)$ for fixed small $\tau = 0.1$; the quantity H^c_γ is the QFI without nonlinearities (Eq. (5.10)). The quadrature measurement in presence on Kerr effect achieves increasingly better performances for increasing values of λ and α, even if the ratio has a slightly oscillating behaviour and there are some regions in which $R < 1$, i.e. the Kerr effect is slightly detrimental.

FI for quadrature measurements with a coherent state probe

Although the optimal QFI is improved by the Kerr effect, we need to find the actual measurement that reaches the quantum bound. We mentioned that for a coherent probe both photon counting and quadrature measurement are optimal when $\lambda = 0$, however they are not optimal if the nonlinear term is present. Indeed, photon counting is not affected at all by the Kerr effect, as the diagonal elements of the density matrix are independent of λ. For this reason we study numerically the effect of nonlinearity on a quadrature measurement. We present the results only for a coherent probe state. In this section we denote the classical Fisher information of a homodyne measurement of the quadrature $\hat{x}_\theta$, maximized over the quadrature phase θ as $F_x(\tau) = \max_\theta \mathcal{F}[\langle x_\theta|\rho_\gamma(\tau)|x_\theta\rangle]$; the optimal quadrature phase depends on α and λ.

We found that in general the quadrature measurement is not optimal, i.e. the Fisher information is always lower than the QFI. This fact is presented in the left panel of Fig. 5.6, for measurements at the optimal time, where we plot the ratio $\overline{R} = F_x(\overline{\tau})/\overline{H}_\gamma(\lambda)$. Here $\overline{H}_\gamma(\lambda)$ is the maximal QFI computed at the optimal time $\overline{\tau}$ and $F_x(\overline{\tau})$ is the FI (optimized over the quadrature phase) at the same time. The ratio is close to one only for λ close to zero or $\alpha \ll 1$. For increasing α and λ the ratio appears to tend asymptotically to $1/3$.

In the small time regime a quadrature measurement is still sub-optimal in presence of nonlinearity, however in some cases such a measurement can perform better than the best possible measurement in the linear case, because the relative improvement of the QFI in this regime is substantial.

In particular, this behaviour seems to increase with increasing nonlinearity λ and increasing input energy α, however we can see from the right panel of Fig. 5.6 that oscillations are present and there are small regions where a quadrature measurement does not give an improvement, i.e. $R < 1$.

5.3.3 Results with optical qutrit states

One may wonder what happens if the optimal Fock states are used as probes, instead of Gaussian states. The Kerr nonlinear term $(\hat{a}^\dagger\hat{a})^2$ clearly does not affect single Fock states, but also a simple superpositions of a Fock state with the vacuum $A|0\rangle + B|n\rangle$ is not affected. The most simple superposition affected by the nonlinear evolution is the optical qutrit state

$$\cos\theta|0\rangle + e^{i\mu}\sin\theta\sin\varphi|1\rangle + e^{i\nu}\sin\theta\cos\varphi|2\rangle, \tag{5.21}$$

where θ is fixed by choosing the mean energy $\bar{n}$ as the relevant parameter, so that $\theta = \arcsin\sqrt{2\bar{n}/(3+\cos 2\varphi)}$. In the linear lossy evolution, these qutrit states approximate the optimal non-Gaussian states when the mean energy $\bar{n}$ is not an integer; this is particularly important for the low energy regime $\bar{n} < 1$ [1].

In general, the maximum value of the QFI obtainable with the state (5.21) is the same regardless of the Kerr term in the evolution, but the maximum happens for different values of the initial parameters and at a different time. This is due to the fact that during the evolution the system is constrained to remain in the subspace of dimension three; so if we optimize on every possible parameter there is no room for improvement left. However, in order to achieve the maximal QFI one should be able to tune the value of the initial parameters for every mean energy $\bar{n}$, and in the nonlinear case also for every value of λ. In particular in the linear case the result must be optimized only over the parameter φ, since the relative phases μ and ν give an optimal result for the value π.

Instead, we consider a setting similar to the one previously used for the coherent states: given a *fixed* initial state we check if the nonlinear evolution brings an improvement. In particular we fix $\mu = \nu = \pi$ and we check the behaviour of the quantum Fisher information for different values of φ, while optimizing over time t. The results are in Fig. 5.7: we find that on average the nonlinear terms brings an improvement for values of $\lambda \approx 1$, i.e. when the nonlinear parameter is approximately equal to the loss parameter to estimate. For higher values of λ we have an oscillatory behaviour and on average the nonlinearity can also be detrimental. Furthermore we found that at fixed small times the nonlinear Kerr term does not always bring an improvement on average when using qutrit states.

Discussion on the role of non-Gaussianity

The nonlinear Kerr interaction makes an initial Gaussian probe non-Gaussian during the evolution and a question arises on whether the observed increase of the QFI may be quantitatively linked to some quantifier of non-Gaussianity or nonclassicality. It would be desirable to identify the underlying characteristic of the state which guarantees the improvement in the estimation, since this would represent a guideline to engineer optimal estimation schemes.

In previous works it has been conjectured [1] that a family of optimal non-Gaussian states exists for any fixed energy, but that non-Gaussianity in itself cannot be a resource. As a matter of fact, some non-Gaussian states are less efficient probes than the optimal Gaussian ones. Hereby we confirm that result. In fact, during its evolution a Gaussian

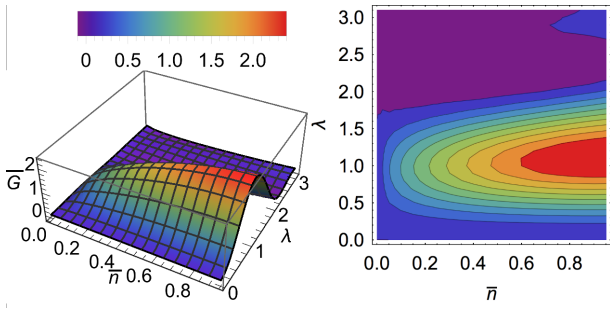

Figure 5.7: Average relative gain of the optimal QFI in presence of non-linearity over the optimal QFI without Kerr effect for qutrit states, shown in percentage. The range of the parameters are $0 < \bar{n} < 1$ and $0 < \lambda < \pi$. On the left, a 3D plot, on the right the corresponding contour plot. Every point in the plot is the average improvement obtained by generating 1000 random values of the parameter φ of the state (5.21) in the range $\left(0, \frac{\pi}{2}\right)$, while the phases are fixed $\mu = \nu = \pi$ and θ is fixed by the choice of the mean energy $\bar{n}$.

input state first becomes non-Gaussian and then it evolves towards the Gaussian state $|0\rangle$, which is the stationary state. This qualitative behaviour is also shown by the relative gain in the estimation of γ in Fig. 5.2. These two quantities, however, do not have a quantitative relation in general, e.g. states leading to the largest improvement at optimal time are not the most non-Gaussian.

Overall, our results show that while the evolution drives the Gaussian input into a set of non-Gaussian states that are more sensitive to loss detection, non-Gaussianity is not a resource in itself. This idea is confirmed by looking at the behaviour of qutrit probe states, which are already highly non-Gaussian: there we find evidences that the Kerr interaction may be detrimental in some regimes, whereas when an improvement is present, the states are non necessarily more non-Gaussian.

Summary

- The estimation of the loss rate of a single-mode bosonic loss channel is an important problem, mostly studied in the linear (Gaussian) case without any Hamiltonian term. Adding a self-Kerr Hamiltonian to the dynamics can be useful for improving the precision of the estimation with an initial Gaussian state.

- The dynamics has two time scales, one given by the loss rate and one given by the strength of the nonlinear interaction. For this reason we estimate the loss rate rather then the total loss (which also includes the evolution time).

- The QFI of coherent or squeezed vacuum states evolving in the nonlinear lossy channel is always higher than the corresponding linear case, in particular this improvement is very relevant at small times. The QFI is computed both via an analytical approximation and with an extensive numerical study.

- The precision quantified by the QFI is not achievable by photon counting and

quadrature measurements. On the other hand, for short interaction times even a suboptimal quadrature measurement offers an improvement in precision compared to the linear case.

- It appears that the improvement in the QFI has no clear quantitative link the non-Gaussianity of the evolved state.

CHAPTER 6

Nonclassicality of anharmonic oscillators ground states

In this chapter we abandon the topic of quantum metrology and we focus on the nonclassical properties of CV quantum states, in particular ground states of anharmonic oscillators. Here, we want to investigate the general idea that nonlinearity is a resource to generate nonclassicality in single-mode bosonic systems of anharmonic oscillators. In particular, we present a quantitative assessment of the phenomenon and we consider specific quantifiers of both nonclassicality and nonlinearity.

The starting point of this analysis lies in Ref. [223], where the authors show that the non-Gaussianity of a ground state can be used to capture and quantify the *nonlinearity* of an anharmonic potential. Using this quantitative definition, the problem reduces to comparing the behavior of non-Gaussianity and nonclassicality measures of the ground states. A quantitative connection between nonclassicality and non-Gaussianity of pure states is in itself an interesting topic and we are going to comment more on this in Chapter 8.

The present investigation is motivated by the fact that new experimental platforms offer the unique opportunity to implement *nonlinear* (or anharmonic) models. The possibility to host non-linearities is within reach of current technologies, in particular for trapped ions [132] and optomechanical systems [251]. It was shown that including nonlinearities in the oscillator opens new possibilities to generate nonclassical states, see e.g. [159, 241, 281].

The quantitative connection between the nonlinear behavior of an oscillatory system and the appearance of nonclassicality, has been tested with similar methods for the Duffing oscillator model [275], in the context of nano-mechanical resonators. The work presented in this chapter, based on [9], is an extension of such observations to more general scenarios: three families of exactly solvable non-linear oscillators and a generic sixth order potential.

Nonlinearity of a potential via non-Gaussianity of the ground state

The first idea to quantify the nonlinearity (intended as the *anharmonicity character*) of a potential would be defining a distance between potential functions and the reference harmonic potential. In general this is not feasible, since potentials do not need to be integrable functions. A different approach follows from the fact that ground states and equilibrium states of anharmonic potentials are not Gaussian, as opposed to those of a

quantum harmonic oscillator. We can thus quantify nonlinearity by the non-Gaussianity of the ground state of a given Hamiltonian model, as proposed in [223]. For this goal we use the relative entropy of non-Gaussianity introduced in Section 1.4.4.

We consider a generic potential $V(x)$ and denote with $|\phi_V\rangle$ the ground state of the corresponding Hamiltonian operator $\hat{p}^2/2 + V(\hat{x})$. By using the non-Gaussianity measure δ in (1.157), the nonlinearity of $V(x)$ is defined as

$$\eta_{\rm NG}[V] \equiv \delta(|\phi_V\rangle\langle\phi_V|) = h\Big(\sqrt{\det\sigma}\Big), \tag{6.1}$$

where σ is the covariance matrix of the ground state $|\phi_V\rangle$. This identity holds because the ground state is pure and the only symplectic invariant of a single-mode state is the determinant of the covariance matrix[1].

An alternative idea to quantify nonlinearity is to use some geometrical distance between the ground states of the potential and the ground state of a reference harmonic state [223]. However, this approach has a downside, because one has to choose a value for the reference frequency ω of the harmonic oscillator, usually by expanding around the minimum, which could be ambiguous for potentials exhibiting more than one minimum.

This entropic measure is more appealing than a geometric one because it does not require to find a reference potential for $V(x)$, but only the covariance matrix of the ground state. This makes $\eta_{\rm NG}$ independent of the specific features of the potential, since we do not need to know the behavior of $V(x)$ near its minimum to compute the reference frequency.

Moreover, $\eta_{\rm NG}$ inherits the property of the non-Gaussianity measure and is invariant under symplectic transformations. This means that $\eta_{\rm NG}$ assigns the same nonlinearity to oscillators which are displaced, rotated in phase space or squeezed, which is a reasonable property for a measure of nonlinearity.

6.1 Exactly solvable anharmonic oscillators

We now analyze quantitatively the relation between the non-linearity of the potential $\eta_{\rm NG}$ and two different figures of merit for the non-classicality of the ground-state. For P-nonclassicality we study the entanglement potential $\mathcal{E}[\rho]$, defined in (1.153) as the entanglement entropy of the state after the interaction with the vacuum through a balanced beam splitter. The entanglement potential is evaluated by expanding the wave function on the Fock space of a harmonic oscillator of unitary frequency and mass, truncating the expansion by ensuring the approximate normalization of the state before and after the beam-splitter. For W-nonclassicality, we compute the renormalized volumed of the negative part of the Wigner function, i.e. ν defined in (1.155). In particular, in this Section we focus on three exactly solvable anharmonic oscillators.

We denote the Wigner function of the ground state as follows

$$W(q,p) \equiv \mathcal{W}[|\phi_V\rangle\langle\phi_V|](q,p)\ , \tag{6.2}$$

[1] In this chapter we compute the non-Gaussianity in nats (natural units of information), meaning that the logarithms appearing in the definition of $h(x)$ in Eq. (1.130) are natural logarithms; in Chapter 8 we use bits (logarithm in base 2).

specifying different potentials with subscripts on $W(q,p)$. In order to maintain consistency with [9] we label the position phase-space coordinate q rather than x.

6.1.1 Modified Harmonic Oscillator

The Modified Harmonic Oscillator (MHO) potential is defined as [42] (throughout this manuscript we choose units such that $\hbar = m = 1$)

$$V_{\mathrm{MHO}}(x) = \frac{\alpha^2 x^2}{2} - \alpha\beta x \tanh(\beta x). \tag{6.3}$$

Here α is a parameter corresponding to the frequency of the unmodified harmonic oscillator, while β determines the deformation of the harmonic potential. The effects of this parameter on the shape of the potential is appreciated from Fig. 6.1, where $V_{\mathrm{MHO}}(x)$ is plotted at a set value of α for different choices of β, showing that an increasing deformation parameter transforms a harmonic potential into a double-well one whose well-depth and separation both increase with β. For small β this potential has a similar behavior to the Duffing oscillator routinely used to model nanomechanical resonators [56, 288], therefore we can think of the MHO as an extension to the Duffing model in the case of strong nonlinearity.

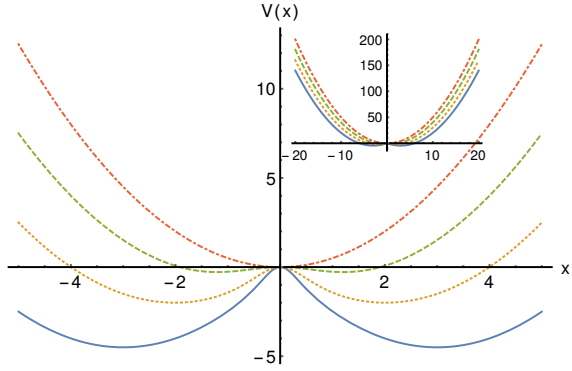

Figure 6.1: The MHO potential with $\beta = 3$ (solid blue), 2 (dotted yellow), 1 (dashed green) and the harmonic potential with unitary frequency and mass (dot-dashed orange); with our choice of units x is measured in units of $\alpha^{-1/2}$, V in units of α and β in units of $\alpha^{1/2}$. The inset represent the same graph at a larger scale, where we see the resemblance to the harmonic potential.

The normalized wave-function of the ground-state of this potential reads [42]

$$\phi_{\mathrm{MHO}}(x) = \frac{\sqrt{2}e^{-\frac{1}{2}\alpha x^2}\cosh(\beta x)}{\sqrt[4]{\frac{\pi}{\alpha}}\sqrt{1+\exp[\beta^2/\alpha]}}. \tag{6.4}$$

The associated energy is $E_0 = (\alpha - \beta^2)/2$. The covariance matrix of such least-energy state can be computed straightforwardly to be

$$\boldsymbol{\sigma}^{\mathrm{MHO}} = \begin{pmatrix} \frac{1}{2\alpha} + \frac{\beta^2}{\alpha^2}\frac{\exp[\beta^2/\alpha]}{1+\exp[\beta^2/\alpha]} & 0 \\ 0 & \frac{\alpha}{2} - \frac{\beta^2}{1+\exp[\beta^2/\alpha]} \end{pmatrix}. \tag{6.5}$$

Its determinant is

$$\det \sigma^{\mathrm{MHO}} = \frac{1}{2} - \frac{\tau^2\left(2\tau^2 e^{\tau^2} - e^{2\tau^2} + 1\right)}{(e^{\tau^2}+1)^2} \tag{6.6}$$

with the dimensionless parameter $\tau = \sqrt{\beta^2/\alpha}$. Such dependence on τ, rather than α and β independently, is common to $\eta_{\mathrm{NG}} = h(\det\sigma)$ and the measure of nonlinearity based on the Bures distance (for the latter, we should choose the unmodified harmonic oscillator with frequency α as a reference). Both measures of nonlinearity increase monotonically with τ.

The Wigner function associated with ϕ_{MHO} can be written in terms of the suitably rescaled phase-space variables $q = \beta x$ and $p = \frac{\beta}{\alpha} y$ as [42]

$$W_{\mathrm{MHO}}(q,p) = e^{-\frac{q^2+p^2}{\tau^2}} \frac{\cosh(2q) + e^{\tau^2}\cos(2p)}{\pi\tau^2(1+e^{\tau^2})}, \tag{6.7}$$

which shows again the key role played by τ and, in turn, that the non-classicality measure based on the volume of the negative part of $W_{\mathrm{MHO}}(q,p)$ is determined by such parameter.

In order to understand how W-nonclassicality and nonlinearity are related to each other, we have studied both quantities against τ. In Fig. 6.2 we report the resulting parametric plot, showing that ν monotonically increases with η_{NG}, thus supporting the idea that a growing degree of anharmonicity of the potential results in increased nonclassicality of the corresponding ground state.

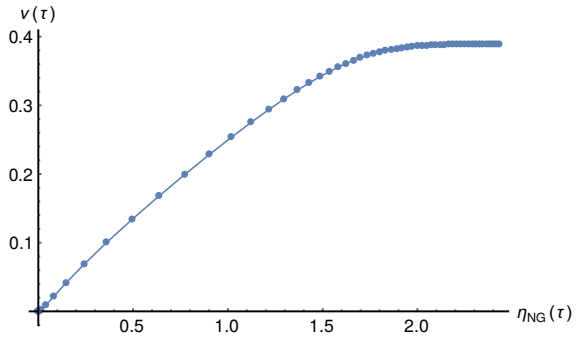

Figure 6.2: Parametric plot of the W-nonclassicality measure $\nu(\tau)$ versus the degree of nonlinearity for the MHO potential and for $\tau \in [0.1, 6]$.

The picture changes significantly as soon as we consider P-nonclassicality quantified by the entanglement potential which can single out more detailed features of quantumness, such as squeezing. Indeed, at variance with what has been found above, such a figure of merit turns out to depend on α and β independently. The reason for such a difference in behavior should be ascribed to the fact that entanglement at the output of a beam splitter can be originated either by a non-Gaussian input state or by Gaussian single-mode squeezing. In other words, nonlinearity is needed to generate W-nonclassicality, while P-nonclassicality may be obtained using just squeezing.

In order to illustrate this clearly, in Fig. 6.3 we show the entanglement potential and squeezing for the MHO both as a function of β for fixed values of τ, and as a function of τ at set values of α. The squeezing in Fig. 6.3 is shown in terms of the ratios

$$r_x = \frac{\sigma_{11}^{\mathrm{MHO}}}{\sigma_{11}^{0}} = 2\sigma_{11}^{\mathrm{MHO}}, \quad r_p = \frac{\sigma_{22}^{\mathrm{MHO}}}{\sigma_{22}^{0}} = 2\sigma_{22}^{\mathrm{MHO}} \tag{6.8}$$

with $\sigma_{11}^{0} = \sigma_{22}^{0} = 1/2$ the variances of position and momentum calculated over the vacuum state of the harmonic potential. Squeezing is found in the ground state of the MHO for either $r_x < 1$ or $r_p < 1$. As it is apparent from Fig. 6.3, the behavior of $\mathcal{E}$ is rather different from ν, and its features may be understood looking at squeezing. In particular, we see that $\mathcal{E}$ grows when the ground state exhibits squeezing.

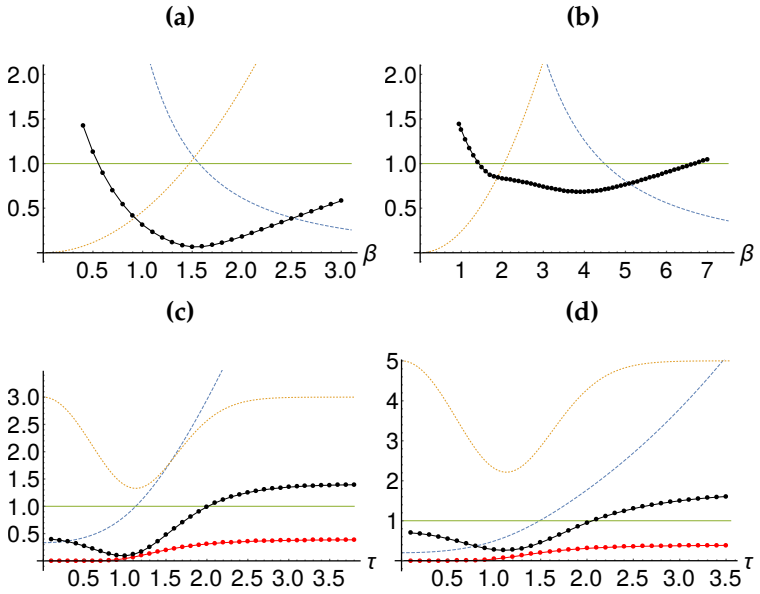

Figure 6.3: Entanglement potential and squeezing for the MHO. In panels **(a)** and **(b)** [**(c)** and **(d)**] we plot r_x (dashed blue curve), r_p (dotted orange curve), the entanglement potential (P-nonclassicality) $\mathcal{E}$ (black dots), and W-nonclassicality ν (red dots) against β [τ] for $\tau = 1$ and $\tau = 3$ [$\alpha = 3$ and $\alpha = 5$]. Squeezing is observed for either $r_x < 1$ or $r_p < 1$ (i.e. variances of the perturbed ground state below the values of the vacuum state of a harmonic oscillator).

6.1.2 Morse potential

The Morse potential has been introduced as an approximation to the potential energy of diatomic molecules as it provides a better description of the vibrational structure than the (quantum) harmonic oscillator [201]. The form of the potential is

$$V_{\mathrm{M}} = D\left(e^{-2\alpha x} - 2e^{-\alpha x}\right), \tag{6.9}$$

where x is the distance from the minimum of the potential, the parameter $D > 0$ determines the depth of the well, while α controls its width. Expanding the two exponentials

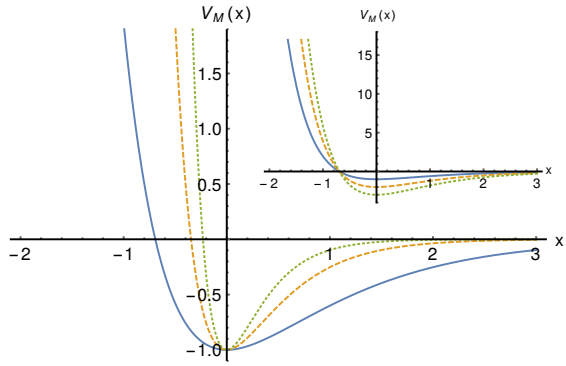

Figure 6.4: The Morse potential $V_{\rm M}(x)$ for $\alpha = 1$ (solid blue), 2 (dashed orange), 3 (dotted green), where V is measured in units of D, x in units of $D^{-1/2}$ and α in units of $D^{1/2}$. The inset shows the potential for $D = 1$ (solid blue), 2 (dashed orange), 3 (dotted green), with x in units of α^{-1} and V and D in units of α^2

for $\alpha \to 0$ at fixed D we get the harmonic limit, which is an oscillator with frequency $\omega_{\rm M} = \sqrt{2D}\alpha$. The potential is plotted in Fig. 6.4 for different values of the parameters.

The Schrödinger equation associated with this potential can be solved analytically, the energy eigenvectors being labelled by two quantum numbers, which we label here N and ν. The first is related to the parameters of the potential as $N = -1/2 + \sqrt{2D}/\alpha$. The second, which can take values $\nu = 0, 1, 2, .., \lfloor N \rfloor$, counts the number of anharmonic excitations of the system. Since we want at least one bound state, we require $N > 0$, so we have the constraint $\alpha < 2\sqrt{2D}$. The limiting case where we have just one bound state (the ground state) is achieved for $\alpha \to 2\sqrt{2D}$. The wave-function of the ground state is

$$\phi_{\rm M}(x) = (2N+1)^N \sqrt{\frac{\alpha}{(N-1)!}} e^{-\alpha x N - (N+\frac{1}{2})e^{-\alpha x}} \tag{6.10}$$

with associated energy $E = -\alpha N^2/2$. The behavior of the nonlinearity of the Morse potential can be understood by looking at the form of the potential in Fig. 6.4, as opposed to the harmonic one [223]. For any fixed value of D (α) we expect an increase (decrease) of nonlinearity for increasing α (D).

The covariance matrix associated with the ground state in Eq. (6.10) is

$$\boldsymbol{\sigma}^{\rm M} = \begin{pmatrix} \frac{2\psi^{(1)}(2N)}{\alpha^2} & 0 \\ 0 & \alpha^2 N \end{pmatrix}, \tag{6.11}$$

where $\psi^{(n)}(z)$ is the polygamma function $\psi^{(n)}(z) = \frac{{\rm d}^{n+1}}{{\rm d}z^{n+1}} \log\Gamma(z)$, $\Gamma(Z)$ being the Euler Gamma function. The determinant of this correlation matrix depends only on N or, equivalently, on the combination $\sqrt{2D}/\alpha$. In this the measure of nonlinearity is a monotonically decreasing functions of N.

The Wigner function for the ground state of the Morse potential reads as follows [89]

$$W_{\rm M}(x,p) = \frac{2(2N+1)^{2N}}{\pi\Gamma(2N)} e^{-2N\alpha x} K_{-2ip/\alpha}\big((2N+1)e^{-\alpha x}\big), \tag{6.12}$$

where $K_\gamma(z)$ is the Macdonald function of (non-integer) order γ. In order to calculate the measure of nonclassicality ν, we rescale the phase-space variables to $q = \alpha x$ and $p = \frac{y}{\alpha}$, and evaluate

$$\iint \mathrm{d}x\,\mathrm{d}y\,|W_{\mathrm{M}}(x,y)| = \iint \mathrm{d}q\,\mathrm{d}p\left|\frac{2e^{-2Nq}}{\pi\Gamma(2N)}(2N+1)^{2N}K_{-2ip}\big((2N+1)e^{-q}\big)\right|, \tag{6.13}$$

which shows that the only relevant parameter is N. The numerical integration of Eq. (6.13) is challenging and was carried out with the aid of the CUBA libraries [124]. The degree of W-nonclassicality ν is found to monotonically decreases with N. The parametric plot of nonclassicality versus nonlinearity in Fig. 6.5 reveals a monotonic behavior, strengthening the link between such features and reinforcing the idea that nonlinearity might play the role of a catalyst for nonclassicality.

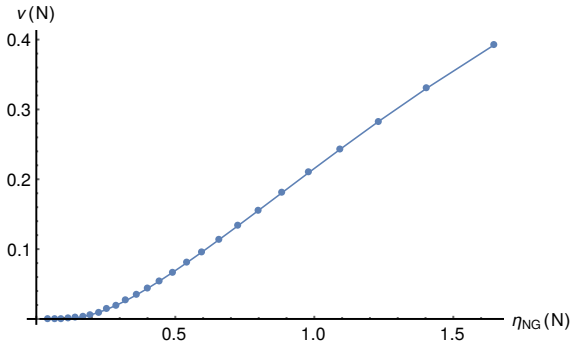

Figure 6.5: Parametric plot of the W-nonclassicality ν versus the degree of nonlinearity η for a Morse potential with $D = 1$ and $\alpha \in [0.15, 2.7]$, i.e. $N \in [0.0238, 8.928]$.

The situation regarding the entanglement potential is completely analogous to what we found for the MHO, as it depends on both parameters. In Fig. 6.6 we report the same kind of graphs, both with N fixed and α fixed, which show that the behavior of $\mathcal{E}$ is explained by the squeezing of the state.

6.1.3 Pöschl-Teller potential

The Pöschl-Teller potential (PT) potential has been studied since the early days of quantum mechanics [88], it has been applied in the context of semiconductor quantum wells [238, 279, 280] and it can also be used to model nonlinear optical properties [304, 305].

In particular we use the modified PT potential, defined as

$$V_{\mathrm{PT}}(x) = -A_{\mathrm{PT}}\cosh^{-2}(\alpha x), \tag{6.14}$$

where $A_{\mathrm{PT}} > 0$ is the depth of the potential and α is connected to its range. The harmonic limit is obtained at fixed A_{PT} for $\alpha \to 0$ and the frequency of the reference harmonic oscillator is $\omega_{\mathrm{PT}} = \sqrt{2A_{\mathrm{PT}}}\alpha$. As for the Morse potential, we have a quantum number s that labels the energy eigenstates and counts the anharmonic excitations. It is related to the parameters of the potential through the relation $A_{\mathrm{PT}} = \frac{1}{2}\alpha^2 s(s+1)$. Therefore, the request

for the existence of at least one bound state translates into $s = \frac{1}{2}\left(-1+\sqrt{1+8A_{\rm PT}/\alpha^2}\right) > 0$. Fig. 6.7 shows the dependence of the PT potential on the position coordinate.

The ground state of the system reads

$$\phi_{\rm PT}(x) = \frac{1}{\pi^{\frac{1}{4}}}\sqrt{\frac{\alpha\Gamma\left(s+\frac{1}{2}\right)}{\Gamma(s)}}\cosh^{-s}(\alpha x), \tag{6.15}$$

with associated energy $E = -\alpha^2 s^2/2$.

The covariance matrix of the ground state is rather involved and is not be reported here, it can however be easily obtained by directly applying x and p operators in the position representation on the wave function (6.15).

In line with the case of the previous two anharmonic potentials studied here, its determinant depends only on s (or, equivalently, on $A_{\rm PT}/\alpha^2$). Again the nonlinearity $\eta_{\rm NG}$ is a monotonically decreasing function of s only.

The Wigner function of the ground state $\phi_{\rm PT}(x)$ in Eq. (6.15) is known analytically for the case of $A_{\rm PT} = \alpha^2$ [42]. In this case, the measure ν is an s-dependent constant, as it can be seen by rescaling the relevant variables as $p' = \frac{p}{\alpha}$, $x' = \alpha x$, $y' = \alpha y$ and evaluating the integral

$$W_{\rm PT}(x,p) = \frac{1}{\pi}\int {\rm d}y\, \phi^*_{\rm PT}\left(x-\frac{y}{2}\right)\phi_{\rm PT}\left(x+\frac{y}{2}\right)e^{-iyp}, \tag{6.16}$$

which embodies the definition of Wigner function.

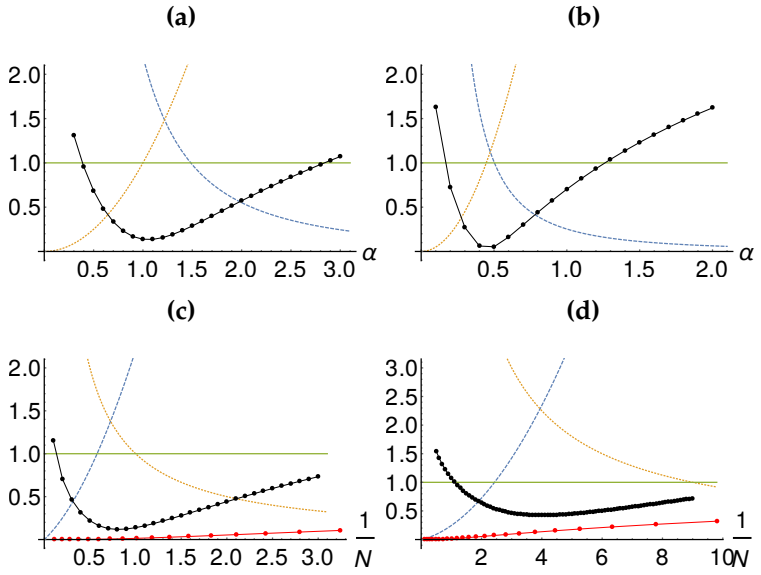

Figure 6.6: Entanglement potential and squeezing for the Morse oscillator. In panels **(a)** and **(b)** [**(c)** and **(d)**] we plot r_x (dashed blue curve), r_p (dotted orange curve), the entanglement potential (P-nonclassicality) $\mathcal{E}$ (black dots), and W-nonclassicality ν (red dots) against α [$1/N$] for $N = 1$ and $N = 5$ [$\alpha = 1$ and $\alpha = 3$]. Squeezing is observed for either $r_x < 1$ or $r_p < 1$ (i.e. variances of the perturbed ground state below the values of the vacuum state of a harmonic oscillator).

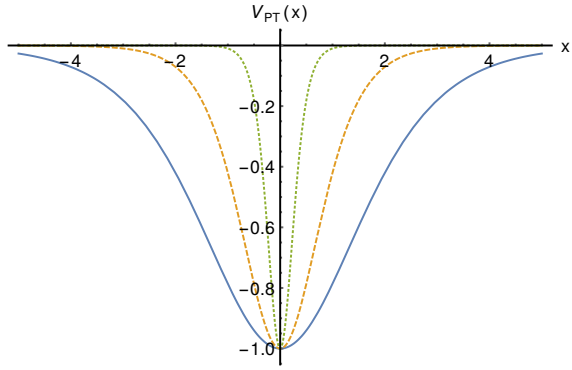

Figure 6.7: The Posh-Teller potential with and $\alpha = 1/2$ (solid blue), 1 (dotted orange) and 3 (dashed green), x in units of $A_{\mathrm{PT}}^{-1/2}$, α in units of $A_{\mathrm{PT}}^{1/2}$ and V_{PT} in units of A_{PT}.

The entanglement potential again depends on both α and s. Plots similar to those valid for the MHO and Morse potential are presented in Fig. 6.8 (without the W-nonclassicality ν).

6.2 Harmonic oscillators with polynomial perturbations

So far we have studied exactly solvable potentials dependent on two parameters and revealed a common behavior: the nonlinearity and the W-nonclassicality ν have the same behavior and depend just on a single effective parameter. On the other hand, the entanglement potential carries a dependence on both the parameters and its different behavior may be understood in terms of the squeezing of the state.

Now we want to address the case of a generic two-parameter perturbation, so we study a physical system composed of a one-dimensional harmonic oscillator with perturbations proportional to x^4 and x^6 respectively. The Hamiltonian of this system thus reads

$$\hat{H} = \frac{1}{2}(\hat{p}^2 + \omega^2 \hat{x}^2) + \epsilon_4 \hat{x}^4 + \epsilon_6 \hat{x}^6 \,. \tag{6.17}$$

As the model is not exactly solvable, the properties of the system are studied using perturbation theory. We notice that Eq. (6.17) may also serve as an approximation for any symmetric (even) potential. In particular also this Hamiltonian can be intuitively considered as a generalization of the static Duffing oscillator.

We do not consider odd powers of $\hat{x}$, nor negative coefficients for the even powers of $\hat{x}$, even when the potential is still bounded from below. We make this choice in order to avoid any ambiguity, which could arise when the potential has more than one minimum. In fact, for such case, the state obtained with the perturbative expansion is not necessarily an approximation to the true ground state, but could be a state associated with a local minimum of energy. Terms proportional to $\hat{x}$ and to $\hat{x}^2$ could in principle be treated in a perturbative way as well. However, they do not give rise to truly anharmonic behavior, and are not considered in this context.

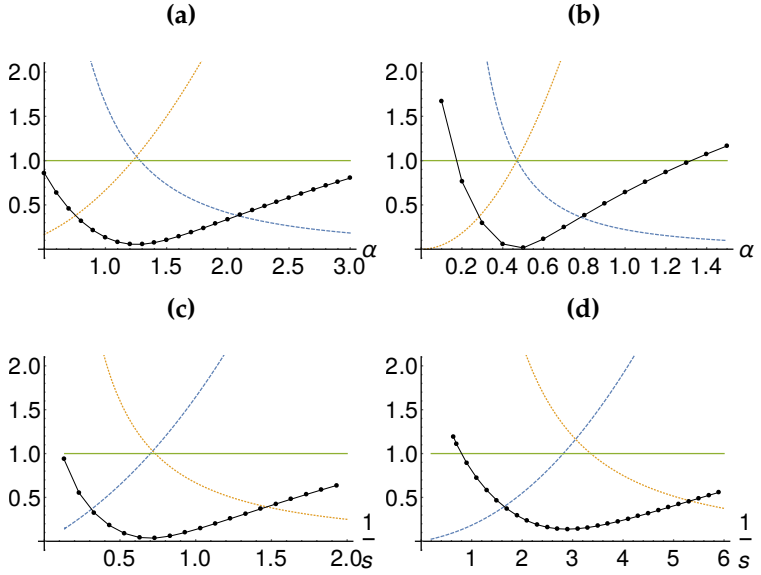

Figure 6.8: Entanglement potential and squeezing for the PT oscillator. Panels **(a)** and **(b)** [**(c)** and **(d)**] show r_x (dashed blue curve), r_p (dotted orange curves), and the entanglement potential $\mathcal{E}$ (black dots)against α $[1/s]$ for $s = 1$ and $s = 5$ [$\alpha = 1$ and $\alpha = 3$].

In order to get insight into the ground states for these Hamiltonians we use first-order time-independent perturbation theory [250]. The formula for the perturbed ground state is the following

$$|\tilde{\psi}\rangle = |0\rangle + \epsilon \sum_{k\neq 0} |k\rangle \frac{V_{k0}}{-\omega k}, \tag{6.18}$$

where $|k\rangle$ denotes a Fock number state of the unperturbed harmonic oscillator and $V_{nk} = \langle n|\hat{V}|k\rangle$ are Fock-basis matrix elements of the perturbation $\hat{V} = \epsilon_4 \hat{x}^4 + \epsilon_6 \hat{x}^6$[2]. Such state is normalized only up to first order in ϵ_4 and ϵ_6, however we work with the normalized version $|\psi\rangle = |\tilde{\psi}\rangle / \langle\tilde{\psi}|\tilde{\psi}\rangle$.

Since the potential is an even function, the normalized state takes the form

$$|\psi\rangle = \sum_{n=0}^{3} \gamma_{2n} |2n\rangle, \tag{6.19}$$

where the coefficients γ_k are

$$\gamma_0 = \frac{1}{C} \quad \gamma_2 = -\frac{\gamma_0}{\sqrt{2}}\left(\frac{45\epsilon_6}{4\omega^3} + \frac{3\epsilon_4}{\omega^2}\right) \quad \gamma_4 = -\gamma_0\sqrt{\frac{3}{2}}\left(\frac{15\epsilon_6}{2\omega^3} + \frac{\epsilon_4}{\omega^2}\right) \quad \gamma_6 = -\sqrt{5}\gamma_0\epsilon_6, \tag{6.20}$$

and the normalization constant C is

$$C = \frac{\sqrt{\omega^2\left(96\omega^6 + 117\epsilon_4^2\right) + 945\omega\epsilon_4\epsilon_6 + 2055\epsilon_6^2}}{4\sqrt{6}\omega^4}. \tag{6.21}$$

[2]For simplicity we assume that ϵ_6 and ϵ_4 are both proportional to a single parameter ϵ in (6.18), and we check the validity of this approximation afterwards.

The Wigner function of this superposition of Fock state reads

$$\begin{aligned} W(q,p) &= \sum_{i,j=0}^{6} \gamma_i \gamma_j{}^* \mathcal{W}[|i\rangle\langle j|](q,p) = \\ &= \sum_{i=0}^{6} |\gamma_i|^2 \mathcal{W}_{|i\rangle}(q,p) + 2\mathrm{Re}\left[\sum_{j=1}^{6}\sum_{i=0}^{j-1} \gamma_i \gamma_j{}^* \mathcal{W}[|i\rangle\langle j|](q,p)\right], \end{aligned} \tag{6.22}$$

where $\mathcal{W}_{|i\rangle}(q,p) = (-1)^n/\pi\, e^{-(q^2+p^2)} L_n\big(2(q^2+p^2)\big)$ are the Wigner functions of Fock states and $L_n(x)$ are Laguerre polynomials. The Wigner transform of the off-diagonal operators $|n\rangle\langle m|$ are given by [27, 62, 227]:

$$\mathcal{W}[|n\rangle\langle m|] = \begin{cases} \frac{(-1)^n}{\pi}\sqrt{\frac{n!}{m!}} e^{-(q^2+p^2)} \Big[\sqrt{2}(q+ip)\Big]^{m-n} L_n^{(m-n)}\big(2(q^2+p^2)\big) & \text{if} \quad m > n \\ \frac{(-1)^n}{\pi}\sqrt{\frac{m!}{n!}} e^{-(q^2+p^2)} \Big[\sqrt{2}(ip-q)\Big]^{m-n} L_m^{(n-m)}\big(2(q^2+p^2)\big) & \text{if} \quad n > m \end{cases}, \tag{6.23}$$

where $L_n^{(k)}(x)$ are the associated Laguerre polynomials.

First-order perturbation theory gives the ground as a finite superposition of Fock states, which makes the Wigner function and the nonlinearity easy to compute. In order to assess the validity of the first order approximation, we have compared such ground state to the state obtained by numerically diagonalizing the Hamiltonian of the system within a truncated Fock space of suitable size. Convergence of the results of such numerical calculations appear to be ensured by using 61 harmonic levels. The corresponding ground state $|\phi_V\rangle$ is then compared to $|\psi\rangle$ using the state fidelity $|\langle\phi_V|\psi\rangle|^2$. For values of ϵ_4 up to 0.1 and ϵ_6 up to 0.03 the fidelity is at least ≈ 0.976.

6.2.1 Nonclassicality and nonlinearity

From the perturbed ground state in Eq. (6.19) we compute the nonlinearity of the perturbing potential. The covariance matrix associated with $|\psi\rangle$ can be thus written as

$$\sigma^{\mathrm{pol}} = \begin{pmatrix} \frac{(1+2\langle\hat{a}^2\rangle+2\langle\hat{a}^\dagger a\rangle-4\langle\hat{a}\rangle^2)}{\omega} & 0 \\ 0 & \omega(1+2\langle\hat{a}^\dagger\hat{a}\rangle-2\langle\hat{a}^2\rangle) \end{pmatrix}, \tag{6.24}$$

with $\hat{a}$ and $\hat{a}^\dagger$ the annihilation and creation operators of the oscillator and

$$\begin{aligned} &\langle\hat{a}^\dagger\rangle = \langle\hat{a}\rangle = 0 \qquad \langle\hat{a}^\dagger a\rangle = 2|\gamma_2|^2 + 4|\gamma_4|^2 + 6|\gamma_6|^2, \\ &\langle\hat{a}^2\rangle = \sqrt{2}\gamma_2\gamma_0{}^* + 2\sqrt{3}\gamma_4\gamma_2{}^* + \sqrt{30}\gamma_6\gamma_4{}^*, \end{aligned} \tag{6.25}$$

An explicit calculation shows that the determinant of σ^{pol}, and in turn the nonlinearity $h(\sqrt{\det\sigma})$, depends on both the perturbative parameters and on the frequency ω. No single-parameter rescaling can be identified in this case, thus entailing the double-dependence highlighted above, which is passed to the W-nonclassicality ν.

Our goal is to highlight the role played by the perturbative parameters, therefore we set $\omega = 1$ and generate random pairs of values (ϵ_4, ϵ_6) (within the appropriate range of

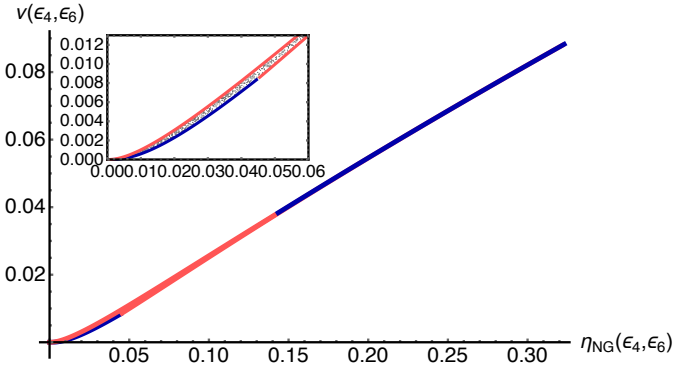

Figure 6.9: Random scatter plot of the W-nonclassicality ν versus the nonlinearity $\eta_{\rm NG}$ for the perturbed harmonic oscillator when parameters ϵ_4 and ϵ_6 are are varied in the range $\epsilon_4 \in [0, 0.1]$, $\epsilon_6 \in [0, 0.03]$; 10^4 random points are generated. The dark blue curve below the points represents $\epsilon_6 = 0$, while the one above the points is the curve for $\epsilon_6 = 0.03$. The light red curve below the points is the one for $\epsilon_4 = 0.1$, while the one above the points is for $\epsilon_4 = 0$. In the inset: zoom on the region $\eta_{\rm NG} \leq 0.6$ to better appreciate the different curves. For higher values of $\eta_{\rm NG}$ the region containing the points become more narrow and all the curves graphically coincide.

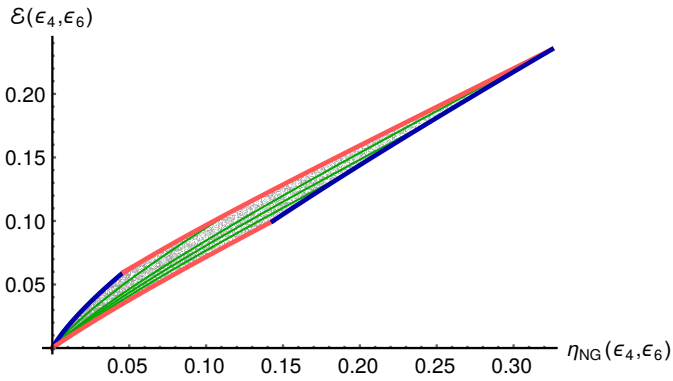

Figure 6.10: Random scatter plot of the entanglement potential (P-nonclassicality) $\mathcal{E}$ versus the nonlinearity $\eta_{\rm NG}$ for the perturbed harmonic oscillator when both parameters ϵ_4 and ϵ_6 are varied in the range; 10^4 random points were generated. The dark blue curve above the points represents $\epsilon_6 = 0$, while the one below the points is the curve for $\epsilon_6 = 0.03$. The light red curve above the points is the one for $\epsilon_4 = 0.1$, while the one below the points is for $\epsilon_4 = 0$. The green curves in the middle are obtained by choosing $\epsilon_6 = k\epsilon_4$, from top to bottom they correspond to the values $k = 2, 1, 0.5, 0.3, 0.1$.

validity of the first-order perturbative approach discussed above) that are then used to compute both the nonclassicality and nonlinearity indicators.

The results shown in Figs. 6.9 and 6.10 showcase a non-monotonic relation between nonlinearity and nonclassicality: the points corresponding to the randomly taken pairs of values for the parameters are distributed within a (narrow) region comprised within four curves, each associated with an extremal value of $\epsilon_{4,6}$. Nonclassicality and nonlinearity

are thus dependent on the details of the system under consideration and are, strictly speaking, non equivalent notions.

However, the region containing the randomly generated points in Fig. 6.9 is very narrow and suggests that the link between W-nonclassicality and the nonlinearity of the potential is indeed correct, since by fixing the value of one quantity the other is *almost* fixed.

On the contrary, for P-nonclassicality the random points in Fig. 6.10 are scattered across a wider region. In Fig. 6.10 we also show that if one varies only a single effective parameter, by fixing the value of either ϵ_4 or ϵ_6 or by keeping their ratio fixed (i.e. $\epsilon_6 = k\epsilon_4$), the behavior of P-nonclassicality measures becomes monotonic with nonlinearity[3].

By inspecting more closely our results, it appears that W-nonclassicality is favoured by the x^6-like nonlinearity, while P-nonclassicality, appears to benefit from a x^4-type of nonlinear effects. As a matter of fact, in Fig. 6.10 the roles of the dark blue and light red curves are inverted with respect to Fig. 6.9. This means that, after choosing the parameters ϵ_4 and ϵ_6 in such a way that the entropic nonlinearity is fixed, the ground state obtained with the maximum value of ϵ_4 generates more entanglement than any other one.

We can thus conclude that the anharmonic character of the potential can be linked to P-nonclassicality of the ground state, but this connection is less stringent than the one between nonlinearity and W-nonclassicality. This result is in perfect agreement with the exactly solvable models, we previously studied.

Summary

- There is an intuitive expectation that the anharmonic charcter of a potential can be regarded as a resource to generate nonclassical ground states. The strict validity of such an expectation, is, however, strongly linked to the specific details of the Hamiltonian model being addressed and to the considered notion of nonclassicality.
- In this quantitive study, the nonlinearity of an anharmonic potential can be quantified via the non-Gaussianity of the ground state of the corresponding Hamiltonian.
- Nonlinearity of the anharmonic oscillator plays a crucial role in the generation of W-nonclassicality (quantified by the negativity of the Wigner funcion), while P-nonclassicality (quantified by the entanglement potential) may be also obtained if the anharmonicity induces just squeezing.
- The solvable anharmonic potentials can be reduced to a single-parameter dependence and give rise to a monotonic relation between nonlinearity and W-nonclassicality.
- For multi-parameter anharmonic potentials (studied perturbatively) a given value of nonlinearity bounds the possible degrees of nonclassicality of the ground state, without *determining* it unambiguously. Even for W-nonclassicality a perfect correspondence with nonlinearity breaks down, but the induced bound is tighter.

[3]The same behavior is shared by the W-noclassicality, but the curves for different value of k are not shown, as the region between the extremal curves in Fig. 6.9 is very narrow.

CHAPTER 7

Backflow of probability and Wigner negativity

The present chapter is dedicated to a peculiar and little-known quantum mechanical effect, the so-called *quantum backflow effect* [302]. This is a counterintuitive behaviour of the quantum mechanical probability current (here studied for a quantum free particle in one dimension): the current may assume negative values even for wave-packets without negative momentum components. Intuitively, this means that a particle with positive momentum can have an increased probability of "going back" for a small fraction of time.

This effect was discovered in connection with the arrival-time problem in quantum mechanics [17], but it was studied in details only several years later in Ref. [33], where a bound for the maximal fraction of the probability that can *flow backwards* during a finite time interval was found. This bound turns out to be an adimensional constant $c_{\mathrm{bm}} \approx 0.04$, independent from the mass of the particle and from the duration of the effect itself; remarkably, this value is also independent from the Planck constant $\hbar$.

More recently, the backflow effect has attracted some more attention: improvements in the numerical estimation of c_{bm} have been addressed [79, 228] and additional bounds, analytical examples, and connections with realistic measurements have been provided [125, 202, 303]. An explicit scheme to experimentally detect backflow in a Bose-Einstein condensate has been proposed [217]. The same behaviour was found also for a particle in a linear potential [189] and for a Dirac particle [190] and an analogue effect for angular momentum has been studied [269].

At variance with the subject of the previous chapter, the backflow effect is a *dynamical* effect, being connected to the free propagation of a particle. However, despite being a dynamical effect, the occurrence of backflow is entirely determined by the properties of the initial quantum state, because the dynamics in the phase space is essentially classical, as we have explained in Sec. 1.4 and as we are going explain in more in details.

Clearly, this backflow effect is an intrinsically quantum phenomenon and we will show that it is intimately connected with negative values of quasiprobability distributions in the phase space, in particular the Wigner function. In some sense, this effects provides a direct and tangible consequence of such negative values; this is consistent with a school of thought which assigns practical and philosophical meaning to *negative probabilities* in quantum mechanics [83, 254].

Starting from these considerations, the main goal of the work we present here is to investigate how the backflow of probability (negativity of the probability current), is

connected to the negativity of the Wigner function. Our results indicate that quantum backflow captures a different and more restrictive notion of nonclassicality, with the negativity of the Wigner function being only a necessary prerequisite for its occurrence. This idea is confirmed by looking at the robustness to noise of this effect: the negativity of the probability current is more easily destroyed than the negativity of the Wigner function itself.

7.1 Phase-space dynamics and quantum backflow effect

7.1.1 Quantum and classical phase-space dynamics

A pure quantum state of a particle moving along a line (coordinate denoted by x) is a continuous variable quantum system and it may be described either by its wave function in the position representation $\psi_t(x) = \langle x|\psi_t\rangle$ or by a phase-space description using the Wigner function. In this chapter we denote the Wigner function of the evolving time-dependent state as:

$$\mathcal{W}[\rho(t)](x,p) \equiv W(x,p,t)\ . \tag{7.1}$$

For systems subject to a potential depending only on the coordinates, i.e. governed by the Hamiltonian

$$\hat{H} = \frac{\hat{p}^2}{2m} + V(\hat{x}), \tag{7.2}$$

the Wigner function obeys the continuity equation

$$\frac{\partial}{\partial t}W(x,p;t) + \operatorname{div}\mathbf{J} = 0, \tag{7.3}$$

where

$$\mathbf{J} = \begin{pmatrix} J_x \\ J_p \end{pmatrix} \tag{7.4}$$

is the *Wigner function flow* of the system in the phase space [28, 150, 262, 266]. This Wigner flow can be decomposed as the product $\mathbf{J} = W\mathbf{v}$, where $\mathbf{v} = \mathbf{J}/W$ may be interpreted as the velocity of the phase space flow. Remarkably, for potentials at most quadratic in x, the velocity field $\mathbf{v}$ coincides with its classical analogue

$$\mathbf{v} = \begin{pmatrix} \dot{x} \\ \dot{p} \end{pmatrix} = \begin{pmatrix} \partial_p H \\ -\partial_x H \end{pmatrix}. \tag{7.5}$$

For this class of potentials the flow is thus Liouvillian, which means $\operatorname{div}\mathbf{v} = 0$, and the Wigner function flows in the phase space as an incompressible fluid. This is equivalent to the "covariant" evolution of the Wigner function under quadratic Hamiltonians in Eq. (1.119).

Some typical quantum effects arise as a consequence of the fact that the Wigner function can take negative values. We can see that in regions where W is negative the Wigner flow $\mathbf{J} = W\mathbf{v}$ takes place in the direction opposite to the velocity $\mathbf{v}$, which, in turn, gives the direction of the classical phase space flow.

7.1.2 The quantum backflow effect

The properties illustrated in the previous section may bear some unexpected results, such as the so-called quantum probability backflow effect. Let us consider a initial wave packet containing only components of positive momentum; the wave function at time $t = 0$ is given by

$$\psi(x,0) = \frac{1}{\sqrt{2\pi\hbar}} \int_{-\infty}^{+\infty} \mathrm{d}p\, e^{\frac{ipx}{\hbar}}\, \phi(p)\Theta(p) \tag{7.6}$$

where $\Theta(p)$ is the Heaviside step function, vanishin for negative values of p. In this situation the Wigner function of the particle is entirely localised in the positive momentum half plane of the phase space.

As we have seen the Wigner flow for a free particle coincides with the classical phase space flow, that is the one given by the velocity

$$\mathbf{v} = \begin{pmatrix} \frac{p}{m} \\ 0 \end{pmatrix}. \tag{7.7}$$

In the positive momentum region, where our particle is localised, the velocity is therefore always in the positive x direction. However, in points where the Wigner function takes negative values, the Wigner flow points in the negative x direction. The volume of the Wigner function in the $x \geq 0$ half plane in phase space coincides with the probability of finding the particle in the positive position semi-axis at a given time:

$$P(t) = \int_{-\infty}^{+\infty} \mathrm{d}p \int_{0}^{+\infty} \mathrm{d}x\, W(x,p;t) = \int_{0}^{+\infty} \mathrm{d}x\, |\psi_t(x)|^2 \,. \tag{7.8}$$

By the continuity equation (7.3), the time derivative of this volume is given by the Wigner flow through the $x = 0$ line in phase space:

$$j(t) := \frac{d}{dt} P(t) = \int_{-\infty}^{+\infty} \mathrm{d}p\, \frac{p}{m}\, W(0,p;t). \tag{7.9}$$

The expression in Eq.(7.9) coincides with the quantum mechanical probability current in the origin, i.e.

$$j(t) = \frac{i\hbar}{2m} \left(\psi_t(0) \frac{\partial \psi_t^*}{\partial x}(0) - \psi_t^*(0) \frac{\partial \psi_t}{\partial x}(0) \right). \tag{7.10}$$

According to classical intuition, one would expect the wave packet described above to move in the positive spatial direction with a constant average velocity and hence the probability $P(t)$ to increase monotonically with time, as the particle moves into the positive position semi-axis. However, this is the case only for states with a sufficiently classical behaviour. If the Wigner function takes negative values, its phase space flow can be in the negative direction even in the positive momentum region. If the negative flow occurs in a sufficiently large section of the $x = 0$ line, the derivative (7.9) can indeed take negative values.

As a consequence, for a generic quantum state, even if in the limit $t \to +\infty$ the probability $P(t)$ globally and monotonically increases, approaching the limiting value $P(t) = 1$, there may exist time intervals in which it is a locally decreasing function of

time. The particle thus appears to "go back" towards the negative semi-axis. In order to quantify the backflow effect, one may consider the maximal amount of such temporary decrease of the probability density:

$$\beta[\psi] := \left| \inf_{t_1<t_2} [P(t_2) - P(t_1)] \right| . \tag{7.11}$$

The increase in probability over a time interval (t_1, t_2) (the most negative values of which we must find to compute backflow) can be expressed in terms of the phase space flow in Eq. (7.9) as follows

$$F(t_1, t_2) := P(t_2) - P(t_1) = \int_{t_1}^{t_2} \mathrm{d}t j(t) . \tag{7.12}$$

Upon considering the incompressible fluid nature of the Wigner flow, one may define a natural motion of phase space points so that this motion has velocity given by the field $\mathbf{v}$: a point initially in (x, p), after a time interval t is mapped to

$$\varphi_t(x, p) = \begin{pmatrix} x + \frac{p}{m} t \\ p \end{pmatrix} . \tag{7.13}$$

Because of the incompressible nature of the flow, the Wigner density remains constant along this motion, that is

$$W(x, p; t) = W(\varphi_{-t}(x, p); 0) , \tag{7.14}$$

as can be seen also from (1.119) upon considering the matrix $\mathrm{diag}[0, 1/m]$ in the quadratic Hamiltonian. Using this result we can express function (7.12) as

$$\begin{aligned} F(t_1, t_2) &= \int_{\mathcal{R}} \mathrm{d}x \, \mathrm{d}p \, W(x, p; t_2) - \int_{\mathcal{R}} \mathrm{d}x \, \mathrm{d}p \, W(x, p; t_1) \\ &= \int_{\varphi_{-t_2}(\mathcal{R})} \mathrm{d}x \, \mathrm{d}p \, W(x, p; 0) - \int_{\varphi_{-t_1}(\mathcal{R})} \mathrm{d}x \, \mathrm{d}p \, W(x, p; 0) \\ &= \int_{\Omega} \mathrm{d}x \, \mathrm{d}p \, W(x, p; 0) , \end{aligned} \tag{7.15}$$

where $\mathcal{R}$ is the $x \geq 0$ half-plane and the region $\Omega = \boldsymbol{\varphi}_{-t_1}(\mathcal{R}) \setminus \boldsymbol{\varphi}_{-t_2}(\mathcal{R})$ is an angular sector in the phase space. In polar coordinates Ω is defined by

$$\frac{\pi}{2} + \arctan\left(\frac{t_1}{m}\right) \leq \phi \leq \frac{\pi}{2} + \arctan\left(\frac{t_2}{m}\right) , \tag{7.16}$$

and no constraint on the radial coordinate. The increase in probability over the time interval (t_1, t_2) may be thus seen as the flow of the Wigner volume initially (at $t = 0$) in the region Ω into the $x \geq 0$ half-plane. If there exists at time $t = 0$ a sector Ω in which the Wigner function has negative integral, then there is also a time interval in which this probability increase is actually negative and the state shows the backflow effect. We refer the reader to [293] for a more detailed analysis of integrals of the Wigner function on angular sectors in phase spaces in the context of quantum harmonic analysis.

7.1.3 Quantum backflow and nonclassicality

The backflow effect cannot be observed for a particle moving according to the classical laws of motion. In this sense its occurrence is a manifestation of the genuine quantum nature of the state under investigation. In the previous Section, we have seen how negativity of the Wigner function is a prerequisite to observe negativity of the probability current, and a question arises about the general connection between the two notions of nonclassicality. In particular we focus on W-nonclassicality; at variance with the previous section we use the actual volume of the negative part of the Wigner function, i.e. Δ defined in (8.2.1) (we omit the dependence on the state) and not the normalized nonclassicality measure ν.

If we choose t_1 and t_2 as the time interval corresponding to the minimum in Eq.(7.11), then $-F(t_1, t_2)$ is equal to the backflow measure of the state $\beta[\psi]$. In this way we may identify the Wigner negativity volume Δ of the initial state as an upper bound to the backflow: if we denote by V_Ω^+ (V_Ω^-) the volume of the positive (negative) part of the initial Wigner function on the sector Ω then, recalling equation (7.15), we may write the following inequality

$$\beta[\psi] = -\left(V_\Omega^+ - V_\Omega^-\right) \leq V_\Omega^- \leq \Delta\,. \tag{7.17}$$

This confirms that W-nonclassicality quantified by the volume Δ is a necessary condition for backflow. Moreover, a question arises on whether a more precise quantitative relation exists between β and Δ. In order to concretely check whether this is the case, we consider an explicit example and analyze in some details the two quantities for superpositions of Gaussian wavepackets.

7.2 Superpositions of Gaussian states

7.2.1 Quantum backflow for superpositions of Gaussian states

The quantum backflow effect is not observed in states with a positive Wigner function. For this analysis, we are going to consider the superposition of two Gaussian momentum wave-packets of width σ centered on different positive momenta. An overview of quantum backflow for such states may be found in [303]. For $\sigma \to \infty$ one recovers a superposition of two plane waves with different momenta, which is the simplest example of a state presenting backflow [33, 302], though it does not correspond to a physical state. In the following, we analyze the backflow for a general normalized superposition with complex coefficients of two Gaussian wave packets. These state are an example of the *Gaussian cat states* [207], introduced as a generalization of the so-called cat states often studied in quantum optics [70, 307].

We are not intersted to systematically study the effect in the whole range of physical parameters. Rather, our main goal is to compare backflow and nonclassicality in some particularly relevant conditions. To this aim, we are interested in finding a state which gives a local (in the parameter space) maximum of the backflow and to study the states in the neighbouring region of the parameter space.

As usual we work in natural units such that $\hbar = 1$ and we choose a particle with unit mass, $m = 1$. We consider following initial state, written in momentum representation

$$\phi_0(p) = N\left[e^{-(p-p_0-\delta)^2\sigma^2} + \alpha e^{i\theta} e^{-(p-p_0)^2\sigma^2}\right], \tag{7.18}$$

where all the parameters are real numbers. The normalization condition fixes the value of N in terms of the other parameters as follows

$$N(\sigma, p_0, \delta, \alpha, \theta) = \left(\frac{2\sigma^2}{\pi}\right)^{\frac{1}{4}} \left(1 + \alpha^2 + 2e^{-\frac{1}{2}\delta^2\sigma^2}\alpha\cos\theta\right)^{-\frac{1}{2}}. \tag{7.19}$$

The time evolved wave function, its expression in position representation and the time dependent probability current in the origin can be calculated analytically, but we do not report their explicit expressions here. One can see, however, that these quantities can be more conveniently expressed in terms of the following rescaled adimensional parameters:

$$\tilde{p}_0 = \sigma p_0 \qquad \tilde{t} = \frac{t}{\sigma^2} \qquad \tilde{\delta} = \sigma\delta\,. \tag{7.20}$$

With this choice, the current $j(\tilde{t})$ can be expressed as the product of a dimensional factor $\frac{1}{\sigma^2}$ with an adimensional oscillating function of the remaining parameters $\tilde{j}(\tilde{t}; \tilde{p}_0, \tilde{\delta}, \alpha, \theta)$. Upon applying a change of variables to the integral in Eq.(7.12) we obtain:

$$F(t_1, t_2) = \int_{\tilde{t}_1}^{\tilde{t}_2} \mathrm{d}\tilde{t}\, j(\tilde{t}) \tag{7.21}$$

with $\tilde{t}_k = \sigma^2 t_k$, $k = 1, 2$, from which it is apparent that the width σ only changes the size of the time interval in which backflow is observed, while the value of the backflow itself only depends on the adimensional parameters $\tilde{p}_0$, $\tilde{\delta}$, α and θ. This is in agreement with Ref. [33], where it is emphasized that the duration of the backflow effect can be changed arbitrarily. However, this extra degree of freedom may be useful if we want to consider states at fixed energy. Indeed, if we want to maximize the backflow at fixed energy E, we can minimize the flux (7.21) as a function of $\tilde{p}_0$, $\tilde{\delta}$, α and θ, and then choose the appropriate value of σ to obtain a state with a given value of energy E.

Clearly, these states are not strictly confined to the positive momentum region. Nonetheless, the total volume of the wave function localized on the negative semi-axis in momentum representation can be arbitrarily reduced by taking a Gaussian centered on a positive momentum sufficiently larger than its width. Indeed, by considering only values of $\tilde{p}_0$ larger than 3 (after fixing $\sigma = 1$), the negative volume is of the order of 10^{-9}, a value corresponding to irrelevant effect on the backflow (we also performed an explicit numerical check).

In Fig. 7.1 we show the probability $P(\tilde{t})$ and current $\tilde{j}(\tilde{t})$ for a given superposition of two Gaussian wavepackets. We can appreciate that the time intervals where probability decreases coincide with the negative regions of the current. According to Eq. (7.12) and since the probability $P(\tilde{t})$ is known analytically, the backflow may be easily computed if we know the time interval which contains the most negative peak of the current. Unfortunately, finding the zeros of the current has to be done numerically. Alternatively,

the backflow may be also computed through a numerical integration of the negative part of the current $\frac{1}{2}\left(\left|\tilde{j}(\tilde{t})\right| - \tilde{j}(\tilde{t})\right)$ over an interval containing the most negative peak. This method does not require the exact knowledge of the zeros, though it requires to check that only the right peak is contained within the integration interval.

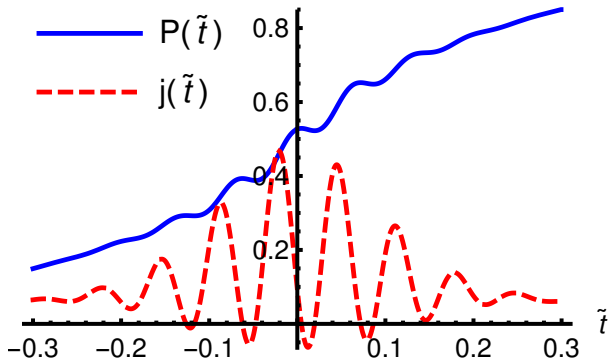

Figure 7.1: The probability $P(\tilde{t})$ (solid blue curve) and the current $j(\tilde{t})$ (dashed red curve) for a superposition of Gaussian wavepackets with $\alpha = 2$, $\tilde{\delta} = 11$, $\tilde{p}_0 = 3$, $\theta = \frac{\pi}{4}$, and $\sigma = 10$. See Eq. (7.18) for details. The value of the current $j(\tilde{t})$ is multiplied by 10 in the figure in order to appreciate its behaviour.

Let us analyze the behaviour of the backflow as a function of the different parameters. At first, we notice that the $\beta[\psi]$ is a decreasing function of $\tilde{p}_0$, at any fixed set of values of the other parameters, see the left panel of Fig. 7.2. Maximum backflow is therefore attained by fixing $\tilde{p}_0$ to its lowest allowed value; as mentioned above we choose $\tilde{p}_0 = 3$ to ensure a vanishing negative momentum component. The effect of the parameter θ is that of shifting the position of negative peaks of the current along the time axis, as it may be seen in Fig. 7.3. Intuition suggests that maximum backflow is obtained for a current with a minimum located in $\tilde{t} = 0$, i.e. $\theta = \pi$. Actually, the central peak is not always the one corresponding to the greatest backflow; nonetheless, in order to simplify our analysis, we focus on a parameter range for which the central peak is indeed the most negative one.

Unless otherwise specified, from now on we fix the values $\tilde{p}_0 = 3$ and $\theta = \pi$ and investigate the dependence of backflow on the parameters α and $\tilde{\delta}$. In particular, we explore the first-quadrant region of the $(\alpha, \tilde{\delta})$ plane bounded by the lines $\alpha = 1$ and $\alpha = 1 + \tilde{\delta}/\tilde{p}_0$ (which is obtained by imposing $\tilde{j}(0) \leq 0$). For different values of θ other regions may be found where backflow is present, but no analytic expression can be found. The backflow $\beta[\psi]$ as a function of α and $\tilde{\delta}$ is shown in Fig. 7.4. We can see that $\beta[\psi]$ shows a maximum, from which it decreases going towards the boundaries of the region. The maximum is obtained for $\alpha \simeq 1.9$, $\tilde{\delta} \simeq 11$, corresponding to $\beta[\psi] \simeq 0.0063$ (a value slightly larger than the one found in Ref. [303]). The region closer to the value $\alpha = 1$ is not shown in the plot as the backflow is not given by the central peak.

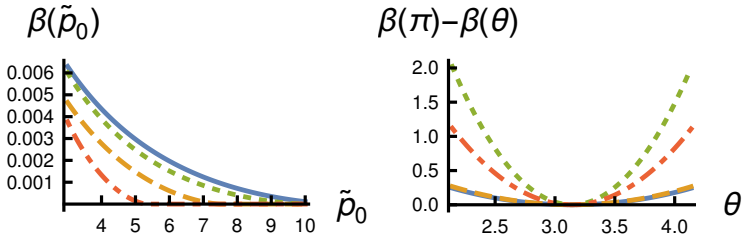

Figure 7.2: Backflow β as a function of θ and $\tilde{p}_0$, the different curves represent a different choice of the couple of parameters α and $\tilde{\delta}$: $\alpha = 2$, $\tilde{\delta} = 11$(solid blue); $\alpha = 3$, $\tilde{\delta} = 15$ (dashed orange); $\alpha = 1.8$, $\tilde{\delta} = 5$ (dotted green); $\alpha = 2.5$, $\tilde{\delta} = 8$ (dot-dashed red). Left panel: β as a function of $\tilde{p}_0$, with $\theta = \pi$. Right panel: the difference between β as a function of θ and β obtained for $\theta = \pi$, with $\tilde{p}_0 = 3$; the values on the ordinate axis are in units of 10^{-4}.

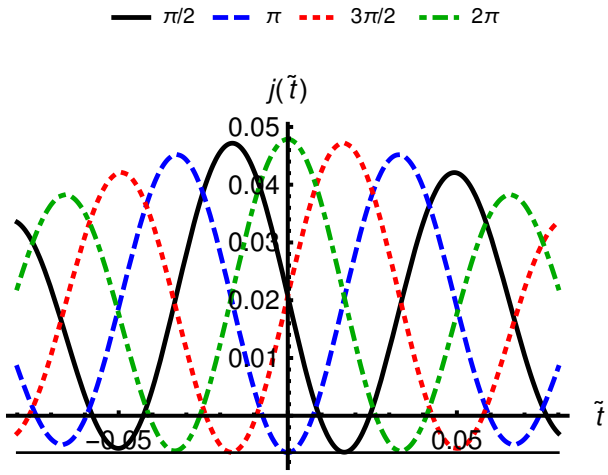

Figure 7.3: The probability current $j(\tilde{t})$ as a function of $\tilde{t}$ for different values of θ at fixed values of the other parameters ($\alpha = 2$, $\tilde{\delta} = 11$ and $\tilde{p}_0 = 3$). The horizontal line highlights that the global minimum corresponds to the central negative peak.

7.2.2 Quantum backflow and Wigner nonclassicality for Gaussian superpositions

The Wigner function of the superposition state in Eq. (7.18) is given by

$$W_0(\tilde{x},\tilde{p}) = \frac{e^{-\tilde{x}^2/2}\left[\alpha^2 e^{-2(\tilde{p}-\tilde{p}_0)^2} + e^{-2\left(\tilde{p}-\tilde{p}_0-\tilde{\delta}\right)^2} + 2\alpha\cos\left(\tilde{x}\tilde{\delta}-\theta\right)e^{-2\left(\tilde{p}-\tilde{p}_0-\frac{\tilde{\delta}}{2}\right)^2}\right]}{\pi\left(1+\alpha^2+2\alpha e^{-\frac{\tilde{\delta}^2}{2}}\cos\theta\right)}\,, \tag{7.22}$$

where, consistently with Eq. (7.20), we used the rescaled variables

$$\tilde{x} = \frac{x}{\sigma} \qquad \tilde{p} = \sigma p\,. \tag{7.23}$$

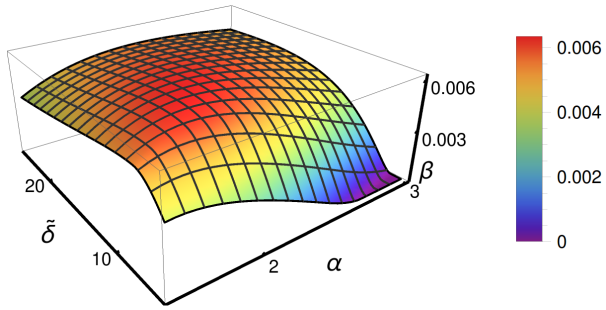

Figure 7.4: The backflow β computed numerically as a function of parameters α and $\tilde{\delta}$ in the range $\alpha \in [1.5, 3]$, $\tilde{\delta} \in [5, 25]$.

Notice that the rescaling is not altering the volume element and that $W_0(\tilde{x}, \tilde{p})$ does not explicitly depend on σ. This means that also the Wigner negativity Δ, as it happens for the backflow β, does not depend on σ.

The Wigner function in Eq. (7.22) is characterized by two Gaussian peaks corresponding to the two momenta p_0 and $p_0 + \delta$ and by an interference region located halfway between the two peaks. In Fig. 7.5 we show a contour plot of the Wigner function, which provides an intuitive explanation to the behaviour of the backflow. On the one hand, the interference effects (and thus the negative regions of the Wigner function) are more pronounced if the the amplitude of the two Gaussians is the same (i.e. for $\alpha = 1$). However, this is not leading to maximum backflow, since the Gaussian peaked at $p_0 + \delta$ prevails in the integration region. These intuitive argument suggests that no monotonic relation between Wigner nonclassicality and quantum backflow shold be found. As a matter of fact, since the positive parts of the Wigner function in the region Ω may compensate for the negative ones, it is possible to find states not showing backflow despite having negative Wigner function. Moreover, we may also find pairs of states with increasing backflow but decreasing negativity. This non monotonic behaviour of the backflow is illustrated in Fig. 7.6, where parametric plots of the backflow as a function of the Wigner negativity are shown for varying α or $\tilde{\delta}$.

Finally, we point out that quantum backflow exhibits *sudden death* for some values of the parameters. As for example, if α is bigger than the threshold value $\alpha = 1 + \tilde{\delta}/\tilde{p}_0$ there is no backflow. Analogue threshold values for $\tilde{\delta}$ at fixed α may be found. On the contrary, Wigner negativity due to the interference fringes dies only asymptotically, i.e. when a single Gaussian state is recovered. This remarkable difference may be observed in both panels of Fig. 7.6, where we have regions with no backflow but nonzero Wigner negativity.

7.3 Backflow and phase space smoothing

We now study the robustness of the backflow effect against the addition of thermal noise, which corresponds to a Gaussian smoothing in the phase space. We start by quickly

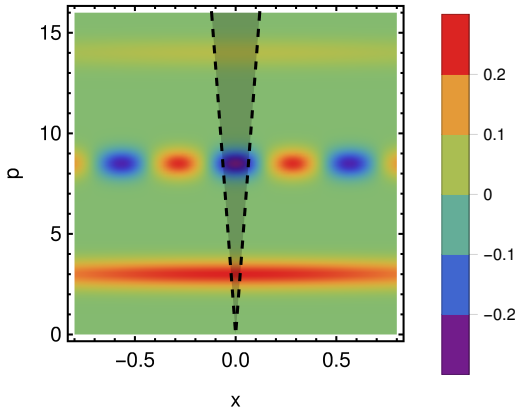

Figure 7.5: Density plot of the Wigner function of the superposition of Gaussian states with the maximum backflow, the integration region Ω is the shadowed region between the two dashed lines corresponding to $p = -\frac{m}{t_1}x$ and $p = -\frac{m}{t_2}x$.

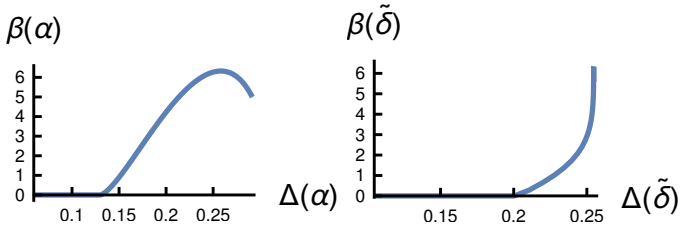

Figure 7.6: Left panel: parametric plot of the backflow β as a function of the nonclassicality Δ for $\tilde{\delta} = 11$ and varying $\alpha \in [1.5, 10]$. Right panel: parametric plot of the backflow β as a function of the nonclassicality Δ for $\alpha = 2$ and varying $\tilde{\delta} \in [1, 20]$.

recalling some notions about s-ordered quasiprobabilities, in order to emphasize the similarity of our analysis to the notion of nonclassical depth.

7.3.1 *s*-ordered quasiprobability distributions

The Wigner function can be generalized to the family of s-ordered quasiprobability distributions [27, 44], which are routinely used in quantum statistical optics to obtain expectation values by averaging over the phase space. A quasiprobability distribution $W(x, p, s)$ is labeled by the index $-1 \leq s \leq 1$, which reflects a particular choice of the ordering of the canonical operators in the expectation value to be computed. For the specific values $s = 1, 0, -1$ we have the Glauber P function (normal ordering), the Wigner function (symmetrical ordering) and the Husimi Q function (antinormal ordering), respectively. For $s < s'$, two quasiprobabilities of different ordering are connected through a Gaussian convolution

$$W(x, p, s) = W(x, p, s') \star G(x, p, s' - s) = \int \mathrm{d}x' \mathrm{d}p' W(x', p', s') G(x - x', p - p', s' - s); \tag{7.24}$$

where $\star$ denotes convolution and the function G is a Gaussian defined as

$$G(x,p,\kappa)=\frac{1}{\pi\kappa}\exp\left[-\frac{x^2+p^2}{\kappa}\right]. \tag{7.25}$$

From Eq. (7.24) one sees that going from $s=1$ to $s=-1$ the distributions gradually become well-behaved and positive definite functions, thanks to the Gaussian smoothing. This is the idea leading to the definition of the nonclassical depth [164]. This quantity is the value of s closer to $s=1$ corresponding to a positive and non-singular distribution for a given state. In other words, the nonclassical depth represents the minimum amount of convolution needed

7.3.2 *s*-dependent current

Here, in order to assess the robustness of backflow against noise, we are going to consider a generalized definition of the probability current based on the s-ordered quasiprobability distributions. Notice that in principle only the Wigner function may be used to compute the current via Eq. (7.9) since the Wigner function is the only s-ordered quasiprobability distribution that has position and momentum probability distributions as marginals.

On the other hand, introducing generalized s-dependent currents is meaningful if we note that the convolution of a Wigner function with a Gaussian represents the Wigner function of the quantum state after the interaction with a thermal environment. Let us consider the master equation of a system interacting with a bosonic bath, expressed in terms of the creation and destruction operators

$$\frac{d\rho}{dt}=\gamma(\bar{n}+1)\mathcal{D}[\hat{a}]\rho+\gamma\bar{n}\mathcal{D}\left[\hat{a}^\dagger\right]\rho \tag{7.26}$$

where γ is the loss rate and $\bar{n}$ is the average photon number of the thermal environment. In terms of the Wigner function, the solution of the above equation may be written as

$$e^{-\tau}W_t(e^{-\tau/2}x,e^{-\tau/2}p)=W_0(x,p)\star G(x,p,-s_\tau), \tag{7.27}$$

where $\tau=\gamma t$ and $s_\tau=-(2\bar{n}+1)(e^\tau-1)$, see e.g. [27, 215, 257] for details. $W(x,p,s)$ is thus the Wigner function of the state obtained from the initial one after the interaction with a noisy environment. Notice that the rescaling due to dissipation, i.e. the exponentials of τ appearing on the l.h.s. of (7.27), plays no role in determining the negativity of the Wigner function and the backflow.

If the initial state has the Wigner function $W_0(x,p)$, the state after the noisy interaction has a Wigner function given by

$$W_0(x,p,s)=W_0(x,p)\star G(x,p,-s), \tag{7.28}$$

where s is a function of the temperature, of the damping coefficient and of the interaction time. At this point, we consider $W_0(x,p,s)$ as the *initial* Wigner function of a mixed state evolving according to the free particle Hamiltonian, and we get an s-dependent and time dependent Wigner function

$$W_t(x,p,s)=W_0\Big(x-\frac{p}{m}t,p,s\Big), \tag{7.29}$$

which can in turn be used to compute the s-dependent current

$$j(t,s) = \int_{-\infty}^{+\infty} \mathrm{d}p \frac{p}{m} W_t(0,p,s). \tag{7.30}$$

We only consider $-1 \leq s \leq 0$, in order to have a smoothing of the initial Wigner function; in terms of ordering this means going from the Wigner towards the Q function.

We stress that this way of proceeding is completely different from considering the backflow of a truly open quantum system, where in general the expression for the probability current is not the same [301].

7.3.3 s-dependent backflow and negative current depth

Having defined an s-dependent current we can straightforwardly apply the definition of backflow (7.12) and obtain an s-dependent backflow. As we can see in Fig. 7.7 the backflow vanishes for a certain $s > -1$, therefore it is less robust than the negativity of the Wigner function. Having more backflow initially (for $s = 0$) usually means that the backflow of the state survives longer (i.e. it disappears for a value of s closer to -1). However, as it may be seen from Fig. 7.7, this is not necessarily the case for any choice of the parameters.

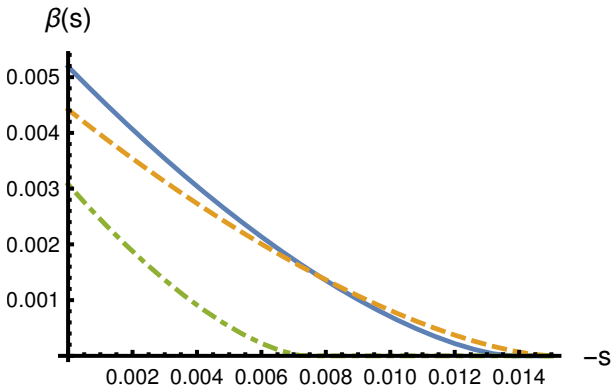

Figure 7.7: Plots of the s-dependent backflow as a function of the Gaussian smoothing parameter s. From top to bottom in the region $s \approx 0$ we have the states with $\alpha = 2$ and $\tilde{\delta} = 7$ (solid blue), $\alpha = 2$ and $\tilde{\delta} = 6$ (dashed orange), $\alpha = 3$ and $\tilde{\delta} = 10$ (dot-dashed green).

In order to better analyze this behaviour we introduce, in analogy with the nonclassical depth, the *negative current depth*, which is defined as follows. Upon denoting by C the subinterval of $s \in [-1, 0]$ leading to a positive s-dependent current in (7.30), then the negative current depth s_m is defined as

$$s_m \equiv \inf_{s \in C}(-s), \tag{7.31}$$

which is a positive quantity bounded between 0 and 1. This quantity provide an alternative quantification of backflow; instead of quantifying how much probability is flowing

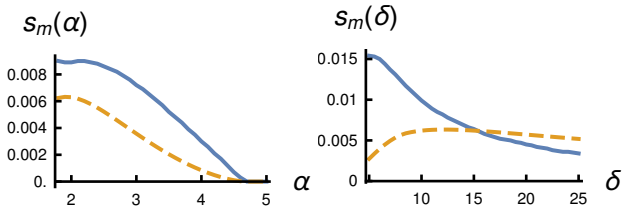

Figure 7.8: The negative current depth (solid blue) and the backflow (dashed orange). Left panel: the quantities are shown as a function of α for $\tilde{\delta} = 11$. Right panel: as a function of $\tilde{\delta}$ for $\alpha = 2$.

backwards we quantify the amount of Gaussian convolution, i.e. noise, needed to destroy the backflow effect of a given initial state.

Fig. 7.8 shows that the negative current depth and the backflow of a quantum state have similar behaviour, but regions where they are not monotonic exist, as it can be seen in the right panel. Upon looking at the values of s_m in Fig. 7.8, and since for all these states the negativities of the Wigner function completely disappear only for $s = -1$, we conclude that the backflow is a very fragile form of nonclassicality. Notice that other criteria for nonclassicality exist and their behaviour for superpositions of Gaussian states in the presence of a thermal environment has been studied [215]. Results have shown that almost all these indicators vanish for a finite Gaussian smoothing, except the visibility of the interference fringes which vanish only asymptotically.

Summary

- The quantum backflow effect is a counterintuitive behaviour observed in the probability current of a one-dimensional free particle, which may be negative even for states with vanishing negative momentum component. As a result, for a particle moving in the positive x direction, the probability of finding it in the region $x < 0$ can *increase* for finite amounts of time during the evolution.
- This effect can be quantified by the maximal amount of probability that can flow in the $x < 0$ region during any time interval.
- Quantum backflow may be described in the phase space, showing that its occurrence is connected to the *classical phase space dynamics* of a *nonclassical initial state*.
- The quantitative measure of backflow has a different behaviour than negative volume of the Wigner function in terms of the defining parameters of the state, in particular it vanishes for some threshold values.
- The negativity of the probability current is a feature which is more easily destroyed by a thermal environment than the negativity of the Wigner function itself.
- Overall, these results suggest that backflow represents a more restrictive and more fragile notion of nonclassicality, and the negativity of the Wigner function is just a necessary condition for its occurrence.

CHAPTER 8

Resource theory of non-Gaussianity and Wigner negativity

This is the last chapter of this Thesis and we can finally use the word *resource* in a a more precise manner, by presenting a (convex) resource theory of non-Gaussianity and Wigner negativity. We have briefly introduced Gaussian states of bosonic systems in Sec. 1.4.2, where we already pointed out that the Gaussian formalism has been the cornerstone of continuous-variable (CV) quantum technology, due to its relative simplicity and to the many physical platforms which can be accurately described by it.

Notwithstanding the vast phenomenology of truly quantum features displayed by Gaussian systems, there are several no-go theorems showing that some protocols cannot be realized in the Gaussian domain. The prime example of such restrictions is found in the task of entanglement distillation [74, 86, 111], a result which has recently been generalized to a large class of quantum resources beyond entanglement [162]. Other similar no-go theorems include: error correction [208], universal quantum computation [169, 191], and more [142, 180]. Furthermore, several CV quantum information protocols can improve their performances when they are implemented with relevant non-Gaussian states and operations. We have seen an example of this for quantum estimation in Chapter 5, but the same is true for teleportation [58, 210, 211] and cloning [38, 57] and many others.

From this discussion it should be clear that non-Gaussian states and operations can be considered crucial elements for the development of CV quantum information technologies. As a matter of fact there have been major research efforts to understand and characterize them and towards their experimental generation. In particular, quantum optical schemes as photon-subtraction and photon-addition have been extensively studied [155, 205, 210, 213, 249].

Roughly speaking, a resource theory would answer questions like "Is it possible to transform a given non-Gaussian state to another one with Gaussian transformations, and how hard is to do so?". However, for reasons that will be explained, no satisfactory resource theory of non-Gaussianity has been developed yet. This fact represents a major obstacle to our understanding of non-Gaussian resources and the development of applications thereof. The work we present in this Chapter has the goal to overcome this obstacle by introducing a general theoretical framework for non-Gaussian resources.

These questions about the manipulation of non-Gaussian states with Gaussian operations is timely, for several reasons. First of all these these operations are becoming a reality in quantum optical experiments [197] and they have proved to be useful, for example, to

counteract the effect of decoherence of non-Gaussian states [84, 163]. Moreover, different protocols that require a non-Gaussian element can be often improved with Gaussian operations. This is the case for entanglement distillation based on photon subtraction, whose performances can be enhanced by implementing local Gaussian operations [49, 87, 309].

Resource theories [59] are a powerful framework to study manipulation of quantum states under some operational restriction on the allowed operations. Entanglement theory is the prototypical example but many others have been recently developed. In particular, general results have been obtained for a vast class of resource theories both in the asymptotic [34] and single-shot regime [116]. In general, a resource theory stems from two interlinked starting points. First, the identification of a set of operations that are regarded, for reasons that depend on the setting at hand, as readily available (*free operations*). For example, these are local operations and classical communication in the resource theory of entanglement. Second, the classification of all possible states in two categories: *free states*, that are considered freely available (typically via free operations) and non-resourceful, and *resource states*. Separable and entangled states are an example of this classifications. The quantification and manipulation of resources via free operations are the central concerns of resource theories.

There are at least two major difficulties towards such a theory in the case of non-Gaussian resources. First, it is natural to identify the set of Gaussian states as free states. However, this set is not convex and therefore non-Gaussianity *per se* cannot be considered a quantum resource of practical relevance in general: in fact, non-Gaussianity can be generated by classical randomness, which is a readily available in most contexts and therefore, from an operational view-point, free. Second, the intrinsic infinite-dimensional character of CV systems implies that some operations (conditioning on the continuous real outcomes of measurements, see below) that are ideally free in various resource theories are, in this context, unfeasible. These two roadblocks have hindered the development of a satisfactory resource theory, namely a theory that is both general and of practical relevance in realistic settings. We try to overcome these roadblocks by adopting a pragmatic approach and incorporating them in our definitions of free operations and states.

Our analysis is based on tools developed to describe quantum systems via their phase-space representation, as reviewed in Sec. 1.4.1. In this formalism, quasiprobability distributions play a central role and their non-positivity is considered as a characteristic trait of quantumness. We have briefly commented about this point, when we introduced nonclassicality in Sec. 1.4.4; however, negativity of quasiprobabilities is a very general feature of quantum theory [66, 81, 82], directly linked to its contextual character [67, 135, 264]. For CV systems, the connection between negativity of the Wigner function and Gaussian states is strong: pure states with a positive Wigner function are only Gaussian, as stated by the Hudson theorem [136, 263]. The situation is more complicated when dealing with mixed states, since there is no equivalent to the Hudson theorem [41, 183, 184]. In particular there exist mixed states that are not mixtures of Gaussian states, yet have a positive Wigner function [85, 103, 126, 138, 149, 216]. Despite this, we are going to introduce a computable resource quantifier based on the negativity of the Wigner function and we are going to show that it is a proper monotone for the resource theory at hand.

The framework presented in this Chapter is based on an analogous one for finite-dimensional systems (discrete variables, DVs), where the challenge to identifying the resource responsible for quantum advantage in quantum computation has led to the formulation of various resource theories [5, 134, 265, 286]. In this context, stabilizer states and Clifford unitaries play the role of Gaussian states and unitaries, respectively. On the other hand, so-called *magic states* play the role of non-Gaussian states. For finite dimensional systems it is natural to define Wigner functions on a finite dimensional state space [110, 194] (opposed to the CV phase space) and in particular for odd-dimensional systems a DV version of the Hudson theorem was proven [117]. For such systems, it has been shown that the negativity of the discrete Wigner function is necessary to obtain a circuit which is both universal and cannot be efficiently simulated with known classical algorithms [185, 226, 239, 285]. Based on this, a computable monotone —dubbed *mana*— has been identified [286]. The monotone that we introduce here can be considered as a CV counterpart of the DV mana.

In the context of CV quantum computation, non-Gaussian operations are known to be necessary to attain universality [169]. Non-Gaussian operations can in turn be enabled by non-Gaussian states via gate teleportation, the Gaussian protocol at the basis of CV measurement-based quantum computation. However, it is not clear in general which non-Gaussian states can play this crucial enabling role [21, 77, 109, 248, 270, 284, 292] and at which cost in terms of circuit synthesis [255]. In addition, some sub-universal CV circuits have been rigorously proven hard to simulate classically. In particular, recent proposals based on non-Gaussian inputs and Gaussian operations and measurements [50, 73, 173] fall clearly in the framework presented here — which then provides quantitative tools for their analysis.

After developing the general framework, we apply it to two tasks. First, we assess and compare the resourcefulness of various non-Gaussian states that have been theoretically proposed or even realized experimentally. In particular, we are going to see that the cubic phase state —a resource that unlocks universality in the context of CV measurement-based quantum computation— has a degree of resourcefulness that can be non-trivially boosted by squeezing operations. Also, we give evidences that photon-added and photon-subtracted states are at most as resourceful as a single-photon Fock state. Second, concerning state manipulation, we evaluate the efficiency of a set of Gaussian simple protocols that consume copies of non-Gaussian inputs to produce more resourceful outputs. These types of resource-concentration protocols are usually a critical point of other resource theories, such as for quantum communication and fault-tolerant DV quantum computation. Our results individuates optimal working points of these concentration protocols, and can thus be used to guide the development of new more efficient ones.

After the completion of the work presented here and in [10], we have become aware of work by R. Takagi and Q. Zhuang [272] covering very similar issues.

8.1 Resource theoretical framework

The ingredients of a resource theory are: free operations, free states, and resource states. The fundamental condition that links these elements is that the set of free states must be closed under the set of free operations —i.e. it must not be possible to obtain a resource state by applying only free operations. This restriction still leaves much freedom in the choice of both free operations and states, and the structure of the resource theory is dictated by this choice. One can choose the free operations and then consequently define free states as the maximal set generated by free operations acting on one fiducial state. Vice-versa, by fixing the set of free states, free operations can be considered as the maximal set that leaves the free states invariant. The freedom left by the abstract formulation is generally restricted by operational issues. Crucially, we are guided by practical considerations regarding the prompt availability of operations such as classical randomness and conditional measurements.

In this section, we introduce a resource theory based on two pragmatical considerations: first, we consider operationally relevant Gaussian transformations, including in particular those that involve conditioning on coarse-grained measurements; second, we consider convex free-state sets. These features set apart our framework from previous studies on the quantification and manipulation of non-Gaussian resources [104–106, 312].

8.1.1 Free operations

The set of free operations is our starting point for the construction of the resource theory. In general, there is a contrast between physically motivated sets of operations and other larger sets with better mathematical properties.

Physically motivated operations are those which, in a given context, can be assumed to be implementable without effort —for example, SLOCC operations in entanglement theory, or stabilizer operations in the resource theory of stabilizer computation. Unfortunately, these operations are usually hard to characterize and other sets of free operations, with better mathematical properties, are often introduced (maximal resource non-generating operations). Even though they do not generate any resource, some amount of resource is typically needed to practically implement them. As said, here we adopt an operational point of view, hence we are not going to deal with these maximal resource non-generating operations.

Ideal and operational Gaussian protocols

Here, we denote with $|\psi_G\rangle$ an arbitrary pure Gaussian state, with $\hat{U}_G$ a Gaussian unitary, and with $\mathcal{S}(\mathcal{H})$ the set of density operators on the Hilbert space $\mathcal{H}$ of an arbitrary (finite) number of bosonic modes. In the context of quantum optics a set of free operations with a strong operational motivation is given by *Gaussian protocols* (GPs), which we define as follows.

Definition 1. *A Gaussian protocol is any map from $\rho \in \mathcal{S}(\mathcal{H})$ to $\sigma \in \mathcal{S}(\mathcal{H}')$ composed of the following operations:*

1. *Gaussian unitaries:* $\rho \to \hat{U}_G \, \rho \, \hat{U}_G^\dagger$.
2. *Composition with pure Gaussian states:* $\rho \to \rho \otimes |\psi_G\rangle\langle\psi_G|$.
3. *Pure Gaussian measurements on subsystems:* $\rho \to Tr_S[\rho \, \mathbb{1} \otimes |\psi_G(\boldsymbol{\alpha})\rangle\langle\psi_G(\boldsymbol{\alpha})|] \, / \, p(\boldsymbol{\alpha}|\rho)$, *with probability density* $p(\boldsymbol{\alpha}|\rho) = Tr[\rho \, \mathbb{1} \otimes |\psi_G(\boldsymbol{\alpha})\rangle\langle\psi_G(\boldsymbol{\alpha})|]$ *where* $\boldsymbol{\alpha}$ *is a vector of continuous measurement outcomes in the real domain.*
4. *Partial trace on subsystems:* $\rho \to Tr_S[\rho]$.
5. *The above quantum operations conditioned on classical randomness or*
   (a) *single measurement outcomes (ideal case)*
   (b) *measurement outcomes falling into finite-size intervals (operational case).*

The above operations encompass what is routinely available in current experiments where CVs are manipulated at the quantum level. They include general quadratic interactions, the generation and control of a large number of bosonic systems, and efficient measurement strategies such as homodyne detection, which correspond to a projection on an infinitely squeezed and unnormalized Gaussian state $|\psi_G\rangle$. Actually, requirement *3.* could be restricted to homodyne detection only, since the projection on any Gaussian state can be obtained via Gaussian unitaries and homodyne detection [111]. In particular, in quantum optical setups, such Gaussian unitaries correspond to inline squeezing operations and passive linear optics circuits [36]. Notice that probabilistic operations are included, therefore a generic *probabilistic* GP Λ_{GP} is a trace non-increasing CP map. Physically, nondeterministic maps come from selecting particular states based on measurement outcomes; this operation cannot generate resource states from free states, not even probabilistically. However we are going to see that it is possible to use nondeterministic free operations to probabilistically concentrate the resource.

The requirements *1.-4.* above are standard in the context of non-Gaussianity quantification [104–106], whereas requirement *5.* needs an explanation. First and foremost, a reasonable request for a *quantum* resource theory is that *classical* randomness should not be regarded as a resource, therefore the inclusion of conditioning on classical randomness. In turn, as anticipated, the latter entails that set of GPs is *convex*. Second, GPs are the CV analogous of the stabilizer operations introduced in Ref. [286] but with some relevant differences due to the infinite dimensional setting. Since the outcomes of projective Gaussian measurements are continuous parameters, single outcomes are obtained with zero probability. Therefore the class of GPs satisfying property *5.a* (*ideal* GPs) contains operations that are unattainable practically; for this reason, in the applications of our resource theory, we mainly consider the subclass of GPs that satisfy condition *5.b* —which we dub *operational* GPs. This subclass is defined by the requirement that every output state must be obtained with finite probability, therefore every conditioning must be done on a finite-size interval of measurement outcomes. The major consequence of choosing operational GPs is that they exclude the possibility to define a resource theory on pure states only, since output states with non-zero probability must be mixed. We remark that this is a peculiar feature of the framework here introduced that is inherently linked to

infinite-dimensional systems, without analogue in the resource theories introduced so far in DV settings.

To conclude this part, we stress again that, from an operational point of view, it is not useful to enlarge the set of GPs, since any operation "easy" to implement in the lab is already included. Not surprisingly however, these physically meaningful free operations are hard to characterize mathematically —similarly to what occurs for other resource theories.

8.1.2 Free states

We consider two classes of free states, both satisfying the standard requirements [34] —in particular, both being closed with respect to GPs. The first class is the most natural choice, and it is given by the maximal set of states that can be generated via GPs —namely, the Gaussian *convex* hull, defined as

$$\mathcal{G} = \left\{ \rho \in \mathcal{S}(\mathcal{H}) \,|\, \rho = \int \mathrm{d}\boldsymbol{\lambda}\, p(\boldsymbol{\lambda}) |\psi_G(\boldsymbol{\lambda})\rangle\langle\psi_G(\boldsymbol{\lambda})| \right\}, \tag{8.1}$$

where $p(\boldsymbol{\lambda})$ is an arbitrary probability distribution. We remark that $\boldsymbol{\lambda}$ in Eq. (8.1) represents the vector of $2n^2 + 3n$ real parameters needed to parametrize an arbitrary n-mode pure Gaussian state. We dub continuous variable quantum states not in the Gaussian convex hull $\mathcal{G}$ as *quantum non-Gaussian* (QnG). Therefore, the theoretical framework derived considering set $\mathcal{G}$ is dubbed the *resource theory of quantum-non-Gaussianity*. We recall that witnesses of QnG states have previously been introduced [85, 103, 126, 138, 149, 216], albeit outside of a resource theoretical context.

Alternatively, one can define the free states as those with a positive Wigner function:

$$\mathcal{W}_+ = \left\{ \rho \in \mathcal{S}(\mathcal{H}) \,|\, W_\rho(\boldsymbol{r}) \geq 0 \right\}, \tag{8.2}$$

where $W_\rho \equiv \mathcal{W}[\rho]$ is the Wigner function of the state ρ; this set is also convex and it is a proper superset of $\mathcal{G}$, i.e. $\mathcal{G} \subset \mathcal{W}_+$. As per the Hudson theorem [136, 263], these two sets coincide when restricted to pure states. We dub continuous variable quantum states with a non-positive Wigner function (states not in the set $\mathcal{W}_+$) as *Wigner negative* (WN). Therefore, the theoretical framework derived considering $\mathcal{W}_+$ is referred to as the *resource theory of Wigner negativity*. We recall that, from an operational point of view, a positive Wigner function is a sufficient condition to have a quantum system that can be efficiently simulated by classical algorithms [185, 226, 239, 287].

As already mentioned, not all Wigner-positive states can be generated using GPs. In this sense, the choice of $\mathcal{W}_+$ as free states of the theory is less natural with respect to choosing $\mathcal{G}$. This is still a valid choice, in the same sense that, for the entanglement resource theory, it is a valid choice to consider the set of states with positive partial transpose. QnG states with positive Wigner function are *bounded* resources: despite the fact that they cannot be generated using GPs, no other resource (*free* resource) can be extracted from them using GPs only —not even when an arbitrary large supply of them is available.

The definition of the set $\mathcal{G}$ allows to specify some additional considerations regarding GPs. An arbitrary GP can be extended to a *deterministic* (trace-preserving) GP Λ_{DGP} by

considering all the possible outcomes. A deterministic GP can be characterized in terms of its free Kraus operators; free means that the trace-decreasing map given by a single Kraus operator is a GP itself. By considering Kraus operators corresponding to all the continuous outcomes of Gaussian measurements, we can write $\Lambda_{\rm DGP}(\rho) = \int {\rm d}\boldsymbol{\lambda} K_{\boldsymbol{\lambda}} \rho K_{\boldsymbol{\lambda}}^\dagger$, where $K_{\boldsymbol{\lambda}} \mathcal{G} K_{\boldsymbol{\lambda}}^\dagger \subset \mathcal{G}$ (disregarding normalization). A different free Kraus representation of $\Lambda_{\rm DGP}$ can be obtained by coarse-graining measurement outcomes, $\Lambda_{\rm DGP}(\rho) = \sum_i K_i \rho K_i^\dagger$, with where $K_i \mathcal{G} K_i^\dagger \subset \mathcal{G}$; in this case every Kraus operator corresponds to an operational GP, *i.e.* it gives an output state with finite probability.

Absence of maximally resourceful states

A relevant observation that can be made at this stage is that no maximally resourceful states exist in the present resource theory —a result that is at odds with the most common resource theories, including entanglement. Namely, there is no resource state that can be transformed via GPs into any other state, in particular any other pure state.

For operational GPs, this is an immediate consequence of the fact that the output states are either mixed (when measurements are involved) or they are the output of a Gaussian unitary operation on the given state. In the latter case a parameter-counting argument immediately proves the claim since, on one hand, Gaussian unitaries on a finite number n of bosonic systems are characterised by a finite number of parameters (namely, the dimension of the affine symplectic group $\mathrm{ISp}(2n, \mathbb{R})$: $2n^2 + 3n$), whereas, on the other hand, a generic pure CV state cannot be specified by a finite number of parameters, due to the infinite dimension of the Hilbert space. A slightly refined argument is valid also for the case of ideal GPs. Again, it is sufficient to consider the case of pure output states. In fact, any ideal GP with pure outputs is an element of the set of (non necessarily positive) linear bounded superoperators Φ that send the set of Gaussian states into itself. These maps Φ have been studied in details in Ref. [65], where it is proven that they are characterised by a finite number of parameters. Therefore, again a parameter-counting argument proves the claim.

The absence of a maximally resourceful state implies relevant consequences that are peculiar to the present resource theory. First, regarding resource quantification, there exist no natural unit for the resource at hand to which all measures can be normalized. Second, regarding resource manipulation, there exist no natural target for resource distillation protocols, nor a natural starting state for resource dilution.

Despite this, notice that there exist at least one class of states that can play the role of maximally resourceful states, the so-called cubic-phase states [115] (see below). It is in fact known that, provided that an arbitrary large supply of these states can be consumed, any state can be generated via ideal GPs [191] (as recalled, magic states play an analogous role for DV stabilizer protocols). In Sec. 8.3.1 we thus consider cubic-phase states more closely. A similar result is suggested to hold true also for Fock states [109].

8.1.3 Monotones

Once the sets of free operations and states are chosen, one can indeed try to quantify a resource. In general, there is no unique way to quantify a resource and different monotones

are usually connected to the performance of different tasks. Moreover, monotones can be used as a tool to assess the feasibility of resource conversion. In the best case scenario, a complete set of monotones can give necessary and sufficient conditions for the conversion between resource states, as in [5].

We can now define both Quantum-non-Gaussianity and Wigner Negativity monotones.

Definition 2. *A Quantum-non-Gaussianity (resp. Wigner Negativity) monotone is a functional from the set of quantum states to non-negative real numbers $\mathcal{M} : \mathcal{S}(\mathcal{H}) \to [0, \infty)$ which satisfies the following properties*

1. $\mathcal{M}(\rho) = 0 \quad \forall \rho \in \mathcal{G}$ *(resp.* $\mathcal{W}_+$*).*
2. *(Monotonicity under deterministic Gaussian protocols)*
   For any trace-preserving GP Λ_{DGP} the monotone must not increase: $\mathcal{M}(\rho) \geq \mathcal{M}(\Lambda_{DGP}(\rho))$.
3. *(Monotonicity on average under probabilistic Gaussian protocols)*
   Given a trace-preserving GP Λ_{DGP} we can express its action in terms of free Kraus operators, we require that the monotone must not increase on average:
   (a) *Ideal case:* $\Lambda_{DGP}(\rho) = \int \mathrm{d}\boldsymbol{\lambda} p(\boldsymbol{\lambda}|\rho)\sigma_{\boldsymbol{\lambda}}$*, where* $\sigma_{\boldsymbol{\lambda}} = \frac{1}{p(\boldsymbol{\lambda}|\rho)} K_{\boldsymbol{\lambda}} \rho K_{\boldsymbol{\lambda}}^\dagger$*. We require that* $\mathcal{M}(\rho) \geq \int \mathrm{d}\boldsymbol{\lambda} p(\boldsymbol{\lambda}|\rho)\mathcal{M}(\sigma_{\boldsymbol{\lambda}})$.
   (b) *Operational case:* $\Lambda_{DGP}(\rho) = \sum_i p_{i|\rho}\sigma_i$*, where* $\sigma_i = \frac{1}{p_{i|\rho}} K_i \rho K_i^\dagger$*. We require that* $\mathcal{M}(\rho) \geq \sum_i p_{i|\rho}\mathcal{M}(\sigma_i)$

Some additional properties that a monotone can enjoy are *faithfulness*: $\mathcal{M}(\rho) > 0 \iff \rho \notin \mathcal{G}$ *(resp.* $\mathcal{W}_+$*)*, *convexity*: $\mathcal{M}(\int \mathrm{d}\nu p(\nu)\rho_\nu) \leq \int \mathrm{d}\nu p(\nu)\mathcal{M}(\rho_\nu)$ for a generic probability distribution $p(\nu)$ and *additivity*: $\mathcal{M}(\rho \otimes \sigma) = \mathcal{M}(\rho) + \mathcal{M}(\sigma)$[1]. If the monotone is convex, monotonicity on average directly implies monotonicity under deterministic operations (*3a* $\implies$ *2*), moreover convexity also gives operational average inequalities from the ideal ones (*3a* $\implies$ *3b*).

Monotones can be used to give bounds on the efficiency of interconversion between resource states. Suppose that Λ is a free operation which converts resource states in a probabilistic manner: it maps k copies of ρ to m copies of a target state σ, i.e. $\Lambda\left(\rho^{\otimes k}\right) = \sigma^{\otimes m}$ with probability p. By virtue of the monotonicity on average (*3b*) we can write

$$\mathcal{M}\left(\rho^{\otimes k}\right) \geq p\mathcal{M}\left(\sigma^{\otimes m}\right), \tag{8.3}$$

where we considered an operational GP to get a finite probability p and we discarded the other conditional states in the sum.

Moreover, additive monotones allow us to express the inequality in terms single letter quantities

$$k\mathcal{M}(\rho) \geq p\, m\mathcal{M}(\sigma). \tag{8.4}$$

[1] In the context of entanglement theory this property is called strong additivity, while weak additivity only requires $\mathcal{M}(\rho^{\otimes n}) = n\mathcal{M}(\rho)$.

This inequality also gives a lower bound for the average conversion ratio [286]. On average we will need to run the probabilistic operation $1/p$ times to obtain a successful outcome, therefore the average number n of copies needed to extract m target states is $\mathbb{E}[n] = k/p$. We can thus rewrite (8.4) as

$$\mathbb{E}[n] = \frac{k}{p} \geq m\frac{\mathcal{M}(\sigma)}{\mathcal{M}(\rho)}, \tag{8.5}$$

i.e., the average number of copies of the input state is lower bounded by the ratio of the monotones times the number of output copies of the protocol. This means that in order to concentrate the resource (*i.e.*, $\mathcal{M}(\sigma)/\mathcal{M}(\rho) > 1$), we need an average conversion ratio smaller than unity $m/\mathbb{E}[n] < 1$.

If free operations converting two resource states in both directions exist, we must have $\mathcal{M}(\rho^{\otimes k}) = \mathcal{M}(\sigma^{\otimes m})$; this is trivially true if the conversion is achieved with a free unitary transformation. It is usually difficult to exactly convert between resource states using a finite number of copies, therefore it is customary to consider conversions in the asymptotic limit of infinite copies. However, we are not going to treat the asymptotic resource theory of QnG in the present work.

Faithful quantum non-Gaussianity monotones

Before going on to introduce our main monotone in Sec. 8.2, which is a non-faithful monotone, we want to mention here two possible ways to define *faithful* QnG monotones.

The non-Gaussianity measure δ introduced in Sec.1.4.4, which we can also call relative entropy of non-Gaussianity, can be considered as a monotone for the resource theory non-Gaussianity, where the set of free states is the non-convex set of Gaussian states. For this reason the relative entropy of non-Gaussianity can be arbitrarily increased by GPs. However, we believe it should be possible to build a QnG monotone by extending this measure to mixed states with a convex roof construction, i.e.

$$\delta_{\mathrm{CR}}[\rho] = \inf_{p_i, |\psi_i\rangle} \sum_i p_i \delta[|\psi_i\rangle] \tag{8.6}$$

where $\rho = \sum_i p_i |\psi_i\rangle\langle\psi_i|$; i can also represent a continuous value, in which case p_i becomes a distribution and the sum is replaced by an integral. The functional δ_{CR} is convex by construction and property *1* and *2* of Definition 2 can easily be proven. We have not been able to prove property *3a* (property *3b* follows by convexity), however we performed some preliminary numerical checks and we conjecture property *3a* to be true.[2]

A second approach to introduce faithful monotones could be to connect the resource theory of quantum non-Gaussianity to the resource theory of coherence; something in this spirit has been proposed for the DV resource theory of magic [203]. For CV, the resource theory of coherence has been generalized to the coherent state basis through a limiting procedure [274]; the resulting coherence monotone is also a monotone for the resource theory of linear optics, i.e. passive Gaussian transformations. This can be interpreted also

[2] After the completion of the work presented in this chapter, a preprint where this conjecture has apparently been solved has appeared [224].

as a resource theory of *nonclassicality* for CV systems, where nonclassical states as those with a negative Glauber-Sudarshan P-function, see Sec. 1.4.4. Remarkably, this resource theory has recently been studied in detail and linked to a metrological interpretation [161, 300]. We stress that this framework is entirely different from ours, since in our resource theory squeezing is assumed to be free.

For our purposes it might be possible to take similar steps and define a resource theory of superpositions of pure Gaussian states. An viable option could be to generalize results from [276], where a general resource theory of superposition of arbitrary non-orthogonal states is presented, for finite dimensions. We leave such questions open for future investigations.

8.2 A computable monotone: continuous-variable mana

Negativity of the Wigner function has long been recognized as an important quantum feature and in particular the volume of the negative part has been introduced as a nonclassicality quantifier (see Sec. 1.4.4). Here we use it to define a resource monotone.

In [286] a computable and additive magic monotone based on the negative values of the discrete Wigner function, dubbed *mana*, was introduced. We call the CV counterpart *CV mana*[3]; it is defined as (all the logarithms in the following are taken to be in base 2 (we measure quantities in bits)

$$\mathrm{W}(\rho) = \log\left(\int \mathrm{d}\boldsymbol{r}\, |W_\rho(\boldsymbol{r})|\right), \tag{8.7}$$

where the integral runs over the whole phase-space $\mathbb{R}^{2n}$, n is the number of modes and $W_\rho(\boldsymbol{r}) \equiv \mathcal{W}[\rho](\boldsymbol{r})$ is the Wigner function of the state ρ. In the next section we explicitly show that this monotone satisfies all the required properties even if it is not convex.

Clearly, the CV mana is a faithful monotone for the resource theory of Wigner Negativity but not for Quantum-non-Gaussianity. This is akin to what happens in entanglement theory for the log-negativity of entanglement [235, 311], depending on whether one considers separable or positive partial transpose states as free states.

The CV mana is an additive monotone, since the Wigner function of separable states can be factorized. This means that the bound (8.5) is valid and we can use the ratio between logarithmic Wigner negativities to lower bound the average number of copies of an input resource state to obtain a certain number of copies of the target state using a probabilistic Gaussian protocol. We remark that this result does not say anything about the actual existence of such protocols.

Similarly to the DV case we can prove that the CV mana is essentially the unique measure which depends on the negative values of the Wigner function, under the assumption that the position of these "negative patches" in phase space do not affect such a measure. The proof follows the same idea of the DV case presented in [286] and lately extended to coherence and entanglement [311].

[3]The manuscript where these results were presented has been accepted for publication, but this monotone is renamed *Wigner logarithmic negativity* (WLN) in the final version. In this Thesis we retain the original name.

As a final remark, notice that the CV mana is *computable* in the sense that its value can usually be assessed by numerical integration. However, in general it is not possible to obtain closed-form expressions, since the analytical integration of the absolute value of a function requires finding the zeros of such function.

8.2.1 Proofs about CV mana

We start by first considering a monotone based the integral of the absolute value of the Wigner function, called Wigner negativity:

$$\mathcal{N}[\rho] = \int \mathrm{d}\boldsymbol{r} |W_\rho(\boldsymbol{r})| - 1\,, \tag{8.8}$$

(this is twice the volume of the negative part of the Wigner function). After proving the properties of this monotone it is easy to generalized them to CV mana.

Wigner negativity

The Wigner negativity (8.8) trivially satisfies property 1 of Def. 2 and in the following we prove that it also satisfies all the properties implied by property 3. The constant factor -1 does not affect the proofs, it is only needed to make the monotone take the value zero on states with a positive Wigner, so we just consider the integral of the Wigner function in the following statements.

1. *Invariance under Gaussian unitaries*

$$\mathcal{N}[\rho] = \mathcal{N}\left[\hat{U}_G \rho \hat{U}_G^\dagger\right] \tag{8.9}$$

   This directly follows from the definition of Wigner function (1.119) by changing the integration variables, since $\det S = 1$.

2. *Invariance under composition with Gaussian states*

$$\mathcal{N}[\rho \otimes \rho_G] = \mathcal{N}[\rho] \tag{8.10}$$

   This property directly follows from the fact that the Wigner function of a tensor product is the product of Wigner functions, see Eq. (1.113), and from the fact the Gaussian states have Gaussian (and thus positive) Wigner functions.

3. *Non-increasing on average under Gaussian measurements*

$$\int \mathrm{d}\boldsymbol{\lambda} p(\boldsymbol{\lambda}) \mathcal{N}[\rho_{\boldsymbol{\lambda}}] \leq \mathcal{N}[\rho] \tag{8.11}$$

   We consider a Gaussian POVM $\int \mathrm{d}\boldsymbol{\lambda} \hat{\Pi}_{\boldsymbol{\lambda}} = \mathbb{1}$, where $\mathcal{W}[\hat{\Pi}_\lambda](\boldsymbol{r})$ are Gaussian functions. Given an initial state ρ we have the unnormalized post-measurement states $\sigma_{\boldsymbol{\lambda}} = \mathrm{Tr}_B\left[\rho \hat{\Pi}_{\boldsymbol{\lambda}}\right]$, the probability density $p(\boldsymbol{\lambda}) = \mathrm{Tr}\left[\rho \hat{\Pi}_{\boldsymbol{\lambda}}\right]$ and the normalized post measurement states $\rho_{\boldsymbol{\lambda}} = \sigma_{\boldsymbol{\lambda}} / p(\boldsymbol{\lambda})$.

Since the Wigner transform is a linear functional and probability density are positive we can write

$$\left|\mathcal{W}\left[\int \mathrm{d}\boldsymbol{\lambda} p(\boldsymbol{\lambda})\rho_{\boldsymbol{\lambda}}\right](\boldsymbol{r})\right| = \left|\int \mathrm{d}\boldsymbol{\lambda} p(\boldsymbol{\lambda})\mathcal{W}[\rho_{\boldsymbol{\lambda}}](\boldsymbol{r})\right|, \tag{8.12}$$

and using linearity again we have that

$$\left|\int \mathrm{d}\boldsymbol{\lambda} p(\boldsymbol{\lambda})\mathcal{W}[\rho_{\boldsymbol{\lambda}}](\boldsymbol{r})\right| = \left|\int \mathrm{d}\boldsymbol{\lambda}\mathcal{W}[\sigma_{\boldsymbol{\lambda}}](\boldsymbol{r})\right|, \tag{8.13}$$

where $\sigma_{\boldsymbol{\lambda}}$ are unnormalized post measurement states, for which the Wigner function is given by (1.112). We can thus write

$$\begin{aligned}\left|\int \mathrm{d}\boldsymbol{\lambda}\mathcal{W}[\sigma_{\boldsymbol{\lambda}}](\boldsymbol{r})\right| &\leq \int \mathrm{d}\boldsymbol{\lambda}|\mathcal{W}[\sigma_{\boldsymbol{\lambda}}](\boldsymbol{r})| = \int \mathrm{d}\boldsymbol{\lambda}\left|(2\pi)^{N'}\int \mathrm{d}\boldsymbol{r}'\mathcal{W}[\rho](\boldsymbol{r},\boldsymbol{r}')\mathcal{W}[\Pi_{\boldsymbol{\lambda}}](\boldsymbol{r}')\right| \\ &\leq \int \mathrm{d}\boldsymbol{\lambda}(2\pi)^{N'}\int \mathrm{d}\boldsymbol{r}'|\mathcal{W}[\rho](\boldsymbol{r},\boldsymbol{r}')\mathcal{W}[\Pi_{\boldsymbol{\lambda}}](\boldsymbol{r}')| = \int \mathrm{d}\boldsymbol{r}'|\mathcal{W}[\rho](\boldsymbol{r},\boldsymbol{r}')|,\end{aligned} \tag{8.14}$$

where we used the integral triangle inequality and the POVM resolution of the identity for the Wigner functions (1.109).

Integrating both sides of this inequality w.r.t. $\boldsymbol{r}$ we get to the sought result:

$$\mathcal{N}\left[\int \mathrm{d}\boldsymbol{\lambda} p(\boldsymbol{\lambda})\rho_{\boldsymbol{\lambda}}\right] \leq \int \mathrm{d}\boldsymbol{\lambda} p(\boldsymbol{\lambda})\mathcal{N}[\rho_{\boldsymbol{\lambda}}] \leq \mathcal{N}[\rho], \tag{8.15}$$

where we also proved monotonicity under trace preserving operations. By taking the appropriate limit these results hold also for homodyne measurements, where $\mathcal{W}[\Pi_{\boldsymbol{\lambda}}](\boldsymbol{r}')$ are proportional to Dirac deltas functions.

4. *Non-increasing under partial trace*

$$\mathcal{N}[\mathrm{Tr}_B\rho_{AB}] \leq \mathcal{N}[\rho_{AB}] \tag{8.16}$$

This property follows from the fact that the Wigner function of a partial trace the marginal of the Wigner function of the bipartite system (cf. Eq. (1.111)), using again the integral triangle inequality as in the previous proof.

5. *Convexity*

$$\mathcal{N}\left(\int \mathrm{d}\nu p(\nu)\rho_{\nu}\right) \leq \int \mathrm{d}\nu p(\nu)\mathcal{N}(\rho_{\nu}) \tag{8.17}$$

Trivially follows from the integral triangle inequality (that we have actually already used in the proof at point 3).

To have an operational Gaussian protocol, i.e. in order to have non-zero conditional probabilities, we need to consider a finite region of the outcome space Ω_i and not a single outcome. Formally this procedure amounts to a coarse-graining of the continuous

outcomes into subsets, thus defining a new POVM. The new effects for discrete outcomes are just obtained by integration $\Pi_i = \int_{\Omega_i} \mathrm{d}\boldsymbol{\lambda}\Pi_{\boldsymbol{\lambda}}$, where the outcome space is partitioned as $\Omega = \cup_i \Omega_i$. The Wigner function of such POVMs is thus a statistical mixture of the original Wigner functions; as a consequence, since the original functions are always positive, the same is true for the coarse grained ones. This implies that the previous proof can straight-forwardly extended to these coarse-grained POVMs. The same inequality for coarse grained POVMs can be obtained by virtue of the convexity of $\mathcal{N}$.

Finally, we remark that the proofs discussed do not rely on the Gaussian character of states and POVM elements, but just on the positivity of their Wigner functions.

CV mana

The CV mana (8.7) can be defined in terms of the Wigner negativity (8.8) as

$$\mathsf{W}[\rho] = \log(\mathcal{N}[\rho] + 1). \tag{8.18}$$

Properties 1, 2 and 4 follow directly from the fact that $\log(x+1)$ is a monotonically increasing function of x.

For the mana the chain of inequalities (8.15) splits in two separate inequalities

$$\mathsf{W}\left[\int \mathrm{d}\boldsymbol{\lambda} p(\boldsymbol{\lambda})\rho_{\boldsymbol{\lambda}}\right] \leq \mathsf{W}[\rho] \tag{8.19}$$

$$\int \mathrm{d}\boldsymbol{\lambda} p(\boldsymbol{\lambda})\mathsf{W}[\rho_{\boldsymbol{\lambda}}] \leq \mathsf{W}[\rho]. \tag{8.20}$$

The the first inequality represents monotonicity under deterministic operations and follows from (8.15) and from the monotonicity of the logarithm. Inequality (8.20) represents monotonicity on average and it is guaranteed by Jensen's inequality

$$\int \mathrm{d}\boldsymbol{\lambda} p(\boldsymbol{\lambda}) \log(\mathcal{N}[\rho_{\boldsymbol{\lambda}}] + 1) \leq \log\left(1 + \int \mathrm{d}\boldsymbol{\lambda} p(\boldsymbol{\lambda})\mathcal{N}[\rho_{\boldsymbol{\lambda}}]\right), \tag{8.21}$$

which holds since the logarithm is a concave function. Notice that the same inequality is true also for the coarse grained case, since Jensen's inequality is valid both for discrete and continuous distributions.

Similarly to what happens in other resource theories, the logarithm makes this monotone additive for separable states $\mathsf{W}[\rho_1 \otimes \rho_2] = \mathsf{W}[\rho_1] + \mathsf{W}[\rho_2]$, but also breaks convexity. To have a convex monotone after the logarithm, the original monotone should be log-convex, $f(px + (1-p)y) \geq f(x)^p f(y)^{1-p}$, which is a stronger requirement than convexity. The lack of convexity is the reason why inequalities (8.19) and (8.20) are not chained as (8.15).

8.2.2 Uniqueness of negativity and mana

The argument given in [286] for the uniqueness of sum negativity can be adapted to CV, even though in this case we need to perform the limit to unphysical infinite energy states. We present the single mode case for simplicity, the argument can be easily generalized to multi-mode states.

We assume to have two states ρ and ρ' with the same negativity (and thus also the same mana) $\mathcal{N}[\rho] = \mathcal{N}[\rho']$; we also assume that $\mathcal{M}_N$ is a generic monotone that depends only on the negative values of the Wigner function, but not on their position in phase space. We define a function $f_\rho(x,y) = |W_\rho(x,y)|$ when $W_\rho(x,p)$ is negative and $f_\rho(x,y) = 0$ everywhere else. We note that $f_\rho(x,p)/\mathcal{N}[\rho]$ is a well defined probability distribution. If ρ and ρ' have negative values we build two ancillary states

$$\begin{aligned} \sigma &= \int \mathrm{d}x\mathrm{d}y f_\rho(x,y)|x\rangle\langle x| \otimes |y\rangle\langle y|, \\ \sigma' &= \int \mathrm{d}x\mathrm{d}y f_{\rho'}(x,y)|x\rangle\langle x| \otimes |y\rangle\langle y|, \end{aligned} \tag{8.22}$$

where $|x\rangle$ are unnormalized position eigenstates, which are the infinite squeezing limit of Gaussian position squeezed states. Therefore we have

$$\mathcal{M}_N[\rho] = \mathcal{M}_N\left[\rho \otimes \sigma'\right] = \mathcal{M}_N\left[\rho' \otimes \sigma\right] = \mathcal{M}_N\left[\rho'\right], \tag{8.23}$$

the two outer equalities are due to the fact that σ and σ' are the limit of a sequence of states in $\mathcal{G}$. The central inequality is due to the fact that the monotone $\mathcal{M}_N$ depends only on the negative value of the values of the Wigner function and not on their position. Note that the two Wigner functions have the same negative values, since the Wigner function of σ and σ' correspond exactly to the probability distribution function $f_\rho/\mathcal{N}[\rho]$ and $f_{\rho'}/\mathcal{N}[\rho']$, since the Wigner functions of $|x\rangle$ is a one dimensional δ function. Equality (8.23) implies that $\mathcal{M}_N$ is a function of $\mathcal{N}$. Suppose that $\mathcal{N}[\rho'] \geq \mathcal{N}[\rho]$, we can always find a new state σ such that $\mathcal{M}_N[\rho'] = \mathcal{M}_N[\rho \otimes \sigma] \geq \mathcal{M}_N[\rho]$, where the last inequalities is due to the weak monotonicity property of monotones. This means that $\mathcal{M}_N$ is a monotonically increasing function of $\mathcal{N}$.

Furthermore, if we require that $\mathcal{M}_N$ is additive, i.e. $\mathcal{M}_N[\rho^{\otimes n}] = n\mathcal{M}_N[\rho]$ we can also follow the proof given in [311] to show that $\mathcal{M}_N$ must correspond to the mana W multiplied by an arbitrary positive constant.

8.3 Resource analysis of classes of pure states

Given its relevance in the general framework just introduced, now we use the CV mana to assess the resourcefulness of some paradigmatic examples of non-Gaussian states. In particular, besides the aforementioned class of cubic phase states, we focus also on states that are of relevance in quantum optical experiments: photon-added, photon-subtracted, and cat states.

In addition to the CV mana, given that we consider pure states only, we also calculate the non-Gaussianity, see Eq. (1.157). As said, the latter is still not proved to be a monotone in our framework, however the comparison between the two quantities is particularly fruitful to single out the properties of the states considered.

8.3.1 Cubic phase state

As recalled, a particularly important non-Gaussian continuous variable state is the so called cubic phase state [115]. For finite squeezing it is defined as

$$|\gamma, r\rangle = \exp\left[i\gamma\hat{x}^3\right]\hat{S}(r)|0\rangle, \tag{8.24}$$

where the squeezing operator $\hat{S}(r) = \exp\left[-\frac{i}{2}r(\hat{x}\hat{p}+\hat{p}\hat{x})\right]$ for $r > 1$ squeezes in momentum and anti-squeezes in position — *i.e.*, the Heisenberg evolution of the position operator is $\hat{S}(r)^\dagger \hat{x}\hat{S}(r) = e^r\hat{x}$. This implies that a squeezing unitary can be used to change the value of γ of a cubic phase *gate* [115]:

$$\hat{S}(r)^\dagger \exp\left[i\gamma\hat{x}^3\right]\hat{S}(r) = \exp\left[i\gamma e^{3r}\hat{x}^3\right]. \tag{8.25}$$

This identity shows that we can "consume" the initial squeezing to enhance the nonlinear parameter by anti-squeezing the state (a Gaussian unitary)

$$|e^{3r'}\gamma, r\rangle = S(-r')|\gamma, r+r'\rangle. \tag{8.26}$$

This means that every monotone must be a function of the effective parameter $e^{3r}\gamma$, since it has to be invariant under Gaussian unitaries:

$$\mathcal{M}(|\gamma, r\rangle) = \mathcal{M}\left(|e^{3r}\gamma, 0\rangle\right) = f\left(e^{3r}\gamma\right). \tag{8.27}$$

As a consequence the contour lines of any monotone on the plane (r, γ) are of the form $\gamma \propto e^{-3r}$. In particular, Eq. (8.27) shows that the resourcefulness of the cubic phase state can be boosted by increasing the initial squeezing.

We remark that in the case of infinite squeezing $r \to \infty$ Eq. (8.26) formally means that we can freely interconvert between ideal cubic phase states with simple Gaussian operations. This is consistent as long we assume to be in the degenerate case where the monotone assumes an infinite value for every cubic phase state, irregardless of the value of γ.

For a pure cubic phase state we can also compute the relative entropy of non-Gaussianity (1.157), which is again invariant for Gaussian unitaries

$$\delta[|\gamma, r\rangle] = h\left(\sqrt{1+9(e^{3r}\gamma)^2}\right), \tag{8.28}$$

where $h(x) = \left(\frac{x+1}{2}\right)\log\left(\frac{x+1}{2}\right) - \left(\frac{x-1}{2}\right)\log\left(\frac{x-1}{2}\right)$; we can explicitly see the dependence on the combination $e^{3r}\gamma$. This measure goes to infinity as $\log\left(e^{3r}\gamma\right)$ for $e^{3r}\gamma \to \infty$, as expected.

We are working with pure states and therefore the Hudson theorem implies that if one measure is zero also the other has to be zero. Furthermore, in this and in the following examples we observe that, as long as both the mana W and the non-Gaussianity δ are functions of a single effective parameter, the two measures are monotonic and thus display the same qualitative behaviour. We remark that the same fact has also been observed

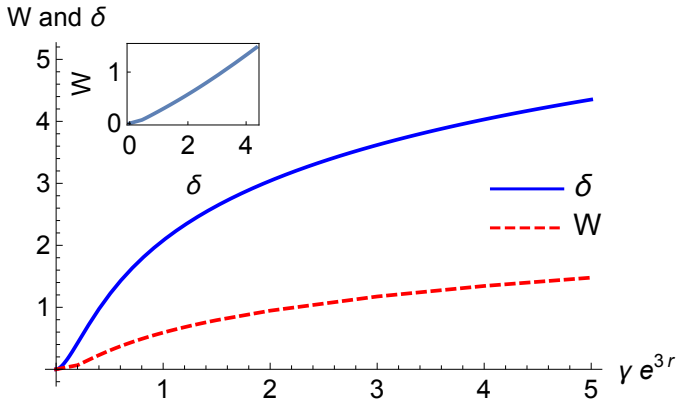

Figure 8.1: Non-Gaussianity δ (solid blue) and mana W (dashed red) of the cubic phase state as a function of their unique parameter γe^{3r}. Inset: parametric plot of the two quantities.

for ground states of anharmonic potentials [9]. Given this heuristic argument, we also expect the mana of the cubic phase state[4] to be a monotonically increasing function of its effective parameter, with a behaviour similar to the measure δ; this is indeed what we observe from a numerical evaluation, see Fig. 8.1. In particular we expect it to diverge like the non-Gaussianity monotone in the limit of infinite squeezing or nonlinearity, in accordance to the intuition from Eq. (8.26).

8.3.2 Photon subtracted/added Gaussian states

The single-mode photon subtracted and photon added Gaussian states are respectively defined as $|\alpha, r\rangle_{\mathsf{sub}} = N_{\mathsf{sub}}^{-1/2}\, \hat{a} D(\alpha) S(r)|0\rangle$ and $|\alpha, r\rangle_{\mathsf{add}} = N_{\mathsf{add}}^{-1/2}\, \hat{a}^\dagger D(\alpha) S(r)|0\rangle$, where $N_{\mathsf{sub}} = \sinh^2 r + |\alpha|^2$ and $N_{\mathsf{add}} = 1 + \sinh^2 r + |\alpha|^2$ are normalization constants. These states have been realized experimentally [18, 19, 25, 205, 212, 213] and they have recently been suggested as non-Gaussian ancillas to implement arbitrary non-Gaussian operations [21]. Multimode photon subtracted and added Gaussian states have also shown a non-trivial interplay with entanglement [289].

We can employ again the invariance under Gaussian operations to get

$$\mathcal{M}[|\alpha, r\rangle_{\mathsf{sub}}] = \mathcal{M}\left[N_{\mathsf{sub}}^{-1/2}\left(e^{i\psi}\sinh|r||1\rangle + \alpha|0\rangle\right)\right] \tag{8.29}$$

$$\mathcal{M}[|\alpha, r\rangle_{\mathsf{add}}] = \mathcal{M}\left[N_{\mathsf{add}}^{-1/2}(\cosh|r||1\rangle + \alpha^*|0\rangle)\right], \tag{8.30}$$

where $r = |r|e^{i\psi}$ and $\mathcal{M}$ represents a generic monotone.

The results above suggest that the maximum amount of resource reachable by these two classes of states is that of a single photon state $|1\rangle$, a result in agreement with the physical intuition about the preparation of these states. Photon subtracted states can be prepared by sending the input state in a high-trasmissivity beam-splitter and then

[4] To compute the mana we have used the analytical Wigner function of the cubic phase state [133], but we do not report the expression here.

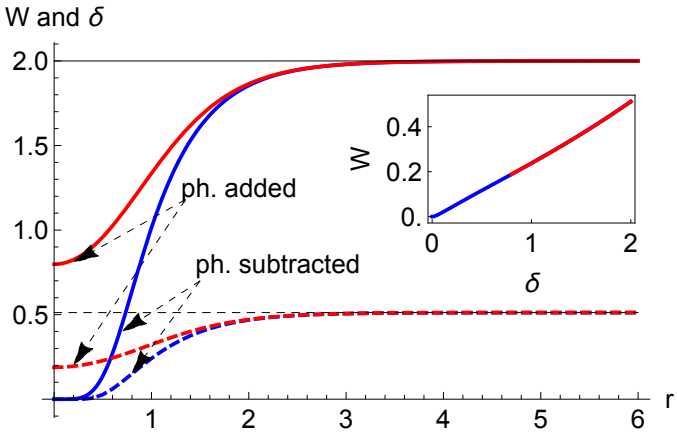

Figure 8.2: Non-Gaussianity δ (full lines) and mana W (dashed lines) of photon subtracted (blue, lower curves) and photon added (red, upper curves) states as a function of r for fixed $|\alpha| = 1$. The horizontal black lines represent the value of the two figure of merit for the state $|1\rangle$. Inset: parametric plot of the two quantities. Since a photon-added state is non-Gaussian for any value of r, both W and δ never go to zero. In the region $\delta \gtrapprox 0.8$ the two parametric curves perfectly overlap.

conditioning on a single photon detection on an output mode. On the other hand, photon addition can be implemented as beam splitting the input state with a single photon state, and then conditioning the output on the detection of no photons. This resource theoretical analysis shows that measurements and ancillary states are indeed equivalent resources in this case, as clearly confirmed by the plot in Fig. 8.2. We remark that while these schemes are appropriate for single mode states, more complicated schemes might be needed for multimode states, see e.g. [24, 237] for photon subtraction.

We can compute the non-Gaussianity (1.157) for these pure states

$$\delta[|\alpha, r\rangle_{\mathsf{sub}}] = h\left(\sqrt{\frac{8}{\left(|\alpha|^2 \mathrm{csch}^2(r)+1\right)^3}+1}\right) \tag{8.31}$$

$$\delta[|\alpha, r\rangle_{\mathsf{add}}] = h\left(\sqrt{\frac{8}{\left(|\alpha|^2 \mathrm{sech}^2(r)+1\right)^3}+1}\right); \tag{8.32}$$

once again this is a function of a single parameter in both cases. In Fig. 8.2 we also observe that non-Gaussianity and mana have the same qualitative behaviour.

8.3.3 Cat states

We now want to complement the intuition we gained with the previous examples on a different class of non-Gaussian states: Schrödinger cat states. We are going to see that the two figures of merit represented by Non-Gaussianity δ and mana W can also display a qualitatively different behaviour.

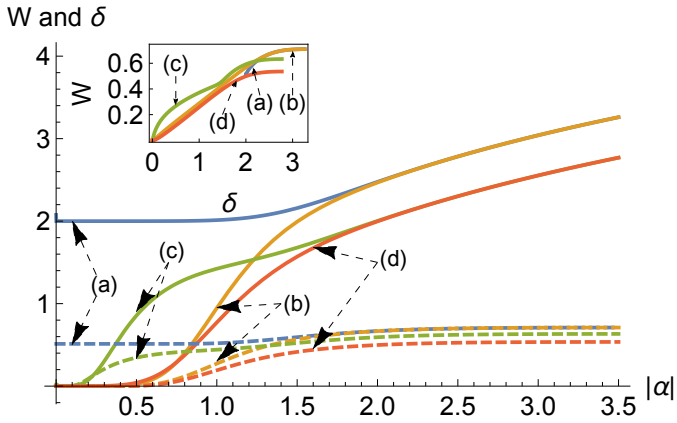

Figure 8.3: Non-Gaussianity δ (full lines) and mana W (dashed lines) of cat states for different values of the parameters as a function of $|\alpha|$. The values of the parameters are (a): $\phi = \pi/4, \theta = \pi$, (b): $\phi = \pi/4, \theta = 0$, (c): $\phi = \pi/8, \theta = \pi$ and (d): $\phi = \pi/8, \theta = 0$. Inset: parametric plot of the same quantities.

We define a cat state as the superposition of two coherent states $|\alpha\rangle$ and $|-\alpha\rangle$ and we keep both the amplitudes and the relative phase as parameters, as follows

$$|\psi(\alpha,\phi,\theta)\rangle = \frac{1}{\sqrt{K}}\Big(\cos\phi|\alpha\rangle + \sin\phi e^{i\theta}|-\alpha\rangle\Big), \tag{8.33}$$

where K is a normalization constant

$$K = 1 + \sin(2\phi)\cos\theta e^{-2|\alpha|^2}. \tag{8.34}$$

The non-Gaussianity $\delta[|\psi(\alpha,\phi,\theta)\rangle]$ is not a function of the absolute value $|\alpha|$ only, but it depends on both angles; we do not report here the cumbersome analytical expression of this quantity. A comparison between the two figures of merit shows that their behaviour is qualitatively the same as a function of ϕ and θ, while they show a remarkable difference as functions of $|\alpha|$. As a matter of fact, while the mana is known to saturate to a finite value for increasing separation between the two Gaussian peaks of the Wigner function [151], the non-Gaussianity diverges, i.e. $\lim_{|\alpha|\to\infty}\delta[|\psi(\alpha,\phi,\theta)\rangle] = \infty$.

This is shown in Fig. 8.3, where we present the two quantities for a choice of parameters ϕ and θ as a function of $|\alpha|$. We stress that even though the two quantities have a different behaviour, they still remain monotonically increasing functions of one another (but not *strictly* monotonic). It is reasonable to ascribe this difference to the fact that non-Gaussianity is sensitive to the distance between the state in question and pure Gaussian states. Given the double-peaked structure of cat states such a distance is bounded to increase indefinitely for large energies. On the other hand the CV mana is clearly insensitive to this.

8.3.4 Comparison at fixed energy

We conclude this section by studying the behaviour of the monotones as a function of the mean number of bosonic excitations $\langle \hat{n} \rangle$, a standard resource in CV quantum information processing. In general there is no one to one relationship between mean energy and any QnG or WN monotone, therefore we consider the maximum value of the monotones for every fixed value of $\langle \hat{n} \rangle$.

For the cubic phase state the problem amounts to maximizing the parameter $e^{3r}\gamma$. We find that the mana of the cubic phase state is a monotonically increasing function of $\langle \hat{n} \rangle$ as intuitively expected. For photon subtracted and photon added Gaussian states the problem amounts to maximizing the probability of the $|1\rangle$ component in (8.29) and (8.30). When $\langle \hat{n} \rangle > 1$ the maximum value of both monotones is the same as for the state $|1\rangle$ and this is achieved for $\alpha = 0$. The photon-subtracted state can also have $\langle \hat{n} \rangle \leq 1$, in this case the maximal value for both monotones is equivalent to that of the state $\sqrt{1 - \langle \hat{n} \rangle}|0\rangle + \sqrt{\langle \hat{n} \rangle}|1\rangle$ [5]. For cat states we restrict to equal amplitudes of the two components, i.e. $\phi = \pi/4$. In this case, for $\langle \hat{n} \rangle > 1$ we have that $\theta = \pi$, i.e. the odd cat state, is always optimal. However, when $\langle \hat{n} \rangle < 1$ the state with $\theta = \pi$ does not exist and we need to numerically find the best angle θ for every value of $\langle \hat{n} \rangle$.

All these findings are summed up in Fig. 8.4, where we report an explicit comparison of the mana W as a function of $\langle \hat{n} \rangle$. We also show points corresponding to Fock states $|n\rangle$, which have an higher value of W than the classes of states we consider. In particular, for $\langle \hat{n} \rangle = 1$ photon subtracted/added Gaussian states and odd cat states reduce to the single photon Fock state $|1\rangle$.

We remark that the same qualitative analysis applies also to the non-Gaussianity δ; however, in this case it can be proven that Fock states have the maximum value of δ at fixed energy [104].

8.4 Negativity Concentration via passive Gaussian operations

We have already recalled that, given an arbitrarily large supply of cubic phase states, it is possible to generate any state via ideal GPs. It is therefore possible to increase the amount of quantum non-Gaussianity of a state, and in particular to distil CV mana. Given the role played by CV mana established by our framework, it is relevant to consider experimentally realistic settings that can concentrate the amount of CV mana via operational GPs. Specifically, taking inspiration from existing CV quantum state engineering protocols based on linear optics, we now want to study the task of concentrating the negativity of the Wigner function from many copies of an input state to a single output state. We know that when a state can be transformed to another via GPs, then the conversion rate is limited by the bound in Eq. (8.5), where we use the CV mana as monotone.

A more general framework which also makes use of single photon sources and general Gaussian measurements detection has been presented in [225] to implement arbitrary

[5] We remark that the maximum value of the monotones is achieved for a vanishing value of the parameters α and r and this corresponds to the limit of a vanishing probability of a successful photon subtraction, i.e. the normalization constant $N_{\text{sub}} \to 0$

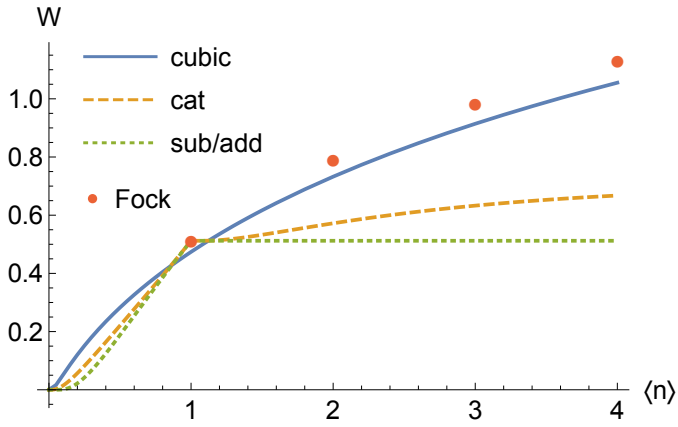

Figure 8.4: Maximal value of the mana as a function of the mean number of bosonic excitations for the considered classes of states, the solid light blue line represents the cubic phase state, the dashed orange line the class of cat states (with equal amplitude) and the dotted green line represents photon subtracted and added Gaussian states, the red dots represents Fock states.

nonlinear potentials. Some general calculations about states obtainable starting from Fock states by applying two-mode interactions and conditional operations based on homodyne post-selection can be found in [109].

8.4.1 Quantitative study of a negativity concentration protocol

Let us exploit the theoretical framework described in the previous section to analyse a quantum state engineering protocol based on beam splitter interaction. In what follows we consider the mana W defined in Eq. (8.7) as the resource monotone. Each probabilistic protocol is indeed a GP Λ that converts k copies of a resource state ρ, into m copies of a state σ, with a given probability p.

Since we focus on the "negativity concentration" properties of these protocols, we introduce two figures of merit. The first one corresponds to the resource gain of the protocol, and it is defined as the relative difference between the mana of the output state and the mana of the input state,

$$\epsilon[\Lambda] = \frac{\mathsf{W}(\sigma) - \mathsf{W}(\rho)}{\mathsf{W}(\rho)}. \tag{8.35}$$

The second figure of merit quantifies the efficiency of the protocol, and it is defined as

$$\eta[\Lambda] = p\,\frac{m\mathsf{W}(\sigma)}{k\mathsf{W}(\rho)} \leq 1\,, \tag{8.36}$$

whose maximum value is one, as a consequence of Eq. (8.4).

In particular, here we focus on a protocol that has been implemented experimentally as described in Refs. [77, 78]: a pair of identical Fock states $\rho = |n\rangle\langle n|$ is mixed at a

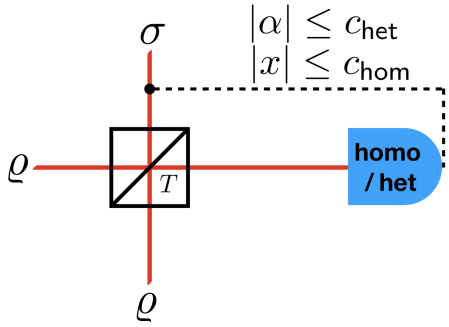

Figure 8.5: Schematic representation of the concentration protocol. The detector represents either an homodyne ("homo") with outcome x or an heterodyne one ("het") with outcomes $\alpha = |\alpha|e^{i\theta}$. The input states are two copies of ρ, while the output state σ is postselected according to the output values of the measurement.

beam-splitter with transmissivity T, and a homodyne detection of the quadrature $\hat{x}$ is performed on one of the two arms, see Fig. 8.5. We also study the case of heterodyne detection for comparison.

To gain intuition about this protocol, consider the output state of the beam splitter, which is of the form $\sum_{p=0}^{2n} f_p|p, 2n-p\rangle$. If we were able to condition on the detection of no photons we would obtain the state $|2n\rangle$, which in turn would imply the concentration of the resource. However, conditioning on the vacuum via Gaussian measurements occurs with zero probability and is therefore unfeasible. The actual protocol works instead conditioning on outcomes that belong to a finite interval around zero. This produces a POVM element which is very close to the ideal projection on the vacuum $|0\rangle\langle 0|$, but with non-zero probability and therefore feasible [77, 78].

In the case of heterodyne detection, the state on the other arm of the beam splitter is kept if the outcome of the measurement is in the range $0 < |\alpha| < c_{\mathsf{het}}$, while we average over the phase θ (note that this makes the POVM elements diagonal in Fock basis). Analogously, in the case of homodyne detection the output is conditioned on the result x falling within the interval $[-c_{\mathsf{hom}}, c_{\mathsf{hom}}]$. Dealing with initial Fock states, these computations are most easily carried out in Fock basis, using the matrix elements of the beam splitter [3] and computing the coarse grained POVM matrix elements:

$$\langle n|\,\hat{\Pi}_{c_{\mathsf{hom}}}\,|m\rangle = \int_{-c_{\mathsf{hom}}}^{c_{\mathsf{hom}}} \mathrm{d}x \langle n|x\rangle\langle x|m\rangle\,, \quad \langle n|\,\hat{\Pi}_{c_{\mathsf{het}}}\,|m\rangle = \int_{-c_{\mathsf{het}}}^{c_{\mathsf{het}}} \mathrm{d}|\alpha| \int_0^{2\pi} \frac{\mathrm{d}\theta}{\pi} \langle n|\alpha\rangle\langle\alpha|m\rangle\,; \tag{8.37}$$

These integrals can be efficiently evaluated for every value of $c_{\mathsf{hom/het}}$. The (unnormalized) conditional state and corresponding probability are then

$$\tilde{\sigma}_{\mathsf{hom}} = \mathrm{Tr}_b\left[\left(U_{\mathsf{bs}}(\rho\otimes\rho)U_{\mathsf{bs}}^\dagger\right)\mathbb{1}\otimes\hat{\Pi}_{c_{\mathsf{hom}}}\right] \quad p_{\mathsf{hom}} = \mathrm{Tr}_a[\tilde{\sigma}_{\mathsf{hom}}]\,, \tag{8.38}$$

and analogously for heterodyne detection. The output states of the concentration protocol are the mixed states $\sigma_{\mathsf{hom}} = \tilde{\sigma}_{\mathsf{hom}}/p_{\mathsf{hom}}$ and $\sigma_{\mathsf{het}} = \tilde{\sigma}_{\mathsf{het}}/p_{\mathsf{het}}$. The Wigner functions can be obtained from the density matrix in Fock basis, by using the previous formulas (6.23).

With homodyne conditioning it is not possible in general to obtain the state $|2n\rangle$, since we would need to condition around a value x where all the wave functions $\langle x|n\rangle = 0$ for $n > 1$. This is possible just in the case of single photon states since the superposition is simply between $|0,2\rangle$ and $|2,0\rangle$ and therefore we could approximate a projection on the vacuum by conditioning the homodyne detection in a region around the zero of $\langle x|2\rangle$, which is obtained for $x_0 = 1/\sqrt{2}$.

In terms of our figures of merits we have $k = 2$ input and $m = 1$ output copies. To start, we study the protocol with two single photon states $|1\rangle$ in input. The protocol efficiency $\eta[\Lambda]$ and the resource gain $\epsilon[\Lambda]$ are plotted in the upper panels of Fig. 8.6 and 8.7, as a function of the heralding parameters c_{het} and c_{hom}, and for different values of T. We observe that $\epsilon \geq 0$ up to certain threshold values of c_{het} and c_{hom}, depending on the the transmissivity T. On the other hand the maximum efficiency can always be achieved for a balanced beam-splitter, since this maximizes the matrix element $\langle 2|\sigma|2\rangle$ of the output states. Typically, these *optimal* values are obtained for values of c_{het} and c_{hom} that in turn corresponds to lower values of ϵ. This trade-off is better highlighted in the lower panels of Fig. 8.6 and 8.7, where we show the efficiency η as a function of the gain ϵ. We observe that we can indeed gain more negativity with heterodyne heralding, since we are approximately creating the state $|2\rangle$, in this case there is a strict trade-off between η and ϵ, i.e. η is a monotonically decreasing function of ϵ.

For homodyne heralding we gain less negativity, but at least for $T = 0.5$, there is an *optimal* region, where *large* values of the two figure of merits can be achieved (*large values* in the sense that they are close to the maximum values that one can achieve via this protocol, by changing the interval width c_{hom}). However, by changing the transmissivity of the beam splitter we observe a monotonically decreasing behaviour of η as a function of ϵ, similarly to the heterodyne case.

We then consider the same protocol with *lossy* Fock states $\rho = \beta|1\rangle\langle 1| + (1-\beta)|0\rangle\langle 0|$ as input (resource) states and by fixing the transmissivity to $T = 1/2$. We observe the same trade-off in the parametric plot in Fig. 8.8: the protocol becomes less effective for decreasing values of β, and the *optimal* region for homodyne measurements is not present anymore for $\beta \lesssim 0.9$.

Finally, we consider Fock states $|n\rangle$ with n up to 5 as input resources (mixed at a balanced beam-splitter) and we plot in Fig. 8.9 η as function of ϵ. All the curves present a similar behaviour, but it is clear that the performances of the protocol in terms of our figures of merit decreases for increasing n.

A remark about negativity concentration

These schemes we studied are *concentration* protocols at the single copy level, in the sense that the single outcome state is more resourceful than a single input state, but two input states must be used.

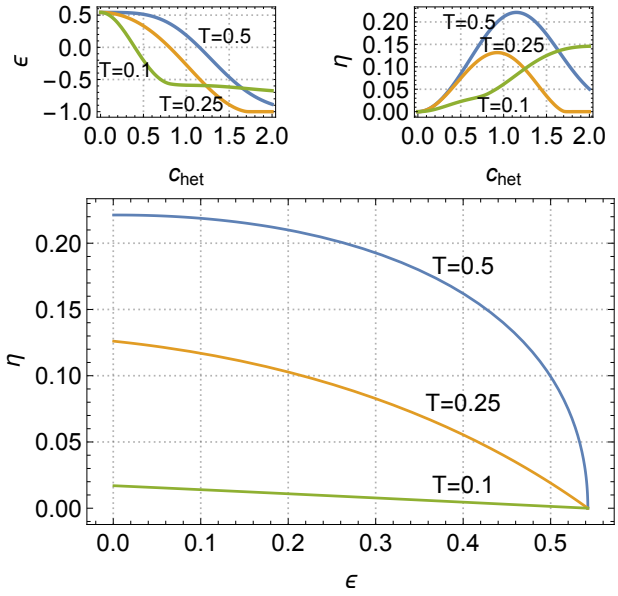

Figure 8.6: **Heterodyne post-selection** Efficiency η and negativity gain ϵ for the heterodyne concentration scheme with two single photon Fock states $|1\rangle$ in input as a function of the conditioning parameter c_{het} for different beam-splitter transmissivities.

In particular, these schemes satisfy the following inequality

$$\frac{\mathsf{W}(\sigma)}{\mathsf{W}(\rho^{\otimes 2})} < 1, \tag{8.39}$$

which is a much stronger constraint than what imposed by the bound (8.3), i.e. the mana of the output state never surpass the mana of the *global* input state, not even probabilistically.

The reason for this bound is that negativity of Fock states is sublinear in n [151], this implies that

$$\mathsf{W}(|2n\rangle) < 2\mathsf{W}(|n\rangle) \tag{8.40}$$

and the mana of the output states is never higher than the one of the state $|2n\rangle$.

One might think that this is true in general for GPs, but this is not the case. We found a simple counter-example to this by considering a two-mode non-Gaussian entangled input state of the form

$$|\psi_{\text{in}}\rangle = \sqrt{1-\beta}|0,0\rangle + \sqrt{\beta}|1,1\rangle.$$

If one mode of this state is measured with an heterodyne detector and the outcome conditioned to be in certain intervals, the remaining state on the other mode is thus the

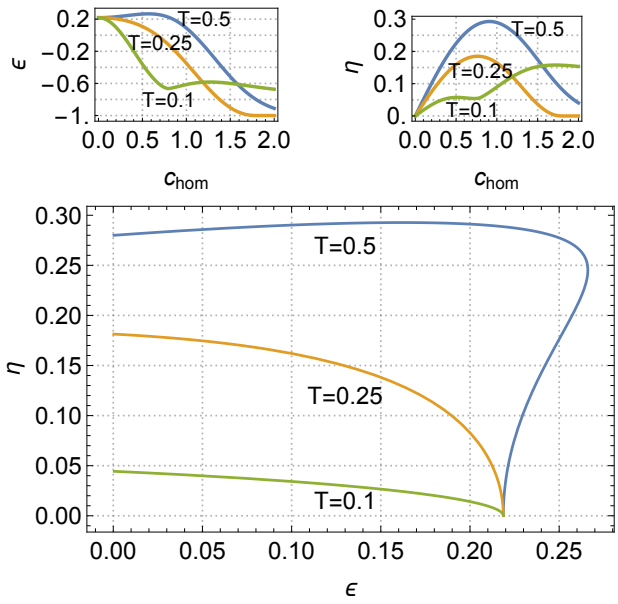

Figure 8.7: **Homodyne post-selection** Efficiency η and negativity gain ϵ for the homodyne concentration scheme with two single photon Fock states $|1\rangle$ in input. Top: both quantities as a function of the conditioning parameter c_{hom} for different beam-splitter transmissivities. Bottom: parametric plot of efficiency and negativity when c_{hom} is varied.

following mixture (we show the unnormalized state):

$$\tilde{\sigma}_{\mathsf{out}} = \int_{\theta_1}^{\theta_2} \frac{\mathrm{d}\theta}{\pi} \int_{\alpha_1}^{\alpha_2} |\alpha|\mathrm{d}|\alpha| \Big[(1-\beta)|\langle\alpha|0\rangle|^2 |0\rangle\langle 0| + \beta|\langle\alpha|1\rangle|^2 |1\rangle\langle 1| + \\ + \sqrt{\beta(1-\beta)} \Big(\langle\alpha|0\rangle\overline{\langle\alpha|1\rangle} |0\rangle\langle 1| + \langle\alpha|1\rangle\overline{\langle\alpha|0\rangle} |1\rangle\langle 0| \Big) \Big]. \tag{8.41}$$

For sufficiently small values of β and conditioning "far" from the origin one can indeed obtain $\mathsf{W}(\sigma_{\mathsf{out}}) > \mathsf{W}(|\psi_{\mathsf{in}}\rangle)$. These outcomes are however very unlikely and the values for the efficiency η are very low; even if the mana is increased we are not close to the saturation of bound (8.3). For example we find that for $\alpha_1 = 2.5$, $\alpha_2 \to \infty$, $\theta_1 = -\pi/6$ and $\theta_2 = +\pi/6$ we have $\mathsf{W}(\sigma_{\mathsf{out}}) - \mathsf{W}(|\psi_{\mathsf{in}}\rangle) \approx 0.05$, however the probability is very small $p_{\mathsf{out}} \approx 5 \cdot 10^{-4}$ and therefore the efficiency is negligible as well $\eta \approx 8 \cdot 10^{-4}$.

Summary

- Understanding the possibilities and limits of manipulating non-Gaussian states with Gaussian operations is a challenging but timely topic of research. Such operations are found to be beneficial in many quantum information protocols involving non-Gaussian states.
- We have introduced a general and physically motivated framework for the resource theory of quantum non-Gaussianity and Wigner Negativity. The free operations,

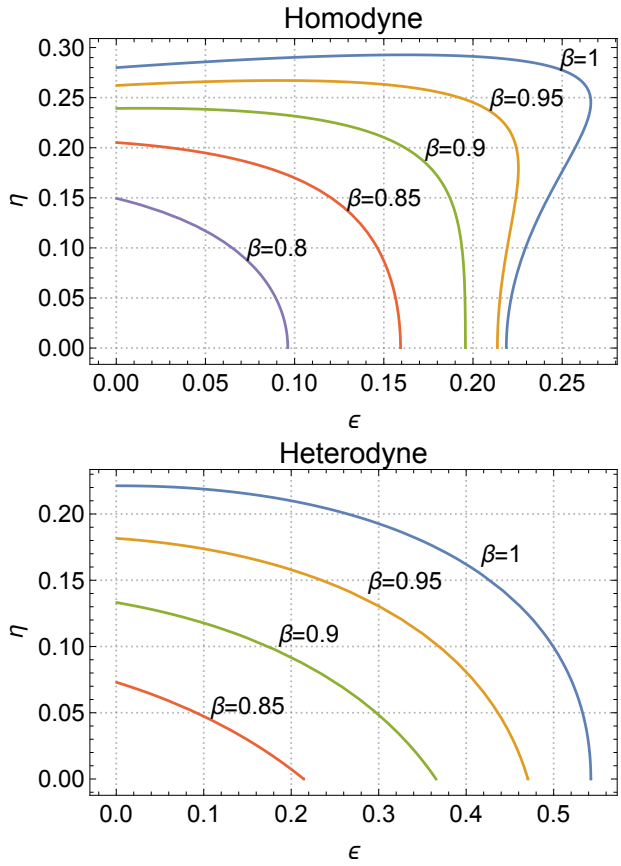

Figure 8.8: Parametetric plot of the efficiency η and the negativity gain ϵ for both the heterodyne and homodyne protocols with two lossy single photon states $(1-\beta)|0\rangle\langle 0| + \beta|1\rangle\langle 1|$ for different values of β.

dubbed Gaussian protocols, are very general and involve all the relevant experimental ingredients, including conditioning on measurement outcomes.

- In this resource theory there is no maximally resourceful state.
- We introduced a computable monotone —the CV mana (or Wigner logarithmic negativity), and used it to gauge the resource content of some classes of experimentally relevant states.
- We studied the efficiency of some resource concentration protocols involving passive interactions and Fock input states.
- The results presented here promote a celebrated quantifier of non-classicality — the volume of the negative part of the Wigner function — to a fully fledged monotone for this resource theory, which is relevant for quantum information processing with infinite-dimensional systems. We argue that this framework will contribute

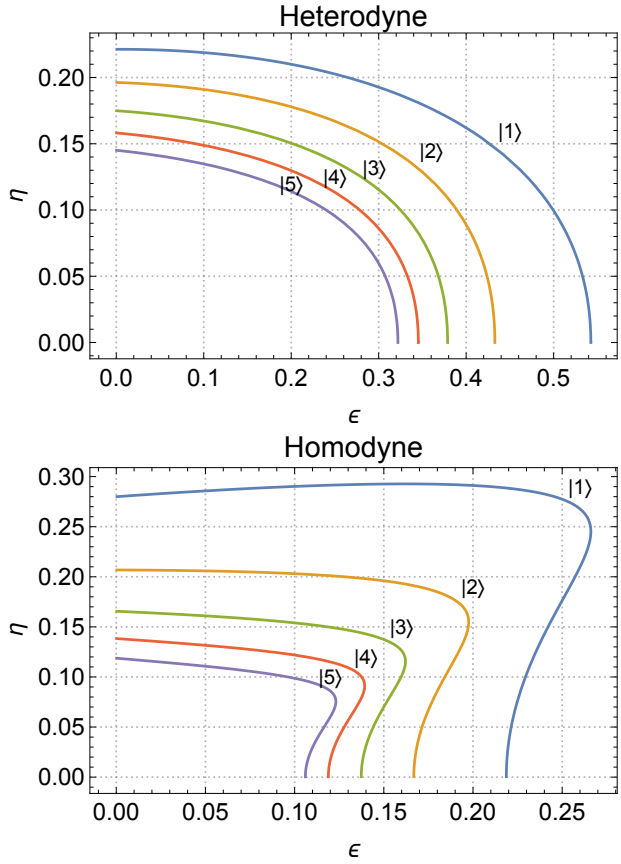

Figure 8.9: Parametetric plot of the efficiency η and the negativity gain ϵ for both the heterodyne and homodyne protocols with two Fock states $|n\rangle$ in input, for $n = 1, \ldots, 5$.

towards the development of sub-universal and universal CV quantum information processing.

- Our framework also incorporates the peculiar feature of CV measurements that finite-probability output states are necessarily mixed. This is of practical relevance when assessing the interconversion rate of state manipulation protocols.

Conclusion and outlooks

In this PhD dissertation we have presented two fairly different main themes, the leitmotiv being the quest to identify "resources" for various tasks. As explained in the introduction, this word has been mostly used in a colloquial manner, to express a slightly vague concept, but also with a more precisely defined meaning in the last chapter.

In the first part we have presented a comprehensive quantum estimation theoretical framework to handle continuously monitored quantum systems, shedding some light on the correct figures of merit to use. The main quantifier of precision in quantum metrology is the QFI, which comes in three flavours for such time-continuous metrological schemes. We dubbed these figures of merit unconditional, effective and ultimate QFI, corresponding respectively to the unconditional dynamics (Markovian master equation), the conditional dynamics (Markovian stochastic master equation) and the unitary global dynamics of system and environment (but still under a Markovian approximation). In particular, the most experimentally relevant quantity is the effective QFI, since it pertains to realistic monitoring strategies and it takes into account both the classical information gained by the specific measurement and the information encoded on the conditional states. On the other hand, the ultimate QFI is mostly used as a theoretical upper bound, derived by assuming that any kind of measurement on the environmental modes is possible.

After laying out these quantum estimation theoretical tools, we have applied them to a couple of concrete and interesting problems involving two level atoms. The first problem we have tackled is magnetometry with large atomic ensembles. The limit of a large number of atoms was essential to obtain analytical results, thanks to a Gaussian approximation. In this physical setup the coupling between the field used for continuous (homodyne) monitoring and the atoms is collective, thereby implementing a time-continuous version of a collective spin measurement. We have shown that this strategy is very powerful to estimate the rotation induced by the magnetic field (which reduces to a displacement in the Gaussian approximation). In particular, we have shown that *both* the classical information coming from the observed photo-current and the QFI of the conditional states exhibit Heisenberg scaling, i.e. quadratic in the number of atoms, even though the initial state of the atoms was assumed to be completely uncorrelated.

The second problem addressed is frequency estimation with two level atoms (here treated more abstractly as qubits) under a noisy dynamical evolution. In this case we have

assumed an initially entangled state, but we have considered a separate environment acting on each qubit. It is well known that for noisy unconditional dynamics (when the environmental modes are not measured) no Heisenberg scaling can be obtained. We have shown that perfectly monitoring the environment restores Heisenberg scaling for two different geometries of the noise: parallel or transverse to the encoding Hamiltonian. These results hold both for photon-counting and homodyne-detection. In the case of parallel noise we have shown that the full information of the noiseless case can be regained, and that by considering GHZ initial states the requirements on the implementation are less stringent. We have shown that for inefficient measurements Heisenberg scaling is lost (for parallel noise; for transverse noise the numerical results are inconclusive), but one can still obtain a non-trivial gain in precision.

The second part of the thesis starts with another quantum estimation problem, involving only the unconditional dynamics; here the parameter to be measured is exactly the coupling with the environment (i.e. the loss rate). We have shown that if the Hamiltonian of the system includes a non-linear self-Kerr interaction it is possible to obtain a higher value for the QFI of the evolved state, with the same initial Gaussian state. However, it is more difficult to reap this advantage, because common measurement strategies do not saturate the quantum Cramér-Rao bound. In the regime of short interaction times we could show that this improvement is significant and can also be witnessed by suboptimal measurements on the state. These results are intriguing; while the nonlinear Hamiltonian is clearly beneficial for initial Gaussian states, it seems hard to draw strong connections with other nonclassical properties of the evolved state, as shown by considering already non-Gaussian initial states.

We have then proceeded to study more closely nonclassical properties of continuous variable systems. For some classes of anharmonic oscillators we have shown that the degree of nonlinearity of the Hamiltonian, quantified by the non-Gaussianity of the ground state, can be quantitatively linked to the nonclassicality of the ground state, even though the details are dependent on the definition of nonclassicality considered. In particular, we have shown that non-Gaussianity and the volume of the negative part of the Wigner function for such ground states are very closely connected. They are monotonic quantities when there is only one effective parameter and being *almost* monotonic when there is more than one effective parameter.

We have also considered the so-called backflow effect arising in the dynamics of a free particle. This effect is completely dependent on the initial state and therefore we have considered it as a nonclassical property of CV states. It can be quantified by the maximal increase in the probability of going in the direction opposite to the direction of motion, during an arbitrary time interval. In particular, we have shown that this quantitative measure of the effect singles out a more fragile degree of quantumness than the one measured by the negativity of the Wigner function.

Finally, the last chapter of this dissertation has been devoted to the construction of a resource theory for non-Gaussian and Wigner-negative states. The crucial ingredient in this theoretical framework are the so-called Gaussian protocols, which we consider as free operations. These include: Gaussian unitaries and Gaussian measurements, ancillary Gaussian states as well as conditioning on classical randomness and on measurement

outcomes. With these operationally motivated free operations one can consider both states outside the convex hull of Gaussian states and states with negative Wigner function as resources. We have proved that CV mana, the logarithm of the integral of the absolute value of the Wigner function, is an additive monotone for this resource theory, albeit an unfaithful one if one considers non-Gaussian states. We have computed this quantity for some classes of pure states, comparing it to the measure of non-Gaussianity; we have also analysed a simple protocol to concentrate the negativity based on passive linear unitaries and Gaussian measurements.

Outlooks

In thesis we have introduced two frameworks. The quantum estimation theoretical framework for continuous measurement was not completely new, but we believe that our way of organising and presenting it, together with the generic numerical tool we have implemented, will be useful to the scientific community. We plan to apply these ideas and tools to many more physical problems, in particular also in the context of *multi-parameter* estimation. We would also like to get in touch with experimental groups, tackling the challenging problem of applying abstract ideas about estimation to actual measurement data.

We also plan to carry out more abstract studies. First, we want to study more in detail the generalized master equations needed to compute the ultimate QFI, in particular with a phase-space approach for CV systems, generalizing the calculations presented in Sec. 3.2.2. Second, the results of Chapter 4 suggest that, whenever we deal with inefficient monitoring, Heisenberg scaling is lost; we plan to attack this question in a general way, possibly generalizing the methods of [160] to conditional dynamics.

The second framework we have introduced is the convex resource theory of non-Gaussianity, is novel, even though very closely related to the finite dimensional version. We will try to use this resource theory to approach more concrete problems, pertaining to CV universal and sub-universal quantum computation. A guide in this studies would be again the path taken by DV resource theories, the final goal possibly being a CV analogue of the results presented in [134].

Bibliography

[1] G. Adesso, F. Dell'Anno, S. De Siena, F. Illuminati, and L. A. M. Souza, "Optimal estimation of losses at the ultimate quantum limit with non-Gaussian states", Phys. Rev. A **79**, 040305(R) (2009) (cit. on pp. 95, 99, 105).

[2] G. Adesso, S. Ragy, and A. R. Lee, "Continuous variable quantum information: gaussian states and beyond", Open Syst. Inf. Dyn. **21**, 1440001 (2014) (cit. on p. 29).

[3] G. S. Agarwal, *Quantum Optics* (Cambridge University Press, 2013) (cit. on p. 157).

[4] Y. Aharonov, D. Falkoff, E. Lerner, and H. Pendleton, "A quantum characterization of classical radiation", Ann. Phys. **39**, 498–512 (1966) (cit. on p. 35).

[5] M. Ahmadi, H. B. Dang, G. Gour, and B. C. Sanders, "Quantification and manipulation of magic states", Phys. Rev. A **97**, 062332 (2018) (cit. on pp. 139, 144).

[6] C. Ahn, H. M. Wiseman, and G. J. Milburn, "Quantum error correction for continuously detected errors", Phys. Rev. A **67**, 052310 (2003) (cit. on p. 76).

[7] C. Ahn, H. Wiseman, and K. Jacobs, "Quantum error correction for continuously detected errors with any number of error channels per qubit", Phys. Rev. A **70**, 024302 (2004) (cit. on p. 76).

[8] N. Akerman, S. Kotler, Y. Glickman, and R. Ozeri, "Reversal of photon-scattering errors in atomic qubits", Phys. Rev. Lett. **109**, 103601 (2012) (cit. on p. 76).

[9] F. Albarelli, A. Ferraro, M. Paternostro, and M. G. A. Paris, "Nonlinearity as a resource for nonclassicality in anharmonic systems", Phys. Rev. A **93**, 032112 (2016) (cit. on pp. xvii, 109, 111, 152).

[10] F. Albarelli, M. G. Genoni, M. G. A. Paris, and A. Ferraro, "Resource theory of quantum non-Gaussianity and Wigner negativity", arXiv:1804.05763 (2018) (cit. on pp. xvii, 139).

[11] F. Albarelli, T. Guaita, and M. G. A. Paris, "Quantum backflow effect and nonclassicality", Int. J. Quantum Inf. **14**, 1650032 (2016) (cit. on p. xvii).

[12] F. Albarelli, M. A. C. Rossi, M. G. A. Paris, and M. G. Genoni, "Ultimate limits for quantum magnetometry via time-continuous measurements", New J. Phys. **19**, 123011 (2017) (cit. on pp. xvi, 41, 44, 59).

[13]F. Albarelli, M. A. C. Rossi, M. G. A. Paris, and M. G. Genoni, "Monitoring time and detectors efficiencies in time-continuous magnetometry", in *Toward a Science Campus in Milan*, edited by P. F. Bortignon, G. Lodato, E. Meroni, M. G. A. Paris, L. Perini, and A.Vicini (2018) (cit. on pp. xvi, 59).

[14]F. Albarelli, M. A. C. Rossi, D. Tamascelli, and M. G. Genoni, "Restoring Heisenberg scaling in noisy quantum metrology by monitoring the environment", arXiv:1803.05891 (2018) (cit. on pp. xvi, 41, 50, 76, 81, 82, 88).

[15]S. Alipour, M. Mehboudi, and A. T. Rezakhani, "Quantum Metrology in Open Systems: Dissipative Cramér-Rao Bound", Phys. Rev. Lett. **112**, 120405 (2014) (cit. on pp. 23, 79).

[16]S. Alipour and A. T. Rezakhani, "Extended convexity of quantum fisher information in quantum metrology", Phys. Rev. A **91**, 1–7 (2015) (cit. on p. 44).

[17]G. Allcock, "The time of arrival in quantum mechanics i. formal considerations", Ann. Phys. **53**, 253–285 (1969) (cit. on p. 123).

[18]A. Allevi, A. Andreoni, F. A. Beduini, M. Bondani, M. G. Genoni, S. Olivares, and M. G. A. Paris, "Conditional measurements on multimode pairwise entangled states from spontaneous parametric downconversion", Europhys. Lett. **92**, 20007 (2010) (cit. on pp. 36, 152).

[19]A. Allevi, A. Andreoni, M. Bondani, M. G. Genoni, and S. Olivares, "Reliable source of conditional states from single-mode pulsed thermal fields by multiple-photon subtraction", Phys. Rev. A **82**, 013816 (2010) (cit. on pp. 36, 152).

[20]E. Andersson, J. D. Cresser, and M. J. W. Hall, "Finding the Kraus decomposition from a master equation and vice versa", J. Mod. Opt. **54**, 1695–1716 (2007) (cit. on p. 84).

[21]F. Arzani, N. Treps, and G. Ferrini, "Polynomial approximation of non-Gaussian unitaries by counting one photon at a time", Phys. Rev. A **95**, 052352 (2017) (cit. on pp. 139, 152).

[22]J. Asbóth, J. Calsamiglia, and H. Ritsch, "Computable Measure of Nonclassicality for Light", Phys. Rev. Lett. **94**, 173602 (2005) (cit. on p. 35).

[23]M. Auzinsh, D. Budker, D. F. Kimball, S. M. Rochester, J. E. Stalnaker, A. O. Sushkov, and V. V. Yashchuk, "Can a Quantum Nondemolition Measurement Improve the Sensitivity of an Atomic Magnetometer?", Phys. Rev. Lett. **93**, 173002 (2004) (cit. on pp. 59, 60).

[24]V. A. Averchenko, V. Thiel, and N. Treps, "Nonlinear photon subtraction from a multimode quantum field", Phys. Rev. A **89**, 063808 (2014) (cit. on p. 153).

[25]M. Barbieri, N. Spagnolo, M. G. Genoni, F. Ferreyrol, R. Blandino, M. G. A. Paris, P. Grangier, and R. Tualle-Brouri, "Non-gaussianity of quantum states: an experimental test on single-photon-added coherent states", Phys. Rev. A **82**, 063833 (2010) (cit. on pp. 36, 152).

[26]O. E. Barndorff-Nielsen and R. D. Gill, "Fisher information in quantum statistics", J. Phys. A **33**, 4481–4490 (2000) (cit. on p. 22).

[27]S. M. Barnett and P. M. Radmore, *Methods in theoretical quantum optics* (Oxford University Press, Oxford, New York, 1997) (cit. on pp. 28, 69, 119, 132, 133).

[28]H. Bauke and N. R. Itzhak, "Visualizing quantum mechanics in phase space", arXiv:1101.2683 (2011) (cit. on p. 124).

[29]F. Benatti, R. Floreanini, and R. Romano, "Complete positivity and entangled degrees of freedom", J. Phys. A **35**, 4955–4972 (2002) (cit. on p. 5).

[30]J. Bertrand and P. Bertrand, "A tomographic approach to Wigner's function", Found. Phys. **17**, 397–405 (1987) (cit. on p. 28).

[31]J. J. Bollinger, W. Itano, D. J. Wineland, and D. J. Heinzen, "Optimal frequency measurements with maximally correlated states", Phys. Rev. A **54**, R4649 (1996) (cit. on p. 59).

[32]R. Boyd, *Nonlinear Optics*, 3rd ed. (Academic Press, Burlington, MA, 2008) (cit. on p. 95).

[33]A. J. Bracken and G. F. Melloy, "Probability backflow and a new dimensionless quantum number", J. Phys. A **27**, 2197–2211 (1994) (cit. on pp. 123, 127, 128).

[34]F. G. S. L. Brandão and G. Gour, "Reversible Framework for Quantum Resource Theories", Phys. Rev. Lett. **115**, 070503 (2015) (cit. on pp. 138, 142).

[35]J. B. Brask, R. Chaves, and J. Kołodyński, "Improved Quantum Magnetometry beyond the Standard Quantum Limit", Phys. Rev. X **5**, 031010 (2015) (cit. on pp. 75, 88).

[36]S. L. Braunstein, "Squeezing as an irreducible resource", Phys. Rev. A **71**, 055801 (2005) (cit. on p. 141).

[37]S. L. Braunstein and C. M. Caves, "Statistical distance and the geometry of quantum states", Phys. Rev. Lett. **72**, 3439 (1994) (cit. on pp. 21, 22).

[38]S. L. Braunstein, N. J. Cerf, S. Iblisdir, P. van Loock, and S. Massar, "Optimal cloning of coherent states with a linear amplifier and beam splitters", Phys. Rev. Lett. **86**, 4938–4941 (2001) (cit. on p. 137).

[39]S. L. Braunstein and P. Van Loock, "Quantum information with continuous variables", Rev. Mod. Phys. **77**, 513 (2005) (cit. on p. 29).

[40]G. Brida, M. Genovese, and I. Ruo Berchera, "Experimental realization of sub-shot-noise quantum imaging", Nature Photon. **4**, 227–230 (2010) (cit. on p. 95).

[41]T. Bröcker and R. F. Werner, "Mixed states with positive Wigner functions", J. Math. Phys. **36**, 62 (1995) (cit. on p. 138).

[42]G. W. Bund and M. C. Tijero, "Mapping Wigner distribution functions into semiclassical distribution functions", Phys. Rev. A **61**, 052114 (2000) (cit. on pp. 111, 112, 116).

[43]D. K. Burgarth, V. Giovannetti, A. N. Kato, and K. Yuasa, "Quantum estimation via sequential measurements", New J. Phys. **17**, 113055 (2015) (cit. on p. 76).

[44]K. E. Cahill and R. J. Glauber, "Density Operators and Quasiprobability Distributions", Phys. Rev. **177**, 1882–1902 (1969) (cit. on p. 132).

[45]K. E. Cahill and R. J. Glauber, "Ordered Expansions in Boson Amplitude Operators", Phys. Rev. **177**, 1857–1881 (1969) (cit. on p. 26).

[46]W. B. Case, "Wigner functions and Weyl transforms for pedestrians", Am. J. Phys. **76**, 937 (2008) (cit. on p. 27).

[47]C. Catana, L. Bouten, and M. Guţă, "Fisher informations and local asymptotic normality for continuous-time quantum Markov processes", J. Phys. A **48**, 365301 (2015) (cit. on p. 76).

[48]C. Catana and M. Guţă, "Heisenberg versus standard scaling in quantum metrology with Markov generated states and monitored environment", Phys. Rev. A **90**, 012330 (2014) (cit. on pp. 44, 76).

[49]O. Černotík and J. Fiurášek, "Displacement-enhanced continuous-variable entanglement concentration", Phys. Rev. A **86**, 052339 (2012) (cit. on p. 138).

[50]L. Chakhmakhchyan and N. J. Cerf, "Boson sampling with Gaussian measurements", Phys. Rev. A **96**, 032326 (2017) (cit. on p. 139).

[51]B. A. Chase and J. M. Geremia, "Single-shot parameter estimation via continuous quantum measurement", Phys. Rev. A **79**, 022314 (2009) (cit. on pp. 59, 71).

[52]S. Chaturvedi and V. Srinivasan, "Solution of the Master Equation for an Attenuated or Amplified Nonlinear Oscillator with an Arbitrary Initial Condition", J. Mod. Opt. **38**, 777–783 (1991) (cit. on p. 97).

[53]R. Chaves, J. B. Brask, M. Markiewicz, J. Kołodyński, and A. Acín, "Noisy Metrology beyond the Standard Quantum Limit", Phys. Rev. Lett. **111**, 120401 (2013) (cit. on pp. 75, 83, 88).

[54]A. Chiruvelli and K. Jacobs, "Rapid-purification protocols for optical homodyning", Phys. Rev. A **77**, 012102 (2008) (cit. on p. 81).

[55]F. Ciccarello, "Collision models in quantum optics", Quantum Meas. Quantum Metrol. **4**, 53–63 (2017) (cit. on p. 10).

[56]A. N. Cleland, *Foundations of Nanomechanics* (Springer-Verlang, Berlin, Heidelberg, 2003) (cit. on p. 111).

[57]P. T. Cochrane, T. C. Ralph, and. Doli ńska, "Optimal cloning for finite distributions of coherent states", Phys. Rev. A **69**, 042313 (2004) (cit. on p. 137).

[58]P. T. Cochrane, T. C. Ralph, and G. J. Milburn, "Teleportation improvement by conditional measurements on the two-mode squeezed vacuum", Phys. Rev. A **65**, 062306 (2002) (cit. on p. 137).

[59]B. Coecke, T. Fritz, and R. W. Spekkens, "A mathematical theory of resources", Inf. Comput. **250**, 59–86 (2016) (cit. on p. 138).

[60]J. Combes, C. Ferrie, Z. Jiang, and C. M. Caves, "Quantum limits on postselected, probabilistic quantum metrology", Phys. Rev. A **89**, 052117 (2014) (cit. on p. 44).

[61]L. Cortez, A. Chantasri, L. P. García-Pintos, J. Dressel, and A. N. Jordan, "Rapid estimation of drifting parameters in continuously measured quantum systems", Phys. Rev. A **95**, 012314 (2017) (cit. on p. 71).

[62]T. Curtright, D. Fairlie, and C. K. Zachos, *A Concise Treatise on Quantum Mechanics in Phase Space* (World Scientific, New Jersey, 2014) (cit. on pp. 27, 119).

[63]J. Dalibard, Y. Castin, and K. Mølmer, "Wave-function approach to dissipative processes in quantum optics", Phys. Rev. Lett. **68**, 580–583 (1992) (cit. on p. 15).

[64]E. G. Dalla Torre, J. Otterbach, E. Demler, V. Vuletic, and M. D. Lukin, "Dissipative Preparation of Spin Squeezed Atomic Ensembles in a Steady State", Phys. Rev. Lett. **110**, 120402 (2013) (cit. on p. 62).

[65]G. De Palma, A. Mari, V. Giovannetti, and A. S. Holevo, "Normal form decomposition for Gaussian-to-Gaussian superoperators", J. Math. Phys. **56**, 052202 (2015) (cit. on p. 143).

[66]J. B. DeBrota and C. A. Fuchs, "Negativity bounds for weyl–heisenberg quasiprobability representations", Found. Phys. **47**, 1009–1030 (2017) (cit. on p. 138).

[67]N. Delfosse, C. Okay, J. Bermejo-Vega, D. E. Browne, and R. Raussendorf, "Equivalence between contextuality and negativity of the wigner function for qudits", New J. Phys. **19**, 123024 (2017) (cit. on p. 138).

[68]R. Demkowicz-Dobrzański, M. Jarzyna, and J. Kołodyński, "Quantum Limits in Optical Interferometry", Prog. Opt. **60**, 345 (2015) (cit. on p. 21).

[69]R. Demkowicz-Dobrzański, J. Kołodyński, and M. Guţă, "The elusive Heisenberg limit in quantum-enhanced metrology", Nat. Commun. **3**, 1063 (2012) (cit. on pp. 75, 79).

[70]V. V. Dodonov and V. I. Man'ko, eds., *Theory of nonclassical states of light* (Taylor & Francis, London New York, 2003) (cit. on p. 127).

[71]A. C. Doherty and K. Jacobs, "Feedback control of quantum systems using continuous state estimation", Phys. Rev. A **60**, 2700–2711 (1999) (cit. on p. 10).

[72]U. Dorner, "Quantum frequency estimation with trapped ions and atoms", New J. Phys. **14**, 043011 (2012) (cit. on p. 62).

[73]T. Douce, D. Markham, E. Kashefi, E. Diamanti, T. Coudreau, P. Milman, P. van Loock, and G. Ferrini, "Continuous-Variable Instantaneous Quantum Computing is Hard to Sample", Phys. Rev. Lett. **118**, 070503 (2017) (cit. on p. 139).

[74]J. Eisert and M. B. Plenio, "Conditions for the Local Manipulation of Gaussian States", Phys. Rev. Lett. **89**, 097901 (2002) (cit. on p. 137).

[75]B. M. Escher, R. L. de Matos Filho, and L. Davidovich, "General framework for estimating the ultimate precision limit in noisy quantum-enhanced metrology", Nature Phys. **7**, 406–411 (2011) (cit. on p. 79).

[76]R.-J. Essiambre and R. W. Tkach, "Capacity Trends and Limits of Optical Communication Networks", Proc. IEEE **100**, 1035–1055 (2012) (cit. on p. 96).

[77]J. Etesse, R. Blandino, B. Kanseri, and R. Tualle-Brouri, "Proposal for a loophole-free violation of Bell's inequalities with a set of single photons and homodyne measurements", New J. Phys. **16**, 053001 (2014) (cit. on pp. 139, 156, 157).

[78]J. Etesse, M. Bouillard, B. Kanseri, and R. Tualle-Brouri, "Experimental generation of squeezed cat states with an operation allowing iterative growth", Phys. Rev. Lett. **114**, 1–5 (2015) (cit. on pp. 156, 157).

[79]S. P. Eveson, C. J. Fewster, and R. Verch, "Quantum Inequalities in Quantum Mechanics", Ann. Henri Poincaré **6**, 1–30 (2005) (cit. on p. 123).

[80]A. Ferraro, S. Olivares, and M. G. A. Paris, *Gaussian states in continuous variable quantum information* (Bibliopolis, Napoli, 2005) (cit. on p. 29).

[81]C. Ferrie, "Quasi-probability representations of quantum theory with applications to quantum information science", Reports Prog. Phys. **74**, 116001 (2011) (cit. on pp. 28, 138).

[82]C. Ferrie and J. Emerson, "Frame representations of quantum mechanics and the necessity of negativity in quasi-probability representations", J. Phys. A **41**, 352001 (2008) (cit. on p. 138).

[83]R. P. Feynman, "Negative probability", in *Quantum Implications: Essays in Honour of David Bohm*, edited by B. Hiley and F. D. Peat (Methuen, London, 1987) Chap. 13, pp. 235–248 (cit. on p. 123).

[84]R. Filip, "Gaussian quantum adaptation of non-Gaussian states for a lossy channel", Phys. Rev. A **87**, 042308 (2013) (cit. on p. 138).

[85]R. Filip and L. Mišta, "Detecting Quantum States with a Positive Wigner Function beyond Mixtures of Gaussian States", Phys. Rev. Lett. **106**, 200401 (2011) (cit. on pp. 138, 142).

[86]J. Fiurášek, "Gaussian Transformations and Distillation of Entangled Gaussian States", Phys. Rev. Lett. **89**, 137904 (2002) (cit. on p. 137).

[87]J. Fiurášek, "Improving entanglement concentration of Gaussian states by local displacements", Phys. Rev. A **84**, 012335 (2011) (cit. on p. 138).

[88]S. Flügge, *Practical Quantum Mechanics* (Springer Berlin Heidelberg, Berlin, Heidelberg, 1971) (cit. on p. 115).

[89]A. Frank, A. L. Rivera, and K. B. Wolf, "Wigner function of Morse potential eigenstates", Phys. Rev. A **61**, 054102 (2000) (cit. on p. 114).

[90]A. Fujiwara, "Strong consistency and asymptotic efficiency for adaptive quantum estimation problems", J. Phys. A. **39**, 12489–12504 (2006) (cit. on p. 22).

[91]G. Spedalieri, S. L. Braunstein, S. Pirandola, "Thermal quantum metrology", 2016 (cit. on p. 95).

[92]S. Gammelmark and K. Mølmer, "Bayesian parameter inference from continuously monitored quantum systems", Phys. Rev. A **87**, 032115 (2013) (cit. on pp. 46, 48, 71).

[93]S. Gammelmark and K. Mølmer, "Fisher Information and the Quantum Cramér-Rao Sensitivity Limit of Continuous Measurements", Phys. Rev. Lett. **112**, 170401 (2014) (cit. on pp. 55, 57, 84).

[94]N. Ganesan and T.-J. Tarn, "Decoherence control in open quantum systems via classical feedback", Phys. Rev. A **75**, 032323 (2007) (cit. on p. 76).

[95]T. Gefen, D. A. Herrera-Martí, and A. Retzker, "Parameter estimation with efficient photodetectors", Phys. Rev. A **93**, 032133 (2016) (cit. on p. 76).

[96]M. G. Genoni, "Cramér-Rao bound for time-continuous measurements in linear Gaussian quantum systems", Phys. Rev. A **95**, 012116 (2017) (cit. on pp. 32, 49).

[97]M. G. Genoni, "Erratum: Cramér-Rao bound for time-continuous measurements in linear Gaussian quantum systems [Phys. Rev. A 95, 012116 (2017)]", Phys. Rev. A **95**, 059908 (2017) (cit. on p. 49).

[98]M. G. Genoni, private communication (cit. on p. 50).

[99]M. G. Genoni, C. Invernizzi, and M. G. A. Paris, "Enhancement of parameter estimation by Kerr interaction", Phys. Rev. A **80**, 033842 (2009) (cit. on p. 96).

[100]M. G. Genoni, L. Lami, and A. Serafini, "Conditional and unconditional Gaussian quantum dynamics", Contemp. Phys. **57**, 331–349 (2016) (cit. on pp. 8, 30, 32, 34, 69).

[101]M. G. Genoni, S. Mancini, and A. Serafini, "Optimal feedback control of linear quantum systems in the presence of thermal noise", Phys. Rev. A **87**, 042333 (2013) (cit. on p. 76).

[102]M. G. Genoni, S. Mancini, and A. Serafini, "General-dyne unravelling of a thermal master equation", Russ. J. Math. Phys. **21**, 329–336 (2014) (cit. on p. 8).

[103]M. G. Genoni, M. L. Palma, T. Tufarelli, S. Olivares, M. S. Kim, and M. G. A. Paris, "Detecting quantum non-Gaussianity via the Wigner function", Phys. Rev. A **87**, 062104 (2013) (cit. on pp. 138, 142).

[104]M. G. Genoni and M. G. A. Paris, "Quantifying non-Gaussianity for quantum information", Phys. Rev. A **82**, 052341 (2010) (cit. on pp. 31, 36, 140, 141, 155).

[105]M. G. Genoni, M. G. A. Paris, and K. Banaszek, "Measure of the non-Gaussian character of a quantum state", Phys. Rev. A **76**, 042327 (2007) (cit. on pp. 36, 140, 141).

[106]M. G. Genoni, M. G. A. Paris, and K. Banaszek, "Quantifying the non-Gaussian character of a quantum state by quantum relative entropy", Phys. Rev. A **78**, 060303 (2008) (cit. on pp. 36, 140, 141).

[107]M. G. Genoni, J. Zhang, J. Millen, P. F. Barker, and A. Serafini, "Quantum cooling and squeezing of a levitating nanosphere via time-continuous measurements", New J. Phys. **17**, 073019 (2015) (cit. on p. 76).

[108]J. M. Geremia, J. K. Stockton, A. C. Doherty, and H. Mabuchi, "Quantum Kalman Filtering and the Heisenberg Limit in Atomic Magnetometry", Phys. Rev. Lett. **91**, 250801 (2003) (cit. on pp. 59, 60, 62).

[109]S. Ghose and B. C. Sanders, "Non-Gaussian states for continuous variable quantum computation via Gaussian maps", J. Mod. Opt. **54**, 855 (2006) (cit. on pp. 139, 143, 156).

[110]K. S. Gibbons, M. J. Hoffman, and W. K. Wootters, "Discrete phase space based on finite fields", Phys. Rev. A **70**, 062101 (2004) (cit. on p. 139).

[111]G. Giedke and J. Ignacio Cirac, "Characterization of Gaussian operations and distillation of Gaussian states", Phys. Rev. A **66**, 032316 (2002) (cit. on pp. 137, 141).

[112]R. D. Gill and B. Y. Levit, "Applications of the van Trees Inequality: A Bayesian Cramér-Rao Bound", Bernoulli **1**, 59 (1995) (cit. on p. 21).

[113]R. J. Glauber, "The quantum theory of optical coherence", Phys. Rev. **130**, 2529–2539 (1963) (cit. on p. 34).

[114]V. Gorini, A. Kossakowski, and E. C. G. Sudarshan, "Completely positive dynamical semigroups of N-level systems", J. Math. Phys. **17**, 821 (1976) (cit. on p. 12).

[115]D. Gottesman, A. Kitaev, and J. Preskill, "Encoding a qubit in an oscillator", Phys. Rev. A **64**, 012310 (2001) (cit. on pp. 143, 151).

[116]G. Gour, "Quantum resource theories in the single-shot regime", Phys. Rev. A **95**, 062314 (2017) (cit. on p. 138).

[117]D. Gross, "Hudson's theorem for finite-dimensional quantum systems", J. Math. Phys. **47**, 122107 (2006) (cit. on p. 139).

[118]J. A. Gross, C. M. Caves, G. J. Milburn, and J. Combes, "Qubit models of weak continuous measurements: markovian conditional and open-system dynamics", Quantum Sci. Technol. **3**, 024005 (2018) (cit. on pp. 8, 10).

[119]G. Guarnieri, J. Nokkala, R. Schmidt, S. Maniscalco, and B. Vacchini, "Energy backflow in strongly coupled non-Markovian continuous-variable systems", Phys. Rev. A **94**, 062101 (2016) (cit. on p. 70).

[120]S. Guha and B. I. Erkmen, "Gaussian-state quantum-illumination receivers for target detection", Phys. Rev. A **80**, 052310 (2009) (cit. on p. 95).

[121]M. Guţă, "Fisher information and asymptotic normality in system identification for quantum Markov chains", Phys. Rev. A **83**, 062324 (2011) (cit. on pp. 24, 55).

[122]M. Guţă and J. Kiukas, "Information geometry and local asymptotic normality for multi-parameter estimation of quantum markov dynamics", J. Mat. Phys. **58**, 052201 (2017) (cit. on p. 76).

[123]J. F. Haase, A. Smirne, J. Kołodyński, R. Demkowicz-Dobrzański, and S. F. Huelga, "Precision Limits in Quantum Metrology with Open Quantum Systems", arXiv:1807.11882 (2018) (cit. on p. 75).

[124]T. Hahn, "Cuba-a library for multidimensional numerical integration", Comput. Phys. Commun. **176**, 712–713 (2007) (cit. on p. 115).

[125]J. J. Halliwell, E. Gillman, O. Lennon, M. Patel, and I. Ramirez, "Quantum backflow states from eigenstates of the regularized current operator", J. Phys. A **46**, 475303 (2013) (cit. on p. 123).

[126]L. Happ, M. A. Efremov, H. Nha, and W. P. Schleich, "Sufficient condition for a quantum state to be genuinely quantum non-gaussian", New J. Phys. **20**, 023046 (2018) (cit. on pp. 138, 142).

[127]T. Heinosaari and M. Ziman, *The Mathematical language of Quantum Theory* (Cambridge University Press, Cambridge, 2011) (cit. on pp. 1, 4, 6).

[128]C. W. Helstrom, *Quantum detection and estimation theory* (Academic Press New York, 1976) (cit. on p. 21).

[129] A. S. Holevo, *Probabilistic and Statistical Aspects of Quantum Theory; 2nd ed.* Publications of the Scuola Normale Superiore Monographs (Springer, Dordrecht, 2011) (cit. on p. 29).

[130] A. S. Holevo, *Statistical Structure of Quantum Theory*, Vol. 67, Lecture Notes in Physics Monographs (Springer-Verlag Berlin Heidelberg, Berlin, Heidelberg, 2001) (cit. on p. 21).

[131] A. S. Holevo and R. F. Werner, "Evaluating capacities of bosonic Gaussian channels", Phys. Rev. A **63**, 032312 (2001) (cit. on p. 31).

[132] J. P. Home, D. Hanneke, J. D. Jost, D. Leibfried, and D. J. Wineland, "Normal modes of trapped ions in the presence of anharmonic trap potentials", New J. Phys. **13**, 073026 (2011) (cit. on p. 109).

[133] O. Houhou, private communication (cit. on p. 152).

[134] M. Howard and E. T. Campbell, "Application of a Resource Theory for Magic States to Fault-Tolerant Quantum Computing", Phys. Rev. Lett. **118**, 090501 (2017) (cit. on pp. 139, 165).

[135] M. Howard, J. Wallman, V. Veitch, and J. Emerson, "Contextuality supplies the 'magic' for quantum computation", Nature **510**, 351–355 (2014) (cit. on p. 138).

[136] R. Hudson, "When is the wigner quasi-probability density non-negative?", Reports Math. Phys. **6**, 249–252 (1974) (cit. on pp. 36, 138, 142).

[137] S. F. Huelga, C. Macchiavello, T. Pellizzari, A. K. Ekert, M. B. Plenio, and J. I. Cirac, "Improvement of Frequency Standards with Quantum Entanglement", Phys. Rev. Lett. **79**, 3865 (1997) (cit. on p. 79).

[138] C. N. Hughes, M. G. Genoni, T. Tufarelli, M. G. A. Paris, and M. S. Kim, "Quantum non-Gaussianity witnesses in phase space", Phys. Rev. A **90**, 013810 (2014) (cit. on pp. 138, 142).

[139] M. R. Hush, I. Lesanovsky, and J. P. Garrahan, "Generic map from non-Lindblad to Lindblad master equations", Phys. Rev. A **91**, 032113 (2015) (cit. on pp. 56, 58).

[140] C. Invernizzi, M. G. A. Paris, and S. Pirandola, "Optimal detection of losses by thermal probes", Phys. Rev. A **84**, 022334 (2011) (cit. on p. 95).

[141] J. S. Ivan, M. S. Kumar, and R. Simon, "A measure of non-gaussianity for quantum states", Quant. Inf. Proc. **11**, 853–872 (2012) (cit. on p. 36).

[142] M. G. Jabbour, R. García-Patrón, and N. J. Cerf, "Interconversion of pure Gaussian states requiring non-Gaussian operations", Phys. Rev. A **91**, 012316 (2015) (cit. on p. 137).

[143] K. Jacobs, *Stochastic Processes for Physicists* (Cambridge University Press, Cambridge, 2010), p. 186 (cit. on pp. 12, 13).

[144] K. Jacobs, *Quantum Measurement Theory and its Applications* (Cambridge University Press, Cambridge, 2014), p. 554 (cit. on pp. 8, 81, 82).

[145] K. Jacobs and P. L. Knight, "Linear quantum trajectories: Applications to continuous projection measurements", Phys. Rev. A **57**, 2301–2310 (1998) (cit. on p. 47).

[146]K. Jacobs and D. A. Steck, "A straightforward introduction to continuous quantum measurement", Contemp. Phys. **47**, 279 (2006) (cit. on p. 8).

[147]E. T. Jaynes and G. Bretthorst, *Probability theory: the logic of science* (Cambridge University Press, Cambridge, 2003) (cit. on p. 21).

[148]H. Jeong, M. S. Kim, T. C. Ralph, and B. S. Ham, "Generation of macroscopic superposition states with small nonlinearity", Phys. Rev. A **70**, 061801 (2004) (cit. on p. 96).

[149]M. Ježek, I. Straka, M. Mičuda, M. Dušek, J. Fiurášek, and R. Filip, "Experimental Test of the Quantum Non-Gaussian Character of a Heralded Single-Photon State", Phys. Rev. Lett. **107**, 213602 (2011) (cit. on pp. 138, 142).

[150]D. Kakofengitis and O. Steuernagel, "The Quantum Liouville Equation is non-Liouvillian", arXiv:1410.4367 (2014) (cit. on p. 124).

[151]A. Kenfack and K. Życzkowski, "Negativity of the Wigner function as an indicator of non-classicality", J. Opt. B **6**, 396 (2004) (cit. on pp. 35, 154, 159).

[152]T. Kiesel, "Classical and quantum-mechanical phase-space distributions", Phys. Rev. A **87**, 062114 (2013) (cit. on p. 34).

[153]A. H. Kiilerich and K. Mølmer, "Estimation of atomic interaction parameters by photon counting", Phys. Rev. A **89**, 052110 (2014) (cit. on p. 71).

[154]A. H. Kiilerich and K. Mølmer, "Bayesian parameter estimation by continuous homodyne detection", Phys. Rev. A **94**, 032103 (2016) (cit. on p. 71).

[155]M. S. Kim, "Recent developments in photon-level operations on travelling light fields", J. Phys. B **41**, 133001 (2008) (cit. on p. 137).

[156]M. S. Kim, W. Son, V. Bužek, and P. L. Knight, "Entanglement by a beam splitter: Nonclassicality as a prerequisite for entanglement", Phys. Rev. A **65**, 032323 (2002) (cit. on p. 35).

[157]G. Kirchmair, B. Vlastakis, Z. Leghtas, S. E. Nigg, H. Paik, E. Ginossar, M. Mirrahimi, L. Frunzio, S. M. Girvin, and R. J. Schoelkopf, "Observation of quantum state collapse and revival due to the single-photon Kerr effect.", Nature **495**, 205–9 (2013) (cit. on p. 96).

[158]J. R. Klauder and E. C. G. Sudarshan, *Fundamentals of Quantum Optics* (Benjamin, New York, 1968) (cit. on p. 28).

[159]A. Kolkiran and G. S. Agarwal, "Quantum Properties of a Nanomechanical Oscillator", 8 (2006) (cit. on p. 109).

[160]J. Kołodyński and R. Demkowicz-Dobrzański, "Efficient tools for quantum metrology with uncorrelated noise", New J. Phys. **15**, 073043 (2013) (cit. on p. 165).

[161]H. Kwon, K. C. Tan, T. Volkoff, and H. Jeong, "Nonclassicality of Light as a Quantifiable Resource for Quantum Metrology", arXiv:1804.09355 (2018) (cit. on p. 146).

[162]L. Lami, B. Regula, X. Wang, R. Nichols, A. Winter, and G. Adesso, "Gaussian quantum resource theories", Phys. Rev. A **98**, 022335 (2018) (cit. on p. 137).

[163]H. Le Jeannic, A. Cavaillès, K. Huang, R. Filip, and J. Laurat, "Slowing quantum decoherence by squeezing in phase space", Phys. Rev. Lett. **120**, 073603 (2018) (cit. on p. 138).

[164]C. T. Lee, "Measure of the nonclassicality of nonclassical states", Phys. Rev. A **44**, R2775–R2778 (1991) (cit. on pp. 34, 133).

[165]E. L. Lehmann and G. Casella, *Theory of point estimation*, 2nd ed, Springer texts in statistics (Springer, New York, 1998) (cit. on pp. 18, 19, 21).

[166]G. Lindblad, "On the generators of quantum dynamical semigroups", Commun. Math. Phys. **48**, 119–130 (1976) (cit. on p. 12).

[167]J. Liu, X. Jing, W. Zhong, and X. Wang, "Quantum Fisher information for density matrices with arbitrary ranks", Commun. Theor. Phys. **61**, 45–50 (2014) (cit. on p. 23).

[168]J. Liu and H. Yuan, "Valid lower bound for all estimators in quantum parameter estimation", New J. Phys. **18**, 093009 (2016) (cit. on p. 24).

[169]S. Lloyd and S. L. Braunstein, "Quantum Computation over Continuous Variables", Phys. Rev. Lett. **82**, 1784–1787 (1999) (cit. on pp. 137, 139).

[170]A. Luis, "Nonlinear transformations and the Heisenberg limit", Phys. Lett. A **329**, 8–13 (2004) (cit. on p. 96).

[171]A. Luis, "Quantum-limited metrology with nonlinear detection schemes", SPIE Rev. **1**, 018006 (2010) (cit. on p. 96).

[172]A. Luis and Á. Rivas, "Nonlinear Michelson interferometer for improved quantum metrology", Phys. Rev. A **92**, 022104 (2015) (cit. on p. 96).

[173]A. P. Lund, S. Rahimi-Keshari, and T. C. Ralph, "Exact boson sampling using Gaussian continuous-variable measurements", Phys. Rev. A **96**, 022301 (2017) (cit. on p. 139).

[174]N. Lütkenhaus and S. M. Barnett, "Nonclassical effects in phase space", Phys. Rev. A **51**, 3340–3342 (1995) (cit. on p. 35).

[175]J. Ma, X. Wang, C.-P. Sun, and F. Nori, "Quantum spin squeezing", Phys. Rep. **509**, 89–165 (2011) (cit. on p. 63).

[176]Y. Ma, M. Pang, L. Chen, and W. Yang, "Improving quantum parameter estimation by monitoring quantum trajectories", arXiv:1807.09543 (2018) (cit. on p. 76).

[177]H. Mabuchi, "Dynamical identification of open quantum systems", Quant. Semiclass. Opt. **8**, 1103 (1996) (cit. on p. 46).

[178]K. Macieszczak, M. Guţă, I. Lesanovsky, and J. P. Garrahan, "Dynamical phase transitions as a resource for quantum enhanced metrology", Phys. Rev. A **93**, 022103 (2016) (cit. on pp. 55, 57).

[179]L. B. Madsen and K. Mølmer, "Spin squeezing and precision probing with light and samples of atoms in the Gaussian description", Phys. Rev. A **70**, 052324 (2004) (cit. on pp. 59, 62).

[180]L. Magnin, F. Magniez, A. Leverrier, and N. J. Cerf, "Strong no-go theorem for Gaussian quantum bit commitment", Phys. Rev. A **81**, 010302 (2010) (cit. on p. 137).

[181] L. Mandel, "Non-classical states of the electromagnetic field", Phys. Scr. **34** (1986) (cit. on p. 34).

[182] L. Mandel and E. Wolf, *Optical coherence and quantum optics* (Cambridge University Press, Cambridge MA, 1995) (cit. on p. 34).

[183] A. Mandilara, E. Karpov, and N. J. Cerf, "Extending Hudson's theorem to mixed quantum states", Phys. Rev. A **79**, 062302 (2009) (cit. on p. 138).

[184] A. Mandilara, E. Karpov, and N. J. Cerf, "Gaussianity bounds for quantum mixed states with a positive Wigner function", J. Phys. Conf. Ser. **254**, 012011 (2010) (cit. on p. 138).

[185] A. Mari and J. Eisert, "Positive Wigner Functions Render Classical Simulation of Quantum Computation Efficient", Phys. Rev. Lett. **109**, 230503 (2012) (cit. on pp. 35, 139, 142).

[186] A. Mari, K. Kieling, B. Melholt Nielsen, E. S. Polzik, and J. Eisert, "Directly Estimating Nonclassicality", Phys. Rev. Lett. **106**, 010403 (2011) (cit. on p. 36).

[187] P. Marian and T. A. Marian, "Relative entropy is an exact measure of non-Gaussianity", Phys. Rev. A **88**, 012322 (2013) (cit. on p. 36).

[188] E. Martínez-Vargas, C. Pineda, F. Leyvraz, and P. Barberis-Blostein, "Quantum estimation of unknown parameters", Phys. Rev. A **95**, 012136 (2017) (cit. on p. 43).

[189] G. F. Melloy and A. J. Bracken, "Probability backflow for a Dirac particle", Found. Phys., 505–514 (1998) (cit. on p. 123).

[190] G. F. Melloy and A. J. Bracken, "The velocity of probability transport in quantum mechanics", Ann. Phys. **7**, 726–731 (1998) (cit. on p. 123).

[191] N. C. Menicucci, P. van Loock, M. Gu, C. Weedbrook, T. C. Ralph, and M. A. Nielsen, "Universal Quantum Computation with Continuous-Variable Cluster States", Phys. Rev. Lett. **97**, 110501 (2006) (cit. on pp. 137, 143).

[192] G. Milburn, A. Mecozzi, and P. Tombesi, "Squeezed-state Superpositions in a Damped Nonlinear Oscillator", J. Mod. Opt. **36**, 1607–1614 (1989) (cit. on p. 97).

[193] G. J. Milburn and C. A. Holmes, "Dissipative quantum and classical liouville mechanics of the anharmonic oscillator", Phys. Rev. Lett. **56**, 2237–2240 (1986) (cit. on p. 96).

[194] C. Miquel, J. P. Paz, and M. Saraceno, "Quantum computers in phase space", Phys. Rev. A **65**, 062309 (2002) (cit. on p. 139).

[195] A. Miranowicz, K. Bartkiewicz, A. Pathak, J. Peřina, Y.-N. Chen, and F. Nori, "Statistical mixtures of states can be more quantum than their superpositions: Comparison of nonclassicality measures for single-qubit states", Phys. Rev. A **91**, 042309 (2015) (cit. on p. 34).

[196] A. Miranowicz, R. Tanas, and S. Kielich, "Generation of discrete superpositions of coherent states in the anharmonic oscillator model", Quantum Opt. **2**, 253–256 (1990) (cit. on p. 96).

[197]Y. Miwa, J.-i. Yoshikawa, N. Iwata, M. Endo, P. Marek, R. Filip, P. van Loock, and A. Furusawa, "Exploring a New Regime for Processing Optical Qubits: Squeezing and Unsqueezing Single Photons", Phys. Rev. Lett. **113**, 013601 (2014) (cit. on p. 137).

[198]K. Mølmer, "Hypothesis Testing with Open Quantum Systems", Phys. Rev. Lett. **114**, 040401 (2015) (cit. on p. 57).

[199]K. Mølmer and L. B. Madsen, "Estimation of a classical parameter with Gaussian probes: Magnetometry with collective atomic spins", Phys. Rev. A **70**, 052102 (2004) (cit. on pp. 59–62).

[200]A. Monras and M. G. A. Paris, "Optimal quantum estimation of loss in bosonic channels", Phys. Rev. Lett. **98**, 160401 (2007) (cit. on pp. 95, 98, 99).

[201]P. Morse, "Diatomic molecules according to the wave mechanics. II. vibrational levels", Phys. Rev. **34**, 57 (1929) (cit. on p. 113).

[202]J. G. Muga, J. P. Palao, and C. Leavens, "Arrival time distributions and perfect absorption in classical and quantum mechanics", Phys. Lett. A **253**, 21–27 (1999) (cit. on p. 123).

[203]C. Mukhopadhyay, S. Sazim, and A. K. Pati, "Coherence makes quantum systems 'magical'", J. Phys. A Math. Theor. **51**, 414006 (2018) (cit. on p. 145).

[204]R. Nair, "Quantum-limited loss sensing: Multiparameter estimation and Bures distance between loss channels", arXiv:1804.02211 (2018) (cit. on p. 95).

[205]J. S. Neergaard-Nielsen, B. M. Nielsen, C. Hettich, K. Mølmer, and E. S. Polzik, "Generation of a superposition of odd photon number states for quantum information networks", Phys. Rev. Lett. **97**, 083604 (2006) (cit. on pp. 137, 152).

[206]S. Ng, S. Z. Ang, T. A. Wheatley, H. Yonezawa, A. Furusawa, E. H. Huntington, and M. Tsang, "Spectrum analysis with quantum dynamical systems", Phys. Rev. A **93**, 042121 (2016) (cit. on pp. 23, 44).

[207]F. Nicacio, R. N. Maia, F. Toscano, and R. O. Vallejos, "Phase space structure of generalized Gaussian cat states", Phys. Lett. A **374**, 4385–4392 (2010) (cit. on p. 127).

[208]J. Niset, J. Fiurášek, and N. J. Cerf, "No-Go Theorem for Gaussian Quantum Error Correction", Phys. Rev. Lett. **102**, 120501 (2009) (cit. on p. 137).

[209]H. I. Nurdin and N. Yamamoto, *Linear Dynamical Quantum Systems* (Springer International, Cham, 2017) (cit. on p. 32).

[210]S. Olivares, M. G. A. Paris, and R. Bonifacio, "Teleportation improvement by inconclusive photon subtraction", Phys. Rev. A **67**, 032314 (2003) (cit. on p. 137).

[211]T. Opatrný, G. Kurizki, and D.-G. Welsch, "Improvement on teleportation of continuous variables by photon subtraction via conditional measurement", Phys. Rev. A **61**, 032302 (2000) (cit. on p. 137).

[212]A. Ourjoumtsev, H. Jeong, R. Tualle-Brouri, and P. Grangier, "Generation of optical 'Schrödinger cats' from photon number states", Nature **448**, 784–786 (2007) (cit. on p. 152).

[213]A. Ourjoumtsev, R. Tualle-Brouri, and P. Grangier, "Quantum Homodyne Tomography of a Two-Photon Fock State", Phys. Rev. Lett. **96**, 213601 (2006) (cit. on pp. 137, 152).

[214]A. M. Ozorio de Almeida, "Entanglement in Phase Space", in *Entanglement and decoherence*, Vol. 768 (Springer Berlin Heidelberg, Berlin, Heidelberg, 2009), pp. 157–219 (cit. on p. 28).

[215]J. Paavola, M. J. W. Hall, M. G. A. Paris, and S. Maniscalco, "Finite-time quantum-to-classical transition for a Schrödinger-cat state", Phys. Rev. A **84**, 012121 (2011) (cit. on pp. 133, 135).

[216]M. L. Palma, J. Stammers, M. G. Genoni, T. Tufarelli, S. Olivares, M. S. Kim, and M. G. A. Paris, "Detecting quantum non-Gaussianity of noisy Schrödinger cat states", Phys. Scr. **2014**, 14035 (2014) (cit. on pp. 138, 142).

[217]M. Palmero, E. Torrontegui, J. G. Muga, and M. Modugno, "Detecting quantum backflow by the density of a Bose-Einstein condensate", Phys. Rev. A **87**, 053618 (2013) (cit. on p. 123).

[218]S. Pang and T. A. Brun, "Quantum metrology for a general Hamiltonian parameter", Phys. Rev. A **90**, 022117 (2014) (cit. on p. 80).

[219]M. G. A. Paris, "Generation of mesoscopic quantum superpositions through Kerr-stimulated degenerate downconversion", J. Opt. B **1**, 662–667 (1999) (cit. on pp. 96, 97).

[220]M. G. A. Paris, "Nearly ideal binary communication in squeezed channels", Phys. Rev. A **64**, 014304 (2001) (cit. on p. 95).

[221]M. G. A. Paris, "Quantum Estimation for Quantum Technology", Int. J. Quant. Inf. **07**, 125 (2009) (cit. on pp. 21–23).

[222]M. G. A. Paris, "The modern tools of quantum mechanics: A tutorial on quantum states, measurements, and operations", Eur. Phys. J. Spec. Top. **203**, 61–86 (2012) (cit. on p. 7).

[223]M. G. A. Paris, M. G. Genoni, N. Shammah, and B. Teklu, "Quantifying the nonlinearity of a quantum oscillator", Phys. Rev. A **90**, 012104 (2014) (cit. on pp. 109, 110, 114).

[224]J. Park, J. Lee, K. Baek, S.-w. Ji, and H. Nha, "Faithful measure of Quantum non-Gaussianity via quantum relative entropy", arXiv:1809.02999 (2018) (cit. on p. 145).

[225]K. Park, P. Marek, and R. Filip, "Nonlinear potential of a quantum oscillator induced by single photons", Phys. Rev. A **90**, 013804 (2014) (cit. on p. 155).

[226]H. Pashayan, J. J. Wallman, and S. D. Bartlett, "Estimating Outcome Probabilities of Quantum Circuits Using Quasiprobabilities", Phys. Rev. Lett. **115**, 070501 (2015) (cit. on pp. 139, 142).

[227]A. Pathak and J. Banerji, "Wigner distribution, nonclassicality and decoherence of generalized and reciprocal binomial states", Phys. Lett. A **378**, 117–123 (2014) (cit. on p. 119).

[228]M. Penz, G. Grübl, S. Kreidl, and P. Wagner, "A new approach to quantum backflow", J. Phys. A **39**, 423–433 (2006) (cit. on p. 123).

[229]V. Peřinová and A. Lukš, "Third-order Nonlinear Dissipative Oscillator with an Initial Squeezed State", J. Mod. Opt. **35**, 1513–1531 (1988) (cit. on p. 97).

[230]V. Peřinová and A. Lukš, "Exact quantum statistics of a nonlinear dissipative oscillator evolving from an arbitrary state", Phys. Rev. A **41**, 414–420 (1990) (cit. on p. 97).

[231]D. Petz and G. Catalin, "Introduction to quantum Fisher information", in *Quantum Probability and Related Topics* (Jan. 2011), pp. 261–281 (cit. on pp. 23, 44).

[232]O. Pinel, P. Jian, N. Treps, C. Fabre, and D. Braun, "Quantum parameter estimation using general single-mode Gaussian states", Phys. Rev. A **88**, 040102 (2013) (cit. on p. 65).

[233]S. Pirandola, "Quantum reading of a classical digital memory", Phys. Rev. Lett. **106**, 090504 (2011) (cit. on p. 95).

[234]D. Plankensteiner, J. Schachenmayer, H. Ritsch, and C. Genes, "Laser noise imposed limitations of ensemble quantum metrology", J. Phys. B **49**, 245501 (2016) (cit. on p. 62).

[235]M. B. Plenio, "Logarithmic Negativity: A Full Entanglement Monotone That is not Convex", Phys. Rev. Lett. **95**, 090503 (2005) (cit. on p. 146).

[236]M. B. Plenio and S. F. Huelga, "Sensing in the presence of an observed environment", Phys. Rev. A **93**, 032123 (2016) (cit. on p. 76).

[237]Y.-s. Ra, C. Jacquard, A. Dufour, C. Fabre, and N. Treps, "Tomography of a Mode-Tunable Coherent Single-Photon Subtractor", Phys. Rev. X **7**, 031012 (2017) (cit. on p. 153).

[238]J. Radovanović, V. Milanović, Z. Ikonić, and D. Indjin, "Intersubband absorption in Pöschl–Teller-like semiconductor quantum wells", Phys. Lett. A **269**, 179–185 (2000) (cit. on p. 115).

[239]S. Rahimi-Keshari, T. C. Ralph, and C. M. Caves, "Sufficient Conditions for Efficient Classical Simulation of Quantum Optics", Phys. Rev. X **6**, 021039 (2016) (cit. on pp. 139, 142).

[240]A. T. Rezakhani, S. Alipour, and M. Hassani, "Continuity of the quantum Fisher information", arXiv:1507.01736 (2015) (cit. on p. 23).

[241]S. Rips, M. Kiffner, I. Wilson-Rae, and M. J. Hartmann, "Steady-state negative Wigner functions of nonlinear nanomechanical oscillators", New J. Phys. **14**, 023042 (2012) (cit. on p. 109).

[242]Á. Rivas and A. Luis, "Precision quantum metrology and nonclassicality in linear and nonlinear detection schemes", Phys. Rev. Lett. **105**, 010403 (2010) (cit. on p. 96).

[243]M. A. C. Rossi, F. Albarelli, and M. G. A. Paris, "Enhanced estimation of loss in the presence of Kerr nonlinearity", Phys. Rev. A **93**, 053805 (2016) (cit. on pp. xvii, 98).

[244]P. Rouchon, "Models and Feedback Stabilization of Open Quantum Systems", arXiv:1407.7810 (2014) (cit. on p. 53).

[245]P. Rouchon and J. F. Ralph, "Efficient quantum filtering for quantum feedback control", Phys. Rev. A **91**, 012118 (2015) (cit. on pp. 50, 53).

[246]J. Rubio, P. Knott, and J. Dunningham, "Non-asymptotic analysis of quantum metrology protocols beyond the cramér–rao bound", J. Phys. Comm. **2**, 015027 (2018) (cit. on p. 24).

[247]. Šafránek, "Discontinuities of the quantum fisher information and the bures metric", Phys. Rev. A **95**, 052320 (2017) (cit. on p. 89).

[248]K. K. Sabapathy and C. Weedbrook, "ON states as resource units for universal quantum computation with photonic architectures", Phys. Rev. A **97**, 062315 (2018) (cit. on p. 139).

[249]K. K. Sabapathy and A. J. Winter, "Non-Gaussian operations on bosonic modes of light: Photon-added Gaussian channels", Phys. Rev. A **95**, 062309 (2017) (cit. on p. 137).

[250]J. J. Sakurai and J. Napolitano, *Modern quantum mechanics*, 2nd (Addison-Wesley, Boston, 2011) (cit. on p. 118).

[251]J. C. Sankey, C. Yang, B. M. Zwickl, A. M. Jayich, and J. G. E. Harris, "Strong and Tunable Nonlinear Optomechanical Coupling in a Low-Loss System", Nat. Phys. **6**, 12 (2010) (cit. on p. 109).

[252]M. Sarovar and G. J. Milburn, "Optimal estimation of one-parameter quantum channels", J. Phys. A **39**, 8487–8505 (2006) (cit. on p. 95).

[253]M. Sasaki, R. Momose, and O. Hirota, "Quantum detection for on-off keyed mixed-state signals with a small amount of thermal noise", Phys. Rev. A **55**, 3222–3225 (1997) (cit. on p. 95).

[254]M. O. Scully, H. Walther, and W. P. Schleich, "Feynman's approach to negative probability in quantum mechanics", Phys. Rev. A **49**, 1562–1566 (1994) (cit. on p. 123).

[255]S. Sefi and P. van Loock, "How to decompose arbitrary continuous-variable quantum operations", Phys. Rev. Lett. **107**, 170501 (2011) (cit. on p. 139).

[256]A. Serafini, *Quantum continuous variables: a primer of theoretical methods* (CRC Press, Boca Raton, 2017) (cit. on pp. 8, 10, 25, 26, 29–32, 34, 65).

[257]A. Serafini, M. G. A. Paris, F. Illuminati, and S. D. Siena, "Quantifying decoherence in continuous variable systems", J. Opt. B **7**, R19–R36 (2005) (cit. on pp. 95, 133).

[258]L. Seveso, F. Albarelli, M. G. Genoni, and M. G. A. Paris, "On the discontinuity of the quantum Fisher information and the validity of the Cramér-Rao bound", *in preparation* (2018) (cit. on p. 89).

[259]L. Seveso and M. G. A. Paris, "Estimation of Hamiltonian parameters beyond the quantum Cramer-Rao bound", arXiv:1712.07858 (2017) (cit. on p. 22).

[260]L. Seveso, M. A. C. Rossi, and M. G. A. Paris, "Quantum metrology beyond the quantum Cramér-Rao theorem", Phys. Rev. A **95**, 012111 (2017) (cit. on p. 22).

[261]T. Shitara, Y. Kuramochi, and M. Ueda, "Trade-off relation between information and disturbance in quantum measurement", Phys. Rev. A **93**, 032134 (2016) (cit. on p. 44).

[262]R. T. Skodje, H. W. Rohrs, and J. VanBuskirk, "Flux analysis, the correspondence principle, and the structure of quantum phase space", Phys. Rev. A **40**, 2894–2916 (1989) (cit. on p. 124).

[263]F. Soto and P. Claverie, "When is the Wigner function of multidimensional systems nonnegative?", J. Math. Phys. **24**, 97 (1983) (cit. on pp. 36, 138, 142).

[264]R. W. Spekkens, "Negativity and contextuality are equivalent notions of nonclassicality", Phys. Rev. Lett. **101**, 020401 (2008) (cit. on p. 138).

[265]D. L. Stahlke, "Quantum interference as a resource for quantum speedup", Phys. Rev. A **90**, 022302 (2014) (cit. on p. 139).

[266]O. Steuernagel, D. Kakofengitis, and G. Ritter, "Wigner flow reveals topological order in quantum phase space dynamics", Phys. Rev. Lett. **110**, 030401 (2013) (cit. on p. 124).

[267]M. Stobińska, G. J. Milburn, and K. Wódkiewicz, "Wigner function evolution of quantum states in the presence of self-Kerr interaction", Phys. Rev. A **78**, 013810 (2008) (cit. on p. 96).

[268]J. K. Stockton, J. M. Geremia, A. C. Doherty, and H. Mabuchi, "Robust quantum parameter estimation: Coherent magnetometry with feedback", Phys. Rev. A **69**, 032109 (2004) (cit. on pp. 59, 60).

[269]P. Strange, "Large quantum probability backflow and the azimuthal angle–angular momentum uncertainty relation for an electron in a constant magnetic field", Eur. J. Phys. **33**, 1147–1154 (2012) (cit. on p. 123).

[270]D. Su, K. K. Sabapathy, C. R. Myers, H. Qi, C. Weedbrook, and K. Brádler, "Implementing quantum algorithms on temporal photonic cluster states", arXiv:1805.02645 (2018) (cit. on p. 139).

[271]S. S. Szigeti, A. R. R. Carvalho, J. G. Morley, and M. R. Hush, "Ignorance is bliss: general and robust cancellation of decoherence via no-knowledge quantum feedback", Phys. Rev. Lett. **113**, 020407 (2014) (cit. on pp. 76, 82).

[272]R. Takagi and Q. Zhuang, "Convex resource theory of non-Gaussianity", Phys. Rev. A **97**, 062337 (2018) (cit. on p. 139).

[273]S.-H. Tan, B. I. Erkmen, V. Giovannetti, S. Guha, S. Lloyd, L. Maccone, S. Pirandola, and J. H. Shapiro, "Quantum illumination with gaussian states", Phys. Rev. Lett. **101**, 253601 (2008) (cit. on p. 95).

[274]K. C. Tan, T. Volkoff, H. Kwon, and H. Jeong, "Quantifying the Coherence between Coherent States", Phys. Rev. Lett. **119**, 190405 (2017) (cit. on pp. 34, 145).

[275]B. Teklu, A. Ferraro, M. Paternostro, and M. G. A. Paris, "Nonlinearity and nonclassicality in a nanomechanical resonator", en, EPJ Quantum Technol. **2**, 16 (2015) (cit. on p. 109).

[276]T. Theurer, N. Killoran, D. Egloff, and M. B. Plenio, "Resource theory of superposition", Phys. Rev. Lett. **119**, 230401 (2017) (cit. on p. 146).

[277]L. K. Thomsen, S. Mancini, and H. M. Wiseman, "Spin squeezing via quantum feedback", Phys. Rev. A **65**, 061801 (2002) (cit. on p. 61).

[278]U. M. Titulaer and R. J. Glauber, "Correlation functions for coherent fields", Phys. Rev. **2529** (1965) (cit. on p. 34).

[279]B. Tong, "Scattering states of the Sech-squared potential", Solid State Commun. **104**, 679–682 (1997) (cit. on p. 115).

[280]B. Tong and N. Kiriushcheva, "Band-gap engineering of a Sech-squared potential in heterojunctions", Phys. Lett. A **229**, 49–52 (1997) (cit. on p. 115).

[281]G. Vacanti, M. Paternostro, G. M. Palma, M. S. Kim, and V. Vedral, "Nonclassicality of optomechanical devices in experimentally realistic operating regimes", Phys. Rev. A **88**, 013851 (2013) (cit. on p. 109).

[282]B. Vacchini, *Lecture Notes on Advanced Quantum Mechanics* (Univeristy of Milan, 2017) (cit. on p. 1).

[283]H. L. Van Trees, *Detection, Estimation, and Modulation Theory* (Wiley, New York, 1967) (cit. on pp. 21, 42).

[284]H. M. Vasconcelos, L. Sanz, and S. Glancy, "All-optical generation of states for "Encoding a qubit in an oscillator"", Opt. Lett. **35**, 3261 (2010) (cit. on p. 139).

[285]V. Veitch, C. Ferrie, D. Gross, and J. Emerson, "Negative quasi-probability as a resource for quantum computation", New J. Phys. **14**, 113011 (2012) (cit. on p. 139).

[286]V. Veitch, S. A. Hamed Mousavian, D. Gottesman, and J. Emerson, "The resource theory of stabilizer quantum computation", New J. Phys. **16**, 013009 (2014) (cit. on pp. 139, 141, 145, 146, 149).

[287]V. Veitch, N. Wiebe, C. Ferrie, and J. Emerson, "Efficient simulation scheme for a class of quantum optics experiments with non-negative Wigner representation", New J. Phys. **15**, 013037 (2013) (cit. on pp. 35, 142).

[288]L. G. Villanueva, R. B. Karabalin, M. H. Matheny, E. Kenig, M. C. Cross, and M. L. Roukes, "A Nanoscale Parametric Feedback Oscillator", Nano Lett. **11**, 5054–5059 (2011) (cit. on p. 111).

[289]M. Walschaers, C. Fabre, V. Parigi, and N. Treps, "Entanglement and Wigner Function Negativity of Multimode Non-Gaussian States", Phys. Rev. Lett. **119**, 183601 (2017) (cit. on p. 152).

[290]X. Wang and B. C. Sanders, "Relations between bosonic quadrature squeezing and atomic spin squeezing", Phys. Rev. A **68**, 033821 (2003) (cit. on p. 63).

[291]C. Weedbrook, S. Pirandola, R. Garcia-Patron, N. J. Cerf, T. C. Ralph, J. H. Shapiro, and S. Lloyd, "Gaussian quantum information", Rev. Mod. Phys. **84**, 621 (2012) (cit. on p. 29).

[292]D. J. Weigand and B. M. Terhal, "Generating grid states from schrödinger-cat states without postselection", Phys. Rev. A **97**, 022341 (2018) (cit. on p. 139).

[293]R. F. Werner, "Wigner quantisation of arrival time and oscillator phase", J. Phys. A **21**, 4565–4575 (1988) (cit. on p. 126).

[294]D. J. Wineland, J. J. Bollinger, W. M. Itano, F. L. Moore, and D. J. Heinzen, "Spin squeezing and reduced quantum noise in spectroscopy", Phys. Rev. A **46**, R6797 (1992) (cit. on p. 59).

[295]H. M. Wiseman, "Quantum trajectories and feedback", PhD (University of Queensland, Jan. 1994), p. 214 (cit. on p. 8).

[296]H. M. Wiseman, "Quantum trajectories and quantum measurement theory", Quant. Semiclass. Opt. **8**, 205–222 (1996) (cit. on p. 46).

[297]H. M. Wiseman and A. C. Doherty, "Optimal Unravellings for Feedback Control in Linear Quantum Systems", Phys. Rev. Lett. **94**, 070405 (2005) (cit. on p. 32).

[298]H. M. Wiseman and G. J. Milburn, *Quantum Measurement and Control* (Cambridge University Press, New York, 2010) (cit. on pp. 8, 14, 17, 32, 46, 52, 83).

[299]W. Xiang-bin, "A theorem for the beam splitter entangler", Phys. Rev. A **66**, 024303 (2002) (cit. on p. 35).

[300]B. Yadin, V. Narasimhachar, F. C. Binder, J. Thompson, M. Gu, and M. S. Kim, "An operational resource theory of continuous-variable nonclassicality", arXiv:1804.10190 (2018) (cit. on pp. 34, 146).

[301]J. M. Yearsley, "Quantum arrival time for open systems", Phys. Rev. A **82**, 012116 (2010) (cit. on p. 134).

[302]J. M. Yearsley and J. J. Halliwell, "An introduction to the quantum backflow effect", J. Phys. Conf. Ser. **442**, 012055 (2013) (cit. on pp. 123, 127).

[303]J. M. Yearsley, J. J. Halliwell, R. Hartshorn, and A. Whitby, "Analytical examples, measurement models, and classical limit of quantum backflow", Phys. Rev. A **86**, 042116 (2012) (cit. on pp. 123, 127, 129).

[304]H. Yildirim and M. Tomak, "Nonlinear optical properties of a Pöschl-Teller quantum well", Phys. Rev. B - Condens. Matter Mater. Phys. **72**, 1–6 (2005) (cit. on p. 115).

[305]H. Yildirim and M. Tomak, "Intensity-dependent refractive index of a Pöschl-Teller quantum well", J. Appl. Phys. **99**, 093103 (2006) (cit. on p. 115).

[306]H. P. Yuen and R. Nair, "Classicalization of nonclassical quantum states in loss and noise: some no-go theorems", Phys. Rev. A **80**, 023816 (2009) (cit. on p. 95).

[307]B. Yurke and D. Stoler, "Generating quantum mechanical superpositions of macroscopically distinguishable states via amplitude dispersion", Phys. Rev. Lett. **57**, 13–16 (1986) (cit. on pp. 96, 127).

[308]B. Yurke and D. Stoler, "The dynamic generation of Schrödinger cats and their detection", Physica B **151**, 298–301 (1988) (cit. on p. 96).

[309]S. Zhang and P. van Loock, "Local Gaussian operations can enhance continuous-variable entanglement distillation", Phys. Rev. A **84**, 062309 (2011) (cit. on p. 138).

[310]W. Zhong, Z. Sun, J. Ma, X. Wang, and F. Nori, "Fisher information under decoherence in Bloch representation", Phys. Rev. A **87**, 022337 (2013) (cit. on p. 89).

[311]H. Zhu, M. Hayashi, and L. Chen, "Axiomatic and operational connections between the l1-norm of coherence and negativity", Phys. Rev. A **97**, 022342 (2018) (cit. on pp. 146, 150).

[312]Q. Zhuang, P. W. Shor, and J. H. Shapiro, "Resource theory of non-Gaussian operations", Phys. Rev. A **97**, 052317 (2018) (cit. on p. 140).